UNIVERSIDADE FEDERAL DE MINAS GERAIS
Escola de Engenharia
Programa de Pós-Graduação em Saneamento, Meio Ambiente e Recursos Hídricos

André Felipe Rocha da Silva

ENHANCING HAZARD MAPPING, EMERGENCY RESPONSE COMPREHENSION, AND LIFE-LOSS ASSESSMENT OF FLOOD EVENTS: a study on probabilistic scenarios and empirical analysis

Belo Horizonte
2025

André Felipe Rocha da Silva

ENHANCING HAZARD MAPPING, EMERGENCY RESPONSE COMPREHENSION, AND LIFE-LOSS ASSESSMENT OF FLOOD EVENTS: a study on probabilistic scenarios and empirical analysis

Tese apresentada ao Programa de Pós graduação em Saneamento, Meio Ambiente e Recursos Hídricos da Universidade Federal de Minas Gerais, como requisito parcial à obtenção do título de Doutor em Saneamento, Meio Ambiente e Recursos Hídricos.

Área de concentração: Hidráulica e Recursos Hídricos

Linha de pesquisa: Avaliação e gerenciamento de impactos e de riscos ambientais

Orientador: Prof. Dr. Julian Cardoso Eleutério

Belo Horizonte
2025

Silva, André Felipe Rocha da.
S586e Enhancing hazard mapping, emergency response comprehension, and life-loss assessment of flood events [recurso eletrônico] : a study on probabilistic scenarios and empirical analysis / André Felipe Rocha da Silva. - 2025.
1 recurso online (187 f. : il., color.) : pdf.

Orientador: Julian Cardoso Eleutério.

Tese (doutorado) - Universidade Federal de Minas Gerais, Escola de Engenharia.

Inclui bibliografia.

1. Engenharia sanitária - Teses. 2. Recursos hídricos - Teses. 3. Mortalidade - Teses. 4. Avaliação de riscos - Modelos matemáticos - Teses. 5. Inundações - Teses. 13. Probabilidade - Teses. I. Eleutério, Julian Cardoso. II. Universidade Federal de Minas Gerais. Escola de Engenharia. III. Título.
CDU: 628(043)

Ficha catalográfica elaborada pelo bibliotecário Reginaldo César Vital dos Santos CRB/6 2165
Biblioteca Prof. Mário Werneck, Escola de Engenharia da UFMG

UNIVERSIDADE FEDERAL DE MINAS GERAIS
Escola de Engenharia
Programa de Pós-Graduação em Saneamento, Meio Ambiente e Recursos Hídricos

"Enhancing Hazard Mapping, Emergency Response Comprehension, And Life-loss Assessment Of Flood Events: A Study On Probabilistic Scenarios And Empirical Analysis"

ANDRÉ FELIPE ROCHA DA SILVA

Tese defendida e aprovada pela banca examinadora constituída pelos Senhores:

Prof. JULIAN CARDOSO ELEUTÉRIO

Profa PRISCILLA MACEDO MOURA

Prof. LUIZ RAFAEL PALMIER

Prof. CARLOS HENRIQUE RIBEIRO LIMA

Prof. PEDRO LUIZ BORGES CHAFFE

Aprovada pelo Colegiado do PG SMARH Versão Final aprovada por

Prof. Eduardo Coutinho de Paula Prof. Julian Cardoso Eleutério
Coordenador Orientador

Belo Horizonte, 10 de junho de 2025.

Documento assinado eletronicamente por **Julian Cardoso Eleuterio, Professor do Magistério Superior**, em 10/06/2025, às 16:55, conforme horário oficial de Brasília, com fundamento no art. 5º do Decreto nº 10.543, de 13 de novembro de 2020.

Documento assinado eletronicamente por **Priscilla Macedo Moura, Professora do Magistério Superior**, em 10/06/2025, às 16:55, conforme horário oficial de Brasília, com fundamento no art. 5º do Decreto nº 10.543, de 13 de novembro de 2020.

Documento assinado eletronicamente por **Pedro Luiz Borges Chaffe, Usuário Externo**, em 10/06/2025, às 17:29, conforme horário oficial de Brasília, com fundamento no art. 5º do Decreto nº 10.543, de 13 de novembro de 2020.

Documento assinado eletronicamente por **Carlos Henrique Ribeiro Lima, Usuário Externo**, em 10/06/2025, às 17:30, conforme horário oficial de Brasília, com fundamento no art. 5º do Decreto nº 10.543, de 13 de novembro de 2020.

Documento assinado eletronicamente por **Luiz Rafael Palmier, Professor do Magistério Superior**, em 10/06/2025, às 17:36, conforme horário oficial de Brasília, com fundamento no art. 5º do Decreto nº 10.543, de 13 de novembro de 2020.

Documento assinado eletronicamente por **Eduardo Coutinho de Paula, Coordenador(a) de curso de pós-graduação**, em 10/09/2025, às 12:54, conforme horário oficial de Brasília, com fundamento no art. 5º do Decreto nº 10.543, de 13 de novembro de 2020.

A autenticidade deste documento pode ser conferida no site https://sei.ufmg.br/sei/controlador_externo.php?acao=documento_conferir&id_orgao_acesso_externo=0, informando o código verificador **4289661** e o código CRC **5409C026**.

Referência: Processo nº 23072.234746/2025-33 SEI nº 4289661

AGRADECIMENTOS

Agradeço especialmente à minha família, que, mesmo na minha ausência durante esses anos, sempre esteve ao meu lado em todas as decisões e me forneceu total apoio de diversas maneiras.

Ao meu orientador, professor Julian, pelo auxílio concedido durante a pesquisa, pelas discussões relacionadas ao tema do trabalho, pelas correções e revisões finais, e pelo trabalho em conjunto em diversos projetos.

À minha orientadora durante o período sanduíche, Heidi Kreibich, pela oportunidade de trabalhar em conjunto e pelo apoio durante a mudança e a estadia no Centro de Pesquisa em Geociências (GFZ) de Potsdam, Alemanha.

Aos membros da banca, pela leitura, revisão e contribuições que proporcionaram o aprimoramento deste trabalho.

À Helena, que, além de auxiliar em diversas situações ao longo da realização desta tese, me trouxe carinho, amor, compreensão e companheirismo durante todo esse período.

Aos amigos do Departamento de Engenharia Hidráulica e Recursos Hídricos, pelas horas compartilhadas na sala 4504 e pelos momentos vividos fora do ambiente universitário.

Aos amigos de Belo Horizonte, Cataguases, Juiz de Fora e de tantos outros lugares que, de alguma forma, contribuíram para minha trajetória.

À comunidade da Universidade Federal de Minas Gerais e, por fim, ao Conselho Nacional de Desenvolvimento Científico e Tecnológico e à Coordenação de Aperfeiçoamento de Pessoal de Nível Superior, pelo apoio concedido ao desenvolvimento desta pesquisa por meio das bolsas de doutorado e doutorado sanduíche.

RESUMO

As inundações representam o desastre natural mais recorrente em escala global, com um aumento significativo na frequência de eventos extremos em decorrência das mudanças climáticas. Esse crescimento, associado à intensificação da urbanização e à consequente ampliação da exposição populacional, eleva substancialmente os riscos, resultando em maior número de pessoas afetadas e de fatalidades. Ainda assim, observa-se uma redução no número médio de indivíduos impactados por evento, o que indica avanços na mitigação de riscos, especialmente por meio de investimentos em Sistemas de Alerta e Evacuação (SAEs). A eficácia desses sistemas pode ser avaliada por meio de modelos de estimativa de perda de vidas, que fornecem informações sobre os impactos potenciais de inundações sob diferentes condições operacionais dos SAEs. No entanto, esses modelos ainda enfrentam importantes limitações, como a representação insuficiente das incertezas hidráulicas, devido aos elevados custos computacionais associados a simulações probabilísticas de alta resolução; a ausência de uma abordagem probabilística que considere a variação temporal e espacial da distribuição populacional; e a limitada representatividade da dinâmica dos agentes envolvidos nos SAEs (autoridades e população), frequentemente baseada em estudos com foco nos Estados Unidos. Esta tese busca explorar essas limitações, avançando na aplicação e compreensão de estimativas de perdas humanas em inundações, em quatro capítulos principais. Primeiramente, introduz-se a modelagem de perdas de vidas por meio da avaliação de diferentes alternativas de SAEs, considerando um cenário hipotético de rompimento de barragem a montante de um vale densamente urbanizado. A análise identifica, por setores ao longo do vale, os momentos ideais e os tempos críticos mínimos para a emissão de alertas que minimizem as fatalidades. Em seguida, desenvolve-se um mapeamento probabilístico do rompimento de uma barragem de terra, utilizando abordagem computacional otimizada. Em um estudo de caso fictício, observa-se que a área de inundação derivada da análise determinística corresponde àquela associada a uma probabilidade de excedência de 40% nos cenários probabilísticos. Na terceira etapa, propõe-se uma nova metodologia para a estimativa probabilística de perdas de vidas, integrando, sob abordagem probabilística, incertezas hidráulicas e as distribuições temporal e espacial da população. Ainda para o estudo de caso anterior, percebe-se que, embora a abordagem determinística produza estimativas medianas superiores às médias ponderadas do método probabilístico, a consideração da variabilidade, expressa pelo desvio padrão, pode inverter esse resultado. Por fim, ao analisar o desempenho dos SAEs durante a inundação de 2021 na Alemanha, com base em pesquisa junto aos residentes afetados, identificam-se lacunas entre a execução prática dos sistemas e as recomendações teóricas. Apesar da emissão oportuna dos alertas, falhas sistêmicas de comunicação comprometeram a resposta da população, sendo estimado que estratégias alternativas de SAEs poderiam ter reduzido as perdas humanas em até 80%. Os resultados, as metodologias propostas, e as discussões desenvolvidas nesta tese contribuem para o aprimoramento das ferramentas de simulação de impactos de SAEs, oferecendo subsídios relevantes para o desenvolvimento de modelos mais robustos, contextualizados e capazes de gerar estimativas mais precisas sobre impactos humanos em inundações.

Palavras-chave: Sistemas de alerta. Avaliação do risco de inundações. Fatalidades em inundações. Rompimento de barragem. Modelo baseado em agentes LifeSim.

ABSTRACT

Floods are the most recurrent natural disaster on a global scale, with a significant increase in the frequency of extreme events driven by climate change. This growth, combined with intensified urbanisation and the resulting expansion of population exposure, substantially raises associated risks, leading to a greater number of people affected and an increase in fatalities. Despite this, a reduction in the average number of individuals impacted per event has been observed, indicating progress in risk mitigation, particularly through investments in Early Warning and Evacuation Systems (EWESs). The effectiveness of these systems can be evaluated using life-loss estimation models, which provide insights into the potential impacts of floods under different operational conditions of EWESs. However, these models still face significant limitations, including the insufficient representation of hydraulic uncertainties, mainly due to the high computational cost of high-resolution probabilistic simulations; the lack of probabilistic approaches that account for temporal and spatial variability in population distribution; and the limited representativeness of agent behavior (authorities and population), which is often based on studies focused on the United States. This thesis aims to explore and address these limitations by advancing the application and understanding of life-loss estimation in flood events across four main chapters. First, life-loss modelling is introduced through the evaluation of different EWES alternatives, considering a hypothetical dam-break scenario upstream of a densely urbanised valley. The analysis identifies, by sector along the valley, the optimal moments and critical minimum lead times for issuing alerts that minimise fatalities. Next, a probabilistic flood mapping method for the failure of an earthen dam is developed using a computationally optimised approach. In a fictional case study, it is observed that the inundation area derived from deterministic analysis corresponds to the area associated with a 40% exceedance probability in probabilistic scenarios. In the third stage, a new methodology is proposed for probabilistic life-loss estimation that integrates, under a probabilistic framework, both hydraulic uncertainties and the temporal and spatial variability of population distribution. Applied to the same case study, the analysis reveals that although deterministic estimates tend to produce higher median values than the probabilistic weighted means, accounting for variability, expressed through standard deviation, can reverse this outcome. Finally, the performance of EWESs during the 2021 flood in Germany is analysed based on surveys conducted with affected residents. The study identifies substantial gaps between the practical implementation of the systems and theoretical recommendations. Despite the timely issuance of alerts, systemic communication failures undermined public response, and it is estimated that alternative EWES strategies could have reduced human losses by up to 80%. The findings, proposed methodologies, and discussions developed in this thesis contribute to improving the simulation tools used to assess the impacts of EWESs. They provide valuable insights for the development of more robust, context-sensitive models that can produce more accurate estimates of human impacts during flood events.

Keywords: Early warning systems. Flood risk assessment. Flood fatalities. Dam breach. Agent-based LifeSim model.

LIST OF FIGURES

LIST OF TABLES

LIST OF ABBREVIATIONS AND ACRONYMS

a and b – Coefficients specific for adjusting empirical data in warning issuance delay

ABM – Agent-Based Model

$A_{i,j}$ – Probability of inundation boundary for each scenario

AT – Arrival time

a_m – Coefficient related to the mobilisation speed

b_m – Coefficient related to the average time for mobilisation

B – Dam-breach event

B_t – Brech top width

b_t – Coefficient related to the effectiveness of the direct alert system

$C_{i,j}$ – Flood hazard class Probability for each scenario

CS – Cross-section

c_t – Coefficient associated with the effectiveness of the indirect alert system

DEM – Digital Elevation Model

EAP – Emergency Action Plan

EWES – Early Warning and Evacuation Systems

F_E – Evacuation rate

F_d – Fatality rate

FN – Fatality-Probability

FEWE – Flood Early Warning And Evacuation

FRM – Flood-Routine Module

HEC – Hydrologic Engineering Center

HC – Hazard Classification

H_d – Dam height

HANZE – Historical Analysis of Natural HaZards in Europe (

HMS – Hydrologic Modelling System

HR – Flood hazard

ICOLD – International Commission on Large Dams

IIE – Internal Erosion

INT – Intermediate

LAU – Local Administrative Unit

L_{cr} – Dam crest length

LOL – Loss of Life

$LOL_{i,j,k}$ – Estimation of loss of life

LLM – Loss of Life Module

η – Manning's roughness value

n – Iteration

N – Estimated loss of life

NAR – Narrow

DWD – National German Weather Service

NDSP – National Dam Safety Policy

NLCD – National Land Cover Database

NUTS – Nomenclature of Territorial Units for Statistics

NRW – North Rhine-Westphalia

N_{par} – Number of people at risk

OT – Overtopping

p – Probability of delay in the decision

$P_{i,j}$ – Dam-breach scenario probability

$P_{i,j,k}$ – Dam-breach and population distribution scenario probability

P_{in} – Inundation boundary probability

P_{LOL} – Probabilistic life-loss estimation

$P_{LOL_{i,j}}$ – Probabilistic life-loss estimation for a given scenario

PL.Dam – Pampulha Lake Dam

$P_{mobilised_t}$ – Proportion of the population who initiate protective action at a given time step

P_{t_h} – Cumulative probability of being mobilised

Pu_t – Population that has not been warned

P_{warned_t} – Proportion of the population receiving the warning at each discrete time interval

Q_p – Peak flow

RAS – River Analysis System

RCEM – Reclamation Consequence Estimating Methodology

RFEWE – Reconstructed scenario of the 2021 flood

RLP – Rhineland-Palatinate

RMSE – Root Mean Square Deviation

S – Dam-breach scenario

σ – Standard deviation

SAE – Sistema de Alerta e Evacuação

SLM – Shelter Loss Module

t – Time [min]

t_f – Breach formation time

t_h – Time [h]

t_p – Peak time

μ – Weighted mean

VAR – Flood variable

W – Alerted population

$\frac{\Delta W}{\Delta t}$ – Rate of the alerted population

WEM – Warning and Evacuation Module

WID – Wide

SUMMARY

1 INTRODUCTION

Floods are among the most frequently occurring natural disasters, resulting in substantial economic and human losses. Over the period from 1998 to 2017, out of more than 7,000 documented global disaster events, floods accounted for 43% of them, resulting in damages exceeding USD 650 billion, impacting over two billion individuals, and causing more than 142,000 fatalities (CRED & UNISDR, 2018). Under a climate change scenario, the frequency of floods, particularly of rare events, has increased globally (WASKO *et al.*, 2021). This increase, coupled with greater exposure due to rapid urbanisation (TELLMAN *et al.*, 2021), intensifies the risk, consequently leading to a higher number of affected individuals and fatalities (MISHRA *et al.*, 2022; ZHANG *et al.*, 2021).

Between 2000 and 2019, the global frequency of reported floods increased by 57compared to the period from 1980 to 1999, affecting 1.65 billion people and resulting in 104,614 deaths (CRED; UNDRR, 2020). Despite the increasing number of flood events and their consequences in recent years, the number of people affected per event has decreased (HU *et al.*, 2018; JONKMAN; CURRAN; BOUWER, 2024; MERZ *et al.*, 2021). This trend could indicate some level of efficiency in implementing flood risk-reduction measures (HAMMOND *et al.*, 2015; SALMAN; LI, 2018). However, flood risk management still faces significant challenges, particularly in addressing the impacts of unprecedented events with magnitudes not previously experienced (KREIBICH *et al.*, 2022).

Enhanced land-use planning, strict legislative measures, and the implementation of strategies such as the establishment of warning systems and evacuation routes constitute effective means to minimise the adverse impacts of flood events (APEL; VOROGUSHYN; MERZ, 2022; KREIBICH; HUDSON; MERZ, 2021; LUMBROSO *et al.*, 2021). In this context, risk assessment plays an important role, offering insights into the comprehension of existing scenarios and the development of prospective strategies to mitigate risks associated with flood dynamics and potentially affected populations (MERZ *et al.*, 2010). Risk assessment depends on the interplay between the probability of an event occurring and its consequences, which are commonly quantified in terms of economic losses and loss of human life. These metrics are considered objective, encompassing factors such as fatalities or monetary value,

making them particularly pertinent to the public perception of disasters (JONKMAN; VAN GELDER; VRIJLING, 2003).

In terms of fatalities, one of the most critical factors during floods is the effectiveness of Early Warning and Evacuation Systems (EWESs) (PETRUCCI, 2022; YARI *et al.*, 2020). An optimal EWES should be robust, capable of early hazard identification, and equipped with efficient communication channels to promptly inform the population at risk (KREIBICH; HUDSON; MERZ, 2021; KULLER; SCHOENHOLZER; LIENERT, 2021). Additionally, an investment in enhancing the population's knowledge of appropriate actions and behaviours in response to flood risks is essential (AERTS *et al.*, 2018; BERGHÄUSER *et al.*, 2023).

One method to assess the effectiveness of these flood EWESs is through life-loss estimation models (CHEN *et al.*, 2023; GE *et al.*, 2022). Life-loss estimation models can be categorised as either empirical or dynamic. The empirical approach combines flood characteristics, such as water depth, flow velocity, rise rate, and warning time, with population exposure and vulnerability to estimate fatality rates. Dynamic models, often referred to as agent-based models, employ a time-varying quantification of event characteristics correlated with flood exposure criteria and thresholds. These agent-based models provide a more detailed simulation of events by modelling individual behaviour and the causes of fatalities (ANSHUKA *et al.*, 2022; ZHUO; HAN, 2020). This detailed simulation is beneficial for evaluating EWES, offering advantages over empirical models (DI MAURO; DE BRUIJN; MELONI, 2012; SHIRVANI; KESSERWANI, 2021).

Numerous agent-based models related to flood risk management have been developed (ANSHUKA *et al.*, 2022). However, most of these models are designed for specific sites and types of floods and have been applied only in limited research contexts. As a result, only two models have been widely used in flood risk assessment (LUMBROSO; DAVISON; WETTON, 2023): the Life Safety Model (LSM) (JOHNSTONE *et al.*, 2005) and the LifeSim model (ABOELATA; BOWLES; MCCLELLAND, 2003).

In the Brazilian context, catastrophic dam failures in Mariana (2015) and Brumadinho (2019), both located in the state of Minas Gerais, resulted in extensive economic,

societal, and environmental repercussions (FERNANDES *et al.*, 2016; GUIMARÃES *et al.*, 2022; ROTTA *et al.*, 2020). These tragedies led to reforms in dam safety regulations, requiring stronger emergency action plans that incorporate high-resolution flood mapping (FERRARI; VACONDIO; MIGNOSA, 2023), assessments of social vulnerabilities among affected populations, and the development of more robust EWES, encompassing elements such as the planning of evacuation routes and the establishment of meeting points. In this context, agent-based life-loss modelling offers valuable insights for addressing these new regulatory requirements.

Despite the significant potential of agent-based life-loss models in evaluating EWES, numerous uncertainties and gaps challenge their application. One major challenge is incorporating the uncertainty inherent in hydraulic modelling into life-loss estimation, which requires consideration of a wide range of potential scenarios (APEL *et al.*, 2004; PATÉ-CORNELL, 1996). This is particularly difficult due to the high computational demands of probabilistic simulations at fine spatial and temporal resolutions when using traditional sampling techniques (TSAI; YEH; HUANG, 2019).

Additionally, population distribution is highly variable across both space and time, introducing further complexity. These spatiotemporal dynamics significantly influence evacuation behaviour and, consequently, the outcomes of life-loss assessments (PENG; ZHANG; SAYAMA, 2024). While some agent-based models, such as LifeSim, incorporate probabilistic approaches to account for uncertainties in specific input parameters, these do not typically encompass uncertainties related to hydraulic processes or dynamic population distributions. Instead, such models focus on uncertainties associated with other inputs, such as the timing of events within the EWES timeline.

Moreover, the representation of this EWES, which involves modelling the behaviours of both authorities and exposed populations, is predominantly informed by research conducted in American contexts. This limits their applicability in regions with different socio-cultural and institutional conditions. Therefore, this thesis research aims to explore these gaps by verifying the potential benefits of integrating probabilistic dam-breach flood modelling and probabilistic spatiotemporal population distribution into life-loss simulations, while enhancing the understanding of EWES during flood events,

particularly regarding authorities and population emergency response times, to generate more accurate life-loss estimates.

1.1 Objectives

This research aims to enhance the application of agent-based life-loss estimation models by integrating uncertainties related to dam-breach hydrodynamic modelling and spatial and temporal population distribution scenarios within a probabilistic framework, while also evaluating empirical data on early warning and evacuation system procedures.

In order to achieve this goal, four specific objectives are proposed:

- Investigating the effectiveness of a sectorised early warning and evacuation systems in mitigating potential life loss within an urban high-density area during flood events;
- Applying a computationally efficient method for probabilistic flood mapping of embankment dam-breach scenarios, leveraging data from historical dam failure;
- Developing a methodological framework for integrating probabilistic embankment dam-breach flood scenarios and spatial and temporal population distribution scenarios into an agent-based life-loss model; and
- Reconstructing and evaluating the early warning and evacuation response during a historical flash flood event through post-event resident surveys, with a focus on its impact on human loss outcomes.

1.2 State of the art

This section provides the context and presents an overview of the key papers and models that form the basis of this thesis. Initially, it emphasises estimating life loss in flood scenarios, providing a comprehensive description and specifications of the life-loss model employed in this study, LifeSim. Following this first section, the four others are designed to align the life-loss review description with other relevant studies corresponding to each specific objective of this research.

1.2.1 Life-loss estimation in flooding events

In estimating fatalities resulting from flood events, there are methodologies grounded in behavioural assessments and macroeconomic indicators to evaluate these consequences (JONGEJAN; JONKMAN; VRIJLING, 2005). However, the monetary specification of loss of life is considered intricate, given the intangible nature of this typology of damage (MERZ *et al.*, 2010). Furthermore, fatalities can also be indirectly linked to flooding. These fatalities are observed beyond the boundaries of inundated areas, such as those resulting from traffic accidents during evacuations and due to post-flood stress. Nevertheless, as most fatalities occur due to direct causes, and as forecasting such behaviour is challenging, loss of life is categorised solely as direct damage. Consequently, this consequence is addressed directly and quantitatively within the risk assessment process, without a monetary assignment (JONKMAN; VAN GELDER; VRIJLING, 2003).

The prospective quantification of direct loss of life occurs through the consideration of three primary factors: firstly, the number of individuals potentially at risk is taken into account; secondly, the effectiveness of evacuation and shelter strategies is assessed to determine the number of people exposed to the event; and finally, the estimation of the fatality rate is considered, which is the ratio of the number of individuals who do not survive to the number of people exposed to the flooding event (JONKMAN; VRIJLING; VROUWENVELDER, 2008).

Several empirical loss of life models address different events, including coastal and riverine floods (BOYD; LEVITAN; VAN HEERDEN, 2005; BRAZDOVA; RIHA, 2014; JONKMAN *et al.*, 2009; JONKMAN; VRIJLING; VROUWENVELDER, 2008; PENNING-ROWSELL *et al.*, 2005; SHOKOOHI; AMIRMORADI, 2025; YAZDANI *et al.*, 2023; ZHAI; FUKUZONO; IKEDA, 2006), as well as dam breaches (BROWN; GRAHAM, 1988; DEKAY; MCCLELLAND, 1993; GE *et al.*, 2021; GRAHAM, 1999; JIAO; LI; MA, 2022; MAHMOUD; WANG; JIN, 2020; PENG; ZHANG; SAYAMA, 2024; PENG; ZHANG, 2012; USBR, 2015). Among the two cited agent-based models, the LifeSim (ABOELATA; BOWLES, 2005b) is noteworthy for its extensive utilisation within American consulting firms and insurance agencies (NEEDHAM; FIELDS; LEHMAN, 2016) and its widespread application in academic works. Its capacity to simultaneously analyse evacuation procedures and loss of life positions the LifeSim model as the

central focus for developing the methodology within this research. A more comprehensive examination of the model is conducted, encompassing detailed specifications and exploring numerous studies that have employed it.

1.2.1.1 LifeSim model

The LifeSim model, initially proposed by Aboelata and Bowles (2005b), has been integrated into a graphical interface by the United States Army Corps of Engineers (USACE). This model simulates the outcomes of exposure to various events, with its methodology linking loss of life to the evacuation of individuals or their success in finding secure shelter. With an agent-based modelling approach, the model is structured using a modular modelling system, where modules exchange information (Figure 1.1) through a database that encompasses multiple layers of geographic information systems. The model comprises four key modules:

1. flood routine module: encompasses a network representation of flood characteristics throughout the area and time;
2. loss of shelter module: simulates the exposure of individuals in structures during events, considering structural damage and submersion criteria;
3. warning and evacuation module: simulates the distribution and dynamics of the at-risk population following the issuance of alerts; and
4. loss of life module: estimates loss of life employing probability distributions of fatality rates derived from historical flood event data.

Figure 1.1 – LifeSim module interactions.

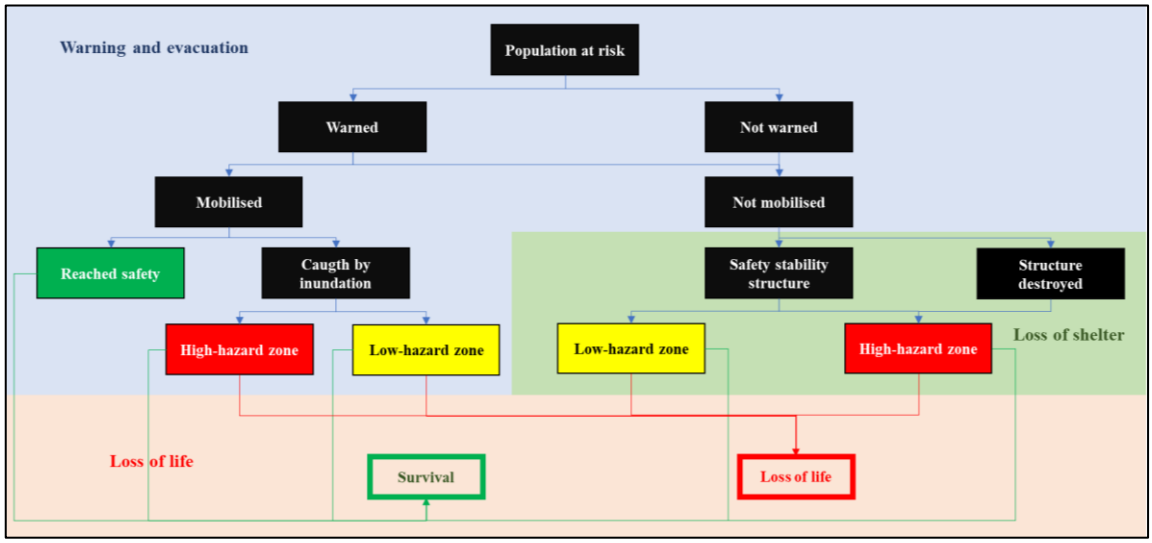

Source: Adapted from (USACE, 2021).

Furthermore, Monte Carlo simulations are employed within LifeSim to account for uncertainties in the warning and evacuation process and the potential for loss of life. Several model parameters can be introduced with uncertainty, examining random and epistemic uncertainties. Consequently, the model's output concerning quantifying loss of life is probabilistic.

The flood routine module contains hydraulic data about the flooding event, encompassing temporal variations in water depth and flow velocity within the analysed region. This module accepts input data from simulations conducted using hydraulic models such as HEC-RAS and FLO-2D. For simulations executed using other hydraulic models, the insertion of water depth and flow velocity data is facilitated through multiple layers, each representing a different time interval and containing corresponding parameter values.

The shelter loss module simulates the population's exposure during each flooding event, accounting for submersion within structures and structural damage. These structures are incorporated into the model through a vector file containing essential information such as geographic location, occupancy type, construction material, number of stories, building elevation relative to the ground, population under the age of 65 and those aged 65 and over.

Regarding submersion within structures, flood zones are physically defined based on the interaction between existing shelters and the summarised depth. Depending on the LifeSim model version, different water depth thresholds define these zones. In assessing structural damage in buildings, stability is defined by criteria that involve flow velocity and depth of damage, while also considering factors such as occupancy type, construction material, and the number of stories in the building. In the LifeSim framework, several criteria can be chosen to assess structural stability, such as those proposed by Davis (1985) and Maijala, Huokona,and Honakakunnas (2001). Once the stability criterion is achieved, leading to the collapse of the structure, the population is relocated to the highest-hazard flood zone. For each predefined risk zone, probabilistic curves are used to estimate the number of fatalities. Further details on these curves will be provided in the subsequent description within the module dedicated to analysing the loss of life.

The warning and evacuation module represents the distribution and behaviour of the population during a flood event. This process involves various milestones, each separated by a time delay, as illustrated in the timeline in Figure 1.2. The timeline commences with identifying an imminent threat and marks the first delay in communicating the threat to the authorities. In both scenarios, no existing studies guide the determination of these time values; thus, users must determine the appropriate times based on the specific characteristics of the analysed case. In contrast, the subsequent three-time delays have been informed by research and supported by studies and equations (SORENSEN; MILETI, 2015c, 2015d, 2015e).

LifeSim incorporates standard curves with an explicit range of uncertainty for these three delays. The uncertainty is inherently present in the delay curves for alert issuance, as they are probability distribution functions. Cumulative probability functions represent the warning diffusion and mobilisation curves, and account for uncertainty. After the evacuation is initiated, the LifeSim routine utilises several criteria and considerations to model the evacuation process and determine whether an agent successfully reaches a safe location.

In identifying the threat and all the delays mentioned in the timeline depicted in Figure 1.2, the user can create their own curves for a specific case and introduce uncertainty into the input data. The accepted distribution types representing uncertainty in the interface include uniform, normal, triangular, and Lindell distributions.

Figure 1.2 – Warning and evacuation timeline.

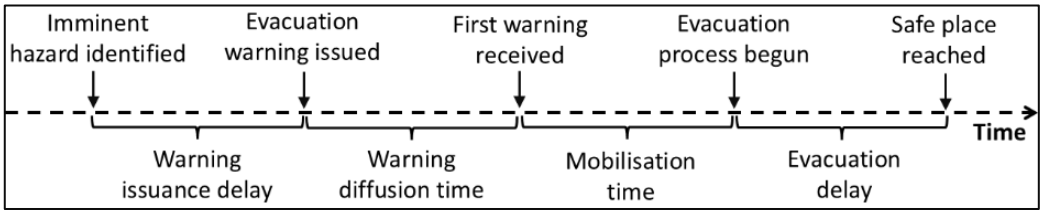

Source: Adapted from (USACE, 2021).

In order to assist in developing these curves to represent delays in warning issuance, diffusion, and mobilisation for any given scenario, Sorensen and Mileti (2015d) created an interview guide consisting of 52 questions. These questions encompass various aspects, including potential threats to the region, characteristics of emergency action plans and alert systems, the population's perception and preparedness, and personal

characteristics of the population. In order to weigh the factors that influence each delay in warning issuance, diffusion, and mobilisation, Sorensen and Mileti (2015c) suggest ranges of weights for each of these factors. These weights are associated with the interview guide and are estimated based on the author's experience in the field. These weights are expected to account for between 25% and 50% of the variance in the curves.

In evacuation dynamics, the Greenshields, Channing and Miller (1935) traffic flow model is employed to represent the effects of traffic density and road capacity on vehicle speed. The original model has been modified to incorporate a minimum speed threshold, determined by stop-and-go conditions. For route determination during evacuation, the Dijkstra (1959) optimisation algorithm is utilised to define the shortest path between the building and the pre-defined meeting point set by the user. The quantity of vehicles is determined by the occupancy rate of these vehicles, as specified by the user. This rate is only considered for individuals evacuating in vehicles, a parameter also defined by the user. If vehicles or individuals are overtaken by flooding during evacuation, stability criteria based on Smith et al. (2017) and Shand et al. (2011) are applied, respectively. If these criteria are exceeded, the affected population is allocated to the highest-hazard flood zone; if not, they are allocated to the lowest-hazard zone.

The loss of life module involves the application of probability distributions for fatality rates to each population allocated in flood zones. These curves were initially derived by McClelland and Bowles (2002) and subsequently updated by Aboelata, Bowles and McClelland (2003) and USACE (2020) through the analysis of 54 historical cases, related mainly to dam-breach events and some other events such as dike failures, flash floods, and regional floods. These cases were subdivided into approximately 250 homogeneous regions based on event characteristics, primarily focusing on dam failure floods. The relative exceedance frequency represents the probability of experiencing a specific fatality rate. Each zone is characterised by a probabilistic distribution based on historical cases. In each iteration of the probabilistic routine, a fatality rate from the hazard functions is sampled for each specific agent (group or individual). Then, a random uniform number between 0 and 1 is assigned to each

individual. If this uniform number exceeds the sampled fatality rate, the individual survives.

The LifeSim routine involves the initial preprocessing of hydraulic data, road networks, and buildings. Hydraulic data is processed to define the flood time series for each structure and road segment. This process utilises the Ramer-Douglas-Peucker algorithm to reduce the number of data points in water depth and flow velocity hydrographs, thereby optimising computational time and memory usage. For road networks, the fastest route between each node is pre-defined using the algorithm proposed by Dijkstra (1959). In the event of traffic jams and flooding on roads, which could necessitate rerouting, the optimal path may change during the simulation. Hydraulic properties are determined at the midpoint of each road segment. Each building is associated with a road segment, and the initial fastest path between the building and an associated safe location is calculated.

The model then simulates each iteration, representing a complete simulation of the warning and evacuation dynamics and their consequences. Iterations are associated with a seed number to ensure the reproducibility of the sampling model. In each iteration, LifeSim samples uncertainty parameters, including input times and curves for the warning and evacuation module, as well as various attributes of individuals and structures. These attributes, for instance, include submergence thresholds, swimming ability, and the highest position reached within a flooded structure. With the sampling set, the dynamic simulation proceeds, and at the end, the exposure for each agent is determined (Figure 1.3). Individuals who were not sampled to receive a warning or take proactive action perform independent time vertical evacuations, relocating to the highest floor, attic, or roof of their building, depending on the sampled attributes of the building. Those who evacuate by car or on foot are subject to sampled evacuation parameters, including willingness to enter the flood and stability criteria. Once exposure conditions are defined, the fatality rate association routine is applied to determine the final condition of each individual. This process is repeated for each iteration, resulting in a probabilistic life-loss estimation.

Nowadays, two versions of LifeSim exist: HEC-LifeSim 1 and LifeSim 2. While HEC-LifeSim 1 accounts for three flood risk zones, the chance, the compromised, and the

safe zones, while LifeSim 2 simplifies this to just two zones: high and low hazard. In the development of LifeSim 2, a comprehensive review and expansion of the database originally organised by McClelland and Bowles (2002) and further refined by Aboelata, Bowles and McClelland (2003), revealed the complexities involved in identifying and characterising an intermediate flood zone (USACE, 2020).

Additionally, the criteria for allocating the population within structures in these zones have been modified. HEC-LifeSim 1 determines the allocation threshold based on flood depth relative to the building's floor. In contrast, within LifeSim 2, there are subgroups for individuals without mobility issues: those who can access the roofs of structures and those who cannot. In the former case, the threshold is defined with reference to the roof, while in the latter case, it is relative to the ceiling of the highest floor within the building. For individuals with mobility issues, the threshold is determined exclusively by the floor of the highest building level. Moreover, the threshold in LifeSim 2 is defined with uncertainty. Mobility in the LifeSim routine is quantified using percentages from the 2017 United States census, which indicate the proportion of individuals under 65 years old with ambulatory difficulty and those over 65 years old with similar issues.

Figure 1.3 – LifeSim flow logic for exposed people.

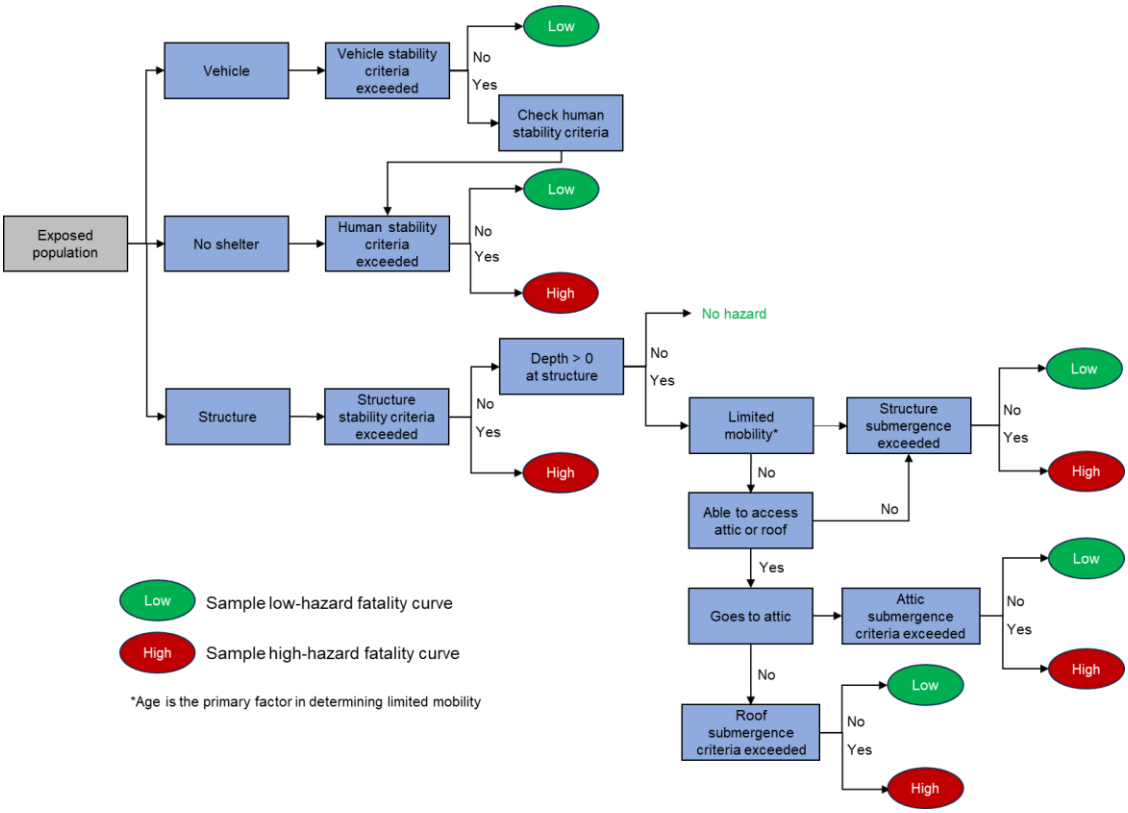

Source: Adapted from (USACE, 2021).

1.2.1.2 Applications of LifeSim in previous studies

Since LifeSim 2 is a recent model, most applications still rely on its previous version, HEC-LifeSim 1, as detailed below.

Risher et al. (2017) applied the model to validate the consequences of a flood event caused by a dike breach in Joso, Japan, in 2015. They observed a significant overestimation of fatalities by an order of magnitude due to the model's inability to accurately represent the actual number of mobilised individuals. In the simulation, only 31% to 35% of the population was accounted for, while in the actual event, it was 70%. Despite conducting tests to reduce the population mobilisation time, the results continued to reveal a limited number of individuals initiating the evacuation process. The authors identified a significant limitation of the model, specifically its capacity to represent evacuations in scenarios characterised by very short flood lead times and in contexts where strong social interactions influence individual risk perception.

Hill, Kavanagh and Lang (2018) conducted a comparative analysis of life-loss estimations using the HEC-LifeSim and Reclamation Consequence Estimating Methodology (RCEM) (USBR, 2015) models for five water reservoirs in Australia, each characterised by varying structural attributes and downstream topography. Their investigation consistently revealed that the HEC-LifeSim model produced higher median estimates of fatalities than the RCEM model under specific conditions. These conditions included scenarios with significant concentrations of at-risk populations close to the reservoir, rapid propagation of flood waves, high severity of flooding, and substantial traffic volumes. Moreover, the authors assessed the advantages of reduced warning times within the HEC-LifeSim framework, resulting in a notable reduction in the 50th percentile estimate of fatalities, from 600 to approximately 240 lives lost. The study underscored the paradoxical possibility that early warnings, in some instances, might result in higher fatalities due to population movements into the risk area during the evacuation process.

Leong-Cuzack et al. (2019) assessed the impact of an alert system by simulating various scenarios involving two water reservoirs in Australia. Their analysis encompassed hydraulic modelling scenarios under dry, rainy, and maximum operational conditions, as well as evacuation scenarios, including no warning, warning

with evacuation, and warning without evacuation. As anticipated, the authors observed a consistent trend of reduced fatalities following the implementation of an effective alert system. However, the study raised an important question regarding whether, at a certain point before the flood event, the at-risk population should remain within structures as a safer alternative to evacuation. Additionally, the authors highlighted the model's potential utility in aiding the classification of threat categories for dams under Australian legislation.

Wang (2019) analysed three case studies of water reservoirs in Australia. The impact of spatial and temporal resolution in water depth and flow velocity grids within hydraulic modelling, road network data quality, and the associated return period of hydrological events was assessed. The study found that temporal resolution exhibited greater sensitivity than spatial resolution variations, highlighting the importance of accurately representing time dynamics in hydraulic modelling. Additionally, Wang (2019) emphasised the significance of segmenting road networks into smaller sections for improved accuracy, particularly in modelling curved road segments. Furthermore, the research underscored the substantial influence of the associated return period on the sensitivity of estimates related to potential loss of life, emphasising the necessity of standardising event frequency selection and the methodology employed for generating hydrological events. These findings underscore the critical importance of considering these factors to enhance the precision and reliability of hydraulic modelling in the context of dam-breach scenarios.

Silva and Eleutério (2021) applied the HEC-LifeSim and RCEM models to analyse the dam-breach disaster at the Fundão tailings dam in Mariana, Minas Gerais, which occurred in 2015. Their findings align with prior research, as observed by Risher et al. (2017), regarding the tendency of overestimation in scenarios characterised by rapid events and high levels of population mobilisation. Similarly, their study corroborated the findings of Hill, Kavanagh and Lang (2018) concerning model comparisons. Hydraulic modelling of the dam-breach event indicated that the floodwaters reached the district of Bento Rodrigues in approximately 23 minutes. However, this timeframe proved insufficient for HEC-LifeSim to accurately represent the evacuation process. Under the most favourable conditions, considering the characterisation of warnings

and evacuations that closely mirrored the actual event, it would have necessitated approximately 49 minutes for an entire population evacuation to be achieved.

El Bilali, Tale and Bouahri (2021) tested two evacuation scenarios in a case study involving a water reservoir in Morocco. One scenario reflected the real conditions with the existing road infrastructure, while the other involved the closure and strategic redirection of specific routes. The effectiveness of the roadway management strategy was evident, leading to a reduction in estimated fatalities in the second scenario. The authors emphasised that, in both scenarios, there was a peak in the estimation of life losses during the initial three hours after the dam breach, followed by a gradual decline in subsequent iterations. This observation aligns with the findings discussed by Leong-Cuzack et al. (2019), underscoring the importance of considering the option for the population to seek refuge in buildings during specific phases of the flooding event.

Kalinina, Spada and Burgherr (2021) applied a model to a hypothetical and representative scenario in Switzerland involving a concrete water reservoir and a downstream valley. Utilising a metamodeling technique based on polynomial chaos expansion, which allows for a higher number of iterations in less time than the original model, the authors assessed the factors contributing most significantly to the variability in estimating life losses. Population parameters, fatality rates in the at-risk zone, and warning delay were identified as the primary drivers of this variability. The authors emphasised that applying the generic metamodel developed could represent a significant advancement compared to current Swiss legislation, which lacks consideration of warning and evacuation processes when evaluating the consequences of dam breaches.

El Bilali et al. (2022) proposed the consideration of hydraulic uncertainties in estimating fatalities resulting from dam breach in an urban region in Morocco. The authors applied McBreach (a tool that automatised the hydraulic model HEC-RAS) for probabilistic simulations of dam failure hydrographs. Exceedance probabilities were linked to the hydrographs through the arrangement of peak flow. Following this, distinct exceedance probabilities were chosen for hydraulic modelling and subsequent simulation in HEC-LifeSim. Finally, the estimation of fatalities was presented conditionally on the probability of flooding. The simulation results revealed an exponential trend in the

arrival time of flooding and loss of life in relation to peak flow. This suggests that using deterministic approaches and linear interpolation for scenarios not explicitly simulated could yield misleading risk interpretations.

Silva and Eleutério (2023a) applied the HEC-LifeSim model to analyse the case of the São Francisco tailing dam failure in Miraí, Brazil, which occurred in 2007. Initially, a validated hydrodynamic model was established, and the actual warning and evacuation processes within HEC-LifeSim were parameterised. The model effectively represented the success of the evacuation, resulting in zero fatalities, which aligns with the observed event. Subsequently, the authors analysed how the scenario could deteriorate under different warning and evacuation strategies. Their findings revealed that delayed warnings and unpreparedness of the population could escalate the loss of life from none, as observed in the actual event, to a maximum rate of approximately 9% of the directly exposed population.

Wang et al. (2024) examined the impacts of non-structural measures, such as disaster identification warnings, urban emergency management responses, evacuation routes, and destination selection, on life-loss estimation in the event of a potential dam breach in a water reservoir in China. Their findings highlighted that the time required for hazard identification and risk communication had the most significant impact on the overall outcome. The authors also emphasised the model's importance and usability in defining optimal evacuation routes, preventing potential road congestion, and identifying the best locations for safe destinations.

1.2.2 Flood early warning and evacuation systems

The assessment of potential life loss and the analysis of flood Early Warning and Evacuation Systems (EWESs) represent pivotal components in the comprehensive evaluation of flood risks. These analyses are essential in ensuring the integrity of critical safety infrastructure and in developing comprehensive emergency preparedness and planning strategies (GE *et al.*, 2022; JIAO; LI; MA, 2022; KULLER; SCHOENHOLZER; LIENERT, 2021). Agent-based life-loss models can be employed to systematically test and assess the efficacy of these flood EWESs by simulating a range of scenarios. Through such simulations, these models enable a detailed

assessment of system performance and its influence on reducing flood-related risks. (CHEN *et al.*, 2023).

In the context of Emergency Action Plans (EAPs) for Dams, several studies employing LifeSim have been documented to illustrate the influence of warning and evacuation systems on estimated loss of life (HILL; KAVANAGH; LANG, 2018; LEONG-CUZACK *et al.*, 2019; SILVA; ELEUTÉRIO, 2023a) and closely correspond to the first specific objective of this research. Furthermore, the study conducted by Silva and Eleutério (2023a) adopts a conceptual approach to EWES, juxtaposing historical events and evaluating the potential impact of various warning and evacuation scenarios compared to recorded fatalities.

Similarly, two additional studies have explored EWES in occurred events but utilising a different agent-based life-loss model known as the Life Safety Model (LUMBROSO; DAVISON; WETTON, 2023). In a study by Lumbroso and Davison (2018), various emergency management interventions during the 1953 flood in Canvey Island demonstrated their potential to mitigate life loss. Lumbroso et al. (2021) applied the Life Safety Model to Brazil's Brumadinho tailings dam failure in 2019. The findings from this study suggest that the loss of life in the Brumadinho incident could have been entirely prevented had an EWES been effectively implemented, with a projected alert time of 15 minutes and a well-prepared population.

1.2.3 Probabilistic dam-breach flood analysis

Considering hydraulic uncertainties in flood modelling is fundamental, as their absence can lead to inaccurate consequences, impacting the quality of risk representation and emergency planning (KHERADMAND *et al.*, 2018; MERZ *et al.*, 2024). Various uncertainties exist in dam-breach hydraulic modelling, such as topographic data (KIM; SANDERS, 2016; TSCHIEDEL; PAIVA, 2018), mathematical simplification type (MARANGOZ; ANILAN, 2022; PANDEY; KNOBLAUCH; ZENZ, 2024), model parameters such as Manning's roughness coefficient (ALMEIDA *et al.*, 2024; KALININA *et al.*, 2020; OGUZHAN; AKSOY, 2020), lack of observed data for calibration (AURELI; MARANZONI; PETACCIA, 2021), rheological models (GHAHRAMANI *et al.*, 2024; MELO; ELEUTÉRIO, 2023), dam-breach geometry (ABDEDOU; SOULAÏMANI; TCHAMEN, 2020; BELLOS *et al.*, 2020; TSAI; YEH;

HUANG, 2019), breach location (MARANZONI; D'ORIA; MAZZOLENI, 2022) and formation time (AHMADISHARAF *et al.*, 2016; BELLO *et al.*, 2022).

LifeSim does not account for hydraulic uncertainties in its flood routine module. This is mainly due to the high computational cost of Monte Carlo simulations for two-dimensional hydrodynamic modelling. An alternative approach emerges as a practical solution to reduce computational demands when controlling truncated hydraulic models, such as the HEC-RAS model (DYSARZ, 2018; HARIRI *et al.*, 2022; PHILIPPUS *et al.*, 2021; WORLEY *et al.*, 2022). This approach facilitates the derivation of weighted failure hydrographs, considering the peak flow (DA SILVA; ELEUTÉRIO, 2023; EL BILALI *et al.*, 2022; SARCHANI; KOUTROULIS, 2022).

However, certain limitations persist in this approach, particularly its failure to account for the breach hydrograph characteristics beyond the peak flow, which are fundamental in determining probabilistic scenarios of dam-breach floods, such as peak time. An alternative approach to addressing this challenge involves the use of optimised sampling methods, which streamline uncertainty analysis by reducing the number of iterations required, such as the Perturbance Moments Method (ISSERMANN; CHANG, 2020; OUBENNACEUR *et al.*, 2018; TSAI; FRANCESCHINI, 2005). In addition to these methods, this thesis explores an alternative approach involving scenario pre-selection and probability assessment (RIZZO; MARANZONI; D'ORIA, 2023).

In the methodology outlined by Rizzo, Maranzoni and D'Oria (2023), handling uncertain input parameters involves a structured discretisation procedure. Within this framework, the range of variability for these input parameters is divided into distinct classes. Thus, each class is distinguished by its uppermost value, which serves as the defining threshold for that class when constructing dam-breach scenarios. The subsequent synthesis of these scenarios relies on the intersection of conditional probabilities associated with each parameter, weighting these scenarios. The determination of probabilities within each class is informed by historical cases or fragility functions (D'ORIA; MARANZONI; MAZZOLENI, 2019). The authors implemented this methodology to assess the probabilistic flood hazard associated with a hypothetical failure of the Mignano dam. In this analysis, both breach size and water level were

considered probabilistic parameters, with the latter demonstrating a higher level of sensitivity.

1.2.4 Flood and population uncertainty into life-loss estimation

Detailed data regarding flood-related fatalities are scarce (PAPAGIANNAKI *et al.*, 2022; PETRUCCI, 2022). Consequently, the calibration and validation of these modelling typologies continue to challenge the widespread adoption of LifeSim. In order to address this issue, it is advisable to encompass all potential scenarios in a probabilistic analysis of the model's parameters.

Nevertheless, it is essential to note that the flood routine within LifeSim cannot currently be evaluated with uncertainty, despite the fact that flood modelling can significantly impact loss estimations (BRUSSEE *et al.*, 2021). The primary factor contributing to the absence of flood uncertainty in life-loss models is the substantial computational demand associated with 2D hydraulic models. Several studies have attempted to assess life loss under probabilistic flood scenarios. De Bruijn, Diermanse and Beckers (2014) introduced an innovative approach to analysing societal flood fatality risk within river deltas in the Netherlands. The authors constructed the Fatality-Probability (FN) curve, which correlates fatalities with their respective probabilities, using Jonkman, Vrijling and Vrouwenvelder (2008) life-loss model. This comprehensive analysis considered uncertainties associated with dike breach locations and evacuation parameters. Similarly, Li, Zhou and Shen (2023) applied a copula function to evaluate the joint probability of storm surge and rainfall, thereby assessing life-loss estimates in the coastal city of Macao. The authors considered eight distinct scenarios of joint probabilities and, similar to De Bruijn, Diermanse and Beckers (2014), constructed FN curves using the Jonkman, Vrijling and Vrouwenvelder (2008) life-loss model.

Maranzoni, D'Oria and Rizzo (2023b), building on the probabilistic flood hazard methodology and case study presented by Rizzo, Maranzoni and D'Oria (2023), proposed a probabilistic mapping of life loss using the empirical model developed by Sun et al. (2014). In addition to flood uncertainty, the authors also accounted for uncertainty in population distribution during business and non-business hours. By simulating 40 scenarios, comprising 20 weighted dam breach scenarios combined with two weighted population distributions, the authors illustrated the spatial distribution of

selected percentiles of loss of life, accompanied by corresponding uncertainty bounds. Peng, Zhang and Sayama (2024) evaluated the impact of varying population distributions during nighttime, commuting, and working hours. Using the Jonkman, Vrijling and Vrouwenvelder (2008) life-loss model, adapted to incorporate key stages of the evacuation process (such as warning issuance, dissemination, and mobilisation times), the authors found that the minimum required warning issuance time to reduce life loss statistically significantly was 214 minutes, 137 minutes, and zero minutes for the respective population distribution conditions.

Specifically related to the LifeSim model, El Bilali et al. (2022) conducted a flood probabilistic analysis using the McBreach tool (GOODELL *et al.*, 2019) to estimate potential life losses in an urban region in Morocco. Analysing with peak flow as the primary variable for scenario weighting can misrepresent the most extreme scenarios, thereby creating a biased perception of risk. In specific cases, the timing of the dam-breach flood's arrival or peak time can emerge as an even more pivotal factor, affording less time for population evacuation and consequently amplifying the overall risk. Additionally, this methodology has the potential for equifinality, where different combinations of breach parameters can result in the same peak flow. This can also lead to similar peak flows occurring at different peak times (DA SILVA; ELEUTÉRIO, 2023). Despite the limitations inherent in weighted scenarios, it is worth mentioning that the probability employed in El Bilali et al. (2022) could potentially be replicated to encompass a probabilistic combination of flood and LifeSim parameter uncertainties.

1.2.5 Warning and evacuation parameterisation

Characterising the delays in the timeline of the warning and evacuation process (Figure 1.2) can be challenging due to the complexity of the process and the representation of population behaviour (AERTS *et al.*, 2018; SIEGRIST; GUTSCHER, 2008). The LifeSim model relies on research that, based on historical evacuation cases, has proposed models and recommendations for estimating delays in the alert and evacuation process (SORENSEN; MILETI, 2015c, 2015d, 2015e). Depending on a specific case study, these models and recommendations may not adequately reflect the local context. Therefore, it is highly recommended to adjust the interview guide developed by Sorensen and Mileti (2015d) and the weight intervals of the questions in

this interview guide (SORENSEN; MILETI, 2015b) to ensure their appropriateness for the local context.

Several studies examining empirical data about warning and evacuation procedures in emergencies have the potential to contribute significantly to a more robust parameterisation of associated delays. Kreibich et al. (2017) assessed emergency responses, drawing from surveys conducted in the aftermath of the German floods in 2002 and 2013. Sorensen et al. (2020) refined the distribution of warning issuance times based on data collected from 20 hurricanes in the USA spanning from 1979 to 2008. Lindell et al. (2020) utilised the US hurricane database to estimate distributions related to preparation times for evacuation, while Lindell et al. (2021) focused on estimating warning diffusion time distributions using the same database for hurricanes. Cao et al. (2022) evaluated warning and public response based on 914 samples collected shortly after hazardous convective weather events in Qingdao. Thieken et al. (2023) conducted an analysis of more than 1,300 responses from an online survey on warning effectiveness in the context of the 2021 floods in Germany. Zhang et al. (2024) investigated the evacuation intentions of residents in Liulin Town, China, under various scenarios involving lead time, risk communication strategies, and mitigation measures, combining survey data collected from 250 residents with agent-based modelling. Also, utilising an agent-based approach, Siam, Lindell and Wang (2024) explored the potential of informal communication channels in disseminating warnings for a tsunami event in Indonesia. Lastly, MacPherson-Krutsky, Brand and Lindell (2025) demonstrated the effectiveness of preparedness workshops in improving the population's preparedness intentions following an earthquake in the Cascadia Subduction Zone (encompassing the United States and Canada).

While some of these studies primarily focus on hurricanes, considered slow-onset events, their methodologies are adaptable to generate valuable insights for rapid-onset events. Specifically, concerning the delay in warning dissemination, the findings from these studies, such as those by Lindell et al. (2021), may offer comparable insights across both event types. Additionally, another avenue for enhancing the parameterisation of warning and evacuation procedures involves the examination of existing alert systems through efficiency testing of sirens (BOPP; DOUVINET, 2022; DOUVINET *et al.*, 2021; SILIÉZAR *et al.*, 2022) or the utilisation of evacuation training

data (ELEUTÉRIO *et al.*, 2024). Several national legislations mandate simulation training, primarily focusing on dam-breach scenarios, and the data collected during such exercises could be leveraged to refine the warning and evacuation systems.

1.3 Methodological abstract

The thesis is structured into four discrete chapters, each associated with a specific objective. These four chapters interact with one another, as depicted in Figure 1.4, to expand the scope and deepen the understanding of life-loss modelling in floods.

Figure 1.4 – Methodology approach of each chapter and its relationship with the others.

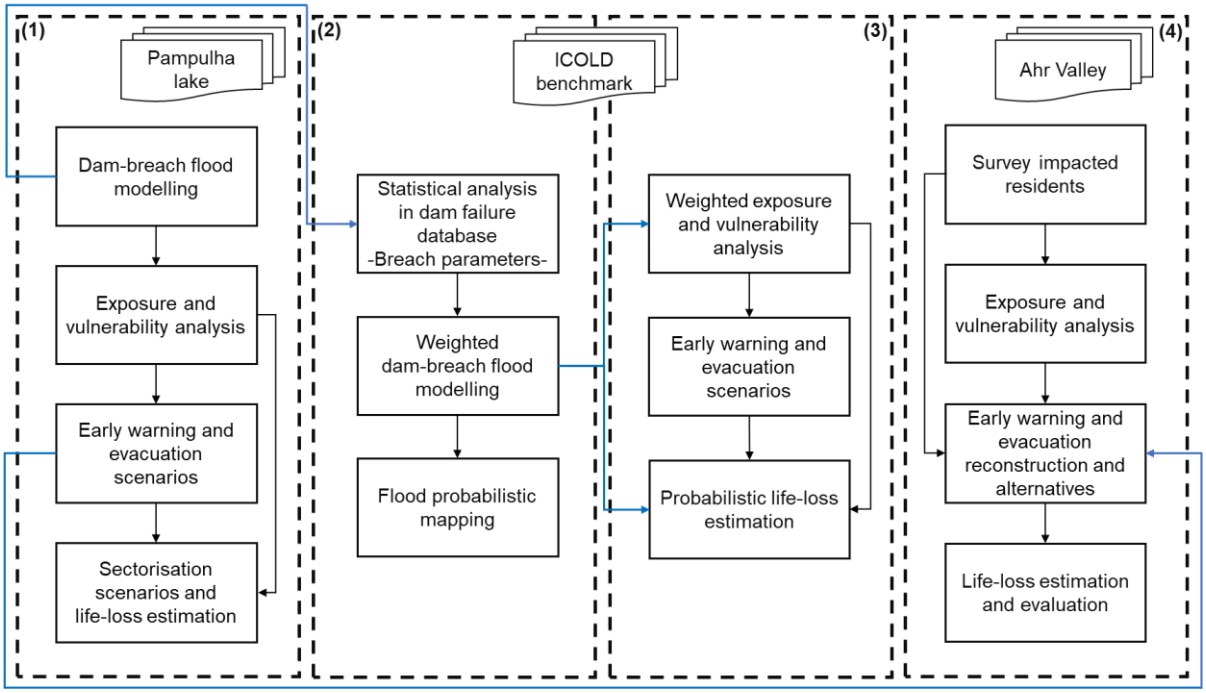

Chapter 1 introduces the use of life-loss estimation in this research by delving into the impact of flood Early Warning and Evacuation Systems (EWESs) within a densely populated urban area. Many EWES scenarios are simulated in this chapter using the agent-based LifeSim life-loss estimation model. The analysis involves an assessment of the sensitivity of LifeSim's outcomes, as well as an exploration of their temporal and spatial correlations. It is important to note that the primary purpose of LifeSim in this chapter is not to ascertain the accurate count of flood-related fatalities or evacuation times. Instead, it aims to evaluate whether different EWES scenarios have the potential to influence the magnitude of life loss, either diminishing or escalating it.

In Chapter 2, the objective is to employ a probabilistic assessment of dam-breach scenarios. This methodological approach draws inspiration from the work of Rizzo, Maranzoni and D'Oria (2023), adapting it for application to embankment dams and utilising a distinct database of dam-breach incidents (BERNARD-GARCIA; MAHDI, 2020). The critical concept here involves defining weighted dam-breach scenarios and mapping flood characteristics considering these weights. This approach is a viable alternative to mitigate the computational demands typically associated with traditional probabilistic mapping techniques such as Monte Carlo simulations. In this chapter, the case study adopted was the benchmark established by the International Commission on Large Dams (ICOLD) (ZENZ; GOLDGRUBER, 2013).

In Chapter 3, the weighted dam-breach flood scenarios developed in Chapter 2 are integrated into the life-loss estimation procedure introduced in Chapter 1. This chapter adapts the methodology of Maranzoni, D'Oria and Rizzo (2023b), substituting the empirical model with the agent-based LifeSim model. The approach improves upon the framework proposed by El Bilali et al. (2022) in integrating agent-based life-loss estimation with flood uncertainty. A significant enhancement involves including weighted scenarios that account for uncertainties related to specific breach characteristics. This approach extends beyond solely relying on simulated peak flow to assign scenario weights, as it may not fully capture critical scenarios about the time available for population evacuation. The approach also considers population distribution as an uncertain input. The case study was the same as the previous chapter, the ICOLD benchmark.

In Chapter 4, a detailed analysis of the EWES during the 2021 flash floods in Germany is conducted, focusing on the most severely affected region, the Ahr Valley in Rhineland-Palatinate. The reconstruction of the EWES relies on reports (KRON *et al.*, 2022; SZÖNYI *et al.*, 2022) and a post-event survey of flood-affected residents (SINGH *et al.*, 2025). The reconstructed EWES is compared to recommended parameterisations derived from historical cases and utilised to estimate life loss through the LifeSim model. After calibrating the model for the reconstructed scenario, alternative realistic approaches are developed, incorporating theoretical parameterisations and forecasting capabilities, and are evaluated to assess the impact of the EWES on life loss.

1.4 Thesis contributions and innovations

This thesis contributes to and introduces innovations in the following topics:

- Consideration of spatial and temporal sectorisation to evaluate the effectiveness of flood Early Warning and Evacuation Systems (EWESs) using agent-based life-loss estimation models;
- application of an already developed and tested probabilistic dam-breach flood mapping method to a different dam typology and using a different dam failure database to define probabilities;
- proposal of a new probabilistic life-loss estimation framework using the agent-based model LifeSim, integrating probabilistic flood modelling and probabilistic population distribution; and
- reconstruction of an EWES for an actual flood event based on official reports and a resident survey, and comparison of this reconstruction with theoretical EWES models in terms of life-loss estimation outcomes.

The upcoming sections pertain to the development of each thesis chapter. Although these chapters are interconnected (Figure 1.4), they were initially designed for independent publication, and some have already been published in different journals. As a result, some redundancy may be present across the chapters, including in the introduction. Additionally, there may be minor inconsistencies in terms of elements and language standards typically used in scientific journals, such as the use of the first person, variations in verb tenses, abbreviations, and figure formatting.

2 EFFECTIVENESS OF A DAM-BREACH FLOOD ALERT IN MITIGATING LIFE LOSSES: A SPATIOTEMPORAL SECTORISATION ANALYSIS IN A HIGH-DENSITY URBAN AREA IN BRAZIL[1]

2.1 Abstract

The integration of Early Warning and Evacuation Systems (EWESs) with estimations for mitigating the loss of life in flood risk assessments marks an advancement towards developing robust emergency action plans for dam breaks. Through the simulation of diverse EWES scenarios, the impact of these systems, coupled with community preparedness on minimising the potential for loss of life, could be calculated. This study was conducted in the theoretical context of a dam break located upstream from a densely populated urban region in Brazil. Hydrodynamic and agent-based models were utilised to estimate potential loss of life across various scenarios and simulations. The Monte Carlo approach, in combination with the LifeSim model, was applied to assess how factors such as warning issuance timing, evacuation strategies and community responses impact the model's outcomes. Sensitivity analysis was performed considering the overall exposed area and specific areas at risk for different spatiotemporal EWES strategies. The results of simulations highlighted the EWES' great potential for risk mitigation and displayed optimal times for warning issuance. The warning diffusion and the protective action initiation parameters proved crucial for improving EWES. The spatiotemporal sectorisation of the alert and evacuation was also an effective strategy to optimise EWES. This methodology should allow for further similar tests and incite EWES improvements based on consistent loss of life alleviation simulations.

2.2 Introduction

Dams located upstream of urban areas present a substantial risk, primarily attributed to the large volume and velocities of water in the possibility of a flood event triggered by their failure (GE *et al.*, 2020; SARCHANI; KOUTROULIS, 2022). The high level of vulnerability and exposure in urbanised downstream valleys intensifies this risk (CHAI; WU, 2023; MISHRA *et al.*, 2022; ZHENG, 2023). Loss of life (LOL) is considered the

[1] This chapter was published by (SILVA; ELEUTÉRIO, 2023b) in: SILVA, A. F. R.; ELEUTÉRIO, J. C. Effectiveness of a Dam-Breach Flood Alert in Mitigating Life Losses: A Spatiotemporal Sectorisation Analysis in a High-Density Urban Area in Brazil. Water, v. 15, n. 19, p. 3433, 2023 b. Disponível em: https://doi.org/10.3390/w15193433.

most severe consequence of floods. This consequence carries significant weight due to its objective quantifiability and crucial role in shaping public perception of disasters (JONKMAN; VAN GELDER; VRIJLING, 2003). From 1998 to 2017, among 7,000 recorded disasters worldwide, 43% were attributed to flood events. These floods resulted in damages exceeding USD 650 billion, affecting over 2 billion people and causing over 142,000 fatalities (CRED & UNISDR, 2018).

The frequency of floods is increasing on a global scale, along with the number of people affected and incurred fatalities (ZHANG *et al.*, 2021). However, the number of people impacted and fatalities per event shows a decreasing trend (HU *et al.*, 2018; MERZ *et al.*, 2021). It indicates advancements in flood risk management and assessment, which is crucial for decision-making in risk mitigation, including resource allocation for structural or non-structural measures (HAMMOND *et al.*, 2015; KREIBICH *et al.*, 2022).

Early warning and evacuation systems (EWES) are essential in minimising LOL during disasters. By providing anticipated alerts and facilitating organised evacuations, these systems play a vital role in mitigating the risk of casualties (KREIBICH; HUDSON; MERZ, 2021; THIEKEN *et al.*, 2023). Different emergency management interventions during the 1953 flood in Canvey Island demonstrated the potential to mitigate LOL (LUMBROSO; DAVISON, 2018). Studies conducted over the 2019 Brumadinho tailing dam failure in Brazil, which led to over 260 fatalities and extensive damages (ROTTA *et al.*, 2020), highlight the potential benefits of early warning systems and population preparedness. According to Lumbroso et al. (2021), loss of life could have been entirely avoided if an EWES was efficiently implemented with a projected alert time of 15 minutes and a well-prepared population. Similarly, the floods experienced in Germany in July 2021, resulting in more than 180 fatalities, underscore the importance of implementing operational forecasting models to enhance warning systems and facilitate an adequate response from the affected population (APEL; VOROGUSHYN; MERZ, 2022; THIEKEN *et al.*, 2023). In contrast, a study conducted over another tailing dam breach that occurred in Brazil in 2007 revealed that if no warning and evacuation had been implemented, fatalities would probably have been another consequence of the accident (SILVA; ELEUTÉRIO, 2023a).

Hence, LOL and EWES analyses effectively evaluate flood risks, ensure the integrity of safety structures, and facilitate comprehensive emergency planning (GE *et al.*, 2022; JIAO; LI; MA, 2022). Numerous models for estimating life losses have been developed since the 1970s (ABOELATA; BOWLES, 2005b; BROWN; GRAHAM, 1988; DEKAY; MCCLELLAND, 1993; FRIEDMAN, 1975; GE *et al.*, 2022; GRAHAM, 1999; HUANG; YU; LI, 2017; JOHNSTONE *et al.*, 2005; JONKMAN; VRIJLING; VROUWENVELDER, 2008; USBR, 2015). Generally, according to Jonkman, Vrijing and Vrouwender (2008), the estimation of life losses in these models is determined by three main factors: the number of people potentially at risk, the effectiveness of evacuation and shelter strategies to determine the number of people exposed to the event and the estimation of the exposure/fatality rate (Equation 1).

$$N = F_d(1 - F_E)N_{par} \quad (1)$$

where: N is the estimated LOL; F_d is the fatality rate; F_E is the evacuation rate; and N_{par} is the number of people at risk.

Models for estimating life losses are classified as empirical, which relates population mortality solely to event characteristics, and mechanistic (agent-based), which provides a more detailed simulation of the flood, allowing for modelling individual behaviour and causes of fatality (JONKMAN *et al.*, 2016). Empirical models are mainly suitable for preliminary and rapid estimation. Agent-based models are recommended when the simulation is conducted to support decision-making processes and assist in selecting measures to reduce flood potential impacts (ZHUO; HAN, 2020).

Among the models currently available, only Life Safety Model (JOHNSTONE *et al.*, 2005) and LifeSim (ABOELATA; BOWLES, 2005b) are built on agent-based principles, which allows for dynamic analyses. HEC-LifeSim 1.0.1 software fully incorporates the agent-based LifeSim model (USACE, 2019). This model stands out as one of the most up-to-date and comprehensive for the proposed purposes, widely used in North American consulting and insurance companies (NEEDHAM; FIELDS; LEHMAN, 2016). It has also been applied in various studies (EL BILALI *et al.*, 2022; EL BILALI; TALEB; BOUTAHRI, 2021; HILL; KAVANAGH; LANG, 2018; KALININA; SPADA; BURGHERR, 2018, 2021; LEONG-CUZACK *et al.*, 2019; SILVA; ELEUTÉRIO, 2023a;

TOMURA *et al.*, 2020; WANG, 2019) and its application is growing in different countries (Australia, Brazil, Morocco, and Switzerland).

However, it still presents some obstacles due to the need for a large quantity and quality input data (LANG, 2018). The model is structured through a modular modelling system, where modules exchange information through a database with multiple layers and tables of geographic information systems. The model has a probabilistic approach by Monte-Carlo analysis and consists of four main modules: the flood-routine module (FRM), which includes a network representing flood characteristics throughout the area and time; the shelter loss module (SLM), which simulates the exposure of individuals in buildings during each event as a result of structural damages and submersion criteria; the warning and evacuation module (WEM), which simulates the distribution and dynamics of the population at risk after the issuance of the alert; and the loss of life module (LLM), which estimates the losses through probability distributions obtained from a set of historical flood events (ABOELATA; BOWLES; MCCLELLAND, 2003; MCCLELLAND; BOWLES, 2002).

A significant advantage of applying these models, which has been little explored in the literature, is the ability to measure, in advance, the efficiency of alert and evacuation systems with different characteristics, such as the decision-making process of stakeholders involved in hazard identification and warning issuance (SORENSEN *et al.*, 2020), the mechanisms of warning dissemination and their influence (KOLL *et al.*, 2023; LINDELL *et al.*, 2021), as well as the preparedness and prior knowledge of the population regarding mobilisation and evacuation to safe places (CHEN *et al.*, 2023; LINDELL *et al.*, 2020). Spatial and temporal sectorisation of alerts and evacuations adapting the system to the specific characteristics of each sector can bring significant benefits in terms of system efficiency (ALAEDDINE *et al.*, 2015; BOPP; DOUVINET, 2022; LEE *et al.*, 2020).

Although some studies developed LOL analysis related to different EWES scenarios, the sectorisation of flood warning and evacuation throughout LOL simulation is still unexplored in literature. Besides, uncertainty analyses related to different EWES scenarios are rare (LUMBROSO *et al.*, 2021; LUMBROSO; DAVISON, 2018; SILVA; ELEUTÉRIO, 2023a). Especially for highly urbanised areas, if simultaneous alert and

evacuation procedures are deployed for significant populations, traffic problems and specific population behaviour characteristics may compromise evacuation, which cannot be appropriately analysed without a sectorisation approach. Therefore, this article aims to explore the potential for enhancing the effectiveness of alert systems through the sectorisation of alerts and evacuations based on the spatial and temporal characteristics of land use and occupancy in the downstream valley. In order to achieve this objective, the hypothetical failure of the Pampulha Lake water dam (Brazil), located upstream of a high-density urban area, is analysed for different alert and evacuation scenarios.

2.3 Case study

As a case study, it was selected the hypothetical failure of the Pampulha Lake Dam (PL.Dam) and its potential LOL for different EWES approaches in its high-density downstream valley, situated in Belo Horizonte City, State of Minas Gerais, in Brazil (Figure 2.1). The area is highly populated, accounting for around 13,381 people potentially exposed to the dam break flood risk.

The PL.Dam collapsed in 1954 because of an internal erosion (piping) caused by inadequate positioning of its drains, resulting in the gradual water flow from the reservoir over the downstream floodplain (Figure 2.2). It led to limited economic losses, once the valley had few urban developments at that time. Four years later the accident, the dam was reconstructed with new configurations of the overflow system and currently has a capacity of 20 hm³ (VIANINI NETO, 2016).

Figure 2.1 – Pampulha Lake reservoir and its dam and downstream valley location.

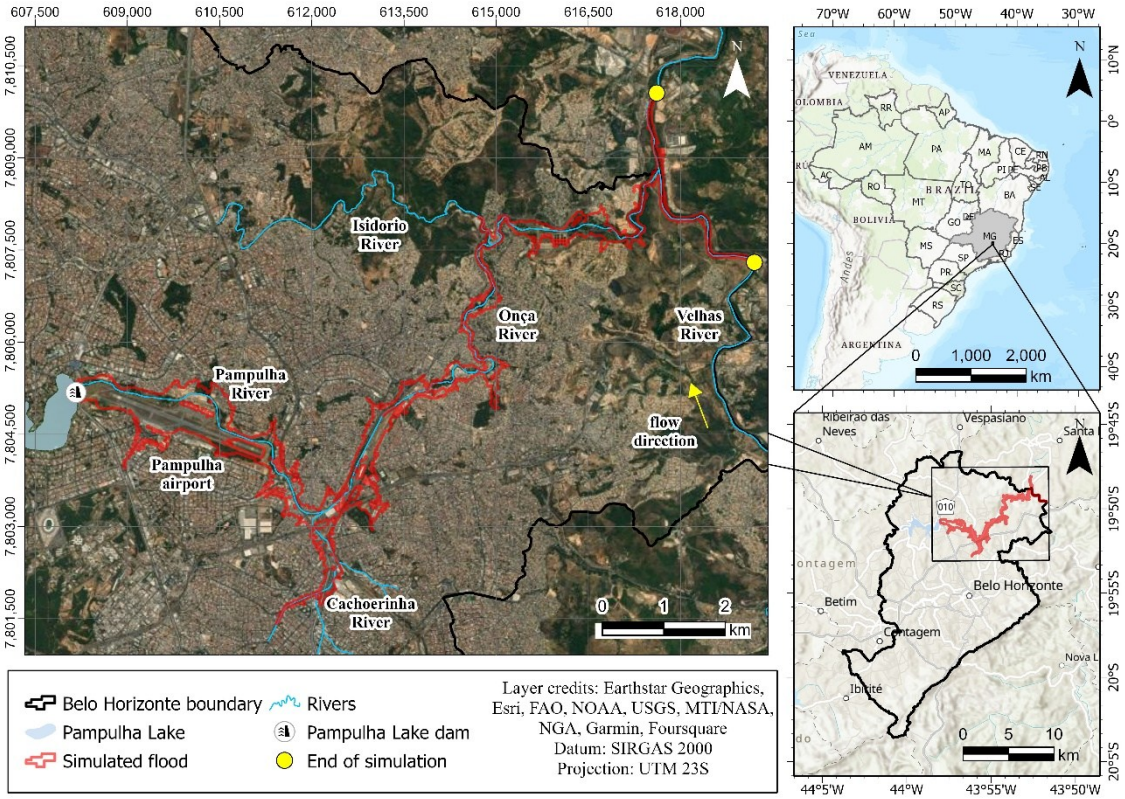

Figure 2.2 – Photos (a) before, (b) during and (c) after the 1954 Pampulha Lake dam failure.

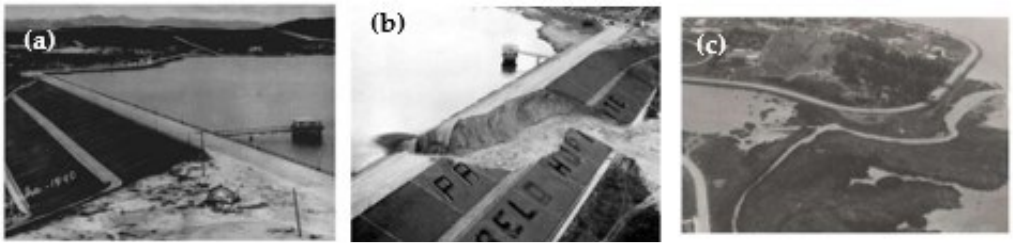

Source: Adapted from (VIANINI NETO, 2016).

A local study achieved hydrodynamic simulations aiming to represent the 1954 accident (VIANINI NETO, 2016). This study also gathered current dam information, which is more relevant for the purpose of this article. Once the conditions are entirely different, we highlight that this article does not intend to match the real flood event or its consequences, considering only the current risk situation. Currently, the dam serves the functions of sediment containment, landscape enhancement, and flood control, and the downstream valley has had a high urbanisation rate since then (Figure 2.3).

Figure 2.3 – Image of the current Pampulha Lake dam downstream valley occupation.

The maximum height of the dam is 20 metres, with a crest at an elevation of 805 metres. It has a width of 20 metres and a length of 450 metres. The spillway system consists of a linear overflow of the side channel type. Additionally, there is an auxiliary tulip overflow (VIANINI NETO, 2016). The contributing basin upstream of its reservoir spans an area of 98.3 km² (VIANINI NETO, 2016). This basin exhibits a pronounced level of urbanisation, closely accompanied by a significant presence of sanitation-related issues. These challenges, in turn, contribute to water quality degradation within the Pampulha Lake (SILVA *et al.*, 2016).

2.4 Materials and methods

In order to understand the spatiotemporal effect of alert and mobilisation, the analyses developed have two main goals: to estimate uncertainty in flood alert and mobilisation times in relation to land use, event time occurrence and anticipation; and to elucidate if alert sectorisation could improve LOL alleviation in the perspective of organising mobilisation according to spatiotemporal event characteristics. In this perspective, the HEC-LifeSim model (USACE, 2019) is used for examining the potential effectiveness of different sectorised and non-sectorised alert and evacuation systems adapted to dam failure floods.

The probabilistic and agent-based simulations in HEC-LifeSim, encompassing its four main modules (flood routine module - FRM; shelter module - SLM; warning and evacuation module - WEM; and loss of life module - LLM), adhere to the timeline for individuals exposed to the flood event (Figure 2.4). Commencing when the imminent threat is identified, the timeline encompasses the first delay associated with the necessary time to issue the warning. Subsequently, the timeline extends until the agent reaches a safe location.

Figure 2.4 – LifeSim modules and their relationship with the methodological approach.

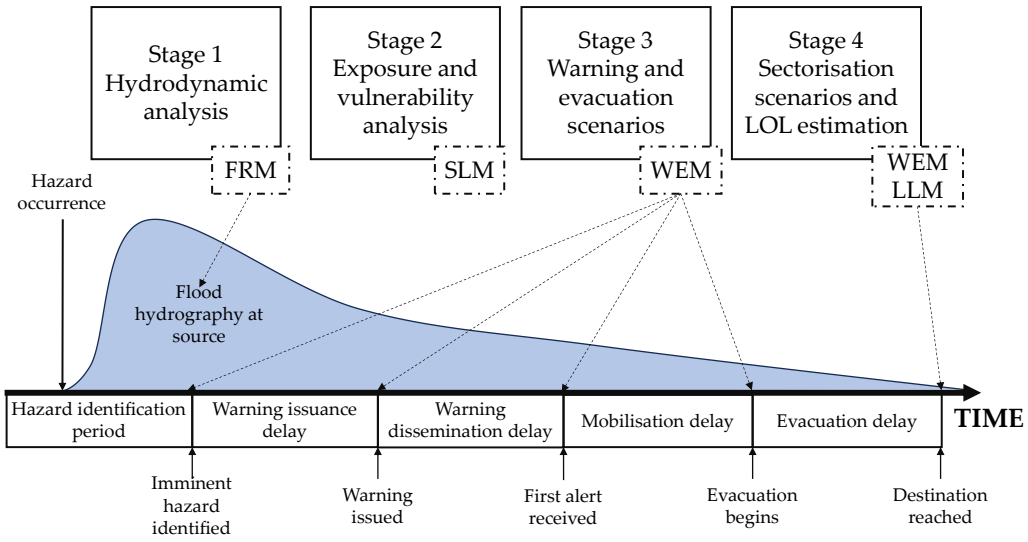

In order to achieve the goals of this article, the development of the proposed analyses is based on the implementation of the different modules of the HEC-LifeSim model, which is organised in this article into four stages (Figure 2.4): 1) Evaluation of potential flood dynamics; 2) Analysis of exposure and vulnerability in the affected area; 3) Development of alert and mobilisation scenarios in order to estimate uncertainty related to EWES; and 4) Development of specific alert and evacuation spatiotemporal scenarios based on the sectorisation of the EWES. Hence, the analysis of the effectiveness of the warning system in terms of LOL alleviation potential is achieved for the different tested scenarios.

The application of the presented methodological stages (Figure 2.4) in the PL.Dam is detailed in the following sections of this article.

2.4.1 Dynamic flood evaluation

The purpose of simulating the flood is solely to determine one specific hypothetical hazardous scenario for enabling LOL analysis and the evaluation of uncertainty and EWES efficiency under different scenarios. Therefore, the analysis of flood dynamics followed the basic premises for a deterministic dam-breach flood analysis (PSOMIADIS *et al.*, 2021).

Based on the dam description (Table 2.1), a piping breach simulation was performed to generate a flood hydrograph, according to Froehlich (2008). A sunny day scenario was considered, taking into account a trigger in the elevation corresponding to the normal operation of the reservoir. Consequently, the influence of the dam spillway system was not considered in this particular case.

Table 2.1 – Dam characteristics by Vianini Neto (2016) to obtain the breach hydrograph, applying the proposed equations of Froehlich (2008).

Parameter	Value
Crest length (m)	450
Height (m)	20
Crest levantino (m)	805
Maximum operation elevation (m)	801
Volume in maximum operation elevation (hm³)	10

The flood wave propagation through the valley was simulated by solving shallow water equations by the Eulerian-Lagrangian method implemented in HEC-RAS 6.4 model (BRUNNER, 2020), considering two-dimensional flow. The digital elevation model, with a resolution of one metre and derived from publicly accessible data (https://bhmap.pbh.gov.br, accessed on 25 July 2023), was used in the study, incorporating necessary modifications to address potential flow limitations caused by singularities. The Manning coefficient of 0.2 was applied to building areas, locations with steep slopes, and immediately downstream of the dam. In contrast, a coefficient of 0.1 was employed for the remaining areas (BRUNNER, 2020). Upstream conditions accounted for the dam-breach outflow hydrograph, while downstream conditions considered the normal depth and average flow during the wet season in the Velhas River (Figure 2.1).

The downstream section of the PL.Dam covered approximately 16.7 kilometres, following the course of the Pampulha River until its confluence with the Onça River, which flows into the Velhas River, marking the municipal boundary of Belo Horizonte

(Figure 2.1). The maximum depths and velocities and the flood wave arrival times are shown in Figure 2.5 and summarised in Table 2.2.

Figure 2.5 – Maximum depths (a) and velocities (b) and arrival time cross-sections for each 30 minutes.

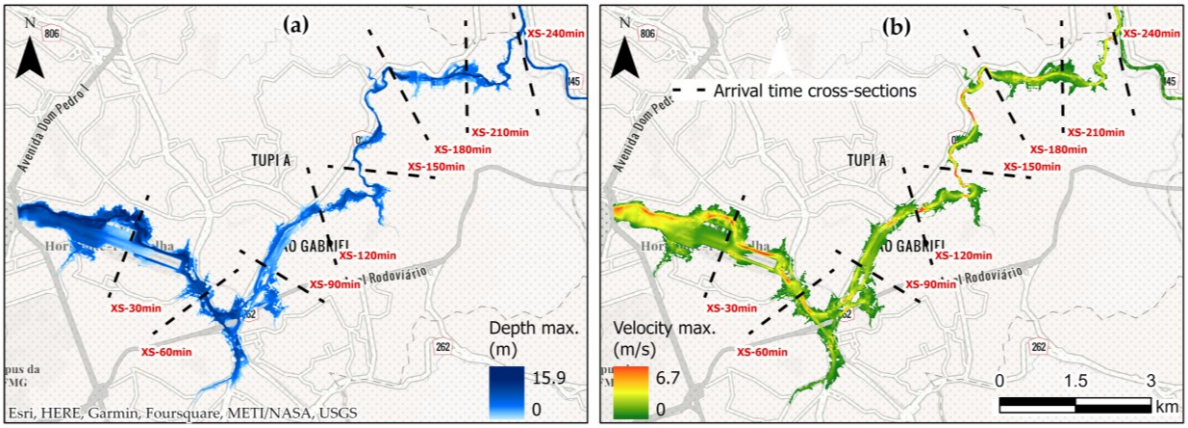

Table 2.2 – Summarised results of the dam-breach simulation in each arrival time cross-section.

Cross-section	Average maximum depth (m)	Average maximum velocity (m/s)
XS-30min	4.8	1.0
XS-60min	3.9	0.9
XS-90min	2.4	0.9
XS-120min	2.8	1.2
XS-150min	4.6	2.9
XS-180min	4.1	1.3
XS-210min	4.0	0.5
XS-240min	4.8	0.9

This flood scenario was the input for the HEC-LieSim flood-routine module (FRM), according to (Figure 2.4), bringing all the required details concerning the flood hydrodynamics through the downstream valley, allowing the computation of flood depths, velocities and flood wave arrival times over the floodplain and the different elements at risk.

2.4.2 Exposure and vulnerability analysis of the valley

Population exposure mapping is essential for characterising elements at risk in areas potentially impacted by flood events (MERZ *et al.*, 2010). Microscale analysis is required to optimise investments by evaluating the cost-benefit ratio of structural and non-structural measures to reduce the risk (MOEL *et al.*, 2015), analysing loss of life, the efficiency of warning systems, and population evacuation (DI MAURO; DE BRUIJN; MELONI, 2012). The LifeSim simulations are based on microscale data.

Exposure and vulnerability analysis was done in order to fulfil the LifeSim Shelter Loss Model (SLM) data input requirements. This analysis involves the representation of buildings as points, wherein information about the structures, such as the number of stories, occupancy type, and construction material, is considered. Additionally, the model requires data regarding the population in these buildings during daytime and nighttime and their mobility patterns. However, a significant challenge lies in acquiring the requisite high-resolution data (PAPROTNY; MENGEL, 2023) to represent the SLM accurately.

Based on the more recent available census data, public municipality layers, and a buffer of 100 metres in the inundation boundary, 38,002 buildings with populations of 101,865 and 106,520 individuals were estimated during daytime and nighttime, respectively. It was observed that approximately 7.5% of the total population in both periods consisted of individuals aged 65 years or older, which was considered as a factor representing the population's mobility characteristics. Besides residential places, the authors considered public places such as schools, hospitals, and companies and population allocation based on census data about work and education characteristics.

It is crucial to acknowledge that the primary focus of this study, as stated in the dynamic flood simulation section, is not to tackle or elucidate the uncertainties related to the analysis of exposure and vulnerability. Instead, the purpose of conducting exposure and vulnerability analysis is solely to parameterise the SLM in order to facilitate LOL analysis and evaluate uncertainty and efficiency within the context of EWES under various scenarios. The estimated population was aggregated within a statistical grid, a geographic unit derived from Brazilian census data with a spatial resolution of 200 x 200 metres, corresponding to a daytime period used in this study (Figure 2.6).

Based on the direct exposure of the population revealed by overlaying the generated exposure maps and the inundation boundary, it is estimated that a daytime rupture event can directly impact a population of 13,381 people. The total number of exposed buildings reaches 4,417, with 3,820 buildings classified as residential, 587 as commercial, and ten public places.

Figure 2.6 – Downstream exposure and vulnerability analysis and the inundation boundary.

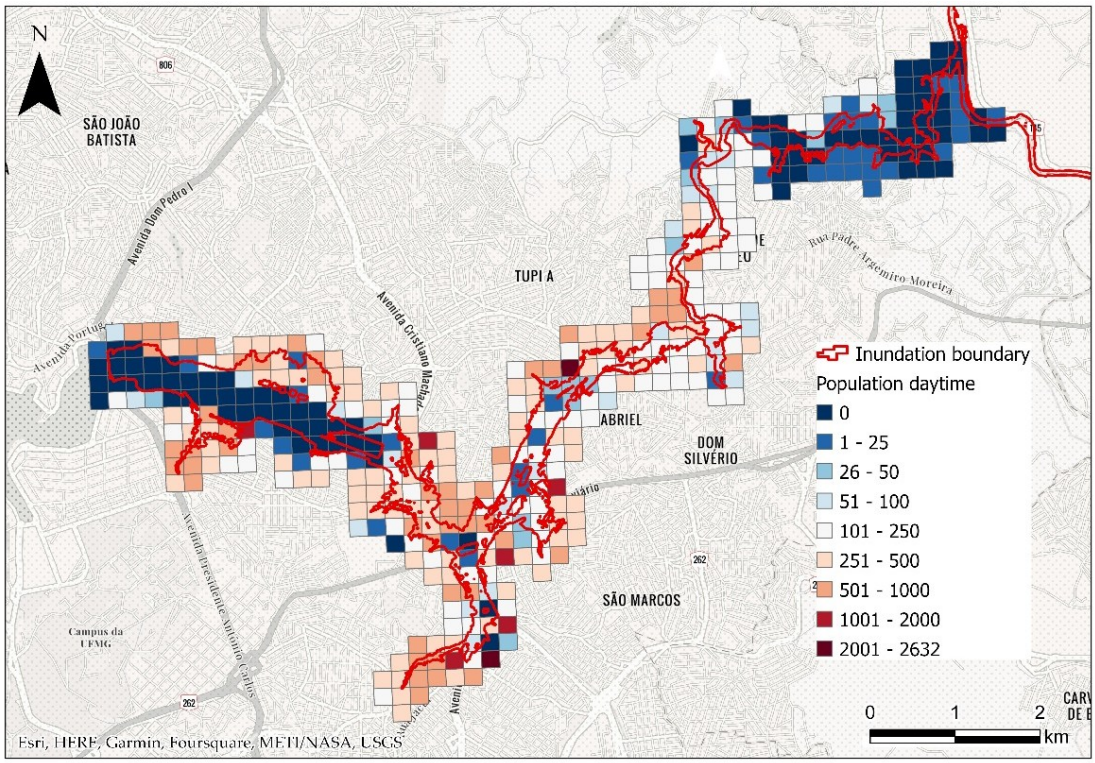

2.4.3 Warning and evacuation scenarios

The timeline depicting the warning and evacuation process is represented in LifeSim under the flood hydrograph in Figure 2.4. The timeline commences with hazard identification and encompasses subsequent stages, including warning issuance, warning dissemination, mobilisation, and evacuation delays, ending when the agent reaches the designated destination.

For the delay in issuing the warning, which is defined as the time from when the managers receive the notification of the imminent hazard to the issuance of an evacuation order to the public, Sorensen and Mileti (2015d) highlight the scarcity of studies on the time it takes to decide to issue an alert. Most of the research conducted over this topic is related to chemical emergencies. However, since many chemical accidents involve fast-moving events that require quick decisions and have a potential for fatalities, the results are relevant to other dangerous situations, such as dam failures. Based on the analysis of these historical cases, Sorensen and Mileti (2015d) present Equation 2 to represent warning issuing delay.

$$p = 1 - e^{(-at^b)} \quad (2)$$

where: p is the probability of delay in the decision; t is the time [min]; and a and b are coefficients specific for adjusting empirical data.

For the delay in warning dissemination, which is the period between the issuance of the warning and when it is received by the population at risk, Sorensen and Mileti (2015c) consider two main factors: the sending of the first alert, which covers the use of technologies, dissemination channels, and repetition of the alert; and the receipt of the first alert, which involves population and event characteristics that influence the alert diffusion process. The authors discuss a specific model of first alert diffusion. Variables that influence it are highlighted, such as direct alert, which is the alert directly received through a communication channel, and indirect alert, which is the alert received through informal messages from friends, neighbours, colleagues, and relatives. Thus, based on the analysis of historical cases of floods, volcanic eruptions, and chemical accidents with a high variability of alert diffusion time, Sorensen and Mileti (2015c) present the following Equation (3).

$$^{\Delta W}/_{\Delta t} = Pu_t * (b_t + c_t - b_t * c_t) \quad (3)$$

where: W is the alerted population; $\frac{\Delta W}{\Delta t}$ is the rate of the alerted population at the time t; Pu_t is the population that has not been warned at the time t; b_t is the coefficient related to the effectiveness of the direct alert system at time t; and c_t is the coefficient associated with the effectiveness of the indirect alert at time t.

For the delay in the initiation of mobilisation, which is the time it takes for the population to take a protective measure after receiving the alert, Sorensen and Mileti (2015e), through the analysis of mobilisation in historical cases of hurricanes, floods, and material accidents, developed a model relating the population's response to the mobilisation speed and the average time for the initiation of mobilisation, as presented below (Equation 4).

$$P_{t_h} = 1 - e^{(-(t_h{}^2)/a_m b_m{}^2)} \quad (4)$$

where: P_{t_h} is the cumulative probability of being mobilised at time t_h; t_h is the time [h]; a_m is the coefficient related to the mobilisation speed; and b_m is the coefficient related to the average time for mobilisation.

Each equation presented above is accompanied by coefficients that depend on population characteristics, the issued alert, and the event under consideration. HEC-LifeSim v 1.0.1 already incorporates the recommended values for these coefficients with an uncertainty range into the warning and evacuation module (WEM). However, it is also possible to define specific coefficients for a particular case and construct customised curves based on them (NEEDHAM *et al.*, 2016).

Regarding evacuation delay, the Greenshields, Channing and Miller (1935) transportation model is used to represent the effects of traffic density and road capacity on vehicle speed. These aspects are quite relevant in the valley downstream of the PL.Dam, where the evacuation process encompasses over 13,000 people. The interaction of these aspects can significantly decrease the speed at which vehicles can reach designated safe areas.

The number of vehicles is obtained by the occupancy rate determined by the user. This rate is only considered for people evacuating in vehicles, a parameter also defined by the user. In order to determine evacuation routes, the Dijkstra's optimisation algorithm (DIJKSTRA, 1959) is employed to identify the path (imported by the OpenStreetMap database) with the shortest time between the building and the corresponding destination.

In this work, Monte Carlo simulations were conducted to analyse the warning and evacuation processes in two parts. The first part involved a sufficiently long interval in representing the time between the hazard identification and the warning issuance, ranging from 0 to 24 hours, starting at the onset of the rupture and characterised by uniform uncertainty. This interval was used to evaluate the optimal response time for the emergency managers. The second part of the analysis focused on the influence of uncertainty in the recommended values of warning dissemination delay and mobilisation time proposed by Sorensen and Mileti (2015c, 2015e). We examined two types of parameterisation — the first type involved fast warning dissemination and a population with high perception and preparedness for mobilisation. The second type consisted of the same warning dissemination rate, but with a population with low levels of perception and preparedness (Figure 2.7). Only the mobilisation pattern was varied

because this aspect has more impact on time and the evacuated percentage of the population achieved than warning dissemination times.

Before these analyses, tests were conducted to assess the evacuation mode (50% on foot and 50% using vehicles, as well as 100% on foot) to identify routes to avoid and the safest evacuation points. The goal was to optimise the evacuation process, whether on foot or using vehicles. However, the results were not highly sensitive to changes in this parameter. Since the region of interest had a significant population, evacuating by vehicles, although it could promote fast displacements, could be limited due to traffic congestion. In contrast, congestion does not affect pedestrian evacuation but may lead to slower speeds than vehicle evacuation in certain situations. Based on these preliminary tests, the 50%/50% on foot and by vehicle evacuation mode was adopted for all the simulations.

Figure 2.7 – Two parts of analysis in the warning and evacuation process and their values: (a) between the hazard identification and the warning issuance; and uncertainties in the recommended values of warning dissemination delay and mobilisation time proposed by Sorensen and Mileti (2015c, 2015e), considering (b) fast warning dissemination and high perception and preparedness of the population and fast warning dissemination and (c) low perception and preparedness of the population.

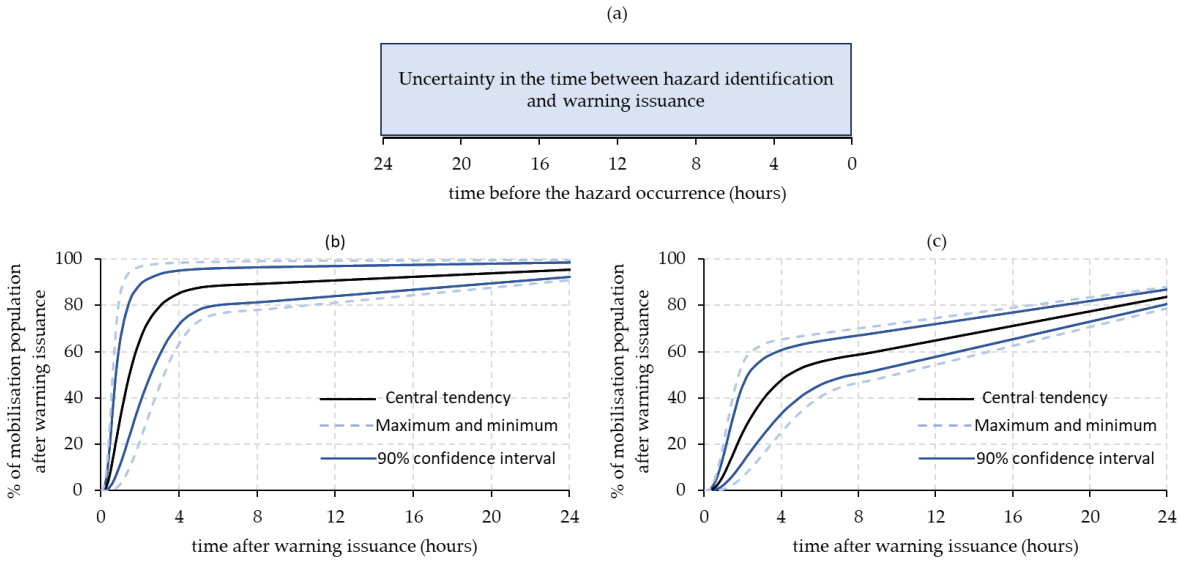

2.4.4 Sectorisation scenarios and LOL estimation

Partitioning the downstream valley into distinct sectors and assessing their outcomes using EWES and LOL simulations allows for identifying unique characteristics and proposing specific actions for each sector. In this study, we choose to evaluate sectors based on local conditions and using the distance of approximately 2 kilometres along

the flow path of the flood wave to determine the sector's limits. This discretisation aligns spatially with the arrival time cross-sections, delineated every 30 minutes. A total of eight sectors were analysed. Among these sectors, the first three exhibited the highest concentration of population and buildings directly impacted by flooding (Figure 2.8).

In HEC-LifeSim, the loss of life module (LLM) involves the application of probability distributions for fatality rates derived from the research conducted by McClelland and Bowles (2002) and subsequently updated by Aboelata, Bowles and McClelland (2003). The updates were based on the analysis of 54 historical cases, further subdivided into approximately 250 homogeneous regions based on event characteristics. The majority of these cases pertained to floods resulting from dam failures.

The LLM involves three distinct curves corresponding to different flood risk zones: the chance zone, which encompasses an area with a high probability of LOL; the compromised zone, representing an area with a moderate probability of LOL; and the safe zone, defining an area with a very low probability of LOL. To determine the risk zone allocation for an agent or groups of agents affected by the flood while inside a building, a submergence threshold is employed, considering the mobility of each agent. If the floodwater surpasses this threshold, the affected agents are allocated to the respective risk zone based on this threshold. When the flood reaches vehicles or agents during the evacuation process, the stability criteria indicated by USACE (2019) are applied. If the floodwater exceeds these criteria, the affected agents are allocated to the chance zone. Conversely, if the stability criteria are not exceeded, the affected agents are assigned to the safe zone.

A recent version, LifeSim v.2.0, has been implemented (USACE, 2023). The Loss of Life Module (LLM) in this new version considers two flood zones: high hazard and low hazard. During the development process, the developed team encountered challenges in identifying and characterising an intermediate flood zone. To address this, they conducted a comprehensive review and expansion of the existing database compiled from the studies conducted by McClelland and Bowles (2002) and Aboelata, Bowles and McClelland (2003). Nevertheless, specific issues were identified in the 2.0 version and reported to the Risk Management Center of the U.S. Army Corps of Engineers. Therefore, the more reliable HEC-LifeSim v.1.0.1 was used for the tests. With some

modifications implemented in the LLM in order to bring it closer to the latest version; the probability distribution curves of fatality rates for high-hazard and low-hazard zones were considered in the model, in which the high-hazard zone combines the chance and the compromised zones, while the low-hazard zone comprises the safe zone.

Ten thousand simulations were conducted using HEC-LifeSim v.1.0.1 to account for uncertainties. These uncertainties encompassed a range of values defined in the Warning and Evacuation Module (WEM) and the application of fatality rate distributions derived from the LLM. The evacuation routes were established utilising road data obtained from OpenStreetMap. Safe destinations were determined based on local plans (Figure 2.8).

Figure 2.8 – Sectors, their number of buildings and population directly impacted by the flood, and the roads and destinations used in EWES and LOL evaluation.

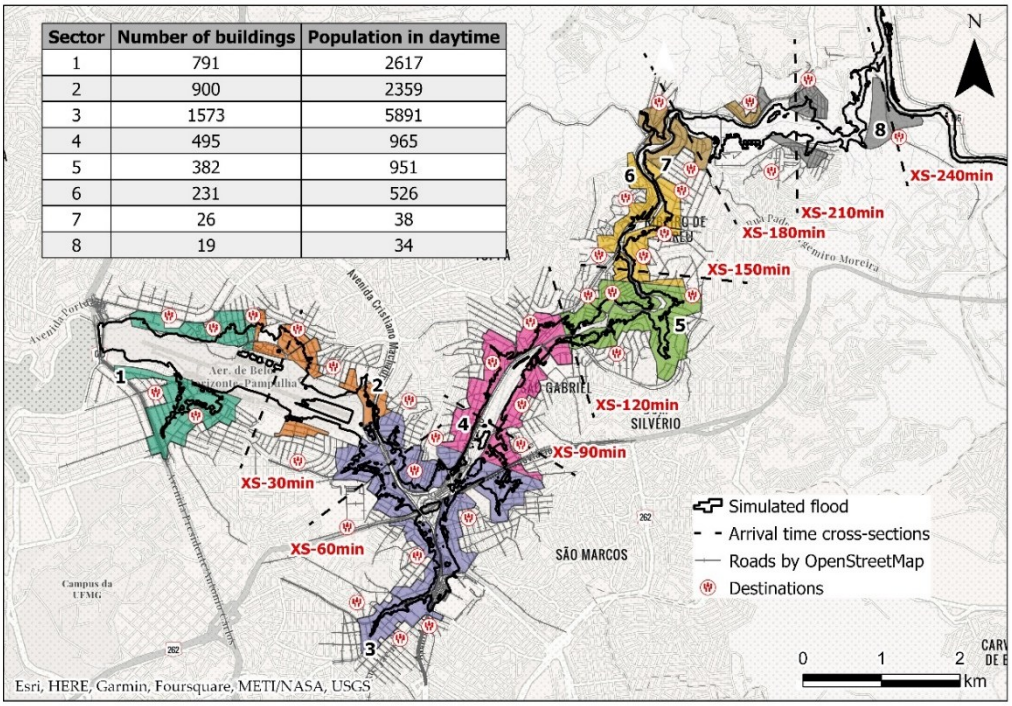

2.5 Results and discussion

An apparent effect can be observed in the potential reduction of fatalities by increasing the alert systems and on-site mobilisation capacity, facilitating a more efficient evacuation in an emergency (Figure 2.9 and Figure 2.10).

Figure 2.9 – Fatality rates for high mobilisation scenario summarised by sector and general estimation.

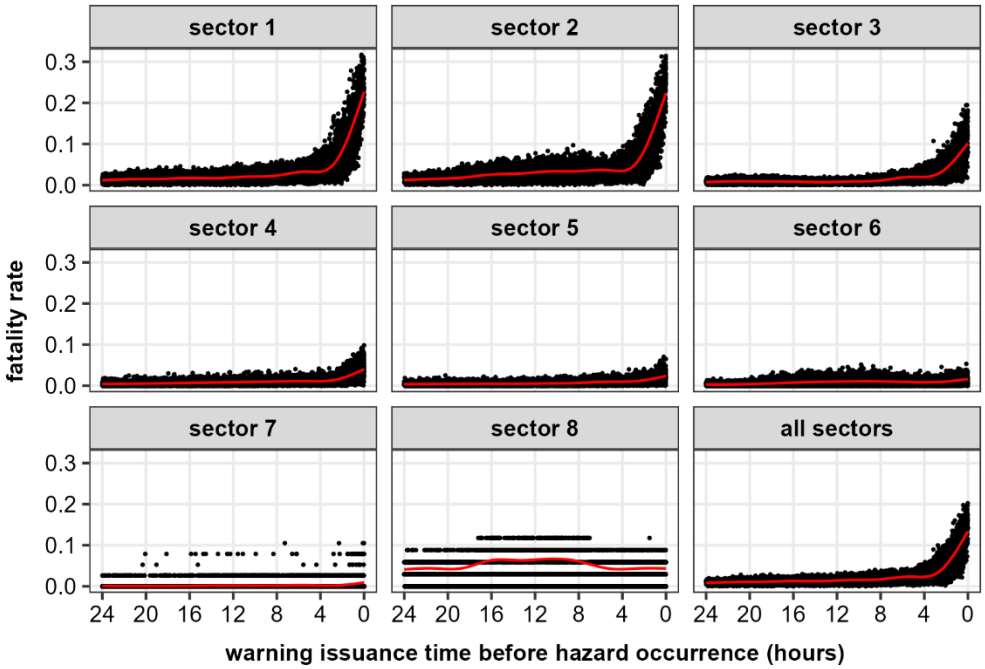

Figure 2.10 – Fatality rates for low mobilisation scenario summarised by sector and general estimation.

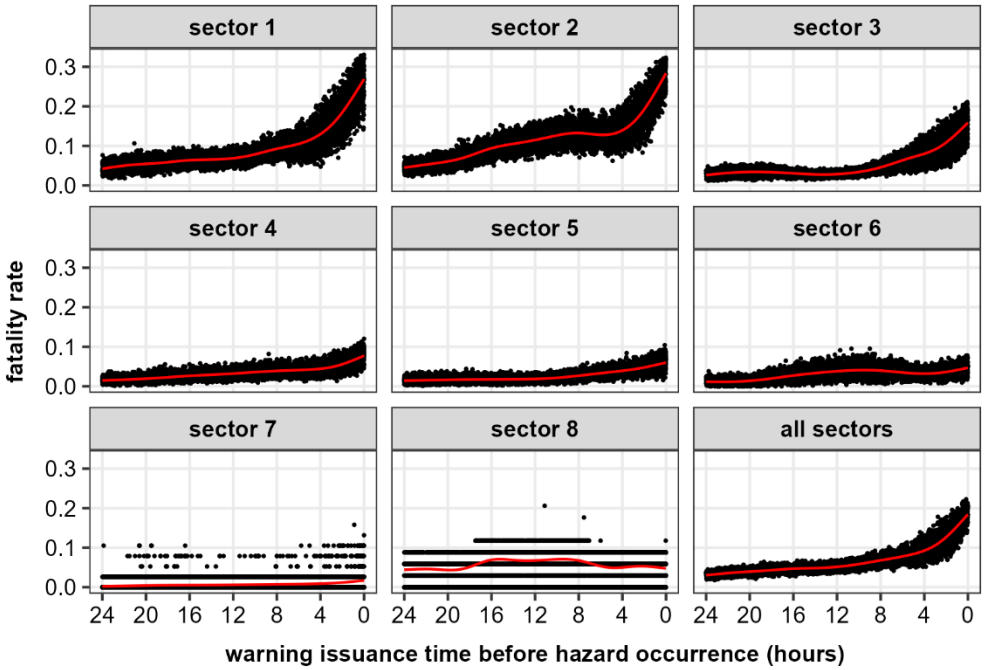

The first three sectors exhibit the highest sensitivity in terms of fatality rates. In cases of high mobilisation, there is an observed trend towards optimising the desired scenario of issuing warnings four hours before the occurrence of the hazard (Figure 2.9). However, in cases of low mobilisation, such a favourable scenario is not observed, as

the likelihood of LOL rates exceeding 0.1 remains prevalent even when alerts are issued up to 12 hours before the dam-breach event, specifically for sectors 1 and 2 (Figure 2.10).

The influence of the warning and evacuation module (WEM) in LOL on the other sectors is comparatively less pronounced compared to the three initial sectors. This observation can be attributed to two primary factors. First, the relatively lower hazard posed by the flood in this area might contribute to a diminished impact on the other sectors. Second, the arrival time of the floodwater, which is around 90 minutes in sector 4, could also permit a longer time for the population reaches safe places. In the last two sectors, the LOL does not demonstrate any apparent relationship with both warning issuance and mobilisation times.

The exclusive impact of mobilisation can be assessed by examining the range of LOL rates estimates for the same time of warning issuance. This range is observed to be wider when the warning is issued closer to the hazard occurrence. It implies that even in an optimal mobilisation scenario, a delay in issuing the warning has a more pronounced impact on the estimation of LOL.

Upon comparing the quantiles of high preparedness and mobilisation (Table 2.3), a significant impact of this delay on the warning and evacuation timeline becomes evident. The median of the low mobilisation scenario is observed to exceed the 0.9 quantile of the high mobilisation scenario. Thus, determining the appropriate curve or range of curves of a specific case study to employ in the LifeSim model becomes an essential step to LOL evaluation. Moreover, the improvement of mobilisation could significantly impact mitigating LOL.

Depending on the specific case study, the pattern curves in the WEM of LifeSim may not accurately represent the local context. Therefore, it is recommended to adjust the definition of the curve locally using equations 2, 3, and 4, along with additional studies on the definition of coefficient equations (SORENSEN; MILETI, 2015b, 2015a). These adjustments can ensure the appropriate application of the curves to the local conditions.

Table 2.3 – Quantiles of LOL for each scenario of mobilisation by sector and general simulation.

Sector	High mobilisation							Low mobilisation						
	0.05	0.25	0.50	0.75	0.90	0.95	0.99	0.05	0.25	0.50	0.75	0.90	0.95	0.99
1	13	33	53	83	176	345	638	106	150	189	276	450	578	738
2	16	38	64	102	165	304	574	108	175	258	327	433	542	692
3	16	38	61	98	200	341	700	128	171	214	347	609	774	1024
4	0	4	7	13	19	26	49	11	21	30	42	54	65	86
5	0	2	5	9	14	18	32	9	15	21	31	44	53	68
6	0	1	3	6	10	12	17	4	9	15	21	26	29	35
7	0	0	0	0	0	1	1	0	0	0	0	1	1	3
8	0	1	2	3	3	3	4	0	1	2	3	3	4	4
All	59	129	197	304	570	1032	1950	416	563	713	1037	1613	2023	2499

In order to examine a more specific influence of mobilisation on estimating LOL, two predetermined instances of warning issuance time were established and simulated. These simulations were designed to evaluate the effects of mobilisation in isolation. In this analysis, the focus was to evaluate the potential gains related to high levels of mobilisation. Values closer to one indicate a more optimised mobilisation, as depicted in the sampled curve of Figure 2.7b. Conversely, values closer to zero signify a less favourable scenario.

It is worth noting that when the warning is issued at the moment of the dam-breach event, the impact of mobilisation does not exhibit a clear trend (Figure 2.11), mainly in the first two sectors, compared to when the warning is issued four hours before the occurrence of the hazard (Figure 2.12).

Even under optimal preparedness and awareness among the population, there is insufficient time to observe a substantial impact on the evaluation of LOL for the first two sectors. However, in the simulation focused on the critical time of four hours, the mobilisation primarily affects these regions.

Figure 2.11 – Fatality rates for high mobilisation scenario summarised by sector when the warning is issued at the moment of dam breach.

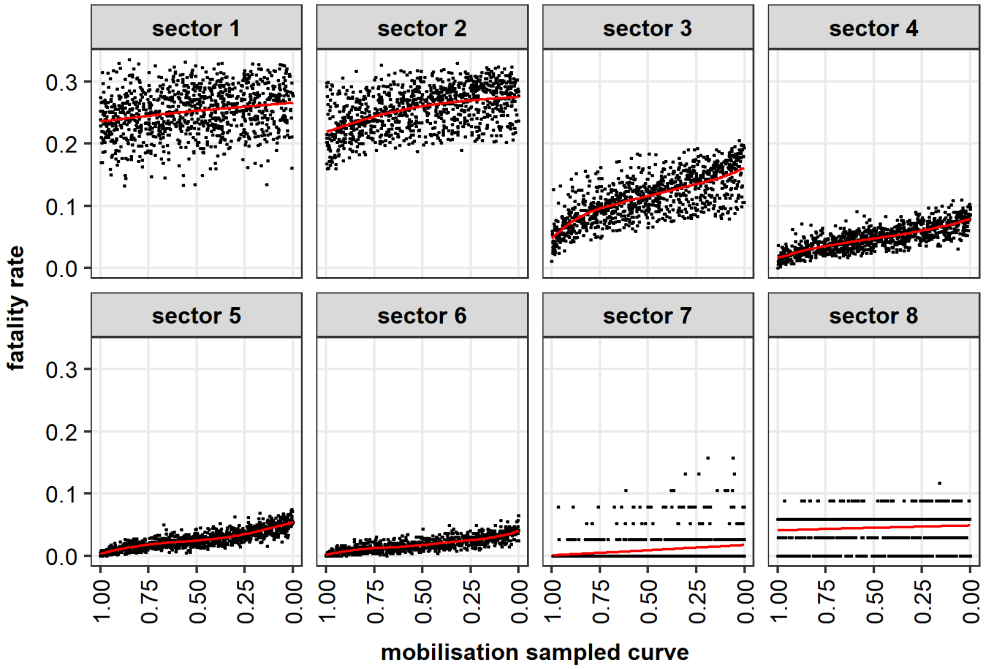

Figure 2.12 – Fatality rates for high mobilisation scenario summarised by sector when the warning is issued four hours before dam breach.

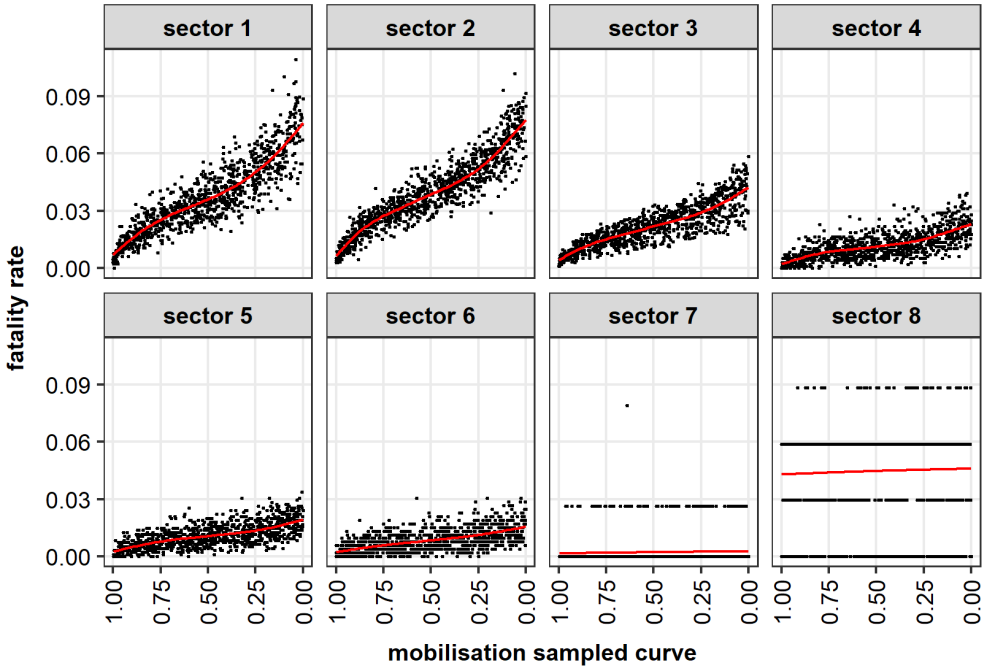

In high mobilisation scenarios, it is concluded that a minimum of four hours was required for anticipated warning issuance for significant alleviation of LOL (Figure 2.9). Three scenarios of sectored downstream areas were analysed to assess if this four-hour timeframe represents an optimal event anticipation and to evaluate the impact of spatial and temporal sectorisation (Figure 2.13). These scenarios involved varying the

time of anticipated warning issuance, ranging from the moment of hazard occurrence to four hours, four to eight hours, and eight to twelve hours. These sectored downstream scenarios were compared to a reference scenario of four-hour fixed warning issuance in a non-sectored downstream valley, with the results summarised within the respective sectors. To isolate the specific impact of warning issuance, the dissemination of this issuance and the mobilisation of the population were set without uncertainty, considering the median curve presented in Figure 2.7b.

Figure 2.13 – Comparison between a non-sectored simulation, where a fixed warning was issued four hours prior to the occurrence of the hazard, and sectored simulations with warnings issued within different time ranges: (a) at the moment of a dam breach and four hours, (b) between four and eight hours, and (c) between eight and 12 hours.

(a) sectored warning issued between the moment and four hours before the dam breach.

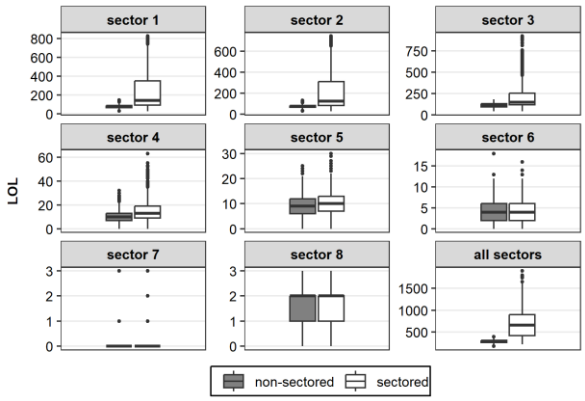

(b) sectored warning issued between four and eight hours before the dam breach.

(c) sectored warning issued between eight and 12 hours before the dam breach.

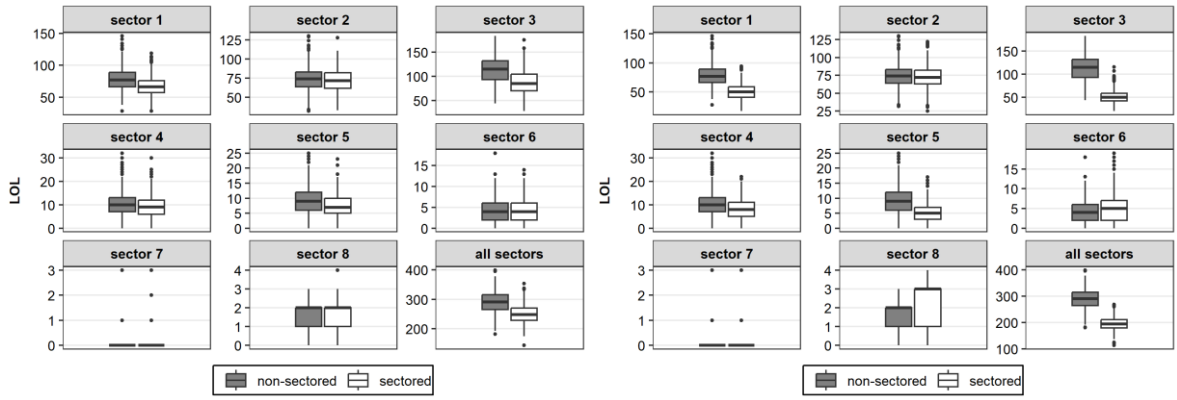

The first four hours (Figure 2.13a) reveal a notable sensitivity in estimating the LOL, particularly within the first three sectors. However, this sensitivity diminishes between four and eight hours (Figure 2.13b), with a minor difference of two fatalities simulated in the second sector. A slight decrease in the mean values of LOL from eight to twelve

hours is also evident (Figure 2.13c), except for the third one, where the mean value experiences a reduction of over 40%.

It suggests that having prior knowledge limited to four hours may not be an optimal scenario for reducing the LOL in the third sector. While the other sectors exhibit stabilisation or only a slight difference in the absolute values of the median after the initial four hours, the LOL in the third sector continues to show significant changes, as a function of their specific vulnerability, exposure, and hydrodynamic characteristics.

It is crucial to maintain awareness, that although the design of an efficient EWES and the strategic implementation of sectorisation can unquestionably result in a notable decrease in the LOL, the perceptions and patterns exposed in this paper can be specific to the actual case study. In other cases, the results may vary. Several studies have unveiled a noticeable trend regarding mitigating LOL in EWES scenarios with different magnitudes. However, it was noticed that during critical junctures, mainly when an imminent hazard is near, the optimal course of action for the population might involve seeking shelter within buildings. This recommendation is based on observations that, during such moments, a significant influx of vehicles can reduce the road capacity, consequently elevating the LOL (EL BILALI; TALEB; BOUTAHRI, 2021; HILL; KAVANAGH; LANG, 2018; LEONG-CUZACK *et al.*, 2019).

The results and specificities of the study underline the importance of LOL simulations in obtaining a deeper understanding of the functioning of the EWES implemented or suggested. These findings and their patterns can help define alternative methods of disseminating warnings and allocating resources to increase awareness and preparedness among at-risk populations.

2.6 Conclusion

The estimation of loss of life (LOL) plays a vital role in flood emergency planning. This study assesses the impact of Early Warning and Evacuation Systems (EWESs) on the potential LOL in the hypothetical scenario of a dam breach at Pampulha Lake. Specifically, the analysis focuses on examining the impact of this event on various sectors located in a downstream valley of the dam.

The LOL estimation revealed that a minimum desirable time for issuing warnings before the hazardous event was four hours, particularly in a scenario with high population mobilisation. Furthermore, it was revealed that the level of preparedness and perception of mobilisation, especially in the initial three sectors, significantly influenced the mitigation of LOL.

2.7 Further research

The proposed sectorisation approach was crucial for understanding the effectiveness of dam-breach flood alerts in mitigating loss of life. It revealed that the effect of different warning and evacuation strategies might influence the areas at risk differently, according to their vulnerability, exposure and the hazard and EWES spatiotemporal characteristics. Therefore, it is recommended that similar approaches be used in other case studies when evaluating EWES effectiveness, especially in high-density population areas.

Furthermore, the estimation inputs for LOL calculations involve several uncertainties. A dam-breach flood event exhibits significant variability due to uncertainties associated with dam-breach parameters (BELLO *et al.*, 2022; RIZZO; MARANZONI; D'ORIA, 2023). Acquiring data for exposure and vulnerability analysis at the microscale, particularly in this case, poses challenges, necessitating the consideration of various hypotheses regarding the transfer of characteristics from another scale to the microscale (PAPROTNY; MENGEL, 2023). Furthermore, relying solely on a sample of historical events to characterise the warning and evacuation processes may not adequately represent the specific circumstances of a region in different contexts from those used in the analysis. In this study, our primary objective was to analyse the impact of LOL alleviation. Further research could consider and discuss these cited sources of uncertainties in the estimation model aiming to enhance understanding of these uncertainties.

3 ENHANCING THE RELIABILITY OF FLOOD HAZARD MAPPING FOR EMBANKMENT DAM-BREACH EVENTS USING PROBABILISTIC SCENARIO SIMULATIONS

3.1 Abstract

The utilisation of high-resolution dam-breach flood mapping is fundamental for effective emergency action planning. Many countries have implemented dam safety regulations that require the use of such mapping detail. However, the accuracy of flood models is often challenged by various sources of uncertainty, which must be considered in dam-breach flood modelling. Traditional methods, such as Monte Carlo simulations, can help address these uncertainties; however, they typically require significant computational resources. This study employs a computationally more efficient approach to flood dam-breach probabilistic modelling, which involves weighting representative scenarios derived from historical dam failure data, followed by probabilistic mapping of critical flood variables, including inundation boundaries, flood hazards, and arrival times. In contrast to the original application, which considers a concrete dam-breach process, we apply this methodology to an embankment dam, incorporating uncertain parameters of breach top width and formation time, and utilising a different dam failure database for the analysis. The results reveal significant variability across simulated scenarios, particularly regarding the dam-breach hydrograph. The deterministic analysis, relying on traditional equations to estimate dam-breach parameters, produces inundation boundaries covering areas with occurrence probabilities exceeding 0.4. Additionally, the deterministic approach closely matches the flood hazard classification derived from the most probable outcomes of the probabilistic approach and predicts a shorter flood arrival time. The probabilistic mapping framework applied in this study provides a holistic view into the inherent uncertainties in dam-breach flood modelling results.

3.2 Introduction

Dams have played a significant role in history, closely intertwined with socioeconomic development in numerous countries (CHEN *et al.*, 2016; ZHANG; GU, 2023). Globally, there are approximately 800,000 dams, with roughly 62,000 falling into the category of large dams, defined as those exceeding a height of 15 metres or having a capacity exceeding three million cubic metres (ICOLD, 2020). Even though they are relatively

rare, with an annual probability of failure around 10^{-4} and 10^{-5} (FOSTER; FELL; SPANNAGLE, 2000; PROSKE, 2018), these structures remain vulnerable to failure, leading to floods that can cause significant damage, depending on the vulnerability and exposure of downstream areas.

Several dam failures have resulted in significant consequences, primarily associated with the loss of human life. Examples include the Banqiao and Shimantan incidents in China, the Vajont disaster in Italy, the Saint Francis incident in the United States, and the Malpasset disaster in France. However, beyond the loss of life, some incidents have also caused extensive environmental damage (FERNANDES et al., 2016; GUIMARÃES et al., 2022; ROTTA et al., 2020), such as the Mariana and Brumadinho tailing dam failures in Brazil.

These events have prompted many countries to establish regulatory frameworks that address dam safety. Currently, several jurisdictions require the preparation of comprehensive Emergency Action Plans (EAPs), including the development of high-resolution flood mapping, to prepare for potential dam failures (FERRARI; VACONDIO; MIGNOSA, 2023). The introduction of these requirements corresponds with a documented reduction in dam failure incidents over time (KALININA; SPADA; BURGHERR, 2020).

Mapping the inundation resulting from a dam breach poses a significant challenge, primarily due to the inherent uncertainties in the process. The field of dam-breach hydraulic modelling deals with various sources of uncertainty, including factors, such as topographic data (KIM; SANDERS, 2016; TSCHIEDEL; PAIVA, 2018), mathematical models simplification (MARANGOZ; ANILAN, 2022; PANDEY; KNOBLAUCH; ZENZ, 2024), model parameters such as Manning's roughness coefficient (ALMEIDA *et al.*, 2024; KALININA *et al.*, 2020; OGUZHAN; AKSOY, 2020), lack of observed data for calibration (AURELI; MARANZONI; PETACCIA, 2021), rheological models (GHAHRAMANI *et al.*, 2024; MELO; ELEUTÉRIO, 2023), dam-breach geometry (ABDEDOU; SOULAÏMANI; TCHAMEN, 2020; BELLOS *et al.*, 2020; TSAI; YEH; HUANG, 2019), breach location (MARANZONI; D'ORIA; MAZZOLENI, 2022) and formation time (AHMADISHARAF *et al.*, 2016; BELLO *et al.*, 2022).

In the context of flood risk assessments, these uncertainties must not be overlooked, as neglecting them can lead to inaccuracies with significant consequences, adversely impacting the quality of risk representation and the effectiveness of emergency planning (APEL *et al.*, 2004, 2009; KHERADMAND *et al.*, 2018; MERZ *et al.*, 2024). Nonetheless, conducting an uncertainty analysis in dam-breach modelling faces a notable obstacle due to the high computational costs, mainly when dealing with traditional two-dimensional models. Within this context, alternative approaches present themselves as viable solutions to mitigate the computational demands. One such approach involves the use of truncated hydraulic models with the control of the HEC-RAS model (DYSARZ, 2018; HARIRI *et al.*, 2022; PHILIPPUS *et al.*, 2021; WORLEY *et al.*, 2022), enabling the derivation of weighted failure hydrographs by the simulated peak flow (DA SILVA; ELEUTÉRIO, 2023; EL BILALI *et al.*, 2022; SARCHANI; KOUTROULIS, 2022).

However, it is essential to acknowledge certain limitations associated with this approach, particularly its inability to account for other breach hydrograph characteristics beyond the peak flow. Another alternative for addressing this challenge involves the utilisation of optimised sampling methods. These methods streamline uncertainty analysis by reducing the number of iterations required and include approaches such as the Perturbance Moments Method (ISSERMANN; CHANG, 2020; OUBENNACEUR *et al.*, 2018; TSAI; FRANCESCHINI, 2005).

In addition to these methods, this paper explores an alternative approach involving scenario pre-selection and associated probability assessment (RIZZO; MARANZONI; D'ORIA, 2023). This method employs a structured discretisation procedure to handle uncertain input parameters, dividing the parameter value range into distinct classes, each defined by its uppermost value. These classes are used to construct dam-breach scenarios, and their synthesis depends on the intersection of conditional probabilities for each parameter, with weighting applied to these scenarios. The probabilities within each class are informed by historical cases or fragility functions (D'ORIA; MARANZONI; MAZZOLENI, 2019). The framework was applied to assess the probabilistic flood hazard linked to a hypothetical Mignano dam failure. Both breach size and water level were treated as probabilistic parameters, with the latter demonstrating greater sensitivity (RIZZO; MARANZONI; D'ORIA, 2023).

This paper extends the previous research by using an alternative dataset (BERNARD-GARCIA; MAHDI, 2020) and shifting the analytical focus from concrete dams, as explored by Rizzo, Maranzoni and D'Oria (2023), to embankment dams, specifically investigating the International Commission on Large Dams (ICOLD) benchmark case study (ZENZ; GOLDGRUBER, 2013). Furthermore, this analysis examines breach top width and formation time, which have traditionally been addressed in embankment dam-breach studies using empirical equations (FROEHLICH, 2008; XU; ZHANG, 2009).

3.3 Case study

The ICOLD benchmark case is a virtual environment introduced during the 12th International Benchmark Workshop on Numerical Analysis of Dams (ZENZ; GOLDGRUBER, 2013). Eight studies were focused on addressing the computational challenges in consequence estimation for risk assessment. Furthermore, additional studies have explored the uncertainties of the breach (DA SILVA; ELEUTÉRIO, 2023; PETER *et al.*, 2018) and rheological parameters (MELO; ELEUTÉRIO, 2023). One of the main advantages of this case study is the availability of detailed data essential for simulations, including dam characteristics, topography, and land use.

A hypothetical embankment dam was situated in a mountainous region, approximately 3.5 kilometres from an urban environment, and terminated in a lake about 17 kilometres away. The hypothetical dam stands at a height of 61 metres, with upstream and downstream slopes of 3:1, a base width spanning 416 metres, and a crest width of 24 metres. The crest extends for 360 metres, creating a reservoir with a capacity of 38 million cubic metres.

The available Digital Elevation Model (DEM) possesses a spatial resolution of 9.5 metres. Land use classifications (Figure 3.1) align with the American National Land Cover Database (NLCD). Manning's roughness coefficient values were determined under the recommended mean values for these classes, as outlined in Brunner (2023). For this study, the dam-breach outflow was computed using the HEC-HMS 4.12 model, assuming a sine wave breach progression and applying the weir flow equation (SINGH, 1996). The simulation of flood wave propagation through the valley involved applying the Eulerian-Lagrangian method to solve the shallow water equations, as implemented

in the HEC-RAS 6.6 model (BRUNNER, 2020), considering two-dimensional flow. Figure 3.1 illustrates the boundary conditions and mesh grid employed in the simulation.

Figure 3.1 – Land use of the ICOLD benchmark case study, grid mesh and boundary conditions used in the simulations.

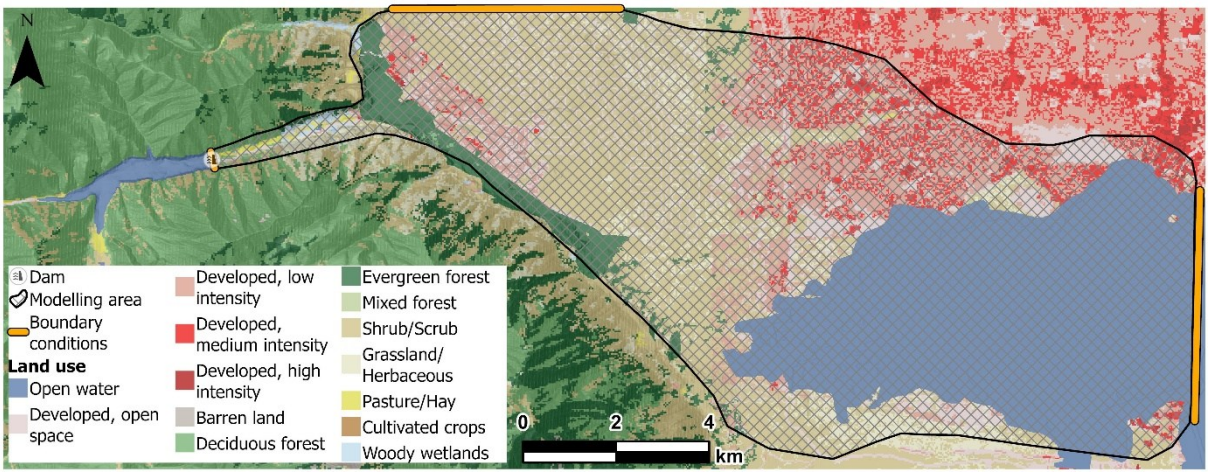

3.4 Probabilistic dam-breach flood modelling

The characterisation of dam-breach formation faces challenges due to the inherently complex and chaotic nature of dam failures (BELLOS *et al.*, 2020). Typically, embankment dams exhibit a trapezoidal breach shape (MACCHIONE; DE LORENZO; GRAZIANO, 2023). In deterministic studies, the geometry and formation time are defined using empirical relationships (FROEHLICH, 2008; XU; ZHANG, 2009).

In the context of a probabilistic approach to dam failure flood modelling, this study exclusively focuses on the uncertainties associated with the breach and its process parameters. Specifically, the study addresses the formation time (t_f) and another parameter that represents breach geometry, the dimensionless breach top width (B_t/L_{cr}), with B_t representing the breach top width and L_{cr}, the dam crest length. Empirical probability distributions for these two input parameters are established using a database compiled by Bernard-Garcia and Mahdi (2020). The methodology proposed by Rizzo, Maranzoni and D'Oria (2023) is adopted to construct weighted scenarios and probabilistically map flood, encompassing probabilistic inundation boundary, expected flood hazard, and expected arrival time. Figure 3.2 illustrates the flowchart of the methodology employed in this paper.

Figure 3.2 – Flowchart methodology for probabilistic mapping of dam-breach flood modelling.

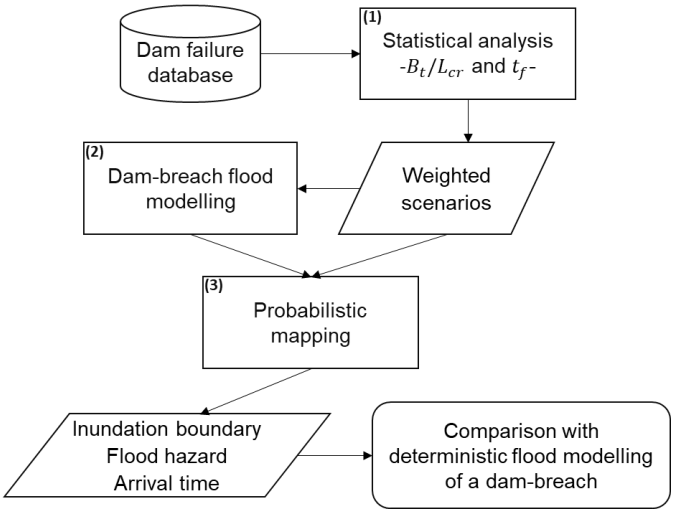

3.4.1 Probabilistc scenarios

In the framework proposed by Rizzo, Maranzoni and D'Oria (2023), uncertainties associated with input parameters are addressed through a spatial discretisation approach. This involves dividing the range of variability into distinct classes, with each upper value in a class representing the input parameter value utilised in the dam-breach scenario. Consequently, each dam-breach scenario ($S_{i,j}$) is characterised by the combination of the dimensionless breach top width (B_t/L_{cr_i}) and the formation time (t_{f_j}) (Figure 3.3). In this paper, higher index i values correspond to narrower breaches, while higher index j values indicate longer breach formation times.

Figure 3.3 – Example of the space discretisation of dimensionless breach top width and the formation time to define the dam-breach scenarios.

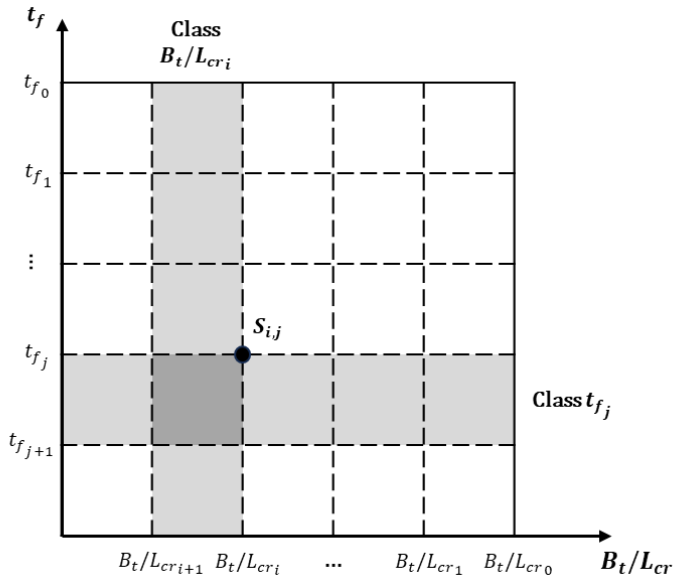

Rizzo, Maranzoni and D'Oria (2023) considered the probability, denoted as $P_{i,j}$ for the $S_{i,j}$ scenario, as the conditional probability when a dam failure event B occurs (Equation 5). Hence, the sum of all scenarios equals one, and in situations where the variables are statistically independent, this relationship can be reformulated, as exemplified in Equation 6.

$$P_{i,j} = P(S_{i,j}|B) = P[(B_t/L_{cr_{i+1}} \leq B_t/L_{cr} \leq B_t/L_{cr_i}) \cap (t_{f_{j+1}} \leq t_f \leq t_{f_j})|B] \quad (5)$$

$$P_{i,j} = P[(B_t/L_{cr_{i+1}} \leq B_t/L_{cr} \leq B_t/L_{cr_i})|B] * P[(t_{f_{j+1}} \leq t_f \leq t_{f_j})|B] \quad (6)$$

The probabilities for the considered input parameters are determined by analysing empirical data from historical dam failures. The subsequent section provides a comprehensive explanation of the database used and details the methodology employed for the analysis.

3.4.2 Dam-breach database analysis

The database compiled by Bernard-Garcia and Mahdi (2020) comprises 3,861 historical dam failure cases, assembled from 196 references, including supplementary databases (FROEHLICH, 2016; WAHL, 2004; XU; ZHANG, 2009; ZHANG *et al.*, 2016). Initially, 2,098 observations were selected, specifically representing failures of embankment dams. Among these observations, 121 provided consistent data on all breach geometry variables, 50 contained consistent data on formation time, and 33 offered consistent data on both variables within the same observation. The dimensionless breach top width used did not account for foundation erosion or valley effects; therefore, the maximum value for this variable was set at 1.

An analysis of the two variables under examination, as depicted in the scatter plot featuring the 33 observations with consistent data (Figure 3.4), showed no statistically significant dependence, as established through the non-parametric Kendall correlation test, with the null hypothesis of independence being accepted (p-value = 0.1611). This finding was further supported by bootstrap analysis, which generated 95% confidence intervals for the correlation coefficient encompassing zero, with 1,000 replicates, reinforcing the absence of a strong relationship. Additionally, attempts to fit non-linear models (including polynomial, exponential, logarithmic, and spline regressions) yielded high residual errors (RMSE), indicating no improvement in explanatory power.

Furthermore, weak correlations observed in the used database support the conclusion that B_t/L_{cr} and t_f can be treated as independent variables.

Figure 3.4 – Scatter plot between formation time and dimensionless breach top width variables in embankment dam failures.

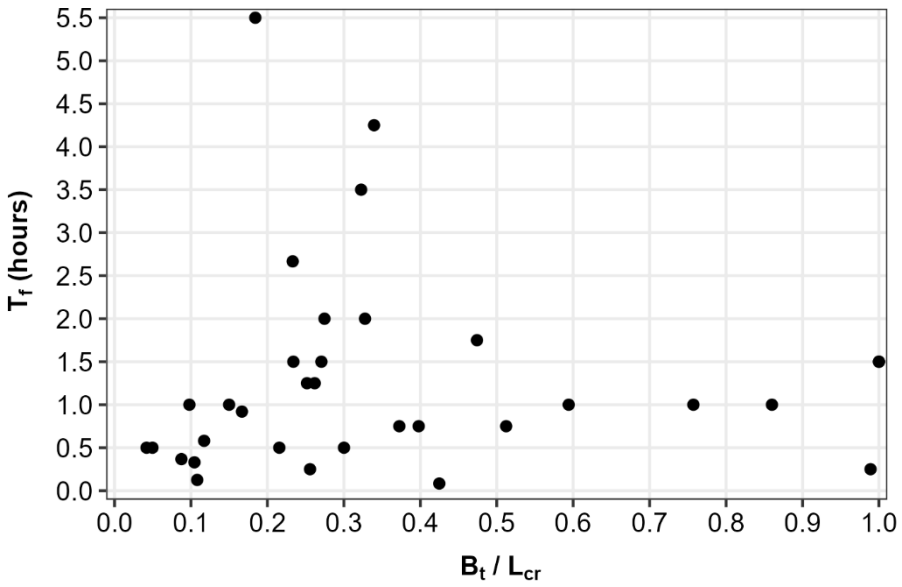

In order to examine potential interrelations among the variables, the multiple comparisons Dunn's test (DINNO, 2017) was applied to assess group influence. The analysis considered the failure mode (overtopping and internal erosion) and the dam shape classifications according to Rosgen (1994), which categorises dams based on crest length (L_{cr}) and the dam height (H_d) (Narrow (NAR) = $L_{cr}/H_d \leq 12$; Intermediate (INT) = $12 < L_{cr}/H_d \leq 40$; and Wide (WID) = $L_{cr}/H_d > 40$). Among the examined variables, a statistically significant group influence was observed only for the dimensionless breach top width, which was affected by both classification groups.

Upon examining the empirical distribution of the 50 observations with consistent formation time data, it is noticed that 46 out of these observations report formation times equal to or less than 2 hours. Only four observations deviate from this trend, corresponding to Banqio Dam in China, Walter Boulin Dam in the United States, Oros in Brazil, and Winston Lake Dam in the United States. Approximately 50% of these observations are concentrated within one hour (Figure 3.5). Based on the analysis of 121 consistent observations categorised by failure mode and dam shape, the empirical distribution of dimensionless breach top width reveals noteworthy trends (Figure 3.6). Wider dams tend to exhibit smaller dimensionless breach top widths, with the

maximum observed value being approximately 0.1 for internal erosion and 0.3 for overtopping. Additionally, the breach top achieves the width of the dam crest only in overtopping failures. Moreover, narrower dams exhibit higher dimensionless breach top width values more frequently.

Figure 3.5 – Histogram of the formation time variable in embankment dam failures.

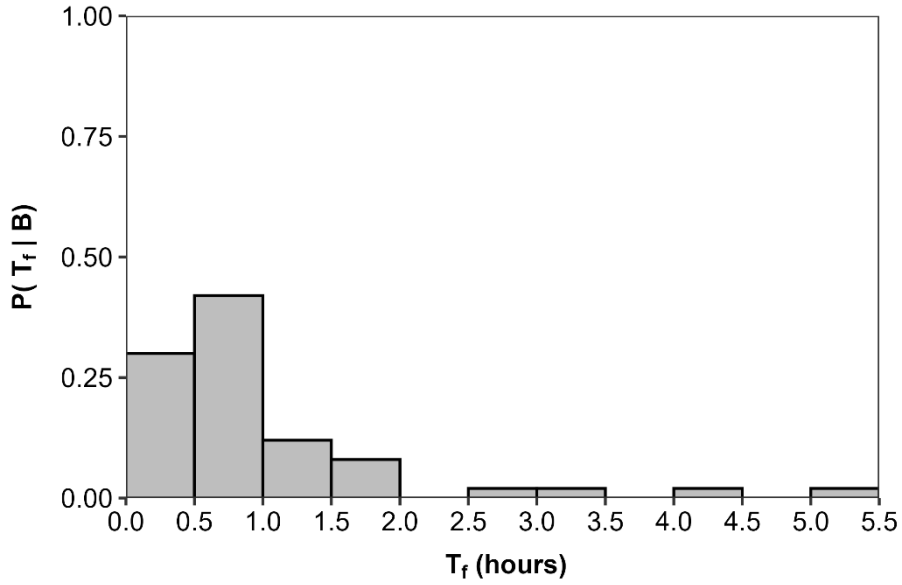

Figure 3.6 – Boxplots of the dimensionless breach top width variable grouped by failure mode and dam shape in embankment dam failures. IEE (Internal Erosion); OT (Overtopping); NAR (Narrow); INT (Intermediate); WID (Wide).

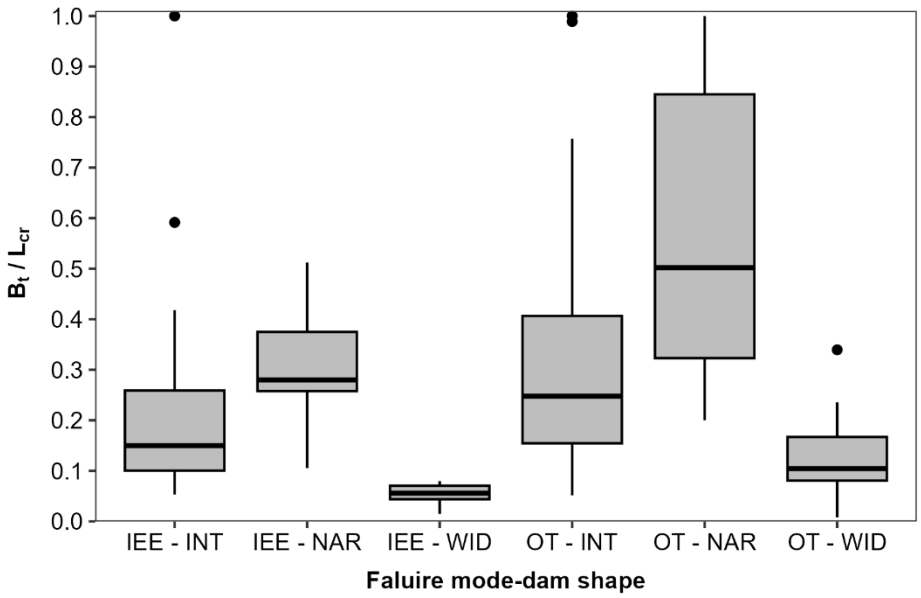

In this study, an overtopping failure dam model is considered, specifically for the ICOLD benchmark dam, which falls under the category of narrow dams ($L_{cr}/H_d =$

5.90). In order to perform the probabilistic mapping, five discretisation classes were established for both parameters. In the case of dimensionless breach top width (18 observations), the class ranging between 0.2 and 0.4 exhibits a higher probability, while the class between 0 and 0.2 displays a lower probability (Figure 3.7). Regarding formation time, the discretisation follows a uniform pattern, with intervals of half an hour up to 2 hours, with a higher probability observed within the 30-minute to 1-hour range. Beyond 2 hours, the last class varies between 2 and 5.5 hours. As noticed in Figure 3.5, only four of the 50 observations fall within this class.

Figure 3.7 – Histogram of the dimensionless breach top width variable with five uniform classes, overtopping and narrow dam shape group.

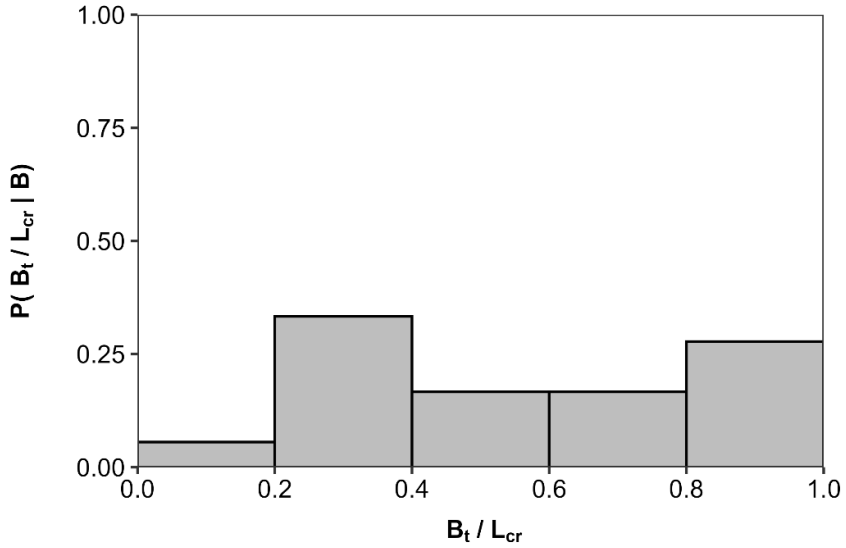

As no dependence is assumed between the dimensionless breach top width and formation time, a probability matrix for each $S_{i,j}$ scenario (Table 3.1) was constructed using Equation 6. Among these scenarios $S_{3,1}$ exhibits the highest probability, while $S_{4,3}$ and $S_{4,4}$ have the lowest probabilities.

Table 3.1 – Probabilities of the dam-breach scenarios for the ICOLD benchmark case study considering overtopping.

$P(S_{i,j}\|B)$		Breach top width (m)					
		$B_{t_0} = 360$	$B_{t_1} = 288$	$B_{t_2} = 216$	$B_{t_3} = 144$	$B_{t_4} = 72$	**Total**
Formation time (h)	$t_{f_0} = 0.5$	0.0833	0.0500	0.0500	0.1000	0.0167	0.300
	$t_{f_1} = 1.0$	0.1167	0.0700	0.0700	0.1400	0.0233	0.420
	$t_{f_2} = 1.5$	0.0333	0.0200	0.0200	0.0400	0.0067	0.120
	$t_{f_3} = 2.0$	0.0222	0.0133	0.0133	0.0267	0.0044	0.080
	$t_{f_4} = 5.5$	0.0222	0.0133	0.0133	0.0267	0.0044	0.080
	Total	0.278	0.167	0.167	0.333	0.055	**1**

As observed in 13 out of the 18 observations within the group of overtopping and narrow dam shapes, the breach height was determined to be equivalent to the dam height. Given the typical trapezoidal breach shape exhibited by embankment dams (MACCHIONE; DE LORENZO; GRAZIANO, 2023), the slope and corresponding breach bottom width were established by calculating the average of the recorded slopes between each dimensionless breach top width (Figure 3.8), resulting in the breach geometries illustrated in Figure 3.9.

Figure 3.8 – Scatter plot between average slope and dimensionless breach top width variables, overtopping and narrow dam shape group.

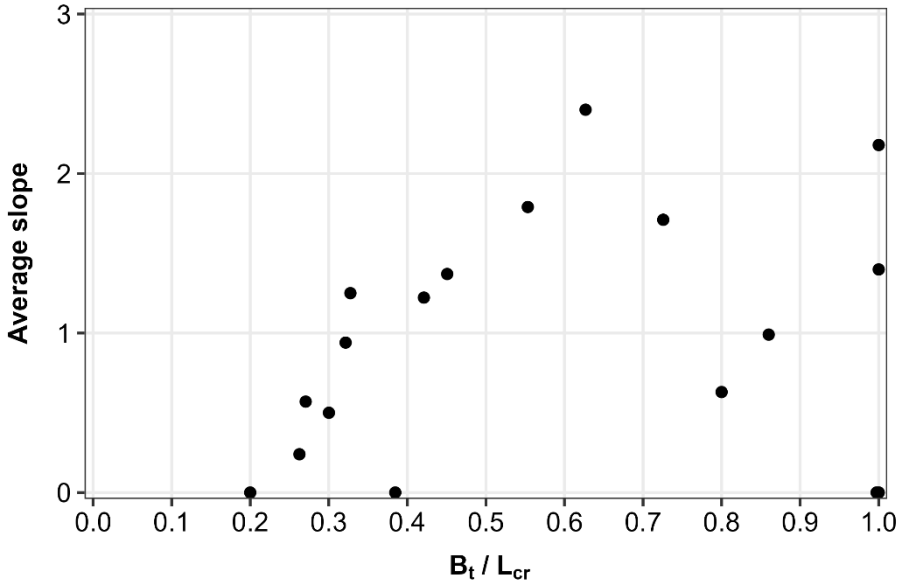

Figure 3.9 – Breach geometry scenarios considered for the ICOLD benchmark case study, overtopping and narrow dam shape group.

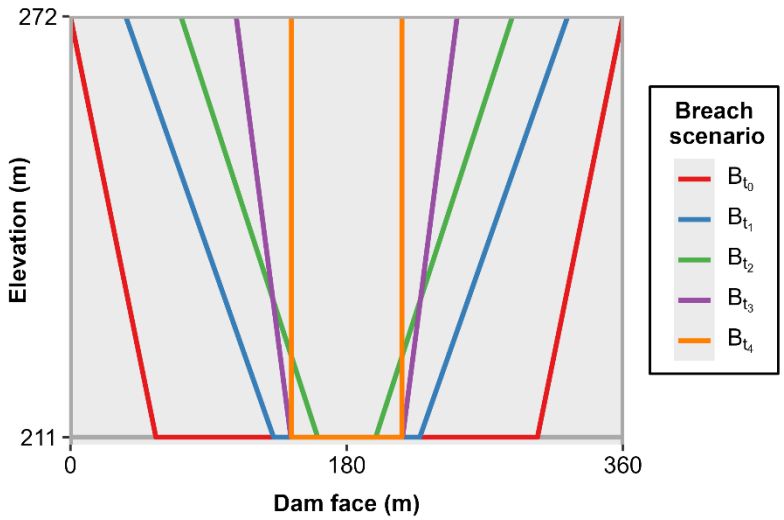

3.4.3 Probabilistic mapping

The breach flow hydrograph for each scenario delineates the influence of breach width and formation time on the flow pattern. In the most impactful scenario ($S_{0,0}$) ,the flow exceeded 50x10^3 m^3/s, while in the less impactful scenario ($S_{2,4}$), the peak is nearly an order of magnitude lower (Figure 3.10, Table 3.2 and Table 3.3). The simulation runtime for an 8-hour model varies depending on the breach formation time: approximately one hour for scenarios with a 30-minute formation time, and around 30 minutes for those with more extended formation periods (Intel Core i7-11800H processor and 16 GB RAM).

Applying Froehlich's (2008) equations, usually used for deterministic approaches of dam-breach flood modelling, for predicting breach characteristics (breach top width of 171 meters, formation time of 34 minutes, and slope of 1:1), it is observed that this scenario would fall between scenarios $S_{4,0}$ and $S_{0,1}$ with a peak flow and peak time of 30.3x10^3 m^3/s and 23 minutes, respectively.

Figure 3.10 – Breach flow hydrograph for each simulated scenario in the context of the overtopping scenario of the ICOLD benchmark dam.

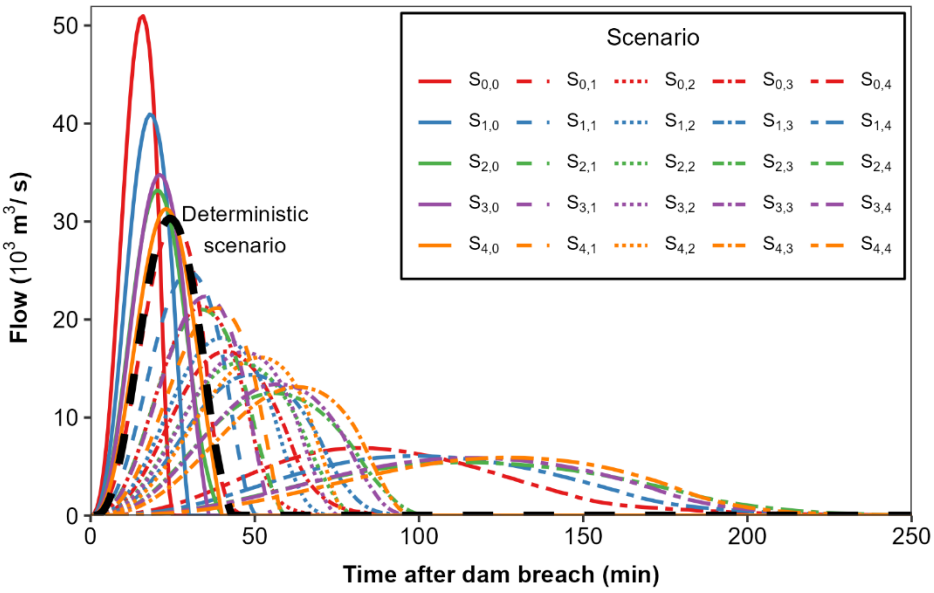

Despite having a wider breach top width and a higher total area (Figure 3.9), the breach B_{t_2} consistently demonstrates a lower peak flow in comparison to B_{t_3} and B_{t_4} across various scenarios. This divergence might be attributed to the narrower bottom width of B_{t_2}, resulting from a steeper average slope. In this context, the progression of the

breach formation, which initiates from the top to the bottom, results in a larger area of B_{t_3} and B_{t_4} as the breach elevation nears its bottom, consequently increasing the volume of water flowing through the breach during this phase of the breach formation.

Table 3.2 – Peak flow (Q_p) of the dam-breach hydrograph for each simulated scenario in the context of the overtopping scenario of the ICOLD benchmark dam.

$Q_p(10^3 m^3/s)$		Breach top width (m)				
		$B_{t_0} = 360$	$B_{t_1} = 288$	$B_{t_2} = 216$	$B_{t_3} = 144$	$B_{t_4} = 72$
Formation time (h)	$t_{f_0} = 0.5$	50.98	40.94	33.16	34.78	31.31
	$t_{f_1} = 1.0$	29.77	24.86	21.02	22.35	21.17
	$t_{f_2} = 1.5$	21.35	18.12	15.58	16.69	16.13
	$t_{f_3} = 2.0$	16.74	14.36	12.48	13.40	13.12
	$t_{f_4} = 5.5$	6.89	6.08	5.43	5.87	5.91

Table 3.3 – Peak time (t_p) of the dam-breach hydrograph for each simulated scenario in the context of the overtopping scenario of the ICOLD benchmark dam.

$t_p(h:min)$		Breach top width (m)				
		$B_{t_0} = 360$	$B_{t_1} = 288$	$B_{t_2} = 216$	$B_{t_3} = 144$	$B_{t_4} = 72$
Formation time (h)	$t_{f_0} = 0.5$	0:17	0:19	0:21	0:22	0:24
	$t_{f_1} = 1.0$	0:26	0:31	0:35	0:36	0:40
	$t_{f_2} = 1.5$	0:35	0:41	0:47	0:48	0:52
	$t_{f_3} = 2.0$	0:43	0:50	0:57	0:58	1:04
	$t_{f_4} = 5.5$	1:22	1:41	1:54	1:58	2:07

In order to analyse the propagation of the breach flow hydrograph, the peak flow and peak time across scenarios were examined at different cross-sections along the length of the downstream valley (Figure 3.11). Besides the breach flow hydrograph section (CS-00), the selected sections include one located at the end of the narrow valley, approximately 3.5 kilometres from the dam (CS-01), another positioned 8.5 kilometres from the dam at the beginning of the flatter reach (CS-02), one situated in the middle of the broader floodplain (CS-03); and the final section just before the lake (CS-04). The last two sections are spaced approximately 2.25 kilometres apart (Figure 3.1).

Between CS-00 and CS-01, there is a slight decrease in peak flow, which is more noticeable in the broader cross-sections of CS-02, CS-03, and CS-04. The peak flow diminishes for $B_{t_{0,1,2,3}}$ along the downstream valley, with values below 10x10^3 m^3/s in CS-04 (Figure 3.12). Additionally, B_{t_4} maintains consistent peak flow values for all simulated formation times, around 5-6x10^3 m^3/s.

Figure 3.11 – Cross-sections utilised for hydraulic analysis.

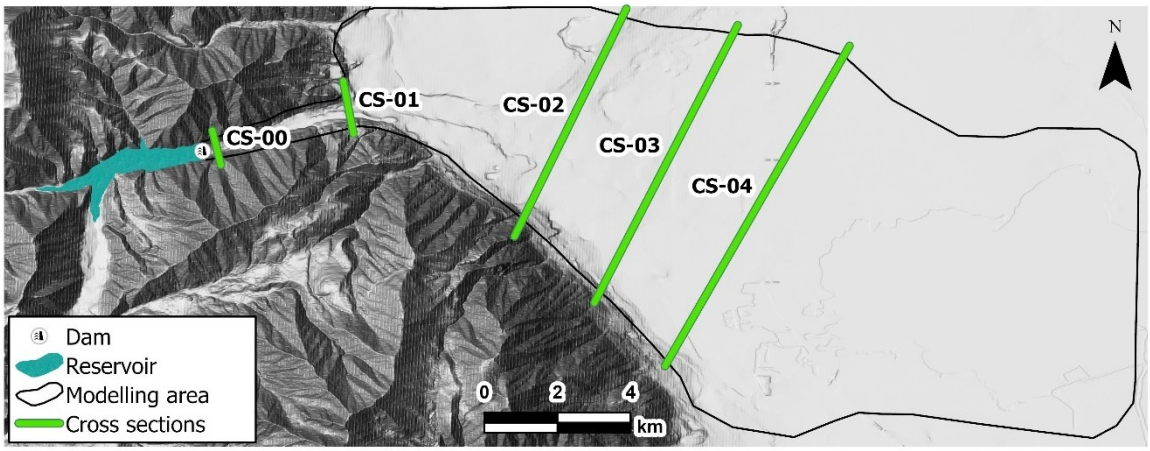

Figure 3.12 – Scatter plot depicting the peak flow and the peak time for each scenario and cross-section in the context of the overtopping scenario of the ICOLD benchmark dam.

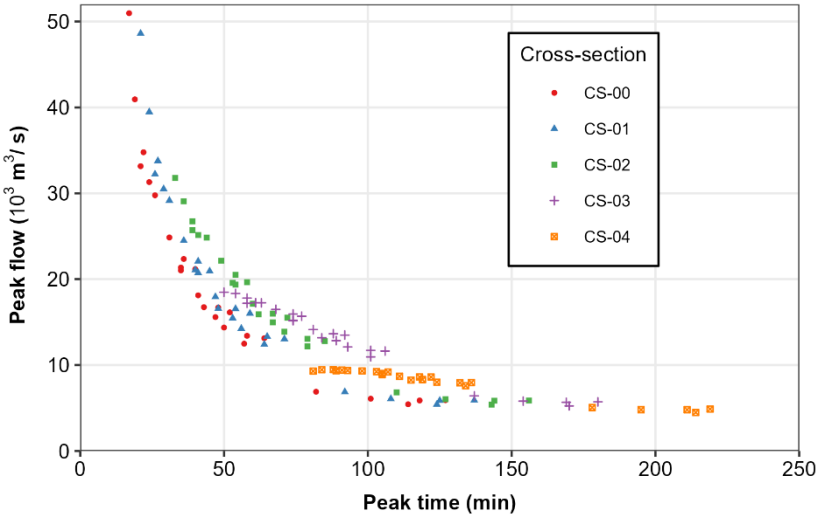

3.4.3.1 Probabilistic inundation boundary mapping

The combination of all probability scenarios leads to the elaboration of a probabilistic inundation boundary map. For each scenario, the (x, y) coordinates exposed to a flood hazard (HR) are allocated to the respective probability $P_{i,j}$ from Table 3.1 (Equation 7). The cumulative sum of all contributions obtained from all $A_{i,j}$ yields the inundation boundary probability, denoted as P_{in} (Equation 8) (RIZZO; MARANZONI; D'ORIA, 2023).

$$A_{i,j}(x,y) = \begin{cases} 0 & \text{if } HR_{i,j}(x,y) = 0 \\ P_{i,j} & \text{if } HR_{i,j}(x,y) > 0 \end{cases} \tag{7}$$

$$P_{in}(x,y) = \sum_{i=0}^{N_{B_t/L_{cr}}-1} \sum_{j=0}^{N_{t_f}-1} A_{i,j}(x,y) \tag{8}$$

Despite the observed disparities of peak flow and peak time among the scenarios (Figure 3.10), in the context of the overtopping of the ICOLD benchmark dam, most of the downstream area remains inundated across all scenarios. Only small portions near the extent boundaries and a larger region to the north exhibit probabilities of inundation below 1, with values dropping below 0.2 for the latter region (Figure 3.13). The total inundated area is 77.4 km^2, with 84.0% of this area being inundated across all scenarios. The deterministic simulated inundation boundary, derived using breach characteristics from Froehlich's (2008) equations, encompasses all areas with probabilities exceeding 0.4, covering 69.3 km^2, representing 90.0% of the total inundated area.

Figure 3.13 – Flood probabilistic inundation boundary map for the overtopping scenario of the ICOLD benchmark dam.

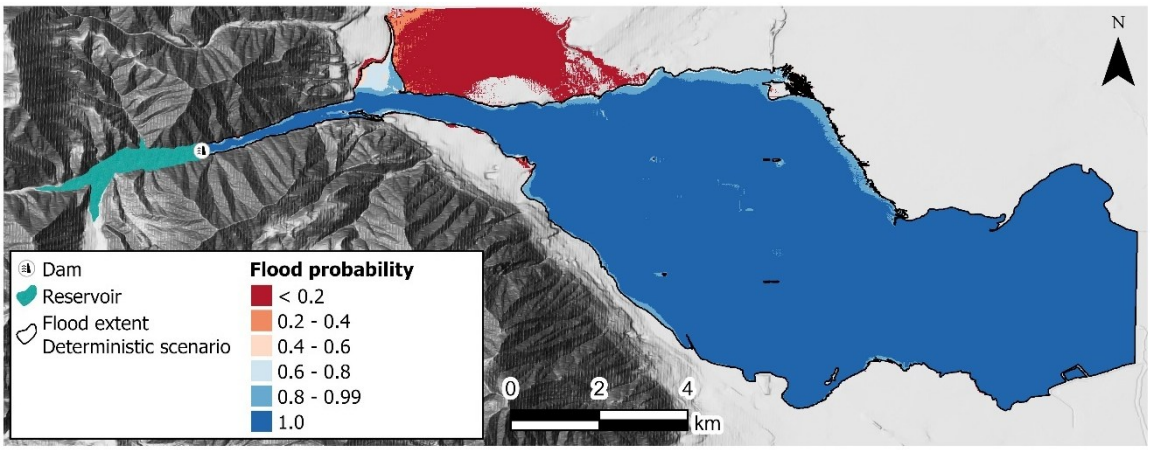

3.4.3.2 Probabilistic flood hazard mapping

The flood hazard denotes the likelihood of a defined flood intensity occurring within a specific region, characterised by particular frequency and magnitude (NOFAL; VAN DE LINDT, 2022). Quantitative methods employed in estimating flood hazards rely on flood variables, such as water depth, flow velocity, and the product of water depth and flow velocity, as common indicators (MARANZONI; D'ORIA; RIZZO, 2023a).

This paper adopts the flood hazard classification (HC) introduced by Smith, Davey and Cox (2014). This choice is motivated by its comprehensive coverage of various exposed elements such as people, vehicles, and buildings, a feature relatively scarce among existing classifications. Additionally, its applicability has been demonstrated in other studies concerning dam-breach assessments (ABDULRAHMAN *et al.*, 2022).

The authors justify the comprehensive coverage of diverse exposed elements due to the essential requirement for a comprehensive risk assessment during an inundation event. The proposed classification delineates six distinct classes, spanning from general safety hazards to conditions deemed unsafe for vehicles and individuals and vulnerable in terms of potential failure in all affected buildings (Table 3.4). Threshold values determine each hazard classification (Table 3.5).

Table 3.4 – Hazard classifications and their respective descriptions as proposed by Smith, Davey and Cox (2014).

Hazard classification	Description
HC 1	Generally safe for vehicles, people and buildings.
HC 2	Unsafe for small vehicles.
HC 3	Unsafe for vehicles, children and the elderly.
HC 4	Unsafe for vehicles and people.
HC 5	Unsafe for vehicles and people. All buildings are vulnerable to structural damage. Some less robust buildings are subject to failure.
HC 6	Unsafe for vehicles and people. All building types are considered vulnerable to failure.

Table 3.5 – Hazard classifications and their respective threshold limits for each variable as proposed by Smith, Davey and Cox (2014).

Hazard classification	Threshold		
	Water depth*flow velocity (m^2/s)	Water depth (m)	Flow velocity (m/s)
HC 1	≤ 0.3	≤ 0.3	≤ 2.0
HC 2	≤ 0.6	≤ 0.5	≤ 2.0
HC 3	≤ 0.6	≤ 1.2	≤ 2.0
HC 4	≤ 1.0	≤ 2.0	≤ 2.0
HC 5	≤ 4.0	≤ 4.0	≤ 4.0
HC 6	> 4.0	-	-

In order to exemplify the expected value and variability of flood variables used in the flood hazard classification, a weighted mean (Equation 9) and standard deviation (Equation 10) were calculated for each variable. The calculation of the weighted mean (μ_{VAR}) for each (x, y) involves the sum of the product of the variable (VAR) and its associated probabilities across all scenarios, while the standard deviation (σ_{VAR}) reflects the variability in the expected value of the variable (RIZZO; MARANZONI; D'ORIA, 2023).

$$\mu_{VAR}(x,y) = \sum_{i=0}^{N_{Bt/Lcr}-1} \sum_{j=0}^{N_{tf}-1} P_{i,j} VAR_{i,j}(x,y) \quad (9)$$

$$\sigma_{VAR}(x,y) = \sqrt{\sum_{i=0}^{N_{Bt/Lcr}-1} \sum_{j=0}^{N_{tf}-1} P_{i,j}[VAR_{i,j}(x,y) - \mu_{VAR}(x,y)]^2} \quad (10)$$

The reach from the dam to CS-02 (Figure 3.11) has the highest weighted mean variable values and standard deviations (Figure 3.14). Conversely, the northern region, which displays a lower probability of inundation, and the area surrounding the lake demonstrate comparatively smaller values for the weighted mean. Furthermore, the latter also exhibits reduced standard deviation values.

Figure 3.14 – Expected, represented by the (X.2) weighted mean, and (X.2) standard deviation values for (a.X) water depth, (b.X) flow velocity, and (c.X) their product for the overtopping scenario of the ICOLD benchmark dam.

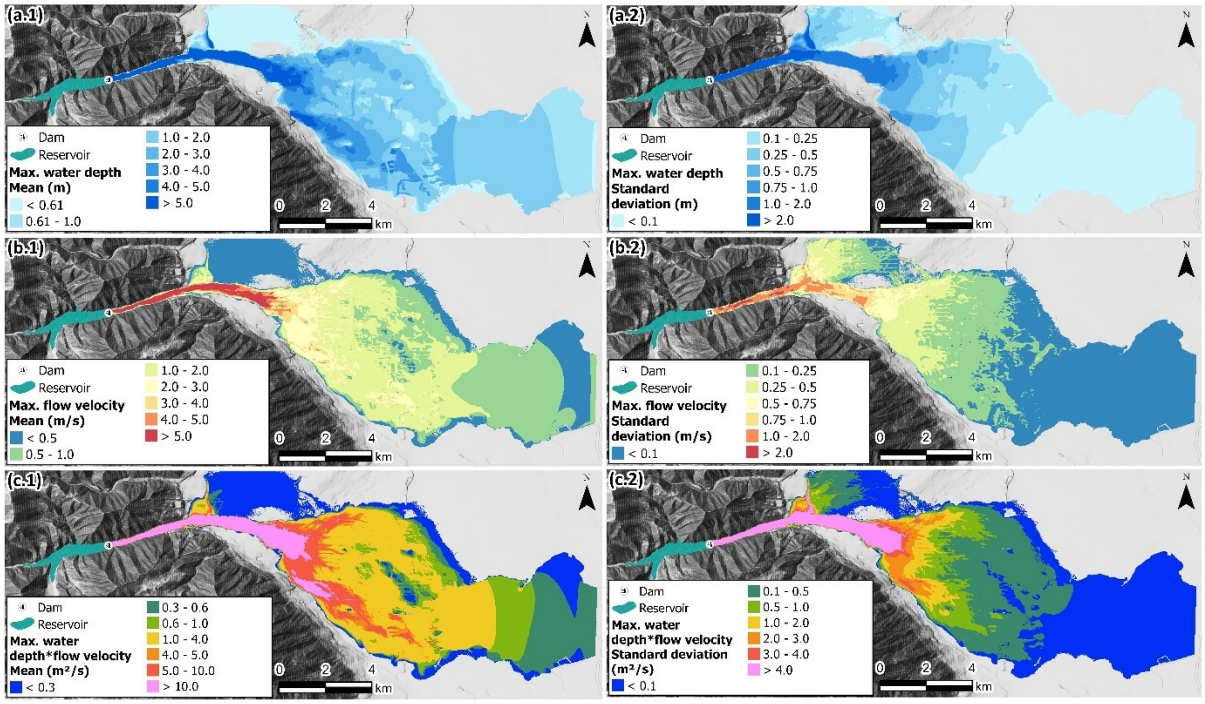

The calculation of the probability for (x, y) coordinates to fall within a specific K hazard classification is determined by Equation 11. The $C_{i,j}$ is assigned to each hazard classification class, representing occurrences across all simulated scenarios in the (x, y) coordinates when a specific hazard classification class is observed (Equation 12) (RIZZO; MARANZONI; D'ORIA, 2023).

$$P_{HC=k}(x,y) = \sum_{i=0}^{N_{Bt/Lcr}-1} \sum_{j=0}^{N_{tf}-1} C_{i,j|HC=k}(x,y) \quad (11)$$

$$C_{i,j|HC=k}(x,y) = \begin{cases} 0 & \text{if } HC_{i,j}(x,y) \neq k \\ P_{i,j} & \text{if } HC_{i,j}(x,y) = k \end{cases} \quad (12)$$

Probabilistic flood hazard mapping shows the highest hazard levels near the dam, where the probability is 1 (Figure 3.15). In the flatter expanse between CS-02 and CS-05 (Figure 3.11), HC 5 and HC 6 are more likely. Further downstream, within the lake area, HC 4 initially displays a higher likelihood, gradually transitioning to HC 3 towards the end of this region. HC 2 exhibits the lowest probability, primarily located along the boundaries of the inundation area. The northern region, characterised by the lowest probability of inundation (Figure 3.13), predominantly indicates HC 1, emphasising its overall safety for vehicles, individuals, and buildings.

Figure 3.15 – Flood hazard probabilistic map for each hazard classification: (a) HC 1; (b) HC 2; (c) HC 3; (d) HC 4; (e) HC 5; and (f) HC 6 — overtopping scenario of the ICOLD benchmark dam.

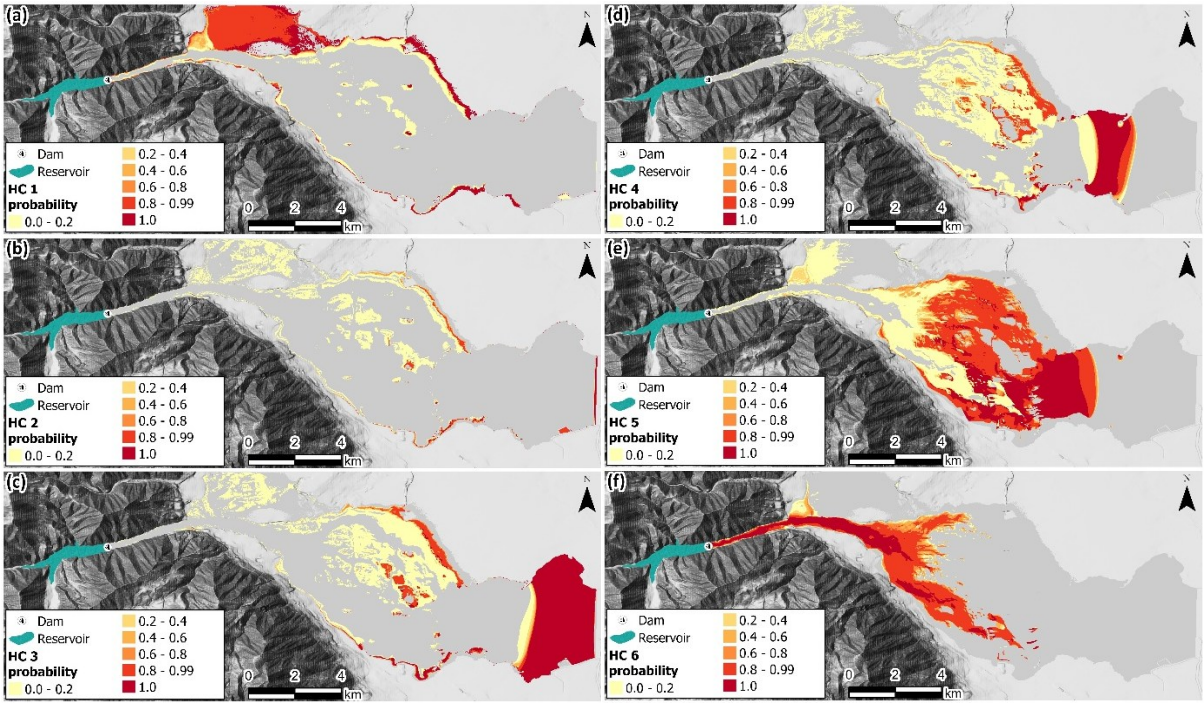

The flood hazard classification based on the deterministic approach using Froehlich's (2008) equations closely matches the most likely hazard class for the valley (Figure 3.16), with a 97.5% agreement. The primary differences arise from HC 6 in the deterministic approach being classified as HC 5 (0.65 km²), mainly affecting the beginning of the flat region between CS-02 and CS-03 (Figure 3.11).

Figure 3.16 – Flood hazard mapping for the (a) most likely class from the probabilistic modelling and the (b) deterministic approach — overtopping scenario of the ICOLD benchmark dam.

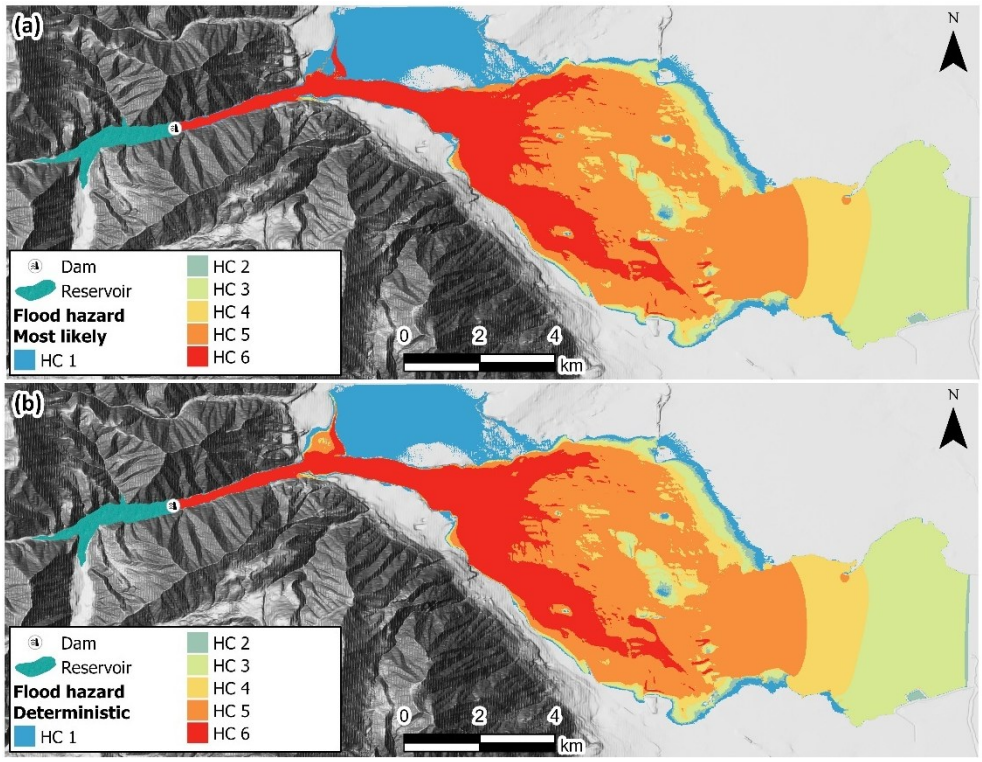

3.4.3.3 Probabilistic arrival time mapping

The arrival time is an additional significant variable, not directly indicative of flood hazard, but essential in dam-breach emergency planning. Numerous studies have underscored the vital role of understanding and mapping the arrival time in mitigating dam-breach flood damages (EL BILALI *et al.*, 2022; LUMBROSO *et al.*, 2021; LUMBROSO; DAVISON, 2018; SARCHANI; KOUTROULIS, 2022; SILVA; ELEUTÉRIO, 2023a, 2023b).

In order to determine the expected value for the flood arrival time and its variability, the computation of the weighted mean flood arrival time (μ_{AT}) is delineated by Equation 13, with AT representing the flood arrival time. The determination of normalised weights $A_{i,j}(x,y)/P_{in}(x,y)$ introduces a form of conditional probability assessment on specific (x,y) coordinates where specific scenarios induce flooding. In cases where $P_{in}(x,y)$ is equal to zero, the probability of the weighted mean tends toward infinity. The weighted mean flood arrival time standard deviation (σ_{AT}) is defined by Equation (14) (RIZZO; MARANZONI; D'ORIA, 2023).

$$\mu_{AT}(x,y) = \begin{cases} \sum_{i=0}^{N_{Bt/Lcr}-1} \sum_{j=0}^{N_{tf}-1} \frac{A_{i,j}(x,y)}{P_{in}(x,y)} AT_{i,j}(x,y) & \text{if } P_{in}(x,y) > 0 \\ +\infty & \text{if } P_{in}(x,y) = 0 \end{cases} \quad (13)$$

$$\sigma_{AT}(x,y) = \sqrt{\sum_{i=0}^{N_{Bt/Lcr}-1} \sum_{j=0}^{N_{tf}-1} \frac{A_{i,j}(x,y)}{P_{in}(x,y)} [AT_{i,j}(x,y) - \mu_{AT}(x,y)]^2} \quad (14)$$

The weighted mean flood arrival time takes approximately 30 minutes to 1 hour to reach the end of the narrower valley region, displaying lesser absolute uncertainty. However, as the flood progresses into flatter regions, both the arrival time and its associated uncertainties increase (Figure 3.17). The northern region, with a probability of inundation lower than 0.2, is affected by only two scenarios ($S_{0,0}$ and $S_{0,1}$), constituting the exclusive inputs used for calculating the probabilistic arrival time in this area. The arrival time mapping illustrates that the difference between these two scenarios widens as the arrival time increases.

Figure 3.17 – (a) weighted mean, (b) deterministic scenario, (c) weighted mean plus standard deviation, and (d) weighted mean minus standard deviation for flood arrival time in the overtopping scenario at the ICOLD benchmark dam.

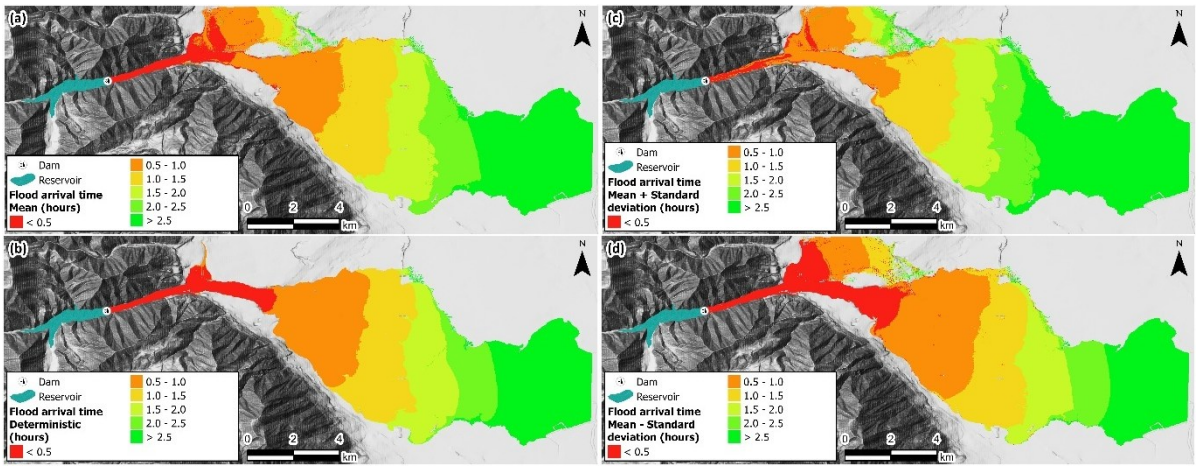

The deterministic approach, derived using breach characteristics from Froehlich's (2008) equations, estimates a shorter flood arrival time than the weighted mean. However, it is visually closer to the weighted mean plus one standard deviation, being slightly slower, with the flood reaching the end of the narrower valley region in approximately 30 minutes.

3.5 Discussion and limitations

Although the probabilistic approach, using predefined scenarios weighted based on historical dam-breach events, is a viable alternative to high-resolution hydrodynamic simulations, specific considerations must be addressed. The assumption that the dimensionless breach top width and formation time are independent may not be entirely accurate, as the physical processes governing dam breaches suggest a relationship between these variables. Some empirical equations for predicting formation time explicitly account for breach width (WAHL, 2004). Our analysis of 33 paired observations did not reveal a statistically significant correlation, but this may be due to the limited sample size rather than a lack of dependence. It is possible to fit a joint probability distribution to this subset to capture potential dependence; however, the small number of data points limits the reliability of such an approach. Treating the variables as independent makes it possible to use larger, separate datasets, with 121 observations for breach geometry and 50 for formation time, which improves the representativeness of the marginal distributions, though it may overlook any existing relationship between them.

Moreover, the definition of scenarios and the discretisation of the variability space of the input parameters can significantly influence the results. In addition to discretisation, another factor affecting the simulations is the number of input parameters selected for analysis. Other parameters, such as breach slope, could also be valuable to investigate. However, the number of simulated scenarios increases proportionally with the multiplication of each discretisation level for the considered parameters. As the number of scenarios grows, one of the key advantages of this methodology, its computational efficiency in high-resolution probabilistic simulations (around 15 hours for a machine with an Intel Core i7-11800H processor and 16 GB RAM), may no longer be as beneficial.

The flood variable outcomes are specific to this case study, as they depend on the characteristics of the dam and the downstream valley. Therefore, generalising these findings to other cases, especially those with different characteristics, is not ideal. The downstream valley, which consists of a narrow section followed by a flat area, results in a similar flood extent across many scenarios. Among the 25 scenarios analysed, only two ($S_{0,0}$ and $S_{0,1}$) cause inundation in the northern region, with inundation

probabilities below 0.2 (Figure 3.13). Although the flood hazard classification is similar between the deterministic and most likely probabilistic approaches (Figure 3.16), probabilistic hazard mapping still provides valuable insights. In all simulation cases, the highest hazard class is expected to occur in the narrow portion of the domain. The probability distribution of hazard classes indicates more significant variability in possible hazard classifications within the flat regions. Regarding flood arrival time, most recommendations for Emergency Action Plans define the self-rescue zone, an important boundary for assigning responsibilities during emergencies, as an area within 10 kilometres or 30 minutes of flood arrival, whichever results in the larger affected area. For this specific case study, all approaches that consider flood arrival time lead to defining the self-rescue zone as the 10 kilometres extent (Figure 3.17). However, using expected flood arrival time and its variability remains essential for other studies, particularly in assessing population vulnerability and risk.

3.6 Conclusions

Accounting for uncertainties in flood risk mapping on a high-resolution scale for dam breaches is widely recommended, including in some national regulations. However, a key challenge in conducting such high-resolution analysis is the significant computational demand associated with uncertainty quantification. This study explores an alternative approach to high-resolution probabilistic dam-breach flood modelling. Specifically, we apply the methodology proposed by Rizzo, Maranzoni and D'Oria (2023), which involves weighting representative scenarios derived from historical dam failure data, and it was initially developed and tested for concrete dams, incorporating breach and reservoir levels at the moment of failure. This study applies the approach to an embankment dam, considering the dimensionless breach top width and formation time, while utilising a different database of dam failures to assign the scenario weights.

For the International Commission on Large Dams (ICOLD) benchmark case study, the probabilistic flood mapping covers an area of 77.4 km^2, with 84.0% of this region having a 100% probability of inundation in the event of a dam failure. The simulated inundation boundary, derived from a deterministic scenario, using breach characteristics estimated by Froehlich's (2008) equations, encompasses all areas with inundation probabilities exceeding 0.4. This area spans 69.3 km^2, representing 90.0% of the total inundated region. Based on the methodology of Smith, Davey and Cox (2014) for

defining hazard classes, the probabilistic flood hazard classification reveals that the narrow portion of the downstream valley has a 100% probability of experiencing the highest hazard levels. In this region, the conditions are unsafe for vehicles and pedestrians, and all building types are considered vulnerable to failure. In contrast, hazard classifications in the flatter portion of the valley are intermediate, still posing risks to vehicles and pedestrians but providing relatively safer conditions for buildings. Furthermore, the expected flood arrival time and its variability, measured by standard deviation, serve as valuable tools for emergency response planning, aiding in developing more robust and effective early warning and evacuation systems.

Probabilistic dam-breach flood mapping provides significantly more informative results than deterministic approaches. Future research could explore the integration of this approach with probabilistic economic damage and human loss estimations. Additionally, further studies should assess the impact of discretisation levels and the number of input parameters considered. Comparative analyses between this approach and traditional probabilistic simulations, such as Monte Carlo methods, could offer deeper insights into its computational efficiency and feasibility. Finally, statistical analysis of dependencies between variables in dam failure databases is recommended to refine probability weighting methods.

4 A METHODOLOGICAL FRAMEWORK FOR LIFE-LOSS ESTIMATION UNDER PROBABILISTIC FLOOD AND EXPOSURE SCENARIOS IN DAM-BREACH EVENTS

4.1 Abstract

Life-loss estimation models, especially agent-based models, hold significant potential for evaluating the effectiveness of early warning and evacuation systems. This is particularly relevant in dam breaches, where stricter regulations are in place to enhance safety, leading to more robust early warning and evacuation systems. However, several limitations persist in this type of modelling. One of them is incorporating hydraulic uncertainties into these simulations, as detailed flood modelling often involves high computational costs. Additionally, population distribution tends to vary spatially and temporally in impacted regions, and integrating this variability into models probabilistically has not yet been fully achieved. This study proposes a framework to address these limitations in life-loss estimation, specifically using the LifeSim agent-based model. The framework builds on LifeSim's existing modelling routines and involves scenario-based simulations that account for varying scenarios of breach top width, breach formation time, and population distribution. Each scenario is assigned a specific probability based on historical dam failure data and the temporal dynamics of population distribution. From this, a probabilistic scenario can be constructed, characterised by its weighted mean and associated variability. In order to validate the framework, it was applied to the benchmark case provided by the International Commission on Large Dams. The weighted mean of the probabilistic scenario generally results in lower estimated fatalities than those produced by deterministic flood modelling approaches. In turn, the deterministic scenarios yield lower estimates than the weighted mean plus one standard deviation. Compared to existing methodologies, the proposed framework represents a significant advancement in accounting for flood characteristics and population distribution uncertainties within agent-based life-loss modelling.

4.2 Introduction

Dams have played a vital role in societal development throughout history. However, their potential failure presents a significant risk to downstream populations (GE *et al.*, 2020; SARCHANI; KOUTROULIS, 2022). In order to mitigate this risk, several national

regulations recommend high-resolution flood mapping and the implementation of a robust Early Warning and Evacuation System (EWES) (FERRARI; VACONDIO; MIGNOSA, 2023; PETRUCCI, 2022; YARI *et al.*, 2020). One of the primary methods for evaluating the effectiveness of such systems is through life-loss estimation models (CHEN *et al.*, 2023; GE *et al.*, 2022). Various approaches can be employed for this purpose, with agent-based models being especially valuable due to their ability to incorporate the dynamics of hazards, emergency planning timelines for issuing warnings, and population behaviour and evacuation processes (LUMBROSO *et al.*, 2021; LUMBROSO; DAVISON, 2018).

Among the most widely adopted tools for assessing flood-related life losses is the agent-based model LifeSim, initially proposed Aboelata et al. (2003) and subsequently developed into a modular simulation framework (USACE, 2020). LifeSim enables the detailed modelling of individual and group behaviour in response to flood events by integrating spatially and temporally varying hydrodynamic data with population characteristics derived from GIS-based layers. The model comprises four primary modules. The flood routine module dynamically represents flood parameters across a networked spatial domain. The shelter loss module assesses population exposure for individuals remaining within structures, taking into account submersion and building collapse criteria. The warning and evacuation module models decision-making and protective action dynamics through a sequence of delays, from hazard recognition to evacuation order issuance, warning dissemination, and population mobilisation. These delays are represented by probabilistic curves capturing uncertainties. Furthermore, the life-loss module estimates fatalities using two distinct probability distributions, depending on individuals' exposure conditions. These fatality rates are derived from empirical data collected from historical flood events (USACE, 2020).

Risk estimation in LifeSim is conducted through Monte Carlo simulations, allowing both epistemic and aleatory uncertainties to be incorporated by repeatedly sampling model inputs. Each simulation iteration, corresponding to a unique combination of sampled parameters, is associated with a seed to ensure reproducibility. LifeSim samples values for input parameters during each iteration, including warning and evacuation timings, as well as structural attributes. Based on these, the model simulates the dynamics of population response. Individuals who are not warned or do not undertake

proactive evacuation engage in time-independent vertical evacuation, relocating within buildings according to sampled structural attributes (e.g., the highest floor, attic, or roof). Those opting for horizontal evacuation are subject to parameters governing movement and safety, such as flood entry willingness and stability criteria. Upon defining the exposure of each agent, the model applies fatality rates to determine life-loss outcomes. This process is repeated across all iterations, yielding a probabilistic estimate of potential fatalities under the defined hazard and population conditions.

The LifeSim model has been applied in various international contexts to estimate the loss of life from dam-breach and flood events. In Switzerland, it was used to develop a generalised life-loss estimation model for dam failures (KALININA; SPADA; BURGHERR, 2021). In Morocco, the model supported traffic management analysis (EL BILALI; TALEB; BOUTAHRI, 2021) and was further employed to propose a probabilistic life-loss assessment for densely populated areas (EL BILALI *et al.*, 2022). In Brazil, LifeSim was applied to evaluate the effectiveness of warning and evacuation procedures in the context of the 2007 São Francisco tailings dam failure (SILVA; ELEUTÉRIO, 2023a), as well as in a hypothetical high-density urban scenario (SILVA; ELEUTÉRIO, 2023b). The model was also used in China to assess the impacts of various non-structural interventions for dam-break floods (WANG *et al.*, 2024). Additionally, it contributed to analysing warning systems and population preparedness during the 2021 flash flood in Germany (SILVA *et al.*, 2025).

While the LifeSim model is beneficial, detailed data regarding flood-related fatalities are scarce (PAPAGIANNAKI *et al.*, 2022; PETRUCCI, 2022). As a result, the calibration and validation of such modelling approaches continue to challenge the broader adoption of LifeSim in prospective studies. In order to address this limitation, it is advisable to incorporate all plausible scenarios within a probabilistic framework that captures the full range of model parameter uncertainties. LifeSim's probabilistic structure already accounts for uncertainties associated with warning dissemination, evacuation processes, and the loss-of-life module.

Nevertheless, it is essential to note that the flood routine within LifeSim cannot currently be evaluated with uncertainty, even though flood modelling can significantly impact loss estimations (BRUSSEE *et al.*, 2021). The primary factor contributing to the

absence of flood uncertainty in life-loss models is the substantial computational demand associated with 2D hydraulic models. Several studies have attempted to assess life loss under probabilistic flood scenarios using empirical models. De Bruijn, Diermanse and Beckers (2014) introduced an innovative approach to analysing societal flood fatality risk within river deltas in the Netherlands. The authors constructed the Fatality-Probability (FN) curve, which correlates fatalities with their respective probabilities, using the Jonkman, Vrijling and Vrouwenvelder (2008) life-loss model. This analysis considered uncertainties associated with dike breach locations and evacuation parameters. Similarly, Li, Zhou and Shen (2023) applied a copula function to evaluate the joint probability of storm surge and rainfall, thereby assessing life-loss estimates in the coastal city of Macao. The authors considered eight distinct scenarios of joint probabilities and, following the approach of De Bruijn, Diermanse and Beckers (2014), constructed FN curves using the Jonkman, Vrijling and Vrouwenvelder (2008) life-loss model.

Another critical input that is not treated probabilistically in LifeSim is population distribution. This factor can vary significantly throughout the day and is particularly sensitive in regions with extensive commercial activity. Several studies have examined the influence of temporal population distribution on life-loss estimates using empirical models. Maranzoni, D'Oria and Rizzo (2023b), building on the probabilistic flood hazard methodology presented by Rizzo, Maranzoni and D'Oria (2023) and applied to a hypothetical failure of the Mignano Dam in Italy, proposed probabilistic mapping of life loss using the empirical model developed by Sun et al. (2014). In addition to flood uncertainty, the authors also accounted for uncertainty in population distribution during business and non-business hours. By simulating 40 scenarios, comprising 20 weighted dam breach scenarios combined with two weighted population distributions, the authors illustrated the spatial distribution of selected percentiles of loss of life, accompanied by corresponding uncertainty bounds. Peng, Zhang and Sayama (2024) evaluated the impact of varying population distributions during nighttime, commuting, and working hours. Using the Jonkman, Vrijling and Vrouwenvelder (2008) life-loss model, adapted to incorporate key stages of the evacuation process (such as warning issuance, dissemination, and mobilisation times), the authors found that the minimum required warning issuance time to reduce life loss statistically significantly was 214, 137, and zero minutes for the respective population distribution conditions.

Specifically related to the LifeSim model, El Bilali et al. (2022) conducted a flood probabilistic analysis using the McBreach tool (GOODELL *et al.*, 2019) to estimate potential life losses in an urban region in Morocco. Exceedance probabilities were linked to the dam-breach hydrographs through the arrangement of peak flow. Following this, distinct exceedance probabilities were chosen for hydraulic modelling and subsequent simulation of life loss. However, using peak flow as the primary variable for scenario weighting can misrepresent the most extreme events, potentially leading to a biased perception of risk. In some instances, the timing of the dam-breach flood's arrival or peak flow may be a more critical factor, as it reduces the available time for evacuation and increases overall risk. Furthermore, this approach may exhibit equifinality, whereby different breach parameter sets produce similar peak flows, potentially occurring at different times (DA SILVA; ELEUTÉRIO, 2023).

This study presents a novel framework for estimating life loss using the LifeSim agent-based model, which explicitly incorporates uncertainties in flood dynamics and population distribution. Expanding upon the methodology proposed by Maranzoni, D'Oria and Rizzo (2023b), our approach replaces the empirical life-loss model with the more detailed and dynamic LifeSim framework. Additionally, this work advances the contributions of El Bilali et al. (2022) by more comprehensively integrating flood-related uncertainty into agent-based life-loss estimations. In addition to temporal population distribution variability, a key innovation of this framework lies in its use of weighted scenarios that capture uncertainty in specific dam-breach parameters. Unlike previous methodologies that rely on peak flow simulations to define scenario weights, our approach allows for the direct consideration of critical variables, such as flood arrival time, which directly influence the window available for effective evacuation. The proposed methodology is demonstrated through its application to the benchmark case study of the International Commission on Large Dams (ZENZ; GOLDGRUBER, 2013).

4.3 Case study

The ICOLD benchmark case is a virtual environment introduced during the 12th International Benchmark Workshop on Numerical Analysis of Dams (ZENZ; GOLDGRUBER, 2013). Eight studies were focused on addressing the computational challenges in consequence estimation for risk assessment. Furthermore, additional studies have explored the uncertainties associated with breach (DA SILVA;

ELEUTÉRIO, 2023; PETER *et al.*, 2018; SILVA; ELEUTÉRIO, 2025) and rheological parameters (MELO; ELEUTÉRIO, 2023).

A hypothetical embankment dam was situated in a mountainous region, approximately 3.5 kilometres from an urban environment, and terminated in a lake about 17 kilometres away. The hypothetical dam stands at a height of 61 metres, with upstream and downstream slopes of 3:1, a base width spanning 416 metres, and a crest width of 24 metres. The crest extends for 360 metres, creating a reservoir with a capacity of 38 million cubic metres.

The dataset provided for the ICOLD benchmark case study includes layers containing crucial information on parcel zones (Figure 4.1) and census blocks (Figure 4.2), which serve as the basis for subsequent analysis. The parcel zone data includes attributes such as land-use type (e.g., residential, commercial) and the number of stories in buildings. The census block data provides demographic information, including population counts, age distribution, and employment characteristics.

Figure 4.1 – Parcel zones of the ICOLD benchmark case study categorised by occupancy type.

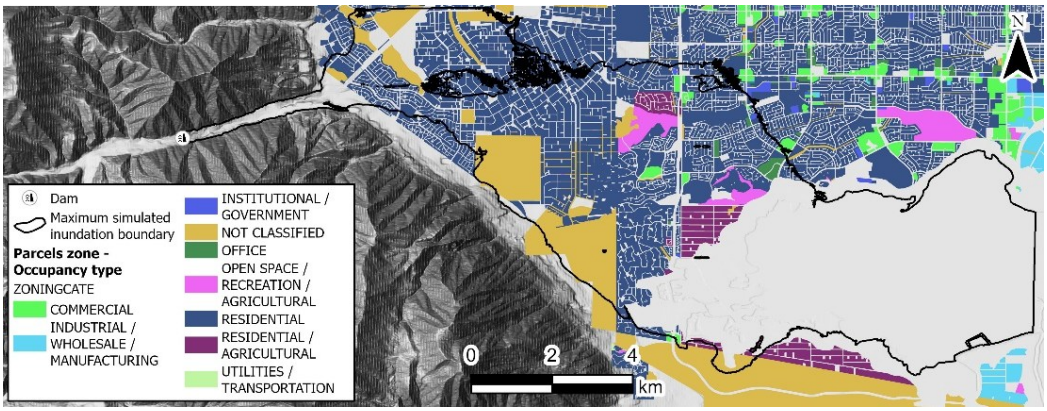

Figure 4.2 – Census blocks of the ICOLD benchmark case study categorised by population.

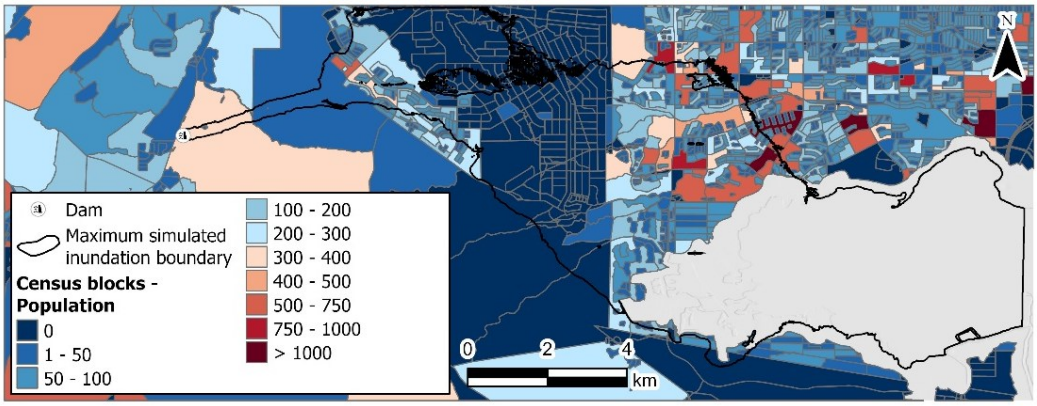

4.4 Probabilistic life-loss estimation framework

The proposed framework is based on an adaptation of the methodology developed by Maranzoni, D'Oria and Rizzo (2023b) for estimating life loss under probabilistic dam-breach flood scenarios and varying population distributions. While their approach employs an empirical life-loss model and primarily focuses on the spatial mapping of fatality outcomes, our framework utilises the agent-based LifeSim model. LifeSim inherently produces probabilistic outputs but does not explicitly incorporate flood dynamics or population distribution uncertainties.

The proposed framework (Figure 4.3) comprises four main stages. First, probabilistic flood modelling of the dam breach is conducted. Second, the temporal distribution of the population within buildings is estimated probabilistically. These probabilistic estimations are achieved by defining discrete scenarios and assigning corresponding weights to each scenario. The third stage involves running LifeSim simulations for all defined scenarios. Finally, life-loss estimates are derived by integrating the simulation results with the assigned scenario weights, producing a probabilistic life-loss assessment. Comparisons between the probabilistic and deterministic approaches are carried out to evaluate the differences in the resulting life-loss estimates. Further details regarding each of these stages are provided in the following sections.

Figure 4.3 – Proposed framework for estimating potential life loss under probabilistic dam-breach flood and population distribution scenarios.

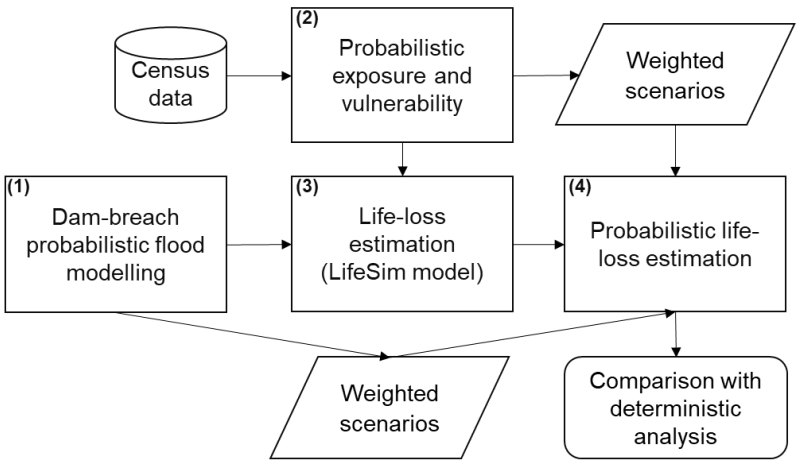

4.4.1 Probabilistic dam-breach flood modelling

Simulating a flood probabilistically following a dam failure presents a significant challenge due to the high computational demands associated with such modelling. In

order to address this, various methodologies have been proposed. One such methodology was adopted in the context of the ICOLD benchmark case study, specifically the probabilistic modelling approach applied by Silva and Eleutério (2025). methodology builds upon the framework introduced by Rizzo, Maranzoni and D'Oria (2023), but is adapted to a different database, dam typology, and set of input parameters.

The probabilistic flood simulation involves discretising the range of variability of key breach parameters into defined classes. The upper value of each class is used as the representative input for dam-breach scenario generation. Each scenario ($S_{i,j}$) is thus characterised by the joint probability of two parameters: the dimensionless breach top width and the breach formation time. In this paper, higher index i values correspond to narrower breaches, while higher index j values indicate longer breach formation times.

Scenario weights were derived using the comprehensive database compiled by Bernard-Garcia and Mahdi (2020), which includes 3,861 historical dam failure records collected from 196 references, supplemented by additional datasets (FROEHLICH, 2016; WAHL, 2004; XU; ZHANG, 2009; ZHANG *et al.*, 2016). From this dataset, 2,098 observations were selected to represent embankment dam failures specifically. Among these, 121 cases included complete data on breach geometry, 50 provided data on breach formation time, and 33 offered both variables within the same record. In the study by Silva and Eleutério (2025), dam shape (narrow, intermediate, and wide) and failure mode (overtopping or piping) were identified as statistically significant grouping variables influencing breach characteristics.

For the ICOLD case study in Silva and Eleutério (2025), which involves a narrow dam subject to overtopping failure, the breach top width and formation time were each discretised into five classes. The probabilities of occurrence (i.e., scenario weights) were then derived based on the characteristics of the selected subset and are summarised in Table 4.1.

Table 4.1 – Probabilities of the dam-breach scenarios for the ICOLD benchmark case study considering overtopping.

$P(S_{i,j}\|B)$		Breach top width (m)					Total
		$B_{t_0} = 360$	$B_{t_1} = 288$	$B_{t_2} = 216$	$B_{t_3} = 144$	$B_{t_4} = 72$	
Formation time (h)	$t_{f_0} = 0.5$	0.0833	0.0500	0.0500	0.1000	0.0167	0.300
	$t_{f_1} = 1.0$	0.1167	0.0700	0.0700	0.1400	0.0233	0.420
	$t_{f_2} = 1.5$	0.0333	0.0200	0.0200	0.0400	0.0067	0.120
	$t_{f_3} = 2.0$	0.0222	0.0133	0.0133	0.0267	0.0044	0.080
	$t_{f_4} = 5.5$	0.0222	0.0133	0.0133	0.0267	0.0044	0.080
	Total	0.278	0.167	0.167	0.333	0.055	**1**

The probabilistic flood mapping covered an area of 77.4 km², considering the maximum simulated extent of the scenario $S_{0,0}$, of which 84.0% of the areas were found to have a 100% probability of inundation in the event of a dam failure. The inundation boundary derived from a deterministic scenario, using breach characteristics estimated by Froehlich's (2008) equations, encompassed all areas where the probability of inundation exceeded 0.4. This deterministic inundation extent covered 69.3 km², corresponding to 90.0% of the total probabilistically inundated area (Figure 4.4).

Figure 4.4 – Flood probabilistic inundation boundary map for the overtopping scenario of the ICOLD benchmark dam.

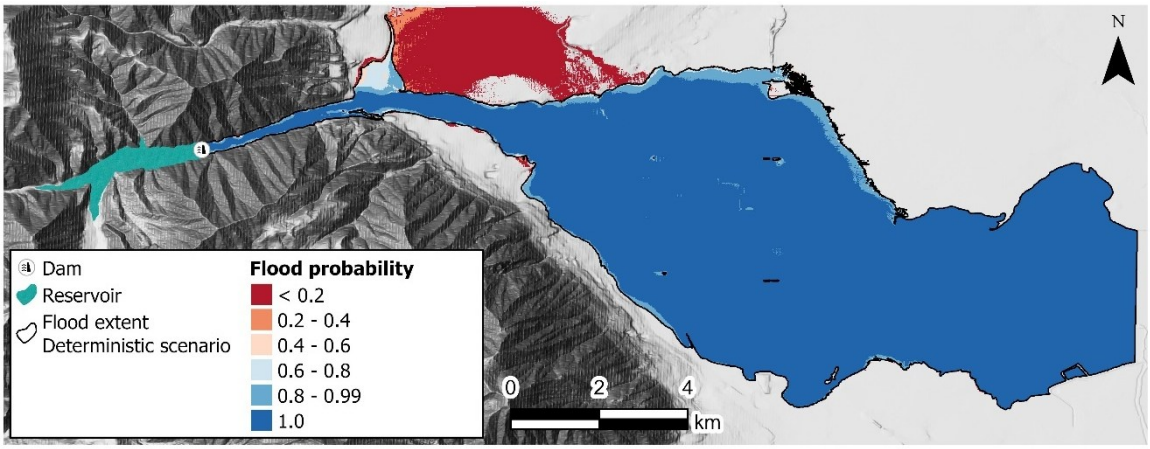

Following the hazard classification methodology proposed by Smith, Davey and Cox (2014), where classes HC 1 to HC 6 denote increasing levels of danger, with HC 1 being the lowest and HC 6 the highest, the probabilistic flood hazard mapping indicates that the narrow downstream valley exhibits a 100% probability of experiencing the most severe hazard levels. In this area, conditions are deemed unsafe for both vehicles and pedestrians, and all types of buildings are considered vulnerable to structural failure. Conversely, the flatter downstream regions are associated with intermediate hazard

classes. While these areas still pose risks to vehicles and pedestrians, they offer relatively safer building conditions (Figure 4.5).

Figure 4.5 – Flood hazard probabilistic map for each hazard classification: (a) HC 1; (b) HC 2; (c) HC 3; (d) HC 4; (e) HC 5; and (f) HC 6 — overtopping scenario of the ICOLD benchmark dam.

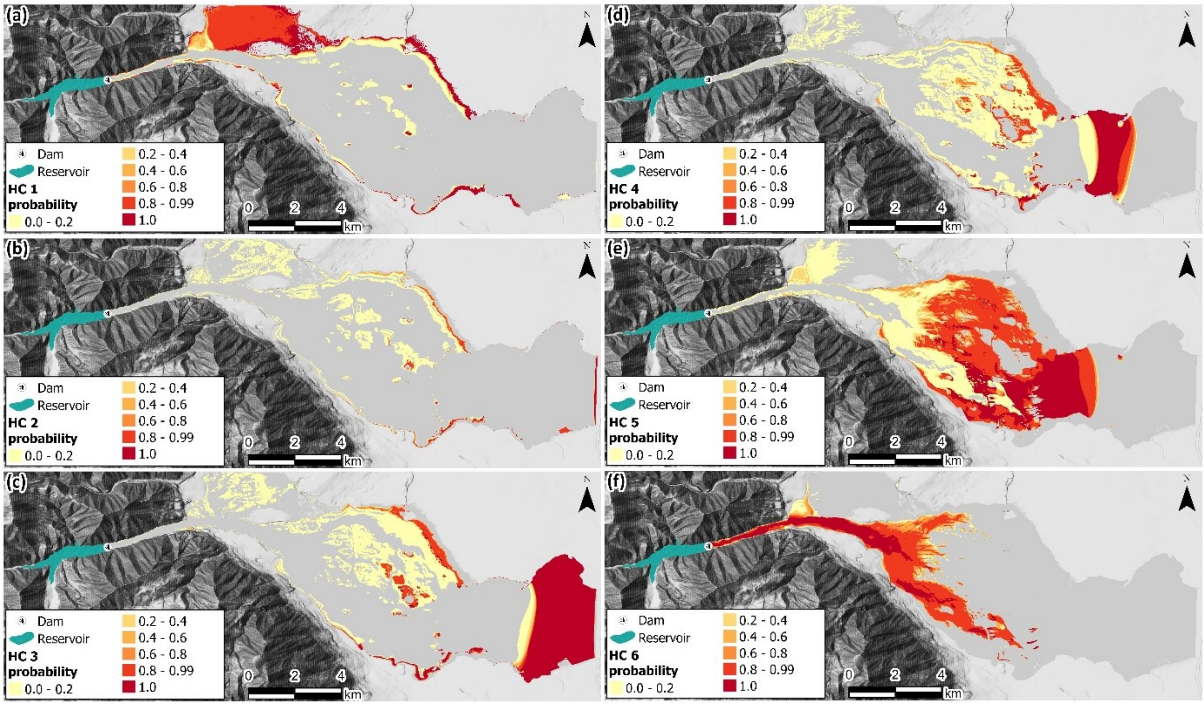

4.4.2 Probabilistic population distribution

The spatial distribution of the population can vary temporally, particularly in regions with a high concentration of commercial activity. In the ICOLD case study, buildings were defined based on parcel zone data (Figure 4.1), while population data were derived from census blocks (Figure 4.2). Buildings classified as utilities, transportation, open space recreation, agricultural, and those without any classification were excluded from the analysis.

Two population distribution scenarios were considered: one representing non-business hours and the other representing business hours. For the non-business hours scenario, census block populations were allocated to residential buildings, weighted by building size and number of floors. In contrast, during business hours, individuals identified as part of the working population were redistributed across all non-residential buildings, also weighted by building size and number of floors. The proportion of individuals aged above and below 65 was also analysed, as the LifeSim model considers age-specific exposure when estimating submergence-related vulnerability

inside buildings. Once the population distribution was completed, the parcel zones were converted into a point shapefile, which was required as input for LifeSim by calculating the centroid of each parcel.

The study area encompasses a total population of 106,325 individuals, including 18,302 people aged 65 and older and 88,023 under the age of 65, distributed across 37,817 parcel zones considered in the analysis. Since the majority of commercial parcel zones are located outside the flood hazard area (Figure 4.1), the number of directly affected individuals in the hazardous dam-breach scenario $S_{0,0}$, varies depending on the time of day. 31,862 individuals are exposed during non-business hours, whereas this number slightly decreases to 31,261 during business hours.

As illustrated in Figure 4.6, most of this variation in residential zones occurs in the flatter downstream areas of the inundation zone, extending over 10 kilometres, where the flood arrival time is approximately 1.5 hours. However, some differences are also observed further downstream in the narrow valley segment, where the flood arrival time is less than 30 minutes (SILVA; ELEUTÉRIO, 2025).

Figure 4.6 – Population variation across parcel zones in the ICOLD benchmark case study between non-business and business hours.

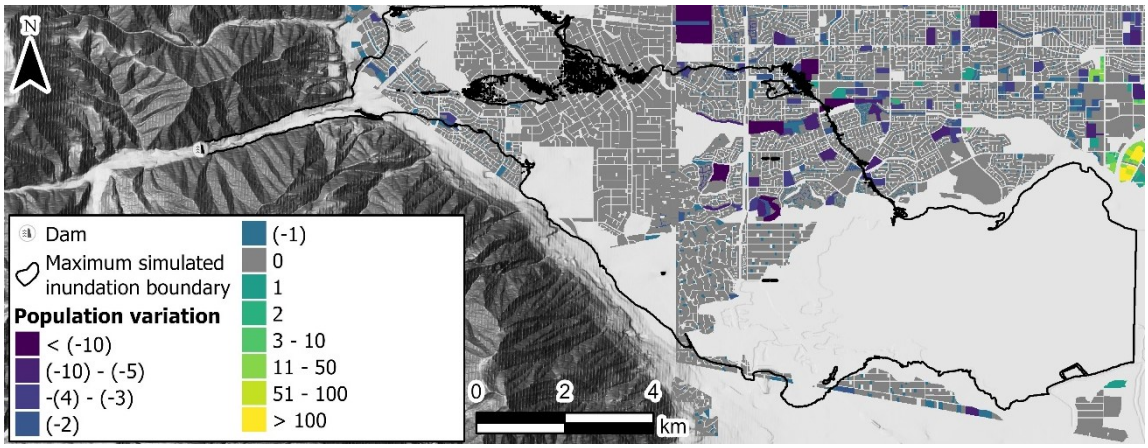

The probabilistic weighting of each scenario was defined following the approach of Maranzoni, D'Oria and Rizzo (2023b). Business hours, referred to as working hours, were defined as the period from 08:00 to 17:00, while non-business hours encompassed all other times of the day. Based on a weekly temporal distribution, the corresponding weights were calculated as 0.268 for business hours and 0.732 for non-business hours.

4.4.3 Probabilistic life-loss estimation

The LifeSim routine employs a fixed seed to ensure the reproducibility of simulations. This guarantees that the sampling of uncertainty parameters remains consistent across iterations when input conditions, such as the structure inventory and the warning and evacuation procedures, are held constant. For instance, the first iteration of each dam-breach and population distribution scenario utilises an identical sampled curve for both warning diffusion and mobilisation processes.

The proposed framework for probabilistic simulation of loss of life builds upon this feature by incorporating probabilistic inputs for both flood and population distribution scenarios. A weighted mean ($\mu_{P_{LOL}}^{(n)}$) and standard deviation ($\sigma_{P_{LOL}}^{(n)}$) are computed for each simulation iteration, as defined in Equations 15 and 16. This approach aggregates the results of multiple flood scenarios, characterised by combinations of the dimensionless breach top width (B_t/L_{cr}) and breach formation time (t_f), along with the population distribution scenario N_{par}. Each combination is associated with a scenario-specific probability weight ($P_{i,j,k}$) and an iteration estimation of loss of life ($LOL_{i,j,k}^{(n)}$).

$$\mu_{P_{LOL}}^{(n)} = \sum_{i=0}^{N_{B_t/L_{cr}}-1} \sum_{j=0}^{N_{t_f}-1} \sum_{k=0}^{N_{N_{PAR}}-1} P_{i,j,k}\, LOL_{i,j,k}^{(n)} \tag{15}$$

$$\sigma_{P_{LOL}}^{(n)} = \sqrt{\sum_{i=0}^{N_{B_t/L_{cr}}-1} \sum_{j=0}^{N_{t_f}-1} \sum_{k=0}^{N_{N_{PAR}}-1} P_{i,j,k}[LOL_{i,j,k}^{(n)} - \mu_{P_{LOL}}^{(n)}]^2} \tag{16}$$

For the ICOLD benchmark case, the weighted mean and standard deviation of life-loss estimation were calculated from an ensemble of 50 scenarios, combining five variations of breach top width, five variations of formation time, and two population distributions.

4.4.4 General LifeSim model inputs, considerations and warning and evacuation scenarios

LifeSim version 2.1.5 (USACE, 2025) was employed to probabilistically assess dam breach fatalities for the ICOLD benchmark case study. Four scenarios were developed

to evaluate the proposed framework, combining variations in warning issuance timing, warning system efficiency, and population preparedness. Table 4.2 summarises the assumptions and configurations applied across the LifeSim modules, with further details provided below within this section.

Table 4.2 – Summary of LifeSim module inputs and parameters for life-loss simulations in the ICOLD benchmark case study.

Module	Input and parameter	Description
Flood routine	Hydraulic data	HEC-RAS simulations of Silva and Eleutério (2025)
Loss of shelter	Buildings	Centroids of the parcel zones
	Population	Census block
	Building stability	Thresholds for engineered constructions as proposed by USACE (2020) based on Clausen and Clark (1990)
	People submergence	Water depth thresholds for the highest reachable floor of the buildings, considering the ages of the defined proportion of people with some mobility issue
Warning and evacuation	First warning issuance	One deterministic scenario assumed warning issuance at the moment of dam failure. In contrast, the probabilistic scenario considered a uniform distribution of warning issuance times, ranging from 24 hours prior to the failure up to the moment of failure
	Warning diffusion delay	Theoretical scenarios based on Sorensen and Mileti (2015c)
	Mobilisation delay	Theoretical scenarios based on Sorensen and Mileti (2015e)
	Road network	Census block boundaries, considering all delineating lines as primary roads according to the OpenStreetMap classification system.
	Safe evacuation places	Set outside the maximum simulated flood extent along the valley
	Evacuation route	Optimal path defined by the Dijkstra (1959) algorithm
	Evacuation delay	Vehicle speed defined by the OpenStreetMap road classification and modified Greenshield traffic flow model (MAHMASSANI *et al.*, 2009). Constant speed of 6.44 km h^{-1} for pedestrians
	Exposure to trapped people	Stability criteria defined by USACE (2020) and based on Smith et al. (2017) for vehicles and Shand et al. (2011) for people.
	Evacuation parameters	Evacuation was assumed to occur with 50% of individuals evacuating by vehicle and 50% on foot. In residential buildings with fewer than four occupants, all warned individuals were assumed to initiate evacuation simultaneously
Loss of life	Fatality rates	Probability distributions for two hazard zones defined by USACE (2020) based on historical cases

Initially, two scenarios with a fixed relative warning issuance time were evaluated, coinciding with the moment of dam failure. The first represents an optimal scenario (S1.1), characterised by a highly effective warning system that utilises multiple communication channels for rapid and widespread alert dissemination, frequent message repetition, and a well-prepared and trained population. The second, a suboptimal scenario (S1.2), reflects a less efficient warning system, relying on limited technological resources and issuing alerts infrequently, thereby constraining timely dissemination. In this case, a significant portion of the population is unlikely to perceive the threat, and their response tends to be largely improvised. The warning dissemination and response curves for these scenarios were adapted from Sorensen and Mileti (2015b, 2015c) (see Appendix, section 4.7.1). Subsequently, two additional scenarios were analysed, in which the relative warning issuance time was treated as a probabilistic variable. A uniform distribution was assumed, ranging from 24 hours before the dam failure to the failure moment. Among these, one scenario reflected optimal warning conditions (S2.1), while the other corresponded to suboptimal conditions (S2.2), consistent with previously described conditions.

Under the optimal warning and high preparedness conditions, the population's evacuation response is characterised by a central tendency, indicating that approximately 85% of individuals commence evacuation within four hours of receiving a warning, with this proportion reaching approximately 95% after 24 hours. Conversely, the situation is considerably more critical in the suboptimal scenario. The central tendency shows that only around 40% of the population begins evacuation within four hours, with the maximum reaching 82.5% after 24 hours (Figure 4.7).

Figure 4.7 – Population mobilised after the warning issuance for the optimal and suboptimal scenarios.

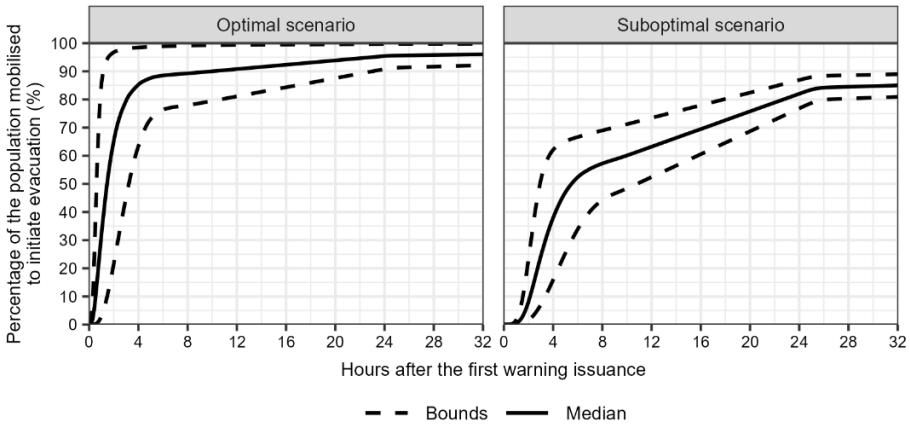

Regarding evacuation dynamics, it was assumed that half of the population evacuated on foot and the other half by car. As the study's primary objective was to evaluate a probabilistic framework, sensitivity analyses related to this assumption were not performed. The evacuation network was defined using census block boundaries. Given that the case study referred to a fictional location, OpenStreetMap data were not applicable; therefore, the boundaries were considered representative of primary roads according to OpenStreetMap classification standards. Evacuation destinations were located along the valley, beyond the maximum simulated flood extent. Furthermore, buildings accommodating more than three individuals were identified, based on the assumption that warning dissemination and population mobilisation did not coincide for all occupants. This threshold also defined the size of the evacuating group in the model.

For the scenarios with a fixed time window for the initial warning issuance, 3,000 iterations were performed. For those incorporating a probabilistic warning time, 12,000 iterations were conducted, based on convergence tests of the estimations (see Appendix, Section 4.7.1). Non-parametric statistical tests were employed to assess the differences in estimated fatalities across scenarios, including those developed by Dunn (1964), Kruskal and Wallis (1952) and Mann and Whitney (1947). Additionally, two deterministic flood scenarios were simulated for both business and non-business hours, based on Froehlich's (2008) equations, which are commonly used in traditional dam-breach flood modelling.

These scenarios, along with the most probable scenario (highest probability of occurrence, weight = 0.1025, represented by the flood scenario $S_{3,1}$ with population distribution during non-business hours), the best-case scenario (lowest estimated fatalities, represented by the flood scenario $S_{4,4}$ with population distribution during business hours), and the worst-case scenario (highest estimated fatalities, represented by the flood scenario $S_{0,0}$ under non-business hours population distribution), were selected from the 50 simulations and used as benchmarks for comparison with the proposed probabilistic framework.

4.5 Results and discussion

4.5.1 Fixed warning issuance time

Regarding the optimal scenario of warning dissemination and population mobilisation (S1.1), the median fatality rate in the weighted mean scenario is 0.089, with an interquartile range of 0.088 to 0.090 (Figure 4.8). The variability around this scenario includes a median value of 0.072 for one standard deviation below the weighted mean (range: 0.067 to 0.074), and a median of 0.107 for one standard deviation above the weighted mean (range: 0.103 to 0.110). Both deterministic scenarios exhibit variability that falls between the weighted mean scenario and the scenario incorporating one standard deviation above the weighted mean. In the non-business hours scenario, the median fatality rate is 0.099, with an interquartile range of 0.096 to 0.103. While for business hours, the median is 0.097, with an interquartile range of 0.094 to 0.100. The deterministic scenarios differ significantly from the weighted mean scenario and associated variability ($p < 0.05$). The only situation in which the probabilistic framework does not yield a statistically significant difference is when comparing the weighted mean plus one standard deviation to the flood scenario $S_{1,0}$ with the population distribution during business hours ($p = 0.291$).

Figure 4.8 – Life-loss estimation for the optimal scenario with the warning issued at the moment of dam failure caused by the overtopping of the ICOLD benchmark dam.

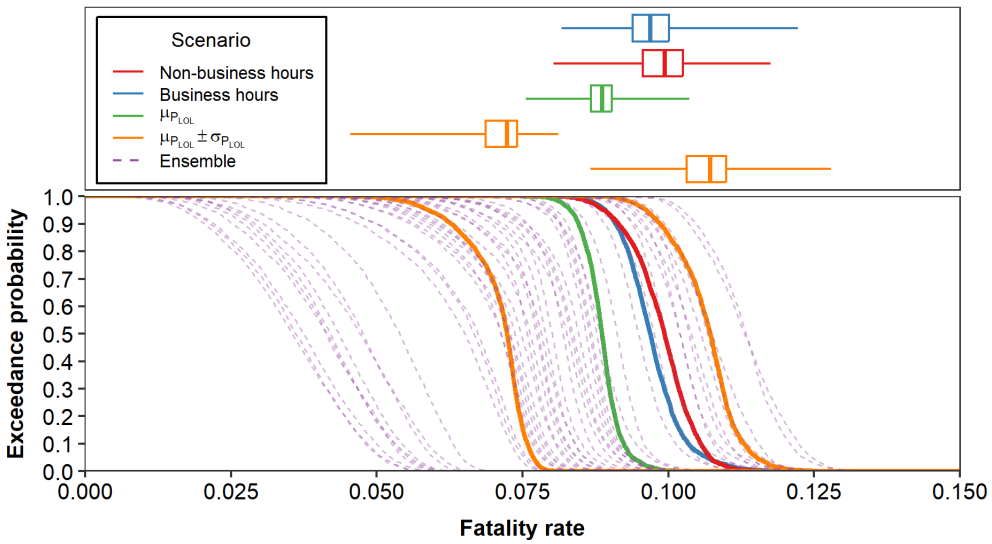

In the suboptimal scenario of warning dissemination and population mobilisation (S1.2), the median fatality rate in the weighted mean scenario is 0.076, with an

interquartile range of 0.075 to 0.077 (Figure 4.9). Variability includes a median of 0.067 for one standard deviation below the weighted mean (range: 0.065 to 0.068), and 0.085 for one standard deviation above (range: 0.083 to 0.087). As with the optimal scenario, both deterministic scenarios fall within the range between the weighted mean and its upper variability bound. In the non-business hours scenario, the median fatality rate is 0.079, with an interquartile range of 0.077 to 0.081. The business hours scenario yields approximately the same values as the non-business hours scenario. Again, the deterministic scenarios differ significantly from the weighted mean scenario and its associated variability ($p < 0.05$). In this case, the probabilistic framework yields statistically significant differences across all simulated scenarios.

Paradoxically, a lower number of fatalities is observed in the suboptimal scenario than in the optimal one. The flood arrival time for most of the affected population ranges from approximately 30 minutes to 1.5 hours. This corresponds to a median population mobilisation of 8% to 51% in the optimal scenario, whereas in the suboptimal scenario, mobilisation ranges from negligible to just 2.5% (Figure 4.7). Consequently, when the warning is issued at the moment of the dam breach, a greater proportion of the population may be on the streets or in transit when the flood reaches populated areas under the optimal warning dissemination and mobilisation conditions. Other studies have reported similar findings employing life-loss agent-based models (SILVA *et al.*, 2025).

Figure 4.9 – Life-loss estimation for the suboptimal scenario with the warning issued at the moment of dam failure caused by the overtopping of the ICOLD benchmark dam.

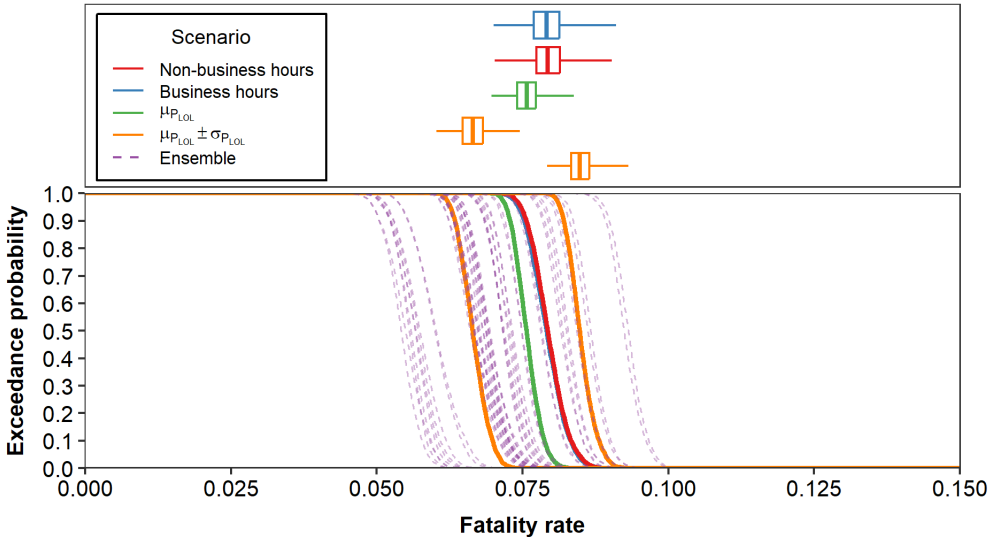

4.5.2 Probabilistic warning issuance time

For optimal warning dissemination and population mobilisation under probabilistic scenarios of warning issuance time, analysis of the estimated fatalities at each hourly interval reveals that five to six hours is the minimum lead time required before the dam breach to issue the warning, thereby statistically significantly reducing the potential loss of life. A more consolidated and consistent reduction, indicated by statistically insignificant differences in estimated fatalities between adjacent hourly intervals, emerges around eight to nine hours before the breach (Figure 4.10). This trend is generally the same across all scenarios. However, in the best-case scenario (represented by the flood scenario $S_{4,4}$ with population distribution during business hours), a significant reduction in estimated fatalities begins when the warning is issued four to five hours before the breach.

Although the required warning lead time remains the same when comparing the weighted mean and its variability with the deterministic scenarios, the estimated fatality values differ significantly across scenarios. The exception is the comparison between the weighted mean and the most probable scenario ($S_{3,1}$ with population distribution during non-business hours, weight = 0.1025), where no significant difference ($p > 0.05$) is observed for any issuance time. In this case, the values are quite similar: for one hour before breach, both the weighted mean and the most probable scenario have a median estimated fatality rate of 0.072 with interquartile ranges of 0.059–0.082 and media of 0.071 and with interquartile ranges 0.059–0.081 respectively; for five to six hours before breach, both have a median of 0.009 (with interquartile ranges of 0.006–0.011 in both cases).

The fatality rates for the non-business and business hours show the same median value of 0.009 for warnings issued five to six hours before the dam breach, with interquartile ranges of 0.007–0.012. This represents a median reduction of 89.1% and 88.0%, respectively, compared to warnings issued one hour before the breach. For warnings issued earlier than five to six hours prior to the breach, no statistically significant differences are observed between business and non-business hours.

Overall, both scenarios exhibit higher estimated fatality rates than the weighted mean. However, no statistically significant differences are found at a high level ($p < 0.001$)

when warnings are issued more than four to five hours before the dam failure. In contrast, these deterministic scenarios show lower estimated fatalities than the weighted mean plus one standard deviation, with statistically significant differences observed across most time intervals. Nevertheless, the weighted mean plus one standard deviation scenario does not exceed the estimated fatalities of the worst-case scenario, represented by $S_{0,0}$ flood scenario under non-business hours population distribution. In this worst-case scenario, the median fatality rates for warnings issued five to six hours before the breach are 0.010 (interquartile range: 0.007–0.013) for the weighted mean plus one standard deviation scenario, and 0.011 (interquartile range: 0.008–0.014) for the worst-case scenario itself.

Figure 4.10 – Estimation of life loss in the optimal scenario, accounting for probabilistic warning issuance between the dam failure and 24 hours before, triggered by overtopping of the ICOLD benchmark dam.

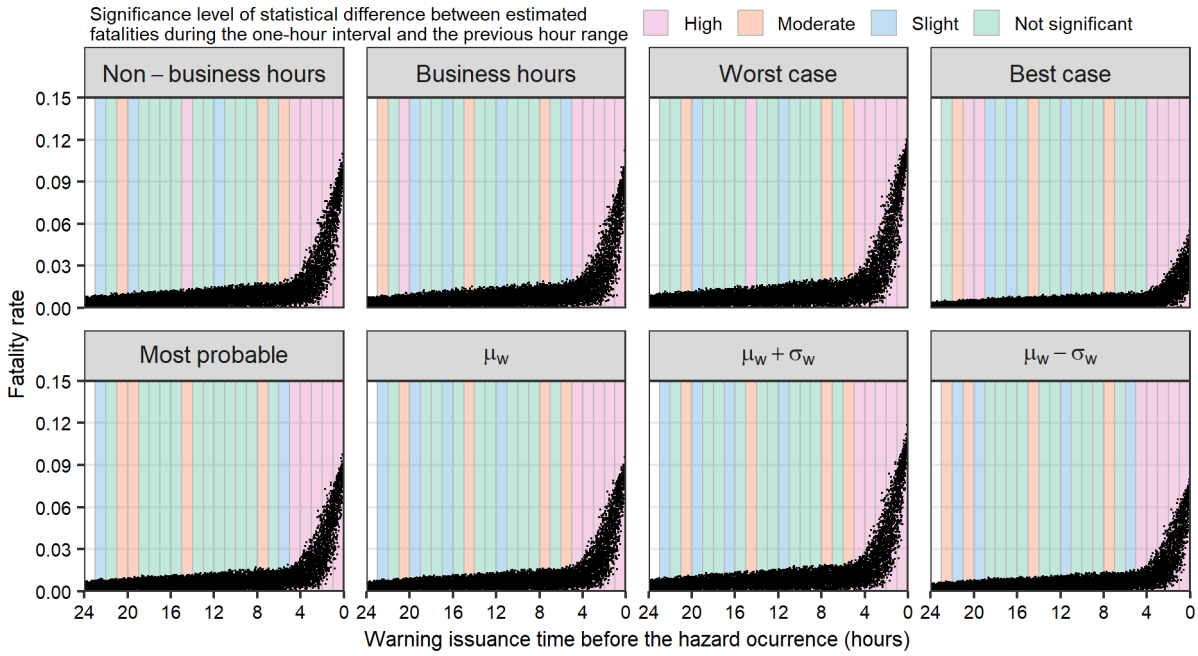

Under suboptimal warning dissemination and population mobilisation, and considering probabilistic scenarios of warning issuance time, there is no defined minimum lead time for statistically significant stabilisation of estimated life loss, neither for deterministic scenarios nor for the weighted mean and its variability. In all cases, an earlier warning consistently significantly reduces life loss compared to the immediately later warning interval (Figure 4.13). This trend can be understood in relation to the timing of warning issuance and its dissemination, as well as the resulting population

response, as illustrated in Figure 4.7. The median population response reaches a maximum of 84% when the warning is issued 24 hours before the dam breach, under the suboptimal scenario of warning dissemination and population mobilisation. This percentage corresponds to a lead time of four hours in the optimal scenario, where neither earlier nor later lead times result in further stabilisation of the life-loss estimates.

The comparisons among the scenarios are consistent with those observed under the optimal warning dissemination and mobilisation case. The weighted mean yields lower fatality estimates than both deterministic scenarios based on Froehlich's (2008) equations. These deterministic scenarios, in turn, produce lower estimates than the weighted mean plus one standard deviation. The worst-case scenario still results in the highest fatality estimates. However, when comparing the weighted mean to the most probable scenario, statistical differences are observed for all warning lead times, except for warnings issued three to four hours and 23 to 24 hours before the dam breach, where no statistically significant difference is found between the estimates.

Figure 4.11 – Estimation of life loss in the suboptimal scenario, accounting for probabilistic warning issuance between the dam failure and 24 hours before, triggered by overtopping of the ICOLD benchmark dam.

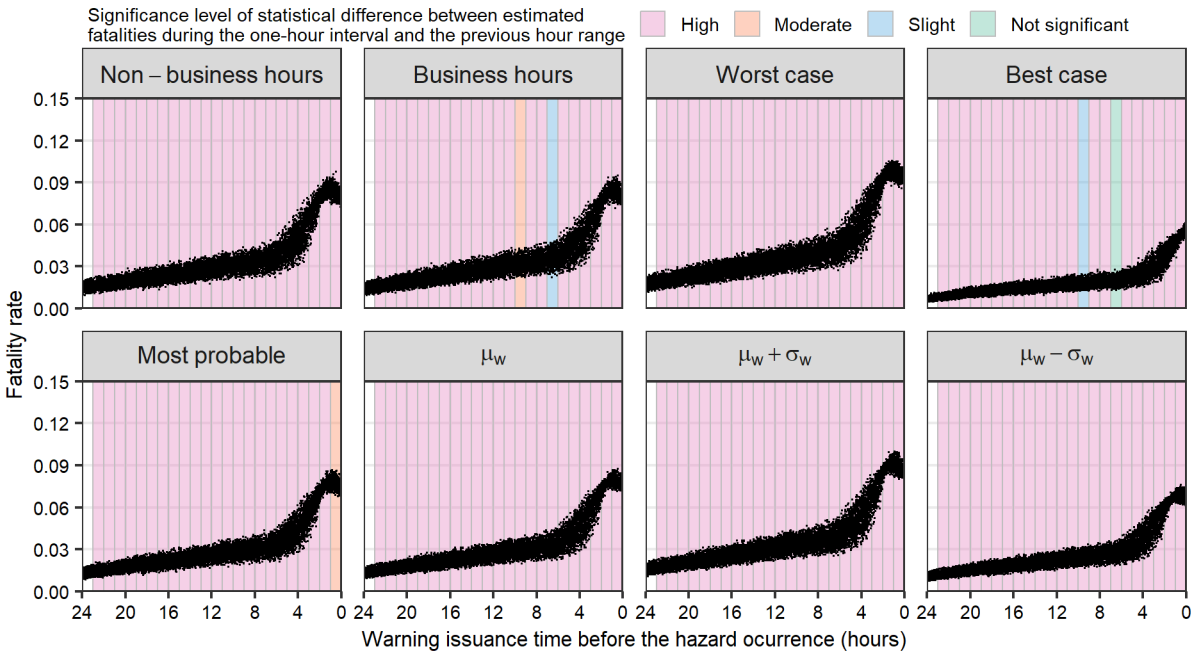

4.6 Conclusion

Agent-based life-loss estimation models are valuable for assessing the potential consequences of implementing mitigation measures to reduce flood-related fatalities. However, they still face limitations in capturing the full range of possible uncertainties. The framework proposed in this paper addresses these limitations by enabling life-loss estimation through an agent-based model that incorporates uncertainties related to flood parameters as well as spatial and temporal variations in population distribution.

This framework extends the work of Maranzoni, D'Oria and Rizzo (2023b) by employing an agent-based model instead of an empirical one, allowing for a more dynamic representation of individual behaviours during flood events. Moreover, it advances the approach of El Bilali et al. (2022) by incorporating a more comprehensive flood scenario weighting process and considering uncertainties in population distribution. While their method weighted scenarios solely based on breach peak flow, the proposed approach uses historical dam failure data to define scenario weights, resulting in a more robust and probabilistic representation of potential outcomes.

The framework is applied to the International Commission on Large Dams (ICOLD) benchmark case, using 50 weighted scenarios. Of these, 25 are related to uncertainties in dam breach parameters, breach top width and formation time, and two are associated with population distribution conditions: business hours and non-business hours. Additionally, two warning dissemination and evacuation conditions are considered, optimal and suboptimal. Two approaches to warning issuance are also analysed, one at the moment of dam failure, and another using a probabilistic issuance between 24 hours before and the time of the breach. Together, these elements are used to represent the dynamics of the warning system within the model.

The weighted mean of the probabilistic scenario generally yields lower estimated fatalities than the deterministic flood modelling scenarios. These deterministic scenarios, in turn, produce lower estimates when compared to the weighted mean plus one standard deviation. The probabilistic warning issuance approach enables the identification of lead times that significantly reduce life loss. In the optimal scenario, a warning issued five to six hours before the dam breach is the minimum required time for significantly reducing life loss. This is observed for the weighted mean (and its

variability) and the deterministic scenarios. However, this trend is not observed for any warning lead time under suboptimal conditions of warning dissemination and population mobilisation.

The patterns observed in this study are specific to the selected case study. Dam characteristics, topography, and population distribution may lead to different patterns when applying the same framework in other contexts. As a direction for future research, this framework could be applied to other case studies and compared with the methodology of El Bilali et al. (2022) and Maranzoni, D'Oria and Rizzo (2023b). Additionally, alternative strategies for calculating the weighted mean could be explored. Rather than weighting each iteration directly, one approach could involve ranking exceedance probabilities within each iteration and then applying the weighted mean to these ranked values. This could broaden the framework's applicability to other agent-based models that incorporate different uncertain input parameters and employ other sampling methods to represent input uncertainties.

4.7 Appendix

4.7.1 Warning dissemination and population mobilisation parameterisation

Several key elements influence how effectively the initial warning is disseminated to the population. These include the variety and technological sophistication of communication channels, the frequency of message broadcasts, and temporal factors such as the time of day (SORENSEN; MILETI, 2015c). In parallel, mobilisation time is shaped not only by the content and clarity of the warning but also by how individuals perceive their personal risk, as well as by situational cues and the perceived severity of the event (SORENSEN; MILETI, 2015e). To capture these complex behavioural processes, theoretical frameworks have been developed, drawing on substantial historical data spanning different types of hazards and previous research findings.

To model the proportion of the population receiving the warning at each discrete time interval (P_{warned_t}), a Rayleigh distribution is applied, supplemented by a parameter that accounts for warnings disseminated through informal or unofficial channels (Equation 17). Two parameters govern this process: b_t, which defines the efficiency of formal communication systems and functions as the shape parameter in the Rayleigh model

(with lower values indicating greater efficiency), and c_t, which captures the effectiveness of non-official communication sources at time t (SORENSEN; MILETI, 2015c). Similarly, the proportion of individuas who initiate protective action at a given time step ($P_{mobilised_t}$) is calculated using a cumulative probability function (Equation 18). Two parameters determine this function: a_m, which controls the overall pace of mobilisation (with smaller values indicating quicker responses), and b_m, the median time at which individuals are likely to begin taking action. Higher b_m values suggest a delayed overall mobilisation process, reflecting scenarios where the population takes longer to react (SORENSEN; MILETI, 2015e). Table 4.3 presents the utilised curves, their respective coefficients, and mobilisation rates for optimal and suboptimal scenarios

$$P_{warned_t} = P_{warned_{t-1}} + \left(\frac{t}{b_t^2} e^{-\frac{t^2}{2b_t^2}}\right) + \left(1 - P_{warned_{t-1}}\right) * \left(P_{warned_{t-1}} * c_t\right) \quad (17)$$

$$P_{mobilised_t} = 1 - e^{(-(t^2)/a_m {b_m}^2)} \quad (18)$$

Table 4.3 – Warning diffusion and mobilisation bounds with their coefficients and rates for the optimal and suboptimal scenarios.

Scenario	Bounds	Warning diffusion			Mobilisation					
		Curve	b_t	b_t	Curve	a_m	b_m	Maximum mobilisation rate		
								8 h	24 h	72 h
Optimal	Upper	Fast	5.0	0.100	Preparedness good perception likely	1.00	25.0	100.0	100.0	100.0
	Most likely		9.5	0.098		1.37	64.0	88.8	95.7	98.6
	Lower		51.5	0.081		1.80	114.0	77.1	91.1	97.2
Suboptimal	Upper	Slow	103.0	0.060	Preparedness poor perception unlikely	1.35	61.8	65.9	88.7	92.8
	Most likely		145.0	0.042		1.79	111.8	57.0	84.2	90.0
	Lower		150.0	0.040		2.20	161.9	48.0	79.8	87.2

A subset of historical case studies is used in the development of the warning diffusion and mobilisation curves implemented in LifeSim, along with their associated uncertainty bounds. Specifically, ten warning diffusion curves, five tailored to daytime and five to nighttime conditions, are recommended in the model. These are derived from six documented events encompassing various hazard types, such as chemical spills, hazardous material releases, volcanic eruptions, and flash floods. In parallel,

nine distinct mobilisation curves are employed, each reflecting different levels of risk perception and population preparedness. Analyses inform these three historical cases involving chemical and hazardous material incidents (SORENSEN; MILETI, 2015c, 2015e; USACE, 2020).

4.7.2 Life-loss model convergence

Figure 4.12 – Mean, standard deviation, skewness, and kurtosis of the estimated fatalities for the following deterministic warning issuance scenarios: (D1.1) optimal dissemination and mobilisation during business hours; (D1.2) optimal dissemination and mobilisation during non-business hours; (D2.1) suboptimal dissemination and mobilisation during business hours; and (D2.2) suboptimal dissemination and mobilisation during non-business hours.

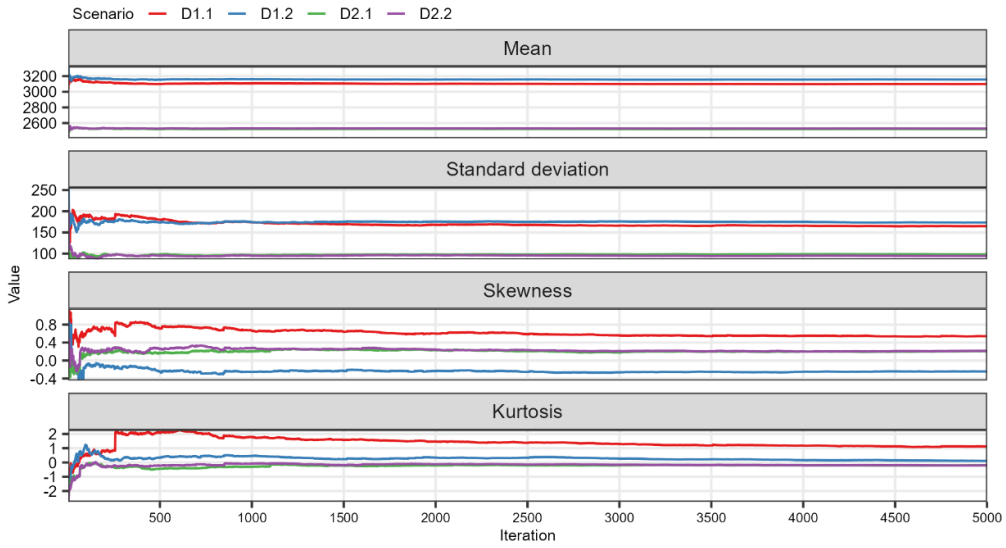

Figure 4.13 – Mean, standard deviation, skewness, and kurtosis of the estimated fatalities for the following probabilistic warning issuance scenarios: (P1.1) optimal dissemination and mobilisation during business hours; (P1.2) optimal dissemination and mobilisation during non-business hours; (P2.1) suboptimal dissemination and mobilisation during business hours; and (P2.2) suboptimal dissemination and mobilisation during non-business hours.

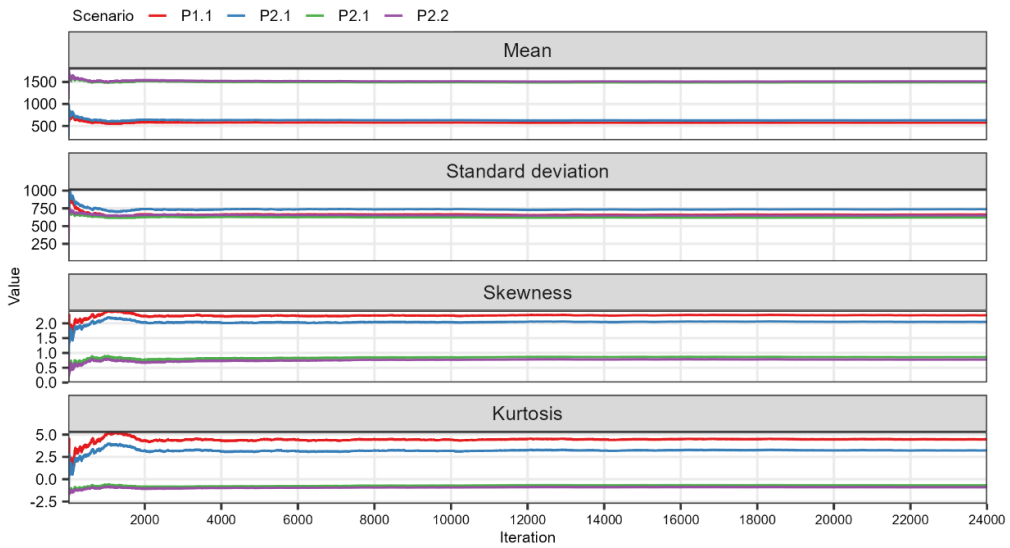

5 ASSESSING THE IMPACT OF EARLY WARNING AND EVACUATION ON HUMAN LOSSES DURING THE 2021 AHR VALLEY FLOOD IN GERMANY USING AGENT-BASED MODELLING[2]

5.1 Abstract

Between 12 and 19 July 2021, a quasi-stationary atmospheric low-pressure system named Bernd caused intense precipitation on already-saturated soil, resulting in severe flooding in Germany, Belgium, and the Netherlands. The Ahr Valley in Rhineland-Palatinate was particularly affected, with approximately 42,000 residents impacted, around 8,800 buildings damaged, and 134 fatalities recorded. The flood in the Ahr Valley significantly exceeded the scenarios outlined in official hazard maps, leaving decision-makers and the public unprepared. Substantial issues occurred with the content, issuance, and dissemination of warnings, thereby reducing the effectiveness of emergency response. We evaluate how human losses in the Ahr Valley might have differed under alternative flood early warning and evacuation (FEWE) scenarios, using the agent-based model LifeSim. To run the model for the 2021 Ahr flood, we utilised a reconstructed modelled time series of water depth and flow velocities and estimated the FEWE timeline based on reports and a post-event survey of the affected population. For the reconstructed FEWE timeline, we identified the first flood warning approximately 13 hours before the peak of the flood upstream of the simulated domain. Only 17.5% of those affected received a warning with evacuation instructions, with most becoming aware of evacuation necessities only after flooding had already reached them. Consequently, only about 34% of the population evacuated their homes or were rescued. Regarding the life-loss estimation, the median of the reconstructed flood overestimates the actual life loss by 28.8%. Simulations of alternative FEWE scenarios indicate a potential life-loss reduction of up to 80% with timely warning dissemination and increased population evacuation. However, scenarios in which the FEWE prompted the population to evacuate at the moment of the imminent hazard at their buildings result in higher human losses. In these cases, vertical evacuation within buildings is more effective. Using a life-loss agent-based

[2]This chapter was published by (SILVA *et al.,* 2025) in: SILVA, A. F. R.; ELEUTÉRIO, J. C.; APEL, H.; KREIBICH, H. Assessing the impact of early warning and evacuation on human losses during the 2021 Ahr Valley flood in Germany using agent-based modelling. **Natural Hazards and Earth System Sciences**, v. 25, n. 4, p. 1501–1520, 2025. Disponível em: https://doi.org/10.5194/nhess-25-1501-2025.

model, such as LifeSim, can support decisions on FEWEs and improve emergency response planning.

5.2 Introduction

Floods represent the most prevalent natural disaster globally (CRED; UNISDR, 2018), and under a climate change scenario, their frequency, particularly of rare events, has increased (WASKO *et al.*, 2021). In Germany, four flood events have been notable in terms of loss of life during the last 40 years. In August 2002, a record-breaking daily rainfall of 314 mm in 24 hours caused flash floods in the Bavarian and Saxon middle hills of Germany. This extreme weather event resulted in the activation of dam spillways, as well as the overtopping and breaching of embankments in many areas, leading to the deaths of 21 people (KIENZLER *et al.*, 2015). Between 31 May and 3 June 2013, precipitation of 346 mm fell on already-saturated soil, affecting 12 of Germany's 16 federal states. Approximately 1,400 kilometres of river networks experienced 100-year flood discharges and some dike breaches, resulting in 14 fatalities (THIEKEN *et al.*, 2022). From 26 May to 9 June 2016, a series of flash floods, including peaks of 100 mm in 2 h in Braunsbach, a small village in Baden-Württemberg, caused significant damage to small and steep catchments, resulting in 11 fatalities (THIEKEN *et al.*, 2022). In July 2021, the most devastating flood event occurred in terms of fatalities. In total, fewer people died in the 40 years between 1980 and 2020, with 159 victims (PAPAGIANNAKI *et al.*, 2022), than in this single 2021 flood event, with 190 victims in Germany (THIEKEN *et al.*, 2023; THIEKEN; ZENKER; BUBECK, 2023).

The extraordinary severe event in July 2021 was caused by a quasi-stationary atmospheric low-pressure system named Bernd. This system brought intense precipitation on already-saturated soil, resulting in severe flooding in the western German states, mainly along the Ahr River, located in the Rhineland-Palatinate state. Hydrologically, the 2021 flood was extreme in terms of the rapid onset of flooding, high flow velocities, and high water depths (KRON *et al.*, 2022). Along the Ahr, about 42,000 inhabitants were affected by the flood, about 8,800 buildings were damaged (DKKV, 2022), and 134 fatalities had occurred (SZÖNYI *et al.*, 2022).

The flood extent significantly exceeded what was outlined in official hazard maps, leaving decision-makers and the population unprepared. This lack of preparedness resulted in numerous issues with the warning content and its issuance and dissemination, compromising the efficiency of residents taking protective measures (SZÖNYI *et al.*, 2022). A survey conducted after the event revealed that 29% of Ahr Valley residents reported not receiving any warning, and among those who were warned, over 40% did not know what to do to protect themselves and their houses. Consequently, 84% of residents were surprised by the magnitude of the flood (THIEKEN *et al.*, 2023).

One of the most critical factors contributing to fatalities during floods is the effectiveness of flood early warning and evacuation (FEWE) systems (PETRUCCI, 2022; YARI *et al.*, 2020). An optimal warning system should be robust, capable of early hazard identification, and equipped with efficient communication channels to promptly inform the population at risk (KREIBICH; HUDSON; MERZ, 2021; KULLER; SCHOENHOLZER; LIENERT, 2021). Additionally, an investment in enhancing the population's knowledge of appropriate actions and behaviours in response to flood risks is essential (AERTS *et al.*, 2018; BERGHÄUSER *et al.*, 2023). This comprehensive approach could significantly mitigate the impact of floods and reduce the likelihood of fatalities.

One method to assess the effectiveness of these FEWE systems is through life-loss estimation models (CHEN *et al.*, 2023; GE *et al.*, 2022). In estimating fatalities from flood events, some methodologies incorporate behavioural assessments and macroeconomic indicators to evaluate the impacts of floods (JONGEJAN; JONKMAN; VRIJLING, 2005). However, assigning a monetary value to the loss of life is complex due to the intangible nature of this type of damage (MERZ *et al.*, 2010). Fatalities can also be indirectly related to flooding, occurring outside the inundated areas through incidents such as traffic accidents during evacuations or deaths due to post-flood stress. Despite these indirect impacts, most fatalities result from direct causes (JONKMAN; VRIJLING, 2008). Since predicting such behaviour is challenging, loss of life is generally classified solely as a direct type of damage. Therefore, risk assessment addresses this metric directly and quantitatively without assigning a monetary value (JONKMAN; VAN GELDER; VRIJLING, 2003).

Life-loss estimation models can be categorised as either empirical or dynamic. The empirical approach integrates some characteristics of the flood event, such as depth, velocity, water rise rate, warning time, and other factors related to the exposure and vulnerability of the population, with a fatality rate. Various empirical models exist for different types of events, including coastal and riverine floods (BOYD; LEVITAN; VAN HEERDEN, 2005; BRAZDOVA; RIHA, 2014; JONKMAN *et al.*, 2009; JONKMAN; VRIJLING; VROUWENVELDER, 2008; PENNING-ROWSELL *et al.*, 2005; YAZDANI *et al.*, 2023; ZHAI; FUKUZONO; IKEDA, 2006) and dam breaks (BROWN; GRAHAM, 1988; DEKAY; MCCLELLAND, 1993; GE *et al.*, 2021; GRAHAM, 1999; JIAO; LI; MA, 2022; MAHMOUD; WANG; JIN, 2020; PENG; ZHANG, 2012; USBR, 2015). Dynamic models, often called agent-based models (ABMs), use a time-varying quantification of event characteristics correlated with flood exposure criteria and thresholds. These models provide a more detailed simulation of events by modelling individual behaviour and the causes of fatalities (ANSHUKA *et al.*, 2022; ZHUO; HAN, 2020). This detailed simulation is beneficial for evaluating FEWE systems, offering advantages over empirical models (DI MAURO; DE BRUIJN; MELONI, 2012; SHIRVANI; KESSERWANI, 2021).

Numerous agent-based models related to flood risk management have been developed (ANSHUKA *et al.*, 2022). However, most of these models are designed for specific sites and types of floods and have been applied only in limited research contexts. As a result, only two models have been widely used in flood risk assessment (LUMBROSO; DAVISON; WETTON, 2023). The Life Safety Model (LSM) (JOHNSTONE *et al.*, 2005) was utilised to assess the impacts of FEWE in the 1953 Canvey Island flood (LUMBROSO; DAVISON, 2018) and in the 2019 Brumadinho tailing dam break event (LUMBROSO *et al.*, 2021). The LifeSim model (ABOELATA; BOWLES, 2005a) was employed to create a generalised life-loss estimation model for dam breaks in Switzerland (KALININA; SPADA; BURGHERR, 2021), for traffic management in Morocco (EL BILALI; TALEB; BOUTAHRI, 2021), and in a proposal for a probabilistic life-loss estimation for densely populated areas in Morocco (EL BILALI *et al.*, 2022). Additionally, it was used to assess warning and evacuation procedures and their impacts in Brazil for the 2007 São Francisco tailing dam failure (SILVA; ELEUTÉRIO, 2023a) and for a hypothetical case in a high-density area

(SILVA; ELEUTÉRIO, 2023b), as well as in order to evaluate the effects of numerous non-structural dam break floods in China (WANG *et al.*, 2024).

The objective of this study is to assess the exceptionally high number of fatalities in the Ahr Valley during the flash flood of 2021. With the help of an ABM, in particular, the effects of FEWE are analysed. Scenarios are used to develop recommendations for improved emergency communication and response. Given the extensive variety of flood types (Needham et al., 2016) and their widespread application in diverse contexts (e.g. flash floods, dike and dam breaches), the agent-based model LifeSim was chosen for this study.

Section 5.3 outlines the data and methods, providing an overview of the agent-based model LifeSim and detailing its principal inputs and operational considerations. A reconstruction of the human consequences of the 2021 Ahr Valley flood is examined, including flood modelling, exposure analysis, and flood early warning and evacuation procedures. The section concludes with an exploration of alternative warning and evacuation scenarios, as well as general parameterisation and considerations regarding the use of LifeSim. Section 5.4 presents and analyses the results of the LifeSim model for human consequence reconstruction and evaluates the impacts of the alternative FEWE scenarios. Section 5.5 highlights the main limitations of the simulations. Finally, Section 5.6 summarises the key findings of this study and suggests areas for further research.

5.3 Data and methods

The concept of assessing the impact of flood early warning and evacuation (FEWE) on loss of life consists of two main parts (Figure 5.1). First, the reconstruction of the 2021 Ahr Valley flood is undertaken to compare the life-loss estimation by the agent-based model LifeSim with the actual values. This involves updating an existing hydraulic model, creating a structure inventory with information on buildings and the population, and reconstructing the warning and evacuation procedures. Second, the impact of alternative scenarios of FEWE is assessed. Once the life-loss model is adjusted to the actual case, two approaches are used to assess the effectiveness of FEWE: one focuses on the efficiency of communication and response using theoretical models of warning dissemination and the mobilisation time taken for the population to

begin evacuation, and the other focuses on the timing for issuing the first flood warning considering forecasting capabilities.

Figure 5.1 – Overview of concept showing methodological components and data relationships for assessing the impacts of early warning and evacuation procedures on life-loss estimation in relation to the 2021 Ahr Valley flood.

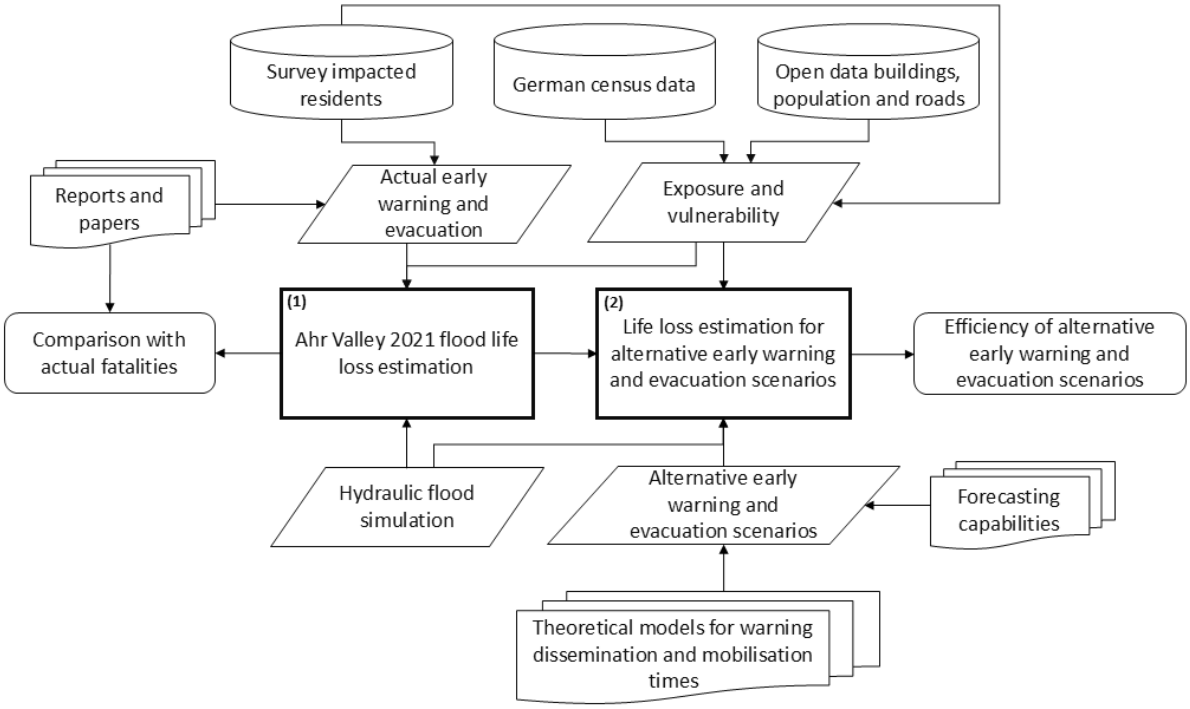

5.3.1 LifeSim agent-based model used to estimate direct flood fatalities

LifeSim was initially proposed by Aboelata et al. (2003) and has since been integrated into a graphical interface by the United States Army Corps of Engineers. This model simulates various outcomes, with a focus on direct life loss resulting from exposure to flood hazards, where the magnitude of life loss is influenced by hydrodynamic parameters and the success of the population in locating adequate shelter during flood events. The model is structured with a modular system in which the agent-based approach allows for the description and simulation of individual and group behaviours. These modules integrate hydrodynamic spatial- and time-dependent data and population characteristic data based on geographic information system layers (USACE, 2020).

The LifeSim model comprises four main modules. The first is the flood routine module, which encompasses a network representation of flood characteristics across the area over time. The shelter loss module, which assesses the exposure of the population

that does not evacuate structures during events, considers submersion and structural damage criteria. The warning and evacuation module models the distribution and dynamics of the at-risk population following the warning issuance. Finally, the loss of life module employs probability distributions of fatality rates derived from historical flood event data to estimate potential fatalities (USACE, 2020). A short description of each module related to life-loss estimation is provided in the following paragraphs based on LifeSim version 2.0 (USACE, 2021).

The flood routine module contains hydraulic data about the flood event, encompassing temporal developments of water depth and flow velocities.

The submersion criteria of the shelter loss module are based on thresholds defined by a triangular distribution, determined by the water depth on the highest floor of a building. For the general population, these thresholds correspond to the ceiling level, while for individuals with mobility issues, they also pertain to the floor level. When access to the building's roof is feasible, the threshold is related to the roof floor. If these thresholds are exceeded, the population is designated into the high-hazard zone, where a specific fatality rate is applied according to the life-loss module. Mobility in the LifeSim routine is quantified using percentages from the 2017 United States census, indicating the proportion of individuals under 65 years with mobility difficulty and those over 65 years with similar issues. The stability criteria depend on the building's construction type, with most criteria based on the consideration of Clausen and Clark (1990). If this stability threshold is reached, the building is considered to be collapsing, and all individuals inside are allocated to high-hazard zones, as in the submersion consideration.

The process of warning and evacuation involves several milestones separated by time delays, as illustrated in Figure 5.2. The timeline begins with the identification of an imminent hazard. The first delay occurs between the identification of the hazard and the decision to issue an evacuation order. Following the issuance of the warning, a second delay represents the time required to disseminate this warning. Once the population receives the warning, a third delay occurs before initiating protective action. These three delays have been identified and substantiated by research, supported by various studies and equations (SORENSEN; MILETI, 2015c, 2015d, 2015e). LifeSim

incorporates standard curves with an explicit range of uncertainty for these three delays. The uncertainty is inherently present in the delay curves for warning issuance, as probability distribution functions represent them. Cumulative probability functions represent the warning diffusion and mobilisation curves, accounting for the inherent uncertainty. After the evacuation is initiated, the LifeSim routine utilises several criteria and considerations to model the evacuation process and determine whether an agent successfully reaches a safe location.

Figure 5.2 – The milestones and respective times between them that represent the warning and evacuation timeline in the LifeSim model.

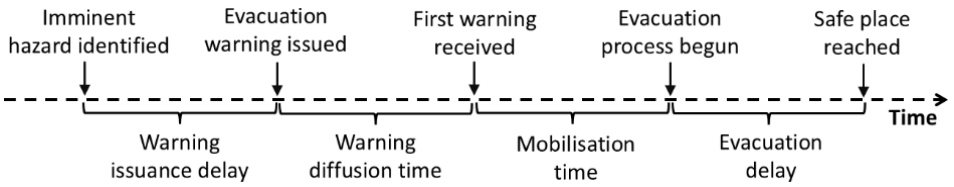

The simulation of the evacuation dynamics employs Greenshield's traffic flow model (MAHMASSANI *et al.*, 2009) to represent the effects of traffic density and road capacity on vehicle speed. This model has been adapted to introduce a minimum speed threshold determined by stop-and-go conditions. The Dijkstra (1959) optimisation algorithm defines the fastest path between the building and the pre-defined meeting point for route determination during evacuation. The quantity of vehicles is determined by their occupancy rate, as specified by the user. The LifeSim model incorporates certain behavioural decisions of the population, such as the non-evacuation depth, which represents the decision to leave or remain in a structure based on a specific water depth, and the willingness to enter flooded roads, indicating a driver's choice to traverse them. Pedestrian evacuation is also considered, based on a pre-defined fraction of the population evacuating by vehicle and on foot. A constant velocity is used for pedestrian evacuation and does not account for traffic density. If vehicles or individuals are overtaken by flooding during evacuation, stability criteria based on Smith et al. (2017) and Shand et al. (2011) are applied, respectively. If these criteria are exceeded, the affected population is allocated to the high-hazard flood zone, and if not, they are allocated to the low-hazard zone.

In the loss of life module, the high-hazard zone refers to situations where the likelihood of dying largely depends on chance, such as being swept downstream, trapped in a

collapsing building, or submerged underwater. In contrast, the low-hazard zone denotes areas where risks exist but are minimal. Each zone is characterised by a probabilistic distribution based on historical cases. In each iteration of the probabilistic routine, a fatality rate is sampled for each specific agent from the hazard functions. Then, a random uniform number between 0 and 1 is assigned to each individual. If this uniform number exceeds the sampled fatality rate, the individual survives.

The computation of risk is performed using Monte Carlo simulations, allowing various model parameters to be introduced with uncertainty, examining random and epistemic uncertainties. Consequently, the model's output concerning the quantification of loss of life is probabilistic (USACE, 2020).

Despite the challenges in acquiring data to understand event dynamics on an agent-based scale (NEEDHAM; FIELDS; LEHMAN, 2016), validation efforts for LifeSim have successfully modelled several significant events. These include Hurricane Katrina in New Orleans, United States; the Kinugawa levee breach in Japan; the Malpasset Dam failure in France; the Kelly Barnes Dam failure in Georgia, the United States; and the Oroville Dam spillway failure in California, the United States (USACE, 2020).

The LifeSim routine involves the initial preprocessing of hydraulic data, road networks, and buildings. Hydraulic data are processed to define the flood time series for each structure and road segment. This process uses the Ramer-Douglas-Peucker algorithm to reduce the number of data points in water depth and flow velocity hydrographs, optimising computational time and memory usage. For road networks, the fastest route between each node is pre-defined using the Dijkstra (1959) algorithm. In the event of traffic jams and flooding on roads, which could necessitate rerouting, the optimal path may change during the simulation. Hydraulic properties are determined at the midpoint of each road segment. Each building is associated with a road segment, and the initial fastest path between the building and an associated safe location is calculated.

The model then simulates each iteration, representing a complete simulation of the warning and evacuation dynamics and their consequences. Iterations are associated with a seed number to ensure reproducibility of the sampling model. For each iteration, LifeSim samples uncertainty parameters such as the warning and evacuation module input times and curves, as well as attributes of people and structures. With the

sampling set, the dynamic simulation proceeds, and at the end, the exposure for each agent is determined. Individuals who were not sampled to receive a warning or take proactive action perform time-independent vertical evacuations, relocating to the highest floor, attic, or roof of their building, depending on the sampled attributes of the building. Those who evacuate by car or on foot are subject to sampled evacuation parameters, including willingness to enter the flood and stability criteria. Once exposure conditions are defined, the fatality rate association routine is applied to determine the final condition of each individual. This process is repeated for each iteration, resulting in a probabilistic life-loss estimation.

5.3.2 Ahr Valley 2021 flood

Between July 12 and 19, a quasi-stationary atmospheric low-pressure system named Bernd brought extreme rainfall to several regions in Europe. The most impacted areas included the federal states of Rhineland-Palatinate (RLP) (Figure 5.3a) and North Rhine-Westphalia (NRW) in western Germany, as well as adjacent regions in Belgium, Luxembourg, and the Netherlands. In Germany, saturated soil due to accumulated precipitation in May and June, which exceeded the average by 10–40%, coupled with an average of 127 mm of rainfall in 72 hours from 12 to 14 July in some catchments, resulted in up to 33 billion euros in damage and 191 fatalities.

Specifically, the Ahr Valley (Figure 5.3b) in RLP was particularly affected with about 42,000 impacted people and 8,800 damaged buildings, resulting in up to 20 billion euros in economic losses and 134 fatalities. The steep slopes of the Ahr Valley caused torrential flows and elevated water levels, with the flow at the Altenahr gauge, upstream of the most affected area (Figure 5.3c), increasing from less than 10 $m^3 s^{-1}$ to up to 700–1200 $m^3 s^{-1}$ within a few hours (DKKV, 2022; KRON *et al.*, 2022; SZÖNYI *et al.*, 2022). A reconstructed water level hydrograph showed a peak of 10.2 metres, significantly higher than the forecasted 5.74 metres, with the discrepancy attributed mainly to forecast uncertainties but also to the clogging of bridges downstream of the Altenahr gauge (APEL; VOROGUSHYN; MERZ, 2022).

Figure 5.3 – Overview of the Ahr Valley and its most impacted area by the 2021 flood. (a) German federal states, highlighting Rhineland-Palatinate and the location of the Ahr Valley catchment. (b) Ahr Valley catchment with drainage system and hillshade base map. (c) Satellite image and local administrative units of the downstream portion and most impacted area of the Ahr Valley, between the cities of Altenahr and Sinzig, at the confluence with the Rhine. Data sources: German federal states and local administrative units – GeoBasis-DE / BKG (2023); rivers and Ahr catchment – global dataset of drainage systems (HE *et al.*, 2024).

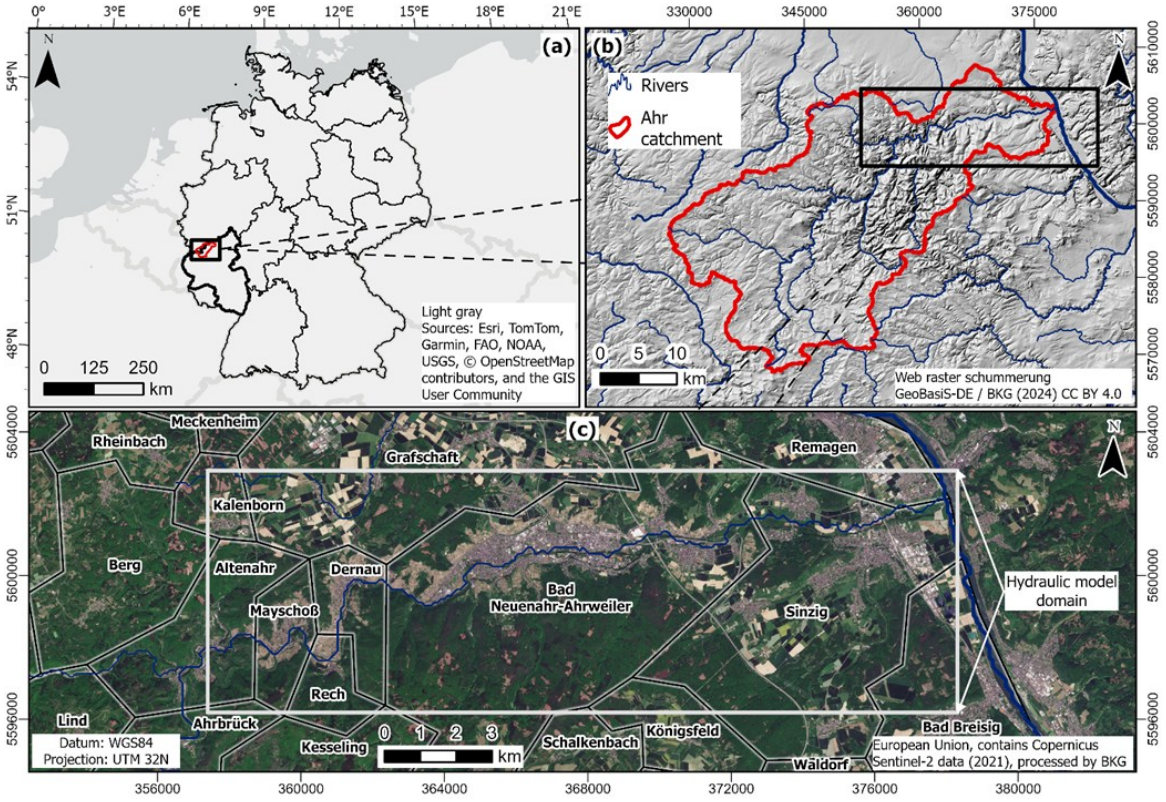

5.3.3 Flood hazard modelling

The 2D raster model RIM2D (APEL; VOROGUSHYN; MERZ, 2022; GHOMASH; APEL; CAVIEDES-VOULLIÈME, 2024; VOROGUSHYN *et al.*, 2024) was used to simulate the 2021 flood event. This simulation updated the model set by Apel, Vorogushyn and Merz (2022), refining the digital elevation model (DEM) resolution from 10 to 5 metres (GHOMASH; APEL; CAVIEDES-VOULLIÈME, 2024). This enhancement improves the accuracy of the results, reducing biases related to resolution impacts on flood characteristics and consequences (BRUSSEE *et al.*, 2021; BRYANT; KREIBICH; MERZ, 2023). Finer resolutions (e.g., 1 and 2 metres) were also tested but had a negligible impact on flood risk estimation, including the risk of loss of life (GHOMASH; APEL; CAVIEDES-VOULLIÈME, 2024). Based on these findings, the 5-metre resolution DEM was selected as the optimal balance between model accuracy and simulation efficiency.

The model domain encompassed the reach between the towns of Altenahr and Sinzig, about 30 kilometres, where the Ahr flows into the Rhine (Figure 5.3c). Land use classification was sourced from Mundialis 2020 (RIEMBAUER *et al.*, 2021), with Manning's roughness values as follows: sealed surface areas (η = 0.02, for simulating flow over tarmac or concrete in built-up areas); forest (η = 0.2); and other classes, including the river channel and floodplains (η = 0.03). The roughness values were calibrated using the Euclidean distance objective function, considering flood extent, flood depth in floodplains, and flood dynamics within the river channel. Regions of the DEM overlaid by building footprints from the OpenStreetMap database were excluded from the hydraulic routine to represent urban flow dynamics more accurately (APEL; VOROGUSHYN; MERZ, 2022).

The reconstructed water level hydrograph at the Altenahr gauge, showing a maximum water depth of 10.2 metres, was used as the upstream boundary condition. A comparison between the maximum water depth layer (Figure 5.4a) and 75 reported water depths revealed a bias of 0.46 metres and a root mean square error of 0.97 metres. To calculate this error metric, a 7.5 metres buffer was applied around the reported markers to gather information from adjacent pixels. The mean depth of inundated pixels within this buffer was then considered. It is important to note that the reported water depths correspond to different vertical datums, including street level, pedestrian walkways, and doorsteps. The simulated flow velocities (Figure 5.4b) are consistent with expectations for such a dynamic event, ranging from 2 to 5 m s^{-1} in the river course and 0.1 to 2 m s^{-1} in built-up areas (APEL; VOROGUSHYN; MERZ, 2022). The maximum simulated water depth predominantly occurred between 12:00 and 4:00 CEST on July 15 (Figure 5.4c).

The LifeSim hydrodynamic module directly accepts input data from simulations conducted using hydraulic models such as HEC-RAS and FLO-2D. For the simulations executed using RIM2D output, the insertion of water depth and flow velocity data was performed through multiple layers, each representing different time intervals and containing parameter values. A 15-minute time series of water depth and flow velocity layers was used as input for the flood routine of the LifeSim model.

Figure 5.4 – Flood characteristics of the 2021 Ahr Valley flood simulated with RIM2D at a resolution of 5 metres. (a) Maximum water depth. (b) Maximum flow velocities. (c) Time of maximum water depth on July 15.

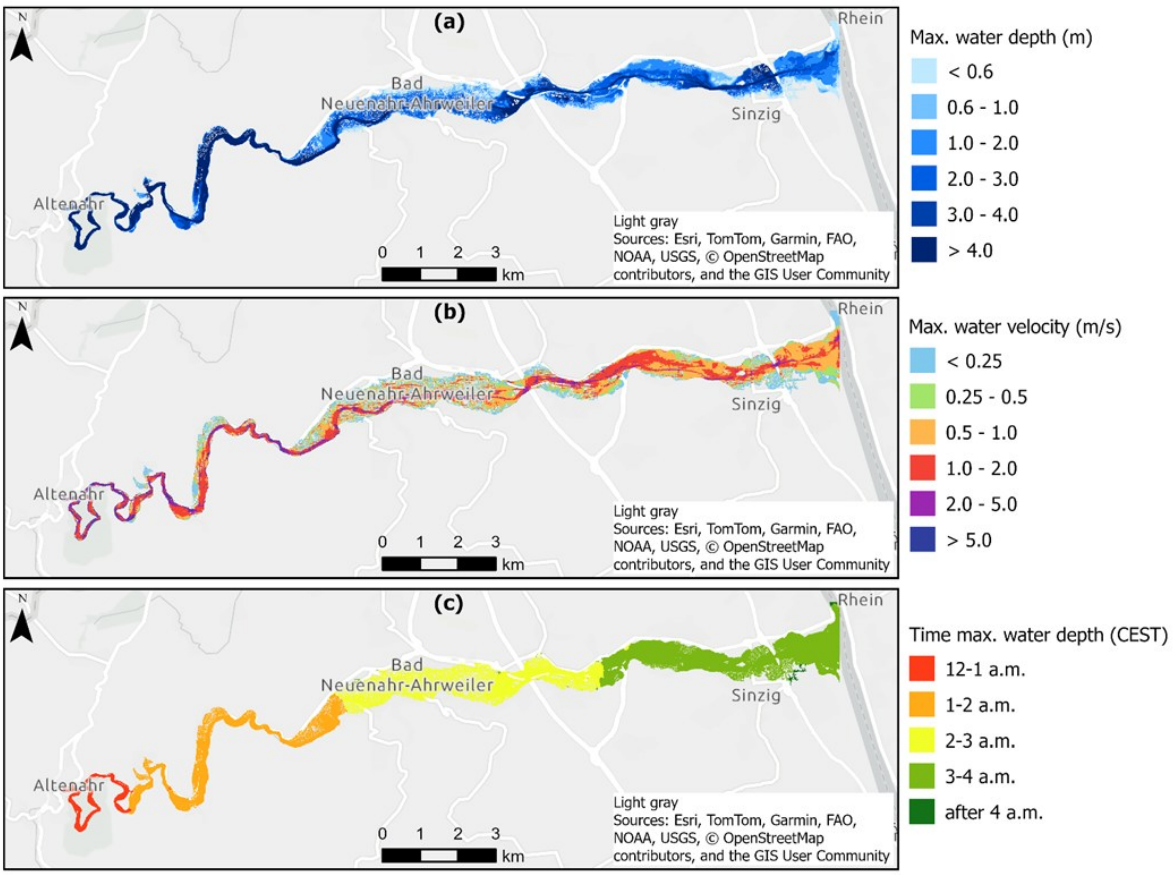

5.3.4 Exposure at a building scale

In order to apply the life-loss model LifeSim, data for each building are required (e.g. number of floors, foundation height, and occupancy type). Similarly, data concerning the number of exposed people and their ages (e.g. more or less than 65 years old) are required. This detailed information was obtained using a combination of available data from OpenStreetMap, the Historical Analysis of Natural HaZards in Europe (HANZE) 2.0.3 database (PAPROTNY, 2023), the 2011 German census, and the Singh et al. (2025) survey result database consolidated after the 2021 event.

Information on the population was sourced from the 100 metres resolution grids of HANZE 2.0.3 for 2020 (PAPROTNY, 2023). The HANZE 2.0.3 population data at this resolution were derived from a disaggregation technique applied to the 1-kilometre resolution population data from the 2011 European GEOSTAT database. This disaggregation considered proportional distribution based on identified human-made structures, such as buildings, impervious surfaces, roads, and streets. In order to

model population growth, a rate of change was used at the Nomenclature of Territorial Units for Statistics (NUTS) 3 level (PAPROTNY; MENGEL, 2023).

Building footprint polygons were obtained from the OpenStreetMap 2021 database, excluding buildings without human occupation potential, such as garages, parking facilities, and toilets. Since we only considered buildings to allocate the population, excluding other man-made structures, we noticed some grids with a 100-metres population resolution in HANZE 2.0.3 lacked buildings overlaying them. In order to address this issue, we first aggregated the 100-metre resolution population data to a 1-kilometre resolution. Then, we redistributed the data to the 100-metre grid, weighted by the HANZE 2.0.3 population at this resolution, but only considering grids with the selected buildings. This approach ensured that there was no grid population without the selected buildings.

In order to allocate the population within the selected buildings, we performed a weighted distribution of the redistributed population from the 100-metre grid, using building size as the weighting factor. After allocating the population to the buildings, the building centroids were moved to the nearest pixel of the RIM2D simulation, as the hydraulic routing has cut out the building footprints (see section 5.3.3).

Age can significantly impact flood fatalities, mainly due to mobility issues (VINET *et al.*, 2012). In the LifeSim routine, age influences the probability of mobility issues and the corresponding submergence threshold criteria. In order to incorporate this information, age demographics from the 2011 German census, provided at a 1-kilometre grid resolution, were used to classify the population in the Ahr Valley region. On average, 24.2% of the population within the selected grids is over 65 years old.

Some crucial building characteristics for the LifeSim model (e.g. number of floors, foundation height and possibility of accessing the attic) were unavailable in the HANZE 2.0.3 and the 2011 German census databases. Consequently, data were supplemented by a post-event survey of flood-affected residents (SINGH *et al.*, 2025). The survey data contain 277 responses from residents of Rhineland-Palatinate. The number of floors was determined based on the proportion of survey responses, assuming that buildings with higher population densities are more likely to have more floors. For example, 0.4% of responses indicated that a building had seven floors, the

maximum reported. Therefore, the 0.4% of buildings with the highest population density were assigned seven floors. Foundation height, defined as the elevation difference between the street and the ground floor, was estimated using responses that provided information on floodwater reaching the ground floor. By comparing estimated water levels inside and outside buildings, an average foundation height of 0.57 metres was determined and applied to all buildings. Additionally, it was estimated that 36.5% of buildings have attic access.

The building stability criterion is defined as 'engineered' according to LifeSim, based on the considerations outlined by Clausen and Clark (1990). For this specific criterion, two curves are considered based on the product of water depth and flow velocity, with a uniform range of uncertainty: the lower-curve threshold is set at 7 m^2 s^{-1}, representing traditional and smaller constructions, and the upper-curve threshold at 10 m^2 s^{-1}, representing high-quality constructions. In the LifeSim routine, a building collapses if the thresholds of the sampled curve are reached and the flow velocities exceed 2 m s^{-1}.

Road networks were imported directly from OpenStreetMap, and safe evacuation places were located outside the inundation zones to simulate the dynamics of an actual evacuation event. Figure 5.5 illustrates the population distribution within buildings at a 100 metres resolution, along with road networks and designated safe places. Buildings within the grids that intersected the 100-metre buffer zone of the inundated boundary were utilised for LifeSim simulations. A total of 10,461 buildings were included, housing 24,076 individuals under 65 years old and 9,467 individuals aged 65 and over.

Figure 5.5 – Overview of exposure at a building scale. Population counts aggregated at a 100-metre grid resolution, buildings and road network along the Ahr Valley, simulated flood extent, and safe places. Data sources: 100-metre grid: HANZE 2.0.3 (PAPROTNY, 2023). Roads and buildings: © OpenStreetMap contributors 2021. Distributed under the Open Data Commons Open Database License (ODbL) v1.0.

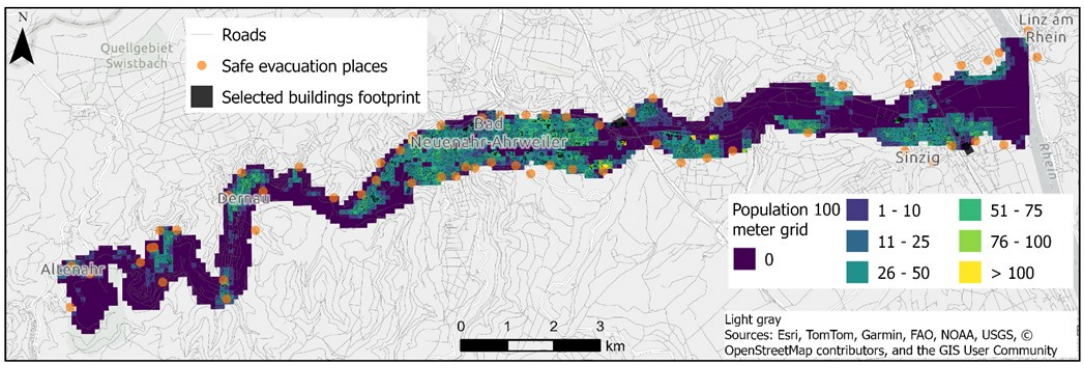

5.3.5 Early warning and evacuation

In Germany, the national German Weather Service (DWD) is responsible for issuing warnings related to extreme weather events, whereas the federal states legally mandate flood warnings (KRON *et al.*, 2022). Regarding the 2021 flood event, the DWD issued the initial weather warning on July 12 at noon CEST. The first flood warning for the Ahr and its tributaries was released on July 14, just before noon CEST, reaching approximately 22,000 people. This warning alerted residents to a rapid water level rise and potential flooding within the next 24 hours. Numerous additional weather and flood warnings were disseminated throughout July 14. For instance, at 23:00 CEST, a warning was issued to Sinzig, Bad Neuenahr-Ahrweiler, and adjacent places with residents living within 50 metres of the Ahr to evacuate their buildings. This significantly underestimated the hazard, as fatalities were later reported in buildings located up to 250 metres from the river. Despite the numerous warnings, the effectiveness of the alert system was severely compromised by miscommunication along the warning chain and a general lack of confidence in the unprecedented severity of the flood (SZÖNYI *et al.*, 2022).

The information provided by the survey conducted by Singh et al. (2025) about the Ahr Valley's warning and evacuation procedures was used for the description of the timeline in LifeSim (Figure 5.2). As the survey had a unit geographic scale of federal state and the flood occurred at different areas and times between 12 and 19 July 2021 in the states, we applied a filter to use only responses from individuals in Rhineland-Palatinate (RLP) affected during the same time window as the high water levels in the simulated domain. Out of 277 responses from RLP, 246 were considered. These respondents reported the occurrence of hazards at their homes between 15:00 CEST on July 14 and 09:00. CEST on July 15. The first flood warning, adopted for this study, was reported at noon CEST on July 14, representing a notification issued 13 hours before the water level peaked at the Altenahr gauge at 01:00 CEST on July 15. As a result, the warning issuance delay in the LifeSim timeline was excluded from the analysis since it occurred before this milestone and would not affect the simulations.

To depict the diffusion of this first warning in the context of the LifeSim routine, we considered the reported lead times from individuals who noted that the warning they received was either a call for evacuation or contained information pertinent to

evacuation. The reported time of hazard occurrence at the buildings was subtracted by the lead time to establish the first warning time for each individual. In instances where no lead time was reported, or the warning lacked evacuation instructions, individuals were assumed to be warned at the moment of their reported hazard occurrence at their building. Notably, 57.0% of those affected by the main event reported receiving a warning. However, only 17.5% received a warning that included explicit evacuation instructions. Some reported no lead time among those who received evacuation instructions, resulting in only 13.8% of the surveyed people receiving an explicit evacuation warning before the flood reached them.

Figure 5.6a illustrates the warning diffusion process based on these assumptions and analyses. Given that the hazard occurrence question was framed in hourly ranges, the curves depict these ranges, which were inserted as a uniform distribution in the model. Additionally, the reported lead times were aligned with the first warning issued by the federal state at noon CEST on July 14. Most individuals were warned or became aware from the night of July 14 and the early morning of July 15, correlating with the most frequently surveyed times of hazard occurrence.

Regarding the mobilisation time, we considered the reported time it took individuals to take protective action after receiving the warning or becoming aware of the hazard. In the survey, the protective actions included several mitigation measures and were not solely focused on evacuation. In order to represent the evacuation dynamics of the event, we considered only responses from individuals who left their homes before or during the flood, as well as those who were rescued. Approximately 34% of the surveyed population left their homes or were rescued, with 6.9% taking immediate action, 5.3% reporting a delay in mobilisation, and 22.0% not specifying when they began protective measures. In order to account for the uncertainty among the 22.0% who did not report a response time, we applied a uniform uncertainty range (Figure 5.6b). This range included an upper curve representing the fastest mobilisation, assuming immediate action for this group, and a lower curve representing the slowest mobilisation, considering six hours (the maximum reported delay).

Regarding the evacuation dynamics, the mean family size on the NUTS 3 scale was used to estimate buildings where all residents were warned and mobilised

simultaneously. Specifically, buildings housing more than three people were identified, as it was assumed that in such cases, the warning and mobilisation of the population do not occur simultaneously. This criterion was also used to define the size of the evacuating group.

The evacuation mode fraction, whether by vehicle or on foot, is a user-defined input in LifeSim. In order to determine this fraction and represent the evacuation dynamics during the 2021 flood event, we conducted multiple runs, adjusting the evacuation mode by 10% in each run. The fraction that produced the closest match to the observed ratio of fatalities occurring indoors versus during evacuation was selected. Specifically, 68.5% of the fatalities (or possibly more) occurred indoors, given the uncertainty regarding victims discovered outside (RHEIN; KREIBICH, 2025). We found that an evacuation mode fraction of 80% by vehicle and 20% on foot most closely matched the indoor fatality ratio, with 69.3%. Consequently, this fraction was chosen to represent the reconstruction scenario (see Figure 5.12 and Table 5.3 in the Appendix, section 5.7.1).

Figure 5.6 – Reconstruction of warning diffusion and mobilisation times in the Ahr Valley 2021 flood based on the post-event survey with flood-affected residents. (a) Warning diffusion curves: cumulative proportion of the population who were warned or became aware of the hazard after the first flood warning. (b) Mobilisation curves: cumulative proportion of the population who initiated an outdoor evacuation after receiving or becoming aware of the hazard.

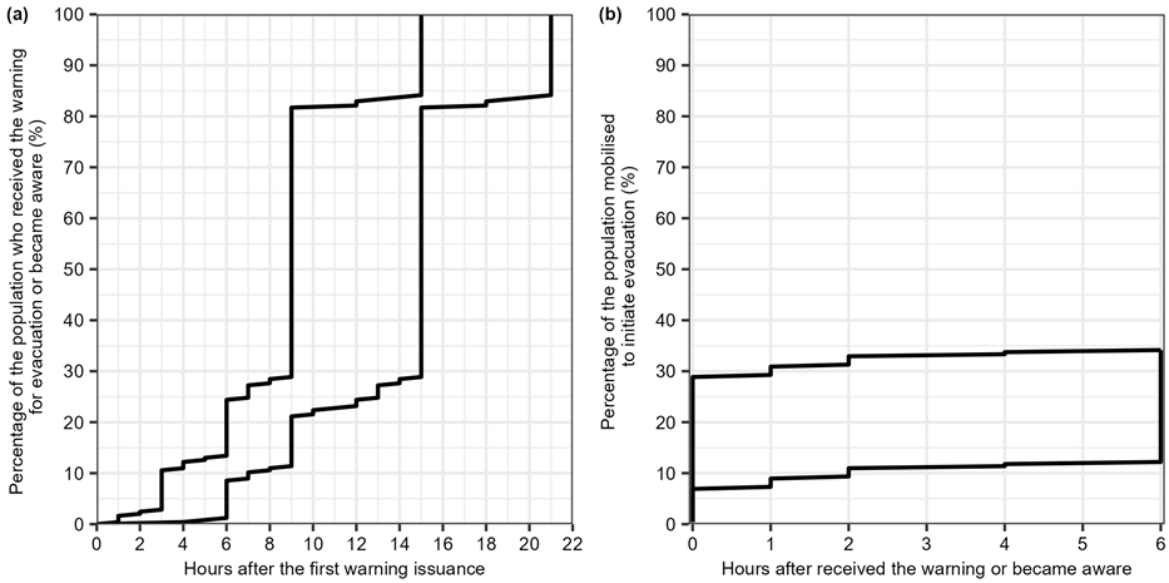

5.3.6 Alternative scenarios of early warning and evacuation

The simulation of alternative warning and evacuation scenarios can illustrate the impact of warning procedures on loss of life (LUMBROSO *et al.*, 2021; LUMBROSO; DAVISON, 2018; SILVA; ELEUTÉRIO, 2023a, 2023b; WANG *et al.*, 2024). For the 2021 Ahr Valley flood, we develop and assess alternative scenarios using two approaches. First, we propose scenarios that alter the warning diffusion and mobilisation curves, drawing on historical cases referenced in the LifeSim recommendations. This approach aimed to represent how different strategies of warning dissemination, as well as varying levels of public perception and preparedness, could impact the number of fatalities without changing the time of first warning issuance. Secondly, we analysed the effect of the timing of the first flooding warning, taking into account the water depth forecasting capabilities for the region.

In order to check the effects of warning diffusion and mobilisation curves, we defined three distinct scenarios, each with its own unique characteristics and implications. The optimal scenario (A1.1) represents a highly effective warning system, employing multiple channels for fast and extensive alert dissemination, with frequent repetition and a well-prepared, trained population. The intermediate scenario (A1.2) features a moderately effective warning system, with a mix of technologies and a population with some awareness of the risks. However, deficiencies in emergency planning affect the likelihood of a high mobilisation rate in a short time. The suboptimal scenario (A1.3) involves a warning system that is less effective, with limited technologies and infrequent warning issuances, hindering fast dissemination. In this scenario, most of the population is unlikely to perceive the threat, and their response is largely improvised. The curves used in these scenarios were proposed by Sorensen and Mileti (2015b, c). The Appendix material (see Appendix, section 5.7.2) provides a detailed description of the equations and their coefficients, as proposed by these authors.

The proposed warning diffusion curves, categorised as ‘fast’, ‘moderate’, and ‘slow’ for daytime scenarios, were utilised in this study. These curves incorporate uncertainty modelled through a triangular distribution. The range extends from the upper bound of the “fast” curve, reflecting rapid dissemination similar to that observed in the 1980 eruption-induced mudflow of the Toutle River, Washington, in the USA, to the lower

bound of the “slow” curve, which aligns with the behaviour seen in the 1987 Nanticoke chemical accident, Pennsylvania, in the USA (SORENSEN; MILETI, 2015c).

Additionally, the proposed mobilisation curves for "preparedness good and perception likely", "preparedness poor and perception likely," and "preparedness poor and perception unlikely" were employed. These curves also utilise a triangular distribution. The uncertainty bounds are derived from the fastest response case of the Confluence (USA) hazardous material flow in 1987, which defined the upper bound for "preparedness good and perception likely," and the slowest case in the database, which corresponded to a similar event in Pittsburgh (USA) in the same year, defining the lower bound for "preparedness poor and perception unlikely". Furthermore, Equation 18 (see Appendix, section 5.7.2) is supplemented by maximum mobilisation rates over different time periods, specifically up to 8, 24, and 74 hours. The two slower response curves have the same coefficients, but different maximum mobilisation rates. These rates represent the maximum population likely to take protective action, with higher mobilisation rates anticipated for longer durations and more optimal scenarios of perception and preparedness (SORENSEN; MILETI, 2015e).

Two additional scenarios were evaluated by integrating the theoretically proposed and empirical curves (Figure 5.7) for the 2021 flood. These scenarios represent a suboptimal warning system, contextualised within empirical curves for warning diffusion (A1.4) and mobilisation (A1.5). This approach enables the analysis of the impact of each delay in the occurred warning timeline process. The suboptimal curves are employed in these scenarios to reflect the realism of the 2021 event characterised by a deficient warning system. Figure 5.7 illustrates the combination of the diffusion and mobilisation process curves for each scenario, including the reconstruction scenario designated as reconstructed flood early warning and evacuation (RFEWE). Table 5.4 (in the Appendix, section 5.7.2) presents the utilised curves, their respective coefficients, and their mobilisation rates for each scenario.

Figure 5.7 – Combination of the warning diffusion and mobilisation curves for each alternative scenario of early warning and evacuation in the first approach. RFEWE (reconstructed scenario of the 2021 flood), A1.1 (optimal scenario), A1.2 (intermediate scenario), A1.3 (suboptimal scenario), A1.4 (suboptimal scenario with an empirical warning diffusion curve), and A1.5 (suboptimal scenario with an empirical mobilisation curve).

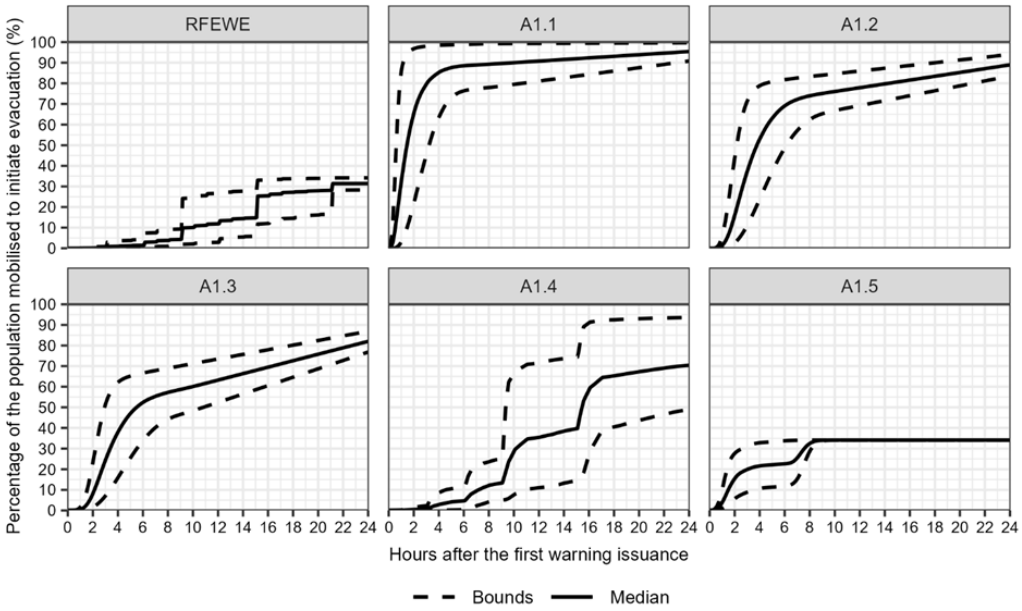

The reconstruction scenario exhibits a more significant delay and lower mobilisation rates in protective action following the first warning issuance compared to the two worst alternative scenarios, A1.4 and A1.5. Most individuals became aware of the hazard only at the time of its occurrence, despite receiving the first warning 13 hours before the peak of the flood, and the low rates of mobilisation were specific characteristics of this event that were not observed in the other events used in the curves proposed in LifeSim. Hence, an even more extreme alternative scenario (A1.6), theoretically worse than the reconstruction, was assessed by simulating only vertical evacuation, excluding any outside evacuation.

In order to assess the timing of the first warning, we employed a uniform distribution to represent the range of possible and reliable times for the first flood warning during the 2021 event. Forecasting techniques indicate that it would be possible to anticipate, with a 75% probability, that the water level at the Altenahr gauge would exceed the 4 m threshold, corresponding to a 100-year event, 17 hours before the peak. This probability would increase to 100% from 8 hours before the peak (NAJAFI *et al.*, 2024). Thus, the potential times for issuing the first warning were considered to fall within a 9-hour window, between 08:00 and 05:00 CEST on July 14. In this second approach,

potential desired times for early warnings that significantly impacted the estimations could be identified (SILVA; ELEUTÉRIO, 2023b). Additionally, the identification of early warnings that could result in traffic jams and, consequently, more people being trapped by the flood during evacuation could be comprehensive (EL BILALI; TALEB; BOUTAHRI, 2021).

When combined with the second approach of analysing different timings for the first warning issuance, the reconstructed empirical warning dissemination (Figure 5.6a) does not represent a realistic scenario. Most surveyed people did not receive an evacuation warning; hence, most of the points on the curve were based on the time of reported hazard occurrence at the surveyed buildings. Using this empirical curve for early warnings issued later than 13 hours before the peak at the Altenahr gauge would suggest that most people would be warned only after the hazard had occurred.

Conversely, issuing warnings earlier than 13 hours before the peak does not align with the dissemination dynamics observed in 2021. Therefore, for warning diffusion and mobilisation delays in the second approach of alternative scenarios, we employed the optimal and suboptimal scenario curves proposed in the first part. This allows for examining the influence of varying warning issuance times on estimating loss of life. Additionally, we included a scenario using the slow theoretical warning dissemination and empirical mobilisation. Table 5.1 summarises the alternative scenarios and their respective warning and evacuation parameterisation considerations. The scenarios for the second approach are designated as A2.1 for the optimal scenario, A2.2 for the suboptimal scenario, and A2.3 for the suboptimal scenario with the empirical mobilisation curve.

Table 5.1 – Overview of all alternative scenarios for early warning and evacuation, considering the timing of the first flood warning issuance, warning diffusion, and mobilisation curves. A1: first approach, analysing warning diffusion and evacuation curves alongside the actual timing of the first flood warning. A2: second approach, focusing on the time window for the first warning issuance based on forecasting capabilities. The numbers in brackets indicate the time window for issuing the first flood warning.

Alternative scenario	Time for issuing the first flood warning before the peak at theAltenahr gauge (h)	Warning diffusion	Mobilisation (preparedness and perception)
A1.1	13	Fast	Good and likely
A1.2	13	Moderate	Poor and likely
A1.3	13	Slow	Poor and unlikely
A1.4	13	Empirical	Poor and unlikely
A1.5	13	Slow	Empirical
A1.6	13	No outside evacuation	
A2.1	U~(8,17)	Fast	Good and likely
A2.2	U~(8,17)	Slow	Poor and unlikely
A2.3	U~(8,17)	Slow	Empirical

5.3.7 Parameterisation and key considerations for using the LifeSim model

LifeSim version 2.1.3 (USACE, 2023) was employed to assess fatalities resulting from the 2021 Ahr Valley flood. A total of 2,000 iterations was sufficient to achieve convergence of the quantiles, standard deviation, and skewness for the probabilistic outcomes in scenarios with a deterministic first warning issuance time (see Figure 5.13 in the Appendix, section 5.7.3). For scenarios with a variable time range for the first warning issuance, 18,000 iterations were conducted, representing approximately 2,000 iterations for each hourly range. Statistical tests, including those developed by Dunn (1964), Kruskal and Wallis (1952) and Mann and Whitney (1947), were performed to compare the differences in estimated fatalities across various scenarios. Table 5.2 provides an overview of the considerations within each LifeSim module used in the analysis.

The modelling domain excluded 15 victims from the upstream cities of Ahrbrück, Dümpelfeld, Müsch, and Dorsel. Among the reported fatalities within the domain, one was associated with a pre-impact case where an individual died of a heart attack due to exhaustion, and another was a post-impact case where an individual was trapped in a collapsing building and subsequently died in a hospital (RHEIN; KREIBICH, 2025).

Table 5.2 – Summary of LifeSim module inputs and parameters for life-loss simulations in the 2021 Ahr Valley flood.

Module	Input and parameter	Description
Flood routine	Hydraulic data	RIM2D flood model of Apel, Vorogushyn and Merz (2022) updated to a resolution of 5 m
Loss of shelter	Buildings	Selection of 2021 OpenStreetMap buildings footprint and their characteristics from post-event survey Singh et al. (2025)
	Population	Number of people indicated by HANZE 2.0.3 for 2020 (PAPROTNY, 2023) and age proportion from the 2011 German census
	Building stability	Thresholds for engineered constructions as proposed by USACE (2020) based on Clausen and Clark (1990)
	People submergence	Water depth thresholds for the highest reachable floor of the buildings, considering the ages of the defined proportion of people with some mobility issue
Warning and evacuation	First flooding warning	Reconstruction: at noon CEST on July 14 (SZÖNYI *et al.*, 2022). Alternative scenarios: U~(8,17) h before peak water depth at the Altenahr gauge
	Warning diffusion delay	Reconstruction: post-event survey answers on warning information, lead time and hazard occurrence. Defined as the uniform distribution between two curves as the reported hazard occurrence time answers are defined by a range of hours. Alternative scenarios: Theoretical scenarios based on Sorensen and Mileti (2015c)
	Mobilisation delay	Reconstruction: post-event survey answers on evacuation, rescue, and time to start protective measures. Alternative scenarios: Theoretical scenarios based on Sorensen and Mileti (2015e)
	Road network	OpenStreetMap
	Safe evacuation places	Set outside the simulated flood extent along the Ahr
	Evacuation route	Optimal path defined by the Dijkstra (1959) algorithm
	Evacuation delay	Vehicle speed defined by the OpenStreetMap road classification and modified Greenshield traffic flow model (MAHMASSANI *et al.*, 2009). Constant speed of 6.44 km h^{-1} for pedestrians
	Exposure to trapped people	Stability criteria defined by USACE (2020) and based on Smith et al. (2017) for vehicles and Shand et al. (2011) for people.
	Evacuation parameters	A total of 80% evacuation by vehicles and 20% on foot. People warned and started evacuation simultaneously in buildings with fewer than four people, based on the mean family size from the 2011 German census
Loss of life	Fatality rates	Probability distributions for two hazard zones defined by USACE (2020) based on historical cases

Thus, for the comparative analysis, we excluded the 15 victims from upstream cities and the pre-impact fatalities. The remaining post-impact fatalities, which could be directly attributed to the flood, were included. This adjustment resulted in a comparison value of 118 victims for evaluating life-loss estimations. The comparisons between the estimated and reported fatality locations were limited to indoor cases due to uncertainties regarding the actual accident locations of victims found outside buildings.

5.4 Results and discussion

5.4.1 Life-loss estimation of the Ahr Valley flood in 2021

The LifeSim median estimate for the number of fatalities is 152, which is 28.8% higher than the actual total of 118. The simulation uncertainties span 140 to 162 fatalities, corresponding to the first and third quartiles, respectively. The extreme range, defined by the minimum and maximum estimated values, spans 99 to 202 fatalities, resulting in a range of 103 fatalities. The median of fatalities inside the buildings is 69.3% of the total estimation, aligning with the reported 68.5% (RHEIN; KREIBICH, 2025).

One reason for the variability in estimations is the sampling of the warning diffusion and mobilisation curve. Figure 5.8 illustrates this influence, showing points near 0.00 meaning iterations where the population is warned or starts the evacuation more slowly (similar to the right curves in Fig. 6), while points nearing 1.00 depict faster responses (similar to the left curves in Fig. 6). In general, the warning diffusion has a similar correlation with the estimated fatalities compared to the mobilisation ($R = -0.29$ and $R = -0.31$, respectively) and this can be observed by analysing the central tendency of the fatalities in different regions of the sampling curves. The same estimated fatality values for warning diffusion and mobilisation levels occur due to the influence of other probabilistic parameters in the model, such as submergence thresholds and stability criteria.

For the warning diffusion, iterations with the sampling curve in the upper quarter (0.75 to 1.00), corresponding to most of the population being warned between 9 hours and 10.5 hours after the first warning issuance (Figure 5.6a), result in a median estimate of 145 fatalities. In contrast, iterations with sampling curves in the lower quarter (0.00 to 0.25), where most of the population becomes aware between 13.5 hours and 15 hours

after the first warning issuance, result in a median estimate of 157 fatalities (Figure 5.8a). Regarding mobilisation, the upper quarter, representing immediate action by 23.4% to 28.9% of the population (Figure 5.6b), has a median of 143 fatalities. Conversely, the lower quarter, representing immediate action by 6.9% to 12.4% of the population, yields a median of 158 fatalities (Figure 5.8b). Furthermore, a joint analysis of warning diffusion and mobilisation underscores the general influence of these input uncertainties. Iterations with sampling curves exclusively in the upper quarter yield a median of 135 fatalities, indicating an overestimation reduction to 14.4% of the estimated fatalities compared to the actual value of 118 (Figure 5.8c).

Figure 5.8 – Relation between estimated fatalities and (a) warning diffusion, (b) mobilisation, and (c) both processes curve samples for the 2021 Ahr Valley flood. Points near 0.00 indicate slower warning dissemination and initiation of evacuation, while points near 1.00 indicate a faster response.

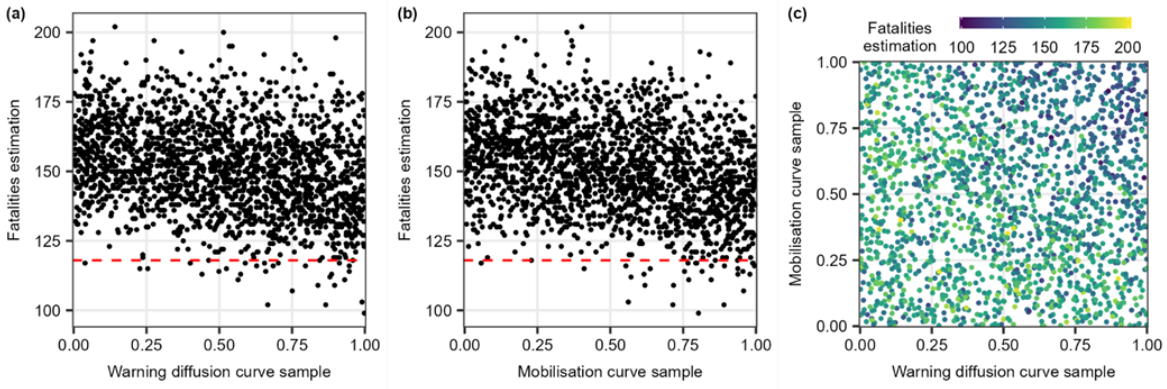

The reported indoor fatalities were 48 (59%), 15 (19%), 10 (12%), 6 (7%), and 2 (3%) for the local administrative units (LAUs) of Bad Neuenahr-Ahrweiler, Sinzig, Dernau, Altenahr and Mayschoss, respectively (RHEIN; KREIBICH, 2025). The mean of the simulations is 59 (57%), 0 (0%), 16 (15%), 11 (11%), and 15 (14%) for the same places, with 3 (3%) more fatalities in Rech. For Bad Neuenahr-Ahrweiler, the model represents the proportion of fatalities. However, it overestimates fatalities for upstream LAUs and underestimates them for Sinzig. This discrepancy may be attributed to the generalisation of the warning and evacuation procedures across the entire modelling domain. During the simulation, the cumulative sampling of the population warned and mobilised is randomly distributed among the buildings within this domain. This likely results in some people being warned later than in the actual event in upstream regions and earlier than in the actual event in downstream regions, thus failing to represent the actual spatial and temporal distribution of the population that began evacuation. Figure

5.9 depicts the spatial distribution of the mean estimated fatalities, aggregated at a 500-metre grid resolution.

Figure 5.9 – Mean of indoor estimated fatalities for the 2021 Ahr Valley flood at a 500-metre grid resolution. Data source – German local administrative units, GeoBasis-DE / BKG (2023); 500-metre grid resolution, GeoGitter GeoBasis-DE / BKG (2020).

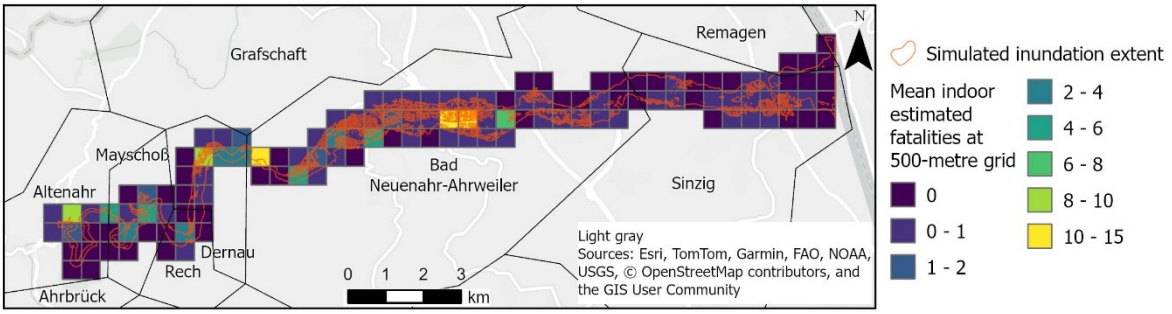

5.4.2 Life-loss estimation of alternative scenarios with improved early warning and evacuation

The reconstructed warning and mobilisation curves indicate a greater delay compared to the alternative scenarios (Figure 5.7). Despite the rapid-onset nature of the flood, the reconstructed warning diffusion curve exhibits a trend similar to that of a slow-onset event. Approximately 80% of the population is warned between 9 and 15 hours after the first alert (Figure 5.6a), mirroring patterns observed in slow-onset hazard events such as hurricanes Katrina (2005) and Rita (2005), and the Boston water contamination event (2010) (LINDELL *et al.*, 2021). In contrast, in the recommendation curves in LifeSim, which are based on historical cases, the warning diffusion times range from 15 minutes for the fastest ones to 3 hours the slower ones for the same rate (USACE, 2020). For the mobilisation time, the only comparable event in the LifeSim database is the 1987 Pittsburgh (USA) hazardous material flow event, which is the worst case of protective action times, where about 40% of the population took protective action approximately 5 hours after becoming aware of the hazard (USACE, 2020).

Figure 5.10 illustrates outcomes from the LifeSim model concerning the initial approach to evaluating alternative scenarios, specifically examining the impacts of warning diffusion and mobilisation curves. The optimal (A1.1), intermediate (A1.2), and suboptimal (A1.3) scenarios show significantly lower reductions in life loss ($p < 0.001$), indicating that the actual scenario (RFEWE) fares worse than theoretical scenarios.

Simulation uncertainties range from 22 to 39, 54 to 74, and 85 to 111 fatalities, representing the interquartile range across these scenarios. Among these scenarios, A1.3, with a median of 98 fatalities, is the closest to the approximate compared to RFEWE. However, the distribution of fatalities within buildings and during evacuation does not mirror the actual event, where 68.5% of fatalities occurred indoors.

Figure 5.10 – Estimated fatalities for the alternative early warning and evacuation scenarios, with a focus on evaluating the warning diffusion and mobilisation curves. RFEWE (reconstructed scenario of the 2021 flood), A1.1 (optimal scenario), A1.2 (intermediate scenario), A1.3 (suboptimal scenario), A1.4 (suboptimal scenario with na empirical warning diffusion curve), A1.5 (suboptimal scenario with an empirical mobilisation curve), and A1.6 (scenario without outside evacuation).

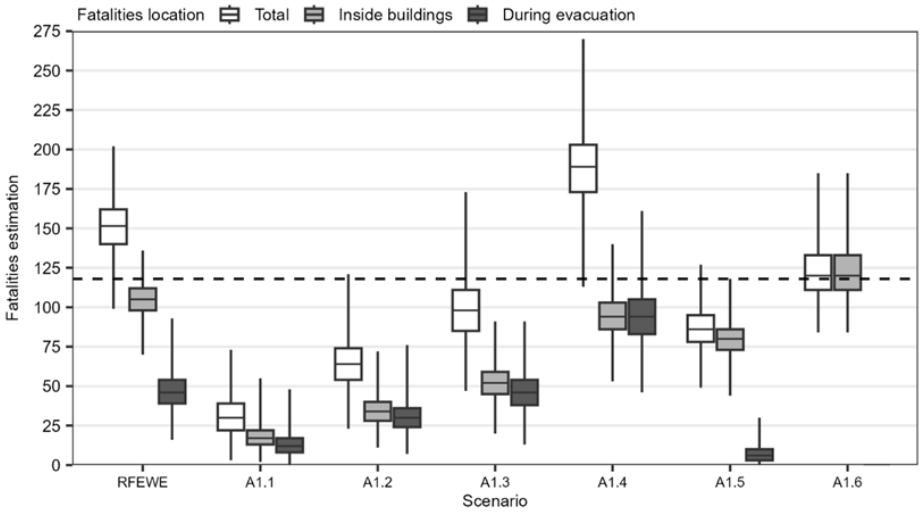

The most critical scenario in terms of estimated fatalities, A1.4, incorporates empirical warning dissemination and a poor preparedness and unlikely perception mobilisation curve. While fatalities within buildings are comparable to RFEWE (86–103 versus 98–112 for the interquartile range), fatalities during evacuation are significantly higher, ranging from 83 to 105, more than double the values of 39 to 54 for RFEWE. Since most individuals became aware shortly before the hazard occurred with empirical warning diffusion, an optimal mobilisation strategy could potentially worsen the situation by increasing the number of people outside buildings when the flood reaches them.

Scenario A1.5 employs a slower theoretical warning diffusion curve in conjunction with empirical mobilisation, highlighting the deficiencies in warning dissemination observed during the 2021 flood. The worst theoretical dissemination curve reduces the interquartile estimated fatality range of 78 to 95. This reduction is primarily due to a

higher rate of the population initiating evacuation promptly after the first warning compared to scenarios RFEWE and A1.4. As shown in Figure 5.7, approximately 34% of the population mobilises within eight hours when considering all possible samplings in the warning and evacuation simulation.

Scenario A1.6 examines a strategy where the population moves to the highest building floors instead of evacuating outside. This approach has an interquartile estimated fatality range of 111 to 133 for the first and third quartiles, exclusively indoors. The findings suggest that for individuals who receive a warning or become aware of the hazard shortly before its occurrence, seeking safety within their buildings is more advantageous than attempting an outside evacuation.

Figure 5.11 presents estimations of potential loss of life relative to the time preceding the water level peak at the Altenahr gauge, which occurred at 01:00 CEST on July 15, marking the issuance of the first flood warning based on forecasting capabilities. The colours indicate the statistical significance level of differences in estimated fatalities, aggregated by hour, between hourly intervals and their anticipated hour range. Concurrently, at the same warning issuance time, uncertainties within the LifeSim approach, such as the warning diffusion and mobilisation curves; probabilistic fatality rates; and structural stability criteria for buildings, vehicles, and individuals, may contribute to variations in the estimated fatality range.

In scenario A2.1, characterised by optimal warning diffusion and mobilisation, the interquartile range of fatalities decreases from 40–74 to 18–32 during the 8–9 and 16–17-hour intervals before 01:00 CEST on 15 July. The analysis identifies a slight statistically significant difference ($0.01 < p < 0.05$) between the 13–14 and 14–15-hour intervals, with the interquartile range of 19–35 fatalities. This is followed by two other slightly significant differences between the earlier intervals. These findings suggest that issuing a warning at least 13 hours in advance is likely optimal for reducing fatalities. However, issuing warnings as early as possible appears crucial for effectiveness, as a non-significant level of statistical difference ($p > 0.05$) is not observed in the comparisons between the hour ranges.

In scenario A2.2, characterised by suboptimal warning diffusion and mobilisation, fatalities decrease from an interquartile range of 138–174 to 66–85 across the extreme

hour ranges. This scenario exhibits a similar pattern to scenario A2.1, with a further reduction in the interquartile range to 74–95 during the 13–14-hour interval. These results underscore the critical importance of issuing warnings as early as possible to mitigate the potential loss of life in this scenario effectively.

Figure 5.11 – Estimated fatalities for the alternative early warning and evacuation scenarios, with a focus on evaluating the time of the first flood warning, highlighting the significance level of the statistical difference between estimated fatalities during the 1-hour interval and the previous hour range. A2.1 (optimal warning diffusion and mobilisation), A2.2 (suboptimal warning diffusion and mobilisation), and A2.3 (optimal warning diffusion and empirical mobilisation).

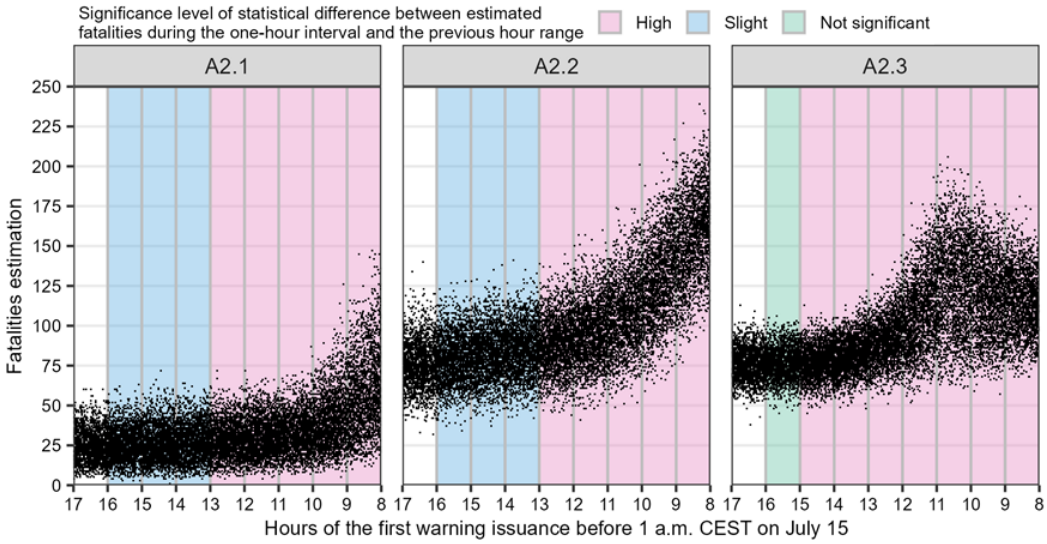

In the suboptimal scenario with the empirical mobilisation curve (A2.3), estimated fatalities decrease from an interquartile range of 102–128 to 39–82 across extreme hour ranges. Fatalities increase from the first extreme hour range to the 10–11-hour interval, with an interquartile range of 103–147, indicating that warnings issued within this interval result in more people being trapped during evacuation. This outcome can be attributed to the combined effect of warning diffusion and mobilisation, the same as scenario A1.5 in Figure 5.7, where the higher rise in the number of people on the streets occurs approximately three hours after the warning is issued, coinciding with the peak of the flood. Following this interval, significant reductions in fatalities ($p < 0.001$) are observed until stabilisation begins approximately 15 hours before the flood peak, suggesting that this is an optimal time for issuing the first flood warning. This scenario underscores the inadequacy of warning dissemination during the 2021 event and its impact on the estimated consequences. Even for later warning issuance times and the same mobilisation behaviour, this scenario can result in lower estimated

fatalities, with a median estimate of 115 fatalities, 24.3% lower than the RFEWE scenario, when the warning is issued between 8 and 9 hours before the peak.

5.5 Discussion of limitations

The LifeSim approach utilises Monte Carlo simulation to address epistemic and aleatory uncertainties. However, when interpreting scenarios, analysing and considering other limitations and uncertainties related to specific inputs and model assumptions are essential.

Although the flood hazard simulation provided a reasonable representation of water depths, flow velocities, and maximum arrival times, even slight variations in the hydrodynamic model could lead to high sensitivity in LifeSim outcomes, depending on the case study. For instance, a test simulation adjusting the water depth time series by subtracting the bias value of 0.46 metres from all pixels across all layers in the hydraulic simulation resulted in a reduced fatality estimate, with the median value decreasing to 126, i.e. 17% lower than the reconstructed scenario. It is important to note that the reported water depths used to calculate the bias correspond to different vertical datums, including street level, pedestrian walkways, and doorsteps. Moreover, this test represents an extreme generalisation of the bias across the entire domain, preliminarily assessing the life-loss model's sensitivity concerning the hydrodynamic simulation for this case study.

Furthermore, other uncertainties and factors could significantly influence life-loss estimation. The hydraulic model does not account for bridges within the simulated domain, potentially altering flood characteristics due to possible clogging, particularly affecting nearby buildings, as observed during the actual flood event. Additionally, building footprints were excluded from the digital elevation model, turning it into a digital surface model to enhance urban flow simulation. For the loss of life estimation, the highest hazard of the adjacent pixels was chosen. This may introduce a bias towards higher fatalities. However, if this is the case it has to be tested by an analysis using the lowest or mean hazard around the buildings.

The detailed information required for building elements in LifeSim results in numerous hypotheses, as obtaining such detailed data is often challenging. Upscaling 100-metre

resolution population data to buildings, weighted by building footprint size, can inaccurately associate a higher population with large areas that actually have a lower population capacity than smaller ones due to verticalisation. Moreover, specific occupancy patterns and individual characteristics are complex to represent using open data. For example, 12 of 15 fatalities in Sinzig were related to people in an inpatient residence, who were not able to leave the building by themselves. Additionally, some building footprints may pertain to commercial or other non-residential sectors, introducing further uncertainty since the population data used only account for residential individuals. The impact of this consideration is less significant during nighttime hazards compared to daytime scenarios when the population distribution varies based on the sectoral distribution of buildings. Furthermore, attributes such as the number of building floors are determined by the post-event survey, potentially lacking accurate representation due to non-representative sampling.

The lack of representative survey sampling can also impact the reconstruction of warning and evacuation processes. Additionally, the reconstruction of these curves for the 2021 Ahr Valley flood aimed to represent the time spent between the warning issuance and the initiation of proactive evacuation actions. Several filters were applied to the survey data to isolate responses related explicitly to evacuation, as the survey initially encompassed a broader context of mitigation measures. Notably, 83% of respondents recognise the need for self-protection only at the moment of the hazard occurrence, which can impact comparative analysis with historical cases, given that the warning diffusion curve is not based on an official warning channel. The content of the warning and the perception of personal impacts significantly influence the mobilisation times (LINDELL *et al.*, 2020). The lack of detailed evacuation information, received by only 17.5% of respondents, combined with 84% being surprised by the flood, likely contributes to the low mobilisation rate. This rate might improve if the population received timely warnings and clear instructions, as 76% of respondents stated they clearly understood what actions to take.

Even when applying a filter to the survey to account for people directly impacted by the main event in the simulated domain, generalising the warning and evacuation process in this domain can lead to overestimating fatalities in upstream regions. The generalisation is necessary due to the lack of precise building location data for survey

respondents. The overestimation arises because there is a 2 to 3-hour difference between the arrival time of the flood in upstream cities compared to downstream areas, and most people were warned only when the flood reached them. As a result, individuals in upstream regions may have taken earlier action than those in the model sampling.

Furthermore, alternative scenarios were developed to incorporate realistic elements into theoretical models and their parameterisation proposed by Sorensen and Mileti (2015b, 2015c). However, most of the cases used to propose the parameterisation of these theoretical models are based on older events primarily focused on the context of the United States. Incorporating recent flood events from diverse locations could enhance the representation of realistic scenarios.

Concerning evacuation dynamics, summarising flood values using the midpoint could distort actual parameter values along roads, especially over extended road lengths. Additionally, LifeSim does not consider prior vehicle conditions on road networks, which could significantly impact the representation of traffic jams, particularly in high-density areas.

5.6 Conclusions

The agent-based model (ABM) LifeSim is used to evaluate the impact of warning system procedures on life-loss estimates during the 2021 Ahr Valley flood. After defining the reconstruction scenario, we evaluated the impact of alternative scenarios for flood early warning and evacuation. The median of the probabilistic LifeSim model results overestimates actual fatalities by 28.8% within the same simulated domain. Nonetheless, the output maintains a consistent proportion of indoor to outdoor fatalities. The distribution of fatalities along the Ahr Valley is overestimated in upstream regions and underestimated in downstream regions. This discrepancy is attributed mainly to generalising the early warning and evacuation processes within the simulated domain, which may lead to variations in evacuation start times across different regions compared to the actual event, particularly in these extreme domain areas.

The 2021 Ahr Valley flood warning diffusion had a significant delay and lower mobilisation rates in protective actions following the first flood warning issuance

compared to the worst theoretical alternative scenarios. The median of estimated fatalities could be reduced by 80% in an optimal theoretical scenario of warning diffusion and mobilisation (scenario A1.1 in Figure 5.10). However, under the actual conditions of warning dissemination, where most of the population was either just warned or became aware when the flood reached them, higher mobilisation rates could result in increased fatalities. In such situations, seeking safe places on the upper floors of buildings is a more effective protective action, as in scenarios without outside evacuation, the median of estimated fatalities is lower than in the reconstructed scenario.

The early flood warning reported 13 hours before the water level peak in the upstream domain appears to be the critical window to effectively reduce fatalities in scenarios with theoretical warning dissemination and evacuation. Thus the existing flood warning system provides information in due time. The problem is rather the information content (spatially distributed water depth forecasts are missing), warning dissemination, and the reaction of the population to the warnings. The presented simulation of early flood warning times underscores the significant impact of the actual poor dissemination during the 2021 event. Even with later warning issuance times, if accompanied by better warning diffusion and the same mobilisation behaviour as observed in the actual event, fatalities could be reduced by 24.3% (scenario A2.3 in Figure 5.11).

Using life-loss ABMs in flood risk assessments can enhance the evaluation of flood hazards and the effectiveness of warning systems. Dynamic simulations over time and space offer valuable insights into optimal intervention timings and critical regions for implementing mitigation measures. The LifeSim model can incorporate both epistemic and random uncertainties, resulting in probabilistic rather than deterministic outcomes. However, several critical aspects of uncertainty must be acknowledged. Efforts are recommended to better represent the variations in warning diffusion and evacuation responses in the specific case study, with benefits incorporating the different responses across various impacted zones. Additionally, ABMs require high-resolution data, which can be challenging to obtain accurately. Comparing these models with empirical ones could enhance the understanding of their differences, as empirical models can be deployed more swiftly, offering faster outcomes in forecasting and nowcasting scenarios.

5.7 Appendix

5.7.1 Fraction of evacuation mode choice

The evacuation mode statistics significantly impact the estimated fatalities across all scenarios and when compared individually ($p < 0.001$). When 100% of the population evacuates on foot, the median number of fatalities is 229, with an interquartile range of 210–245. In contrast, if the entire population evacuates by vehicles, the median number of fatalities decreases to 133, with an interquartile range of 124–142. These differences affect only fatalities during the evacuation, with extreme median values ranging from 38 to 124 (Figure 5.12 and Table 5.3).

Figure 5.12 – 2021 Ahr Valley flood estimated fatalities and their location for several fractions of evacuation mode.

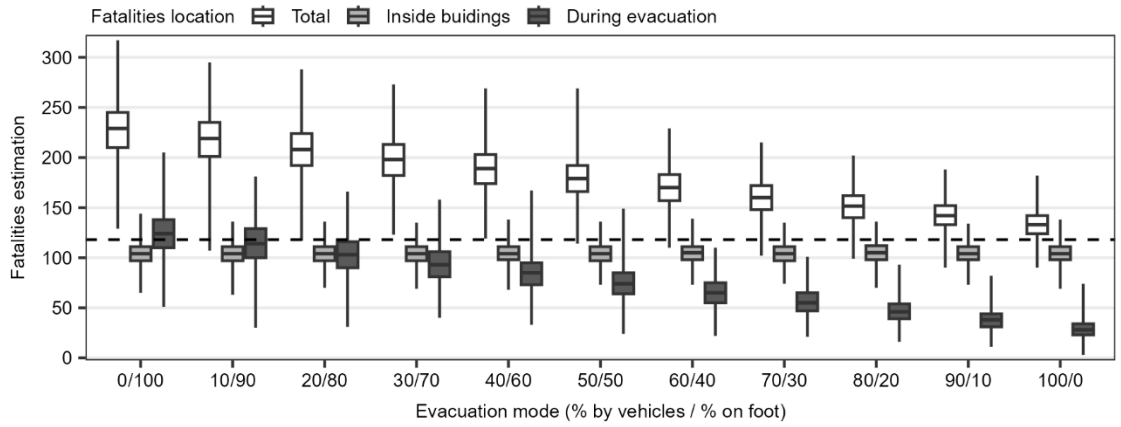

Table 5.3 – 2021 Ahr Valley flood estimated fatalities statistics for several fractions of evacuation mode.

Evacuation mode (% by vehicles / % on foot)	Fatalities estimation							Fraction of indoor fatalities (%)
	Median	First quartile	Third quartile	Minimum	Maximum	Median inside structures	Median during evacuation	
0/100	229	210	245	129	317	104	124	45.4
10/90	219	201	235	107	295	104	114	47.5
20/80	208	192	224	117	288	104	103	50.0
30/70	198	182	213	123	273	104	93	52.5
40/60	189	174	203	119	269	104	85	55.0
50/50	179	166	192	114	269	104	74	58.1
60/40	170	157	183	110	229	105	65	61.8
70/30	160	148	172	102	215	104	55	65.0
80/20	151.5	140	162	99	202	105	46	69.3
90/10	142	133	152	90	188	104	38	73.2
100/0	133	124	142	90	182	104	28	78.2

Although the evacuation mode of 100% of the population evacuating by vehicles results in a fatality count closest to the actual number (118), the scenario where 80% evacuate by vehicles and 20% on foot most matches the proportion of indoor fatalities. This scenario shows a fraction of indoor fatalities at 69.3%, compared to 68.5% in the actual event.

5.7.2 Alternative warning and evacuation scenarios

The principal factors affecting the dissemination of the first warning include the number of channels, their technologies, frequency, and the time of day (SORENSEN; MILETI, 2015c). Factors influencing most mobilisation times include, in addition to the warning content and perception of personal impacts, environmental cues and impact intensity (SORENSEN; MILETI, 2015e). Theoretical models are proposed to represent each of these processes based on an extensive database of historical cases involving various hazard sources and previous studies.

In order to estimate the population warned within a specific minute time step (P_{warned_t}), the Rayleigh distribution can be employed in conjunction with a specific rate of unofficial means of warning (Equation 19). This model is influenced by two key coefficients: b_t and c_t. The coefficient b_t represents the effectiveness of the broadcast channels utilised and serves as the shape parameter of the Rayleigh distribution. Conversely, c_t indicates the efficiency of non-official broadcast means at time step t. Low values of b_t correspond to more efficient broadcast channels, whereas higher values of c_t correlate with an increased rate of the population being warned through informal means. (SORENSEN; MILETI, 2015c). For mobilisation, the proportion of population who being mobilised at minute time t ($P_{mobilised_t}$) is described by Equation 20. This probability depends on the mobilisation speed coefficient (a_m) and the median time for individuals to initiate mobilisation (b_m). As a_m decreases from a value of 2, the response time accelerates. Conversely, when a_m increases, the response time decelerates. Additionally, higher values of b_m indicate a longer duration to complete the initiation of protective action (SORENSEN; MILETI, 2015e).

$$P_{warned_t} = P_{warned_{t-1}} + \left(\frac{t}{b_t^2} e^{-\frac{t^2}{2b_t^2}}\right) + \left(1 - P_{warned_{t-1}}\right) * \left(P_{warned_{t-1}} * c_t\right) \quad (19)$$

$$P_{mobilised_t} = 1 - e^{(-(t^2)/a_m {b_m}^2)} \quad (20)$$

A specific selection of these cases is utilised to define the proposed curves and their uncertainty bounds in LifeSim. There are ten recommended curves (five for each period of the day) for warning diffusion in LifeSim, derived from six historical cases, including chemical spills, hazardous material flow, volcanic eruptions, and flash floods. Additionally, nine mobilisation curves are combined with levels of perception and preparedness, based on evaluations of three cases involving chemical and hazardous material accidents (SORENSEN; MILETI, 2015c, 2015e; USACE, 2020). Table 5.4 presents the utilised curves, their respective coefficients, and mobilisation rates for each scenario.

Table 5.4 – First approach of alternative scenarios of early warning and evacuation. Warning diffusion and mobilisation bounds with their coefficients and rates for various scenarios: A1.1 (optimal scenario), A1.2 (intermediate scenario), A1.3 (suboptimal scenario), A1.4 (suboptimal with empirical warning diffusion curve), and A1.5 (suboptimal with empirical mobilisation curve).

Alternative scenario	Bounds	Warning diffusion			Mobilisation					
		Curve	b_t	c_t	Curve	a_m	b_m	Maximum mobilisation rate		
								8 h	24 h	72 h
A1.1	Upper	Fast	5.0	0.100	Preparedness good perception likely	1.00	25.0	100.0	100.0	100.0
	Most likely		9.5	0.098		1.37	64.0	88.8	95.7	98.6
	Lower		51.5	0.081		1.80	114.0	77.1	91.1	97.2
A1.2	Upper	Moderate	58.0	0.080	Preparedness poor perception likely	1.35	61.8	81.5	95.0	98.5
	Most likely		100.0	0.060		1.79	111.8	74.3	90.0	95.0
	Lower		142.0	0.043		2.20	161.9	67.1	85.0	92.0
A1.3	Upper	Slow	103.0	0.060	Preparedness poor perception unlikely	1.35	61.8	65.9	88.7	92.8
	Most likely		145.0	0.042		1.79	111.8	57.0	84.2	90.0
	Lower		150.0	0.040		2.20	161.9	48.0	79.8	87.2
A1.4	Upper	Empirical			Preparedness poor perception unlikely	1.35	61.8	65.9	88.7	92.8
	Most likely					1.79	111.8	57.0	84.2	90.0
	Lower					2.20	161.9	48.0	79.8	87.2
A1.5	Upper	Slow	103.0	0.060	Empirical					
	Most likely		145.0	0.042						
	Lower		150.0	0.040						

5.7.3 Life-loss model convergence

Figure 5.13 illustrates the estimated fatalities mean, standard deviation, skewness, and kurtosis over model iterations for the reconstruction scenario and the first approach of alternative scenarios. The results indicate that 2,000 iterations are sufficient for the convergence of these statistics.

Figure 5.13 – Estimated fatalities mean, standard deviation, skewness, and kurtosis trace for reconstructed scenario of the 2021 flood and for the alternative early warning and evacuation scenarios, which focus on evaluating the warning diffusion and mobilisation curves: RFEWE (reconstructed scenario of the 2021 flood), A1.1 (optimal scenario), A1.2 (intermediate scenario), A1.3 (suboptimal scenario), A1.4 (suboptimal with empirical warning diffusion curve), and A1.5 (suboptimal with empirical mobilisation curve).

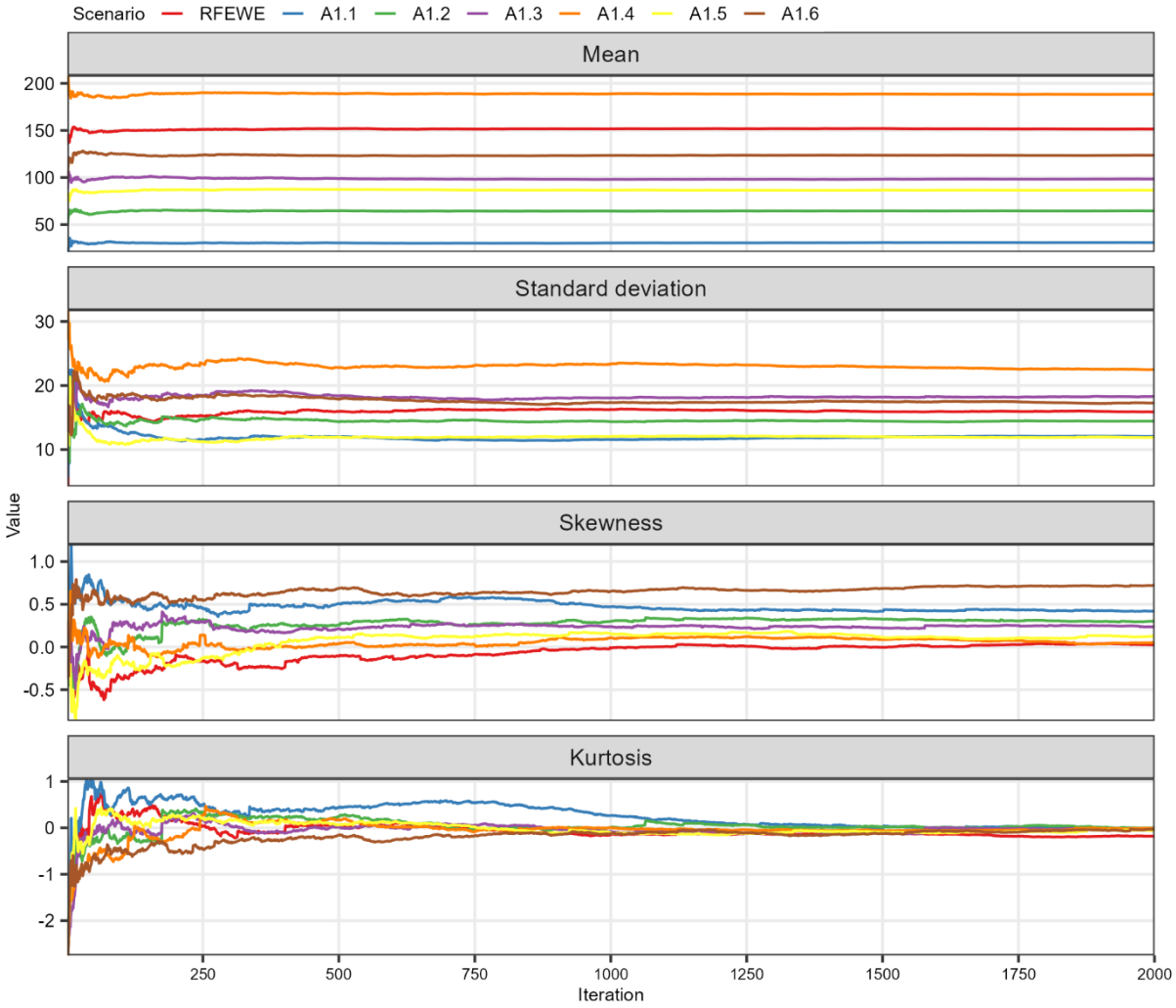

6 CONCLUSIONS AND RECOMMENDATIONS

Life-loss estimation methods represent a powerful tool for evaluating the effectiveness of flood Early Warning and Evacuation Systems (EWESs), particularly through the application of agent-based models. However, several uncertainties remain in this field. Although specific inputs, such as life-loss probability thresholds and warning and evacuation times, are already treated with associated uncertainties, the flood hazard itself is generally not considered a probabilistic input. This omission is primarily due to the high computational cost associated with probabilistic simulations when using traditional sampling techniques. Furthermore, the temporal and spatial variability of population distribution is typically not incorporated probabilistically, despite its potential to significantly affect quantitative estimates of exposed individuals, especially in areas dominated by commercial activities. Additionally, the models used to parameterise EWESs are primarily based on North American contexts, which limits their applicability to other regions.

This thesis explores these challenges through four interconnected chapters. First, the LifeSim agent-based model is used to assess the effectiveness of EWES through spatial and temporal sectorisation of the exposed area. Second, a probabilistic dam-breach flood mapping method is applied to a different dam typology, using an alternative dam failure database to define breach probabilities. Third, a novel framework is developed that integrates probabilistic flood modelling and probabilistic population distribution into LifeSim to improve life-loss estimation. Finally, an occurred EWES response is reconstructed using official reports and resident surveys, and then compared to theoretical EWES scenarios to evaluate its performance.

In the first chapter, the LifeSim model is applied to a densely urbanised valley downstream of a water accumulation dam in Belo Horizonte, Minas Gerais, Brazil, to evaluate the effectiveness of EWES. A sectorised approach is used to identify optimal times for issuing flood warnings. The analysis reveals that the first three downstream sectors are the most sensitive in terms of potential fatalities. In high-mobilisation scenarios, issuing warnings four hours before dam failure significantly reduces life loss. However, under low-mobilisation conditions, even a twelve-hour advance warning does not reduce the likelihood of life-loss rates exceeding 0.1, especially in the two most critical sectors.

This analysis underscores the value of agent-based modelling in EWES planning. By assessing the effectiveness of different warning issuance times under varying warning dissemination and mobilisation scenarios, LifeSim supports the prioritisation of critical sectors and identifies strategic phases within the EWES timeline (Figure 1.2) where targeted investments can enhance emergency response and reduce fatalities.

For the second chapter, an alternative approach to high-resolution probabilistic dam-breach flood modelling is explored. Specifically, the methodology proposed by Rizzo, Maranzoni, and D'Oria (2023) is applied, which involves weighting representative scenarios based on historical data on dam failures. Initially applied to concrete dams, this approach is extended to embankment dams by considering dimensionless breach top width and formation time, and employing a different failure database to assign scenario weights.

In the ICOLD (International Commission on Large Dams) benchmark case study and considering 25 weighted scenarios, probabilistic flood mapping indicates that 77.4 km^2 are potentially inundated, with 84.0% of this area having a 100% probability of flooding. The deterministic flood boundary encompasses all areas with inundation probabilities greater than 0.4, covering an area of 69.3 km^2. The narrow valley downstream exhibits a 100% probability of the highest hazard classes, implying unsafe conditions for vehicles, pedestrians, and buildings. Conversely, the flatter valley areas show intermediate hazard levels. Flood arrival time is also considered, particularly in defining the self-rescue zone, typically understood as the area within 10 kilometres or 30 minutes of flood arrival, whichever is greater. In this case, all approaches using arrival time define the self-rescue zone as extending 10 kilometres downstream.

This flood scenario-weighting methodology offers a computationally efficient alternative to traditional probabilistic dam breach modelling. Although it simplifies the process by limiting the number of input parameters and scenarios, it still provides robust results and enables integration with other consequence modelling frameworks. These advantages make it particularly suitable for coupling with life-loss estimation models, as explored in the third chapter.

The third chapter presents a novel life-loss estimation framework that explicitly integrates uncertainties in flood dynamics and population distribution into the LifeSim

agent-based model. Building upon the methodology developed by Maranzoni, D'Oria, and Rizzo (2023b), the empirical life-loss model is replaced by the more detailed LifeSim framework. This thesis also extends the contributions of El Bilali et al. (2022) by incorporating flood-related uncertainty more comprehensively. The framework leverages the reproducibility of sampled uncertainty parameter values within the LifeSim model to construct a probabilistic scenario, represented by its weighted mean and associated variability.

Applied to the ICOLD case study again, this framework incorporates 50 weighted scenarios, comprising a combination of 25 scenarios that reflect flood hazard uncertainties and two scenarios that represent population distributions during both business and non-business hours. The results show statistically significant differences between probabilistic and deterministic life-loss estimates. Probabilistic simulations generally yield lower fatality estimates than deterministic ones, while the probabilistic mean plus one standard deviation produces higher estimates, emphasising the importance of uncertainty quantification.

In addition to combining hydraulic uncertainties with temporal and spatial variability in population exposure, this chapter marks a substantial advancement in life-loss modelling by incorporating scenario weighting based on variables beyond peak discharge. The probabilistic flood modelling approach employed in this study enables the consideration of additional variables, such as flood arrival time, which are crucial for assessing the feasibility of evacuation. The arrival time of the flood wave can, in many cases, be more consequential than its peak magnitude, as it directly affects the window of opportunity for self-rescue. Moreover, relying solely on peak flow for scenario weighting risks overlooking the issue of equifinality, wherein different breach parameter combinations produce similar peak discharges but result in significantly different arrival times and, consequently, life-loss outcomes.

Finally, in the last chapter, the LifeSim model is used to assess the impact of EWES procedures on life-loss outcomes during the 2021 Ahr Valley flood in Germany. Alternative EWES strategies are evaluated based on a reconstruction scenario developed from official reports and survey data. The median life-loss estimate from the probabilistic LifeSim simulation overestimates actual fatalities by 28.8%, but accurately

captures the proportion of fatalities that occur indoors versus outdoors. Analysis reveals that significant delays in warning diffusion and lower mobilisation rates following initial alerts contributed to higher mortality. In an optimal theoretical scenario of timely warning diffusion and high mobilisation, fatalities could have been reduced by up to 80%. However, higher mobilisation rates could have led to more fatalities under the actual conditions of warning dissemination, where many individuals were only alerted upon direct exposure to the flood. In these circumstances, seeking shelter on upper floors proved to be a more effective protective action.

The results show that the critical opportunity to reduce fatalities was available during early warnings issued prior to peak flood levels upstream. Therefore, the primary issues in the 2021 flood were not the timeliness of warnings, but the inadequacy of warning content (e.g., absence of spatially distributed flood forecasts), ineffective dissemination strategies, and insufficient population response.

The final chapter of the thesis highlights the discrepancy between local EWES response times and those assumed in theoretical models. The delays in warning dissemination and mobilisation for the 2021 flood were significantly worse than in even the most pessimistic theoretical scenarios. This highlights the importance of understanding local emergency conditions when using agent-based models to simulate EWES performance and enhance consequence estimation accuracy.

This thesis demonstrates and explores several limitations associated with the application of life-loss agent-based models. However, additional challenges continue to hinder their practical implementation, beyond the intrinsic limitations of the models themselves, which have already been discussed in this study. Even with observed reductions in fatalities per event, the preparedness of authorities and populations tends to improve mainly for events of similar or lower magnitude, whereas unprecedented events still cause greater damage than previous extremes (KREIBICH *et al.*, 2022). Moreover, although the inclusion of uncertainty in risk analyses is widely recommended, effectively communicating this uncertainty remains a significant challenge. Statistical representations are often complex for practitioners and decision-makers to interpret, thereby limiting their practical utility (PAPPENBERGER; BEVEN, 2006; POORTVLIET *et al.*, 2019).

Additional limitations are directly associated with the LifeSim model. This modelling approach requires high-resolution data on population and buildings, which is often difficult to obtain through open datasets, particularly for undeveloped countries and small regions, thereby increasing simulation uncertainty. Moreover, prior traffic conditions on roads cannot currently be incorporated, which may notably affect simulation results, particularly during rush hours and in densely populated areas. Also, summarising hazard variables at the midpoint of road segments can lead to inaccurate representations, especially across long reaches.

Based on the findings of this study, several areas are recommended for future research:

- Although agent-based life-loss models are better suited for EWES analyses, empirical life-loss models could be valuable for rapid assessments and prioritisation of investment areas. Regional empirical models developed for Italy (YAZDANI *et al.*, 2023) and Iran (SHOKOOHI; AMIRMORADI, 2025) demonstrate this potential. With available databases regarding exposure and vulnerability from past events (PAPAGIANNAKI *et al.*, 2022; PAPROTNY *et al.*, 2024) or with investments aimed at flood fatalities-related data acquisition (BRÁZDIL *et al.*, 2024), regional empirical models could be developed;
- while this study considers breach top width and formation time as uncertain inputs for dam-breach simulations, further research could examine other parameters. Besides, comparative analyses between this approach and traditional Monte Carlo-based probabilistic simulations could provide additional insights into computational efficiency and feasibility, especially with new model versions capable of running on graphics processing units (e.g., HEC-RAS 2025 and RIM2D);
- this study leverages the LifeSim sampling routine to define a probabilistic scenario for each iteration. However, alternative strategies, such as ranking fatality estimates for each weighted scenario and calculating the weighted mean based on each rank-specific value, could enable this approach to other agent-based models that do not follow the same sampling scheme as LifeSim. Furthermore, using different case studies, the proposed framework could be compared to those developed by El Bilali et al. (2022) and Maranzoni, D'Oria,

and Rizzo (2023b). Historical dam failures, such as Brumadinho (Brazil, 2019) and Malpasset (France, 1959), offer valuable opportunities for such comparisons, enabling the evaluation of both the models themselves and their effectiveness in simulating past events;

- one key advantage of LifeSim is its ability to generate detailed outputs on agent behaviour for each simulation iteration. Although the generation and analysis of this detailed output currently require substantial manual effort, future research could leverage these results to analyse optimal evacuation routes, prioritise warnings for specific regions, identify areas more suitable for vertical rather than horizontal evacuation strategies, and investigate individual risk patterns; and
- finally, theoretical models representing EWES dynamics may diverge significantly from actual emergency management practices. Incorporating data from training exercises conducted under local urban flood contingency plans and dam failure emergency action plans could help develop more context-specific models. These models would enhance understanding of local warning issuance times, dissemination processes, and population behavioural responses.

REFERENCES

ABDEDOU, A.; SOULAÏMANI, A.; TCHAMEN, G. W. Uncertainty propagation of dam break flow using the stochastic non-intrusive B-splines Bézier elements-based method. **Journal of Hydrology**, v. 590, n. February, p. 125342, 2020. Disponível em: https://doi.org/10.1016/j.jhydrol.2020.125342

ABDULRAHMAN, K. Z.; FARIS, M. R.; IBRAHIM, H. M.; YOUSIF, O. S. Q.; GHAFOOR, A. A.; OTHMAN, L. S.; KARAKOUZIAN, M. Hypothetical failure of the Khassa Chai dam and flood risk analysis for Kirkuk, Iraq. **Natural Hazards**, p. 1–19, 2022. Disponível em: https://doi.org/10.1007/s11069-022-05371-2

ABOELATA, M.; BOWLES, D. LIFESim: a model for estimating dam failure life loss. **International Symposium on Stochastic Hydraulics 2005: 23 and 24 May 2005. Nijmegen - The Netherlands**, p. 87–89, 2005 a.

ABOELATA, M.; BOWLES, D. S. **LIFESim: A Model for Estimating Dam Failure Life Loss**. Logan, Utah,: *[s. n.]*, 2005 b.

ABOELATA, M.; BOWLES, D. S.; MCCLELLAND, D. M. A model for estimating dam failure life loss. *In*: 2003, Launceston, Tasmania, Australia. **Australian Committee on Large Dams Risk Workshop**. Launceston, Tasmania, Australia: *[s. n.]*, 2003. p. 18.Disponível em: https://doi.org/10.1061/40694(2003)11

AERTS, J. C. J. H.; BOTZEN, W. J.; CLARKE, K. C.; CUTTER, S. L.; HALL, J. W.; MERZ, B.; MICHEL-KERJAN, E.; MYSIAK, J.; SURMINSKI, S.; KUNREUTHER, H. Integrating human behaviour dynamics into flood disaster risk assessment. **Nature Climate Change**, v. 8, n. 3, p. 193–199, 2018. Disponível em: https://doi.org/10.1038/s41558-018-0085-1

AHMADISHARAF, E.; KALYANAPU, A. J.; THAMES, B. A.; LILLYWHITE, J. A probabilistic framework for comparison of dam breach parameters and outflow hydrograph generated by different empirical prediction methods. **Environmental Modelling and Software**, v. 86, p. 248–263, 2016. Disponível em: https://doi.org/10.1016/j.envsoft.2016.09.022

ALAEDDINE, H.; SERRHINI, K.; MAIZIA, M.; NÉRON, E. A spatiotemporal optimization model for the evacuation of the population exposed to flood hazard. **Natural Hazards and Earth System Sciences**, v. 15, n. 3, p. 687–701, 2015. Disponível em: https://doi.org/10.5194/nhess-15-687-2015

ALMEIDA, I. M.; SANTOS, H. A.; DE VASCONCELOS COSTA, O.; GRACIANO, V. B. Uncertainty reduction in flood areas by probabilistic analyses of land use/cover in models of two-dimensional hydrodynamic model of dam-break. **Stochastic Environmental Research and Risk Assessment**, v. 38, n. 4, p. 1335–1350, 2024. Disponível em: https://doi.org/10.1007/s00477-023-02635-6

ANSHUKA, A.; VAN OGTROP, F. F.; SANDERSON, D.; LEAO, S. Z. A systematic review of agent-based model for flood risk management and assessment using the ODD protocol. **Natural Hazards**, v. 112, n. 3, p. 2739–2771, 2022. Disponível em: https://doi.org/10.1007/s11069-022-05286-y

APEL, H.; ARONICA, G. T.; KREIBICH, H.; THIEKEN, A. H. Flood risk analyses - How detailed do we need to be? **Natural Hazards**, v. 49, n. 1, p. 79–98, 2009. Disponível em: https://doi.org/10.1007/s11069-008-9277-8

APEL, H.; THIEKEN, A. H.; MERZ, B.; BLOCHL, G. Flood risk assessment and associated uncertainty. **Natural Hazards and Earth System Science**, v. 81, n. 2, p. 343–347, 2004. Disponível em: https://doi.org/10.5194/nhess-9-289-2009

APEL, H.; VOROGUSHYN, S.; MERZ, B. Brief communication: Impact forecasting could substantially improve the emergency management of deadly floods: case study July 2021 floods in Germany. **Natural Hazards and Earth System Sciences**, v. 22, n. 9, p. 3005–3014, 2022. Disponível em: https://doi.org/10.5194/nhess-22-3005-2022

AURELI, F.; MARANZONI, A.; PETACCIA, G. Review of Historical Dam-Break Events and Laboratory Tests on Real Topography for the Validation of Numerical Models. **Water (Switzerland)**, v. 14, n. 2, p. 1–21, 2021. Disponível em: https://doi.org/10.3390/w14020264

BELLO, D.; ALCAYAGA, H.; CAAMAÑO, D.; PIZARRO, A. Influence of Dam Breach Parameter Statistical Definition on Resulting Rupture Maximum Discharge. **Water**, v. 14, 2022. Disponível em: https://doi.org/doi.org/10.3390/w14111776

BELLOS, V.; TSAKIRIS, V. K.; KOPSIAFTIS, G.; TSAKIRIS, G. Propagating dam breach parametric uncertainty in a river reach using the HEC-RAS software. **Hydrology**, v. 7, n. 4, p. 1–14, 2020. Disponível em: https://doi.org/10.3390/hydrology7040072

BERGHÄUSER, L.; BUBECK, P.; HUDSON, P.; THIEKEN, A. H. Identifying and characterising individual flood precautionary behaviour dynamics from panel data. **International Journal of Disaster Risk Reduction**, v. 94, p. 103835, 2023. Disponível em: https://doi.org/10.1016/j.ijdrr.2023.103835

BERNARD-GARCIA, M.; MAHDI, T.-F. **A Worldwide Historical Dam Failure's Database**. V1. *[S. l.]*: Borealis, 2020. Disponível em: https://doi.org/doi/10.5683/SP2/E7Z09B

BOPP, E.; DOUVINET, J. Alerting people prioritising territories over technologies. A design framework for local decision makers in France. **Applied Geography**, v. 146, 2022. Disponível em: https://doi.org/10.1016/j.apgeog.2022.102769

BOYD, E.; LEVITAN, M.; VAN HEERDEN, I. Further specification of the dose-response relationship for flood fatality estimation. *In*: 2005, **US-Bangladesh workshop on innovation in windstorm/storm surge mitigation construction. National Science Foundation and Ministry of Disaster & Relief, Government of Bangladesh. Dhaka**. *[S. l.: s. n.]* p. 19–21.

BRÁZDIL, R.; FATUROVÁ, D.; ŠULC MICHALKOVÁ, M.; ŘEHOŘ, J.; CALETKA, M.; ZAHRADNÍČEK, P. Spatiotemporal variability of flash floods and their human impacts in the Czech Republic during the 2001–2023 period. **Natural Hazards and Earth System Sciences**, v. 24, n. 10, p. 3663–3682, 2024. Disponível em: https://doi.org/10.5194/nhess-24-3663-2024

BRAZDOVA, M.; RIHA, J. A simple model for the estimation of the number of fatalities due to floods in central Europe. **Natural Hazards and Earth System Sciences**, v. 14, n. 7, p. 1663–1676, 2014. Disponível em: https://doi.org/10.5194/nhess-14-1663-2014

BROWN, C. A.; GRAHAM, W. J. Assessing the threat to life from dam failure 1. **JAWRA Journal of the American Water Resources Association**, v. 24, n. 6, p. 1303–1309, 1988.

BRUNNER, G. W. **HEC-RAS. River Analysis System. Hydraulic Reference Manual - Version 6.0**. U.S. Army Corps of Engineers, Davis, California, United States: *[s. n.]*, 2020.

BRUNNER, G. W. **HEC-RAS 2D User's Manual**. U.S. Army Corps of Engineers, Davis, California, United States: *[s. n.]*, 2023.

BRUSSEE, A. R.; BRICKER, J. D.; DE BRUIJN, K. M.; VERHOEVEN, G. F.; WINSEMIUS, H. C.; JONKMAN, S. N. Impact of hydraulic model resolution and loss of life model modification on flood fatality risk estimation: Case study of the Bommelerwaard, The Netherlands. **Journal of Flood Risk Management**, v. 14, n. 3, p. 1–15, 2021. Disponível em: https://doi.org/10.1111/jfr3.12713

BRYANT, S.; KREIBICH, H.; MERZ, B. Bias in Flood Hazard Grid Aggregation. **Water Resources Research**, v. 59, n. 9, 2023. Disponível em: https://doi.org/10.1029/2023WR035100

CAO, Y.; ZHANG, N.; ZHANG, X.; ZHANG, J. Warning dissemination and public response in China's new warning system: evidence from a strong convective event in Qingdao City. **Journal of Risk Research**, v. 25, n. 1, p. 67–91, 2022. Disponível em: https://doi.org/10.1080/13669877.2021.1905694

CHAI, J.; WU, H.-Z. Prevention/mitigation of natural disasters in urban areas. **Smart Construction and Sustainable Cities**, v. 1, n. 1, p. 4, 2023. Disponível em: https://doi.org/10.1007/s44268-023-00002-6

CHEN, C.; KOLL, C.; WANG, H.; LINDELL, M. K. An interdisciplinary agent-based evacuation model: integrating the natural environment, built environment, and social

system for community preparedness and resilience. **Natural Hazards and Earth System Sciences**, v. 23, n. 2, p. 733–749, 2023. Disponível em: https://doi.org/10.5194/nhess-23-733-2023

CHEN, J.; SHI, H.; SIVAKUMAR, B.; PEART, M. R. Population, water, food, energy and dams. **Renewable and Sustainable Energy Reviews**, v. 56, p. 18–28, 2016. Disponível em: https://doi.org/10.1016/j.rser.2015.11.043

CLAUSEN, L.; CLARK, P. B. The development of criteria for predicting dambreak flood damages using modelling of historical dam failures. *In*: 1990, **International conference on river flood hydraulics**. : John Wiley & Sons Ltd. Hydraulics Research Limited, Wallingford, England, 1990. p. 369–380.

CRED & UNISDR. **Economic Losses, Poverty and Disasters1998-2017**. Brussels, Belgium and Geneva, Switzerland: *[s. n.]*, 2018.

CRED; UNDRR. **The human cost of disasters: an overview of the last 20 years (2000-2019)**. *[S. l.: s. n.]*. Disponível em: https://doi.org/https://doi.org/10.18356/79b92774-en.

CRED; UNISDR. **Economic Losses, Poverty and Disasters 1998-2017**. *[S. l.: s. n.]*. Disponível em: https://doi.org/10.13140/RG.2.2.35610.08643.

DA SILVA, A. Â. C. L.; ELEUTÉRIO, J. C. Identifying and testing the probability distribution of earthfill dam breach parameters for probabilistic dam breach modeling. **Journal of Flood Risk Management**, 2023. Disponível em: https://doi.org/10.1111/jfr3.12900

DAVIS, S. A. **Business Depth Damage Analysis Procedure**. Research Report 85-R-5, Virginia, United States: *[s. n.]*, 1985.

DE BRUIJN, K. M.; DIERMANSE, F. L. M.; BECKERS, J. V. L. An advanced method for flood risk analysis in river deltas, applied to societal flood fatality risk in the Netherlands. **Natural Hazards and Earth System Sciences**, v. 14, n. 10, p. 2767–2781, 2014. Disponível em: https://doi.org/10.5194/nhess-14-2767-2014

DEKAY, M. L.; MCCLELLAND, G. H. Predicting Loss of Life in Cases of Dam Failure and Flash Flood. **Risk Analysis**, v. 13, n. 2, p. 193–205, 1993. Disponível em: https://doi.org/10.1111/j.1539-6924.1993.tb01069.x

DI MAURO, M.; DE BRUIJN, K. M.; MELONI, M. Quantitative methods for estimating flood fatalities : towards the introduction of loss-of-life estimation in the assessment of flood risk. **Natural Hazards**, v. 63, p. 1083–1113, 2012. Disponível em: https://doi.org/10.1007/s11069-012-0207-4

DIJKSTRA, E. W. A Note on Two Problems in Connexion with Graphs. **Numer. Math.**, v. 1, p. 269–271, 1959. Disponível em: https://doi.org/10.1007/BF01386390

DINNO, A. **dunn.test: Dunn's Test of Multiple Comparisons Using Rank Sums**. *[S. l.: s. n.]* Disponível em: https://CRAN.R-project.org/package=dunn.test

DKKV. **Opfer- und Schadensdaten der Flut 2021 in Rheinland-Pfalz**. Bonn, Germany: *[s. n.]*, 2022.

D'ORIA, M.; MARANZONI, A.; MAZZOLENI, M. Probabilistic Assessment of Flood Hazard due to Levee Breaches Using Fragility Functions. **Water Resources Research**, v. 55, n. 11, p. 8740–8764, 2019. Disponível em: https://doi.org/10.1029/2019WR025369

DOUVINET, J.; SERRA-LLOBET, A.; BOPP, E.; KONDOLF, G. M. Are sirens effective tools to alert the population in France? **Natural Hazards and Earth System Sciences**, v. 21, n. 10, p. 2899–2920, 2021. Disponível em: https://doi.org/10.5194/nhess-21-2899-2021

DUNN, O. J. Multiple comparisons using rank sums. **Technometrics**, v. 6, n. 3, p. 241–252, 1964. Disponível em: https://doi.org/10.1080/00401706.1964.10490181

DYSARZ, T. Application of python scripting techniques for control and automation of HEC-RAS simulations. **Water**, v. 10, n. 10, 2018. Disponível em: https://doi.org/10.3390/w10101382

EL BILALI, A.; TALEB, A.; BOUTAHRI, I. Application of HEC-RAS and HEC-LifeSim models for flood risk assessment. **Journal of Applied Water Engineering and Research**, v. 9, n. 4, p. 336–351, 2021. Disponível em: https://doi.org/10.1080/23249676.2021.1908183

EL BILALI, A.; TALEB, I.; NAFII, A.; TALEB, A. A practical probabilistic approach for simulating life loss in an urban area associated with a dam-break flood. **International Journal of Disaster Risk Reduction**, v. 76, p. 103011, 2022. Disponível em: https://doi.org/10.1016/j.ijdrr.2022.103011

ELEUTÉRIO, J. C.; GUIMARÃES, M. T. G. G.; BEZERRA, R. G.; SILVA, A. F. R.; CAMILO, B. K. Simulados de rompimentos de barragem possibilitam o aprimoramento de sistemas de alerta e evacuação relacionados a inundações? *In*: 2024, Curitiba. **IV Encontro Nacional de Desastres**. Curitiba: Associação Brasileira de Recursos Hídricos, 2024. p. 1–4.Disponível em: https://files.abrhidro.org.br/Eventos/Trabalhos/241/IV-END0205-1-20240713-162504.pdf. Acesso em: 20 nov. 2024.

FERNANDES, G. W. *et al.* Deep into the mud: ecological and socio-economic impacts of the dam breach in Mariana, Brazil. **Natureza e Conservação**, v. 14, n. 2, p. 35–45, 2016. Disponível em: https://doi.org/10.1016/j.ncon.2016.10.003

FERRARI, A.; VACONDIO, R.; MIGNOSA, P. High-resolution 2D shallow water modelling of dam failure floods for emergency action plans. **Journal of Hydrology**, v. 618, 2023. Disponível em: https://doi.org/10.1016/j.jhydrol.2023.129192

FOSTER, M.; FELL, R.; SPANNAGLE, M. The statistics of embankment dam failures and accidents. **Canadian Geotechnical Journal**, v. 37, n. 5, p. 1000–1024, 2000. Disponível em: https://doi.org/10.1139/t00-030

FRIEDMAN, D. G. Computer simulation in natural hazard assessment. 1975.

FROEHLICH, D. C. Embankment Dam Breach Parameters and Their Uncertainties. **Journal of Hydraulic Engineering**, v. 134, n. 12, p. 1708–1721, 2008.

FROEHLICH, D. C. Predicting Peak Discharge from Gradually Breached Embankment Dam. **Journal of Hydrology**, v. 21, n. 11, 2016. Disponível em: https://doi.org/10.1061/(ASCE)HE.1943-5584.0001424.

GE, W.; JIAO, Y.; WU, M.; LI, Z.; WANG, T.; LI, W.; ZHANG, Y.; GAO, W.; VAN GELDER, P. Estimating loss of life caused by dam breaches based on the simulation of floods routing and evacuation potential of population at risk. **Journal of Hydrology**, v. 612, n. PA, p. 128059, 2022. Disponível em: https://doi.org/10.1016/j.jhydrol.2022.128059

GE, W.; SUN, H.; ZHANG, H.; LI, Z.; GUO, X.; WANG, X.; QIN, Y.; GAO, W.; VAN GELDER, P. Economic risk criteria for dams considering the relative level of economy and industrial economic contribution. **Science of the Total Environment**, v. 725, 2020. Disponível em: https://doi.org/10.1016/j.scitotenv.2020.138139

GE, W.; WANG, X.; LI, Z.; ZHANG, H.; GUO, X.; WANG, T.; GAO, W.; LIN, C.; VAN GELDER, P. Interval Analysis of the Loss of Life Caused by Dam Failure. **Journal of Water Resources Planning and Management**, v. 147, n. 1, p. 04020098, 2021. Disponível em: https://doi.org/10.1061/(asce)wr.1943-5452.0001311

GHAHRAMANI, N.; ADRIA, D. A. M.; RANA, N. M.; LLANO-SERNA, M.; MCDOUGALL, S.; EVANS, S. G.; TAKE, W. A. Analysis of Uncertainty and Sensitivity in Tailings Dam Breach-Runout Numerical Modelling. **Mine Water and the Environment**, 2024. Disponível em: https://doi.org/10.1007/s10230-024-00970-w

GHOMASH, S. K. Bin; APEL, H.; CAVIEDES-VOULLIÈME, D. Are 2D shallow-water solvers fast enough for early flood warning? A comparative assessment on the 2021 Ahr valley flood event. **Natural Hazards and Earth System Sciences**, v. 24, n. 8, p. 2857–2874, 2024. Disponível em: https://doi.org/10.5194/nhess-24-2857-2024

GOODELL, C.; RAEBURN, R.; KARKI, A.; JOHNSON, D.; MONK, S.; LEE, A. Probabilistic Dam Breac Modeling Using HEC-RAS And McBreach. *In*: 2019, **Journal of Chemical Information and Modeling**. *[S. l.: s. n.]* p. 1689–1699.

GRAHAM, W. **A Procedure for Estimating Loss of Life Caused by Dam Failure. DSO-99-06Sedimentation & River Hydraulics**. Denver, Colorado: *[s. n.]*, 1999.

GREENSHIELDS, B. D.; CHANNING, W.; MILLER, H. A study of traffic capacity. *In*: 1935, Washington DC, United States. **XIV Annual Meeting of the Highway Research Board Held at Washington**. Washington DC, United States: Highway Research Board, 1935. p. 448–477.

GUIMARÃES, R. N.; MOREIRA, V. R.; CRUZ, J. R. A.; SALIBA, A. P. M.; AMARAL, M. C. S. History of tailings dam failure: Impacts on access to safe water and influence on the legislative framework. **Science of the Total Environment**, v. 852, n. August, p. 158536, 2022. Disponível em: https://doi.org/10.1016/j.scitotenv.2022.158536

HAMMOND, M. J.; CHEN, A. S.; DJORDJEVIĆ, S.; BUTLER, D.; MARK, O. Urban flood impact assessment: A state-of-the-art review. **Urban Water Journal**, v. 12, n. 1, p. 14–29, 2015. Disponível em: https://doi.org/10.1080/1573062X.2013.857421

HARIRI, S.; WEILL, S.; GUSTEDT, J.; CHARPENTIER, I. A balanced watershed decomposition method for rain-on-grid simulations in HEC-RAS. **Journal of Hydroinformatics**, v. 24, n. 2, p. 315–332, 2022. Disponível em: https://doi.org/10.2166/hydro.2022.078

HE, C.; YANG, C. J.; TUROWSKI, J. M.; OTT, R. F.; BRAUN, J.; TANG, H.; GHANTOUS, S.; YUAN, X.; DE QUAY, G. S. A global dataset of the shape of drainage systems. **Earth System Science Data**, v. 16, n. 2, p. 1151–1166, 2024. Disponível em: https://doi.org/10.5194/essd-16-1151-2024

HILL, P.; KAVANAGH, C.; LANG, S. Applications of Simulation Model to Estimate Potential Loss of Life. *In*: 2018, Viena, Austria. **XXVI International Congress on Large Dams**. Viena, Austria: ICOLD, 2018.

HU, P.; ZHANG, Q.; SHI, P.; CHEN, B.; FANG, J. Flood-induced mortality across the globe: Spatiotemporal pattern and influencing factors. **Science of the Total Environment**, v. 643, p. 171–182, 2018. Disponível em: https://doi.org/10.1016/j.scitotenv.2018.06.197

HUANG, D.; YU, Z.; LI, Y. Calculation method and application of loss of life caused by dam break in China. **Natural Hazards**, v. 85, n. 1, p. 39–57, 2017. Disponível em: https://doi.org/10.1007/s11069-016-2557-9

ICOLD. **Bulletin XX PREPRINT: Current state-of-practice in risk-informed decision-making for the safety of dams and levees**. Paris, France: *[s. n.]*, 2020.

ISSERMANN, M.; CHANG, F. J. Uncertainty analysis of spatiotemporal models with point estimate methods (PEMs)-the case of the ANUGA hydrodynamic model. **Water (Switzerland)**, v. 12, n. 1, p. 1–16, 2020. Disponível em: https://doi.org/10.3390/w12010229

JIAO, H.; LI, W.; MA, D. Assessment of life loss due to dam breach using improved variable fuzzy method. **Scientific Reports**, v. 12, n. 1, p. 1–7, 2022. Disponível em: https://doi.org/10.1038/s41598-022-07136-0

JOHNSTONE, W. M.; SAKAMOTO, D.; ASSAF, H.; BOURBAN, S. Architecture, modelling framework and validation of BC hydro's virtual reality life safety model. *In*: 2005, **International Symposium on Stochastic Hydraulics**. *[S. l.: s. n.]* p. 87–89.

JONGEJAN, R. B.; JONKMAN, S. N.; VRIJLING, J. K. Methods for the economic valuation of loss of life. *In*: 2005, Nijmegen, The Netherlands. **Conference on International Law and Management of Large-Scale Risks**. Nijmegen, The Netherlands: IAHR, 2005. p. 1–8.

JONKMAN, S. N.; CURRAN, A.; BOUWER, L. M. Floods have become less deadly: an analysis of global flood fatalities 1975–2022. **Natural Hazards**, v. 120, n. 7, p. 6327–6342, 2024. Disponível em: https://doi.org/10.1007/s11069-024-06444-0

JONKMAN, S. N.; MAASKANT, B. B.; KOLEN, B. B.; NEEDHAM, J. T. J. Loss of life estimation - Review, developments and challenges. *In*: 2016, Lyon, France. **III European Conference on Flood Risk Management**. Lyon, France: *[s. n.]*, 2016.Disponível em: https://doi.org/10.1051/e3sconf/20160706004

JONKMAN, S. N.; MAASKANT, B.; BOYD, E.; LEVITAN, M. L. Loss of life caused by the flooding of New Orleans after hurricane Katrina: Analysis of the relationship

between flood characteristics and mortality. **Risk Analysis**, v. 29, n. 5, p. 676–698, 2009. Disponível em: https://doi.org/10.1111/j.1539-6924.2008.01190.x

JONKMAN, S. N.; VAN GELDER, P. H. A. J. M.; VRIJLING, J. K. An overview of quantitative risk measures for loss of life and economic damage. **Journal of Hazardous Materials**, v. 99, n. 1, p. 1–30, 2003. Disponível em: https://doi.org/10.1016/S0304-3894(02)00283-2

JONKMAN, S. N.; VRIJLING, J. K. Loss of life due to floods. **Journal of Flood Risk Management**, v. 1, n. 1, p. 43–56, 2008. Disponível em: https://doi.org/10.1111/j.1753-318x.2008.00006.x

JONKMAN, S. N.; VRIJLING, J. K.; VROUWENVELDER, A. C. W. M. Methods for the estimation of loss of life due to floods: a literature review and a proposal for a new method. **Natural Hazards**, v. 46, p. 353–389, 2008. Disponível em: https://doi.org/10.1007/s11069-008-9227-5

KALININA, A.; SPADA, M.; BURGHERR, P. Alternative life-loss rates for failures of large concrete and masonry dams in mountain regions of OECD countries. *In*: 2018, Trondheim, Norway. **XXVIII International European Safety and Reliability Conference, ESREL 2018**. Trondheim, Norway: *[s. n.]*, 2018. p. 9.Disponível em: https://doi.org/10.1201/9781351174664-213

KALININA, A.; SPADA, M.; BURGHERR, P. Probabilistic Analysis of Dam Accidents Worldwide: Risk Assessment for Dams of Different Purposes in OECD and Non-OECD Countries with Focus on Time Trend Analysis. **Risk Analysis**, v. 40, n. 9, p. 1723–1743, 2020. Disponível em: https://doi.org/10.1111/risa.13536

KALININA, A.; SPADA, M.; BURGHERR, P. Quantitative Assessment of Uncertainties and Sensitivities in the Estimation of Life Loss Due to the Instantaneous Break of a Hypothetical Dam in Switzerland. **Water**, v. 13, n. 3414, p. 22, 2021. Disponível em: https://doi.org/10.3390/w13233414

KALININA, A.; SPADA, M.; VETSCH, D. F.; MARELLI, S.; WHEALTON, C.; BURGHERR, P.; SUDRET, B. Metamodeling for uncertainty quantification of a flood

wave model for concrete dam breaks. **Energies**, v. 13, n. 14, 2020. Disponível em: https://doi.org/10.3390/en13143685

KHERADMAND, S.; SEIDOU, O.; KONTE, D.; BARMOU BATOURE, M. B. Evaluation of adaptation options to flood risk in a probabilistic framework. **Journal of Hydrology: Regional Studies**, v. 19, n. July, p. 1–16, 2018. Disponível em: https://doi.org/10.1016/j.ejrh.2018.07.001

KIENZLER, S.; PECH, I.; KREIBICH, H.; MÜLLER, M.; THIEKEN, A. H. After the extreme flood in 2002: Changes in preparedness, response and recovery of flood-affected residents in Germany between 2005 and 2011. **Natural Hazards and Earth System Sciences**, v. 15, n. 3, p. 505–526, 2015. Disponível em: https://doi.org/10.5194/nhess-15-505-2015

KIM, B.; SANDERS, B. F. Dam-Break Flood Model Uncertainty Assessment: Case Study of Extreme Flooding with Multiple Dam Failures in Gangneung, South Korea. **Journal of Hydraulic Engineering**, v. 142, n. 5, p. 05016002, 2016. Disponível em: https://doi.org/10.1061/(asce)hy.1943-7900.0001097

KOLL, C.; LINDELL, M. K.; CHEN, C.; WANG, H. Emergency Warning Dissemination in a Multiplex Social Network. **JASSS**, v. 26, n. 1, 2023. Disponível em: https://doi.org/10.18564/jasss.4946

KREIBICH, H. *et al.* The challenge of unprecedented floods and droughts in risk management. **Nature**, v. 608, n. 7921, p. 80–86, 2022. Disponível em: https://doi.org/10.1038/s41586-022-04917-5

KREIBICH, H.; HUDSON, P.; MERZ, B. Knowing what to do substantially improves the effectiveness of flood early warning. **Bulletin of the American Meteorological Society**, v. 102, n. 7, p. E1450–E1463, 2021. Disponível em: https://doi.org/10.1175/BAMS-D-20-0262.1

KREIBICH, H.; MÜLLER, M.; SCHRÖTER, K.; THIEKEN, A. H. New insights into flood warning reception and emergency response by affected parties. **Natural Hazards and**

Earth System Sciences, v. 17, n. 12, p. 2075–2092, 2017. Disponível em: https://doi.org/10.5194/nhess-17-2075-2017

KRON, W.; BELL, R.; THIEBES, B.; THIEKEN, A. H. The July 2021 flood disaster in Germany. *In*: 2022, Tokyo, Japan. **HELP Global Report on Water and Disasters 2022, Secretariat of the High-level Experts and Leaders Panel on Water and Disasters (HELP)**. Tokyo, Japan: *[s. n.]*, 2022. p. 12–44.

KRUSKAL, W. H.; WALLIS, W. A. Use of ranks in one-criterion variance analysis. **Journal of the American statistical Association**, v. 47, n. 260, p. 583–621, 1952. Disponível em: https://doi.org/10.1080/01621459.1952.10483441

KULLER, M.; SCHOENHOLZER, K.; LIENERT, J. Creating effective flood warnings: A framework from a critical review. **Journal of Hydrology**, v. 602, n. June, p. 126708, 2021. Disponível em: https://doi.org/10.1016/j.jhydrol.2021.126708

LANG, S. Current Australian and international practices for dam failure consequence assessments. *In*: 2018, Melbourne, Victoria, Austrália. **AUSTRALIAN COMMITTEE ON LARGE DAMS CONFERENCE**. Melbourne, Victoria, Austrália: Comitê Nacional Australiano de Grandes Barragens, 2018. p. 1–6.

LEE, Y. H.; KIM, H. Il; HAN, K. Y.; HONG, W. H. Flood evacuation routes based on spatiotemporal inundation risk assessment. **Water (Switzerland)**, v. 12, n. 8, 2020. Disponível em: https://doi.org/10.3390/w12082271

LEONG-CUZACK, T.; NIELSEN, C.; KAVANAGH, C.; WATT, S. Quantitative Assessment of Dam Safety Emergency Management Using HEC-LifeSim: Is it feasible? *In*: 2019, Auckland, New Zealand. **ANCOLD Conference**. Auckland, New Zealand: ANCOLD, 2019. p. 11.

LI, Y.; ZHOU, W. H.; SHEN, P. Flood risk assessment of loss of life for a coastal city under the compound effect of storm surge and rainfall. **Urban Climate**, v. 47, 2023. Disponível em: https://doi.org/10.1016/j.uclim.2022.101396

LINDELL, M. K.; SORENSEN, J. H.; BAKER, E. J.; LEHMAN, W. P. Community response to hurricane threat: Estimates of household evacuation preparation time

distributions. **Transportation Research Part D: Transport and Environment**, v. 85, 2020. Disponível em: https://doi.org/10.1016/j.trd.2020.102457

LINDELL, M. K.; SORENSEN, J. H.; EARL, J. B.; LEHMAN, W. P. Community Response to Hurricane Threat: Estimates of Warning Diffusion Time Distributions. **Natural Hazards Review**, v. 22, n. 2, p. 0402100, 2021. Disponível em: https://doi.org/10.1061/(ASCE)NH.1527

LUMBROSO, D.; DAVISON, M. Use of an agent-based model and Monte Carlo analysis to estimate the effectiveness of emergency management interventions to reduce loss of life during extreme floods. **Journal of Flood Risk Management**, v. 11, p. S419–S433, 2018. Disponível em: https://doi.org/10.1111/jfr3.12230

LUMBROSO, D.; DAVISON, M.; BODY, R.; PETKOVŠEK, G. Modelling the Brumadinho tailings dam failure, the subsequent loss of life and how it could have been reduced. **Natural Hazards and Earth System Sciences**, v. 21, n. 1, p. 21–37, 2021. Disponível em: https://doi.org/10.5194/nhess-21-21-2021

LUMBROSO, D.; DAVISON, M.; WETTON, M. Development of an agent-based model to improve emergency planning for floods and dam failures. **Journal of Hydroinformatics**, v. 25, n. 5, p. 1610–1628, 2023. Disponível em: https://doi.org/10.2166/hydro.2023.194

MACCHIONE, F.; DE LORENZO, G.; GRAZIANO, A. A. Study of key aspects in simplified modelling of man-made earthen dams breaching: breach shape, erosion process and hydraulics. **Journal of Hydrology**, v. 620, 2023. Disponível em: https://doi.org/10.1016/j.jhydrol.2023.129425

MACPHERSON-KRUTSKY, C.; BRAND, B. D.; LINDELL, M. K. Do engagement best practices motivate preparedness intentions? Data from earthquake workshops for Spanish speakers. **Risk Analysis**, 2025. Disponível em: https://doi.org/10.1111/risa.17712

MAHMASSANI, H. S.; DONG, J.; KIM, J.; CHEN, R. B.; PARK, B. **Incorporating weather impacts in traffic estimation and prediction systemsFHWA-JPO-09-065,**

EDL 14497. Washington, DC 20590: *[s. n.]*, 2009. Disponível em: https://rosap.ntl.bts.gov/view/dot/3990.

MAHMOUD, A. A.; WANG, J. T.; JIN, F. An improved method for estimating life losses from dam failure in China. **Stochastic Environmental Research and Risk Assessment**, v. 34, n. 8, p. 1263–1279, 2020. Disponível em: https://doi.org/10.1007/s00477-020-01820-1

MAIJALA, T.; HUOKUNA, M.; HONKAKUNNAS, T. **Rescue Actions Based on Dam-Break Flood Analysis. The Use of Physical Models in Dam-Break Flood Analysis**. Helsinki, Finland: *[s. n.]*, 2001.

MANN, H. B.; WHITNEY, D. R. On a test of whether one of two random variables is stochastically larger than the other. **The annals of mathematical statistics**, v. 18, n. 1, p. 50–60, 1947. Disponível em: https://doi.org/10.1214/aoms/117773049

MARANGOZ, H. O.; ANILAN, T. Two-dimensional modeling of flood wave propagation in residential areas after a dam break with application of diffusive and dynamic wave approaches. **Natural Hazards**, v. 110, n. 1, p. 429–449, 2022. Disponível em: https://doi.org/10.1007/s11069-021-04953-w

MARANZONI, A.; D'ORIA, M.; MAZZOLENI, M. Probabilistic Flood Hazard Mapping Considering Multiple Levee Breaches. **Water Resources Research**, v. 58, n. 4, p. 1–26, 2022. Disponível em: https://doi.org/10.1029/2021WR030874

MARANZONI, A.; D'ORIA, M.; RIZZO, C. Quantitative flood hazard assessment methods: A review. **Journal of Flood Risk Management**, v. 16, n. 1, 2023 a. Disponível em: https://doi.org/10.1111/jfr3.12855

MARANZONI, A.; D'ORIA, M.; RIZZO, C. Probabilistic mapping of life loss due to dam-break flooding. **Natural Hazards**, 2023 b. Disponível em: https://doi.org/10.1007/s11069-023-06285-3

MCCLELLAND, D. M.; BOWLES, D. S. **Estimating life loss for dam safety risk assessment - A review and new approachInstitute for Water Resources U.S. Army Corps of Engineers**. Logan, Utah: *[s. n.]*, 2002.

MELO, M.; ELEUTÉRIO, J. Probabilistic Analysis of Floods from Tailings Dam Failures: A Method to Analyze the Impact of Rheological Parameters on the HEC-RAS Bingham and Herschel-Bulkley Models. **Water (Switzerland)**, v. 15, n. 16, 2023. Disponível em: https://doi.org/10.3390/w15162866

MERZ, B.; BLÖSCHL, G.; JÜPNER, R.; KREIBICH, H.; SCHRÖTER, K.; VOROGUSHYN, S. Invited perspectives: safeguarding the usability and credibility of flood hazard and risk assessments. **Natural Hazards and Earth System Sciences**, v. 24, n. 11, p. 4015–4030, 2024. Disponível em: https://doi.org/10.5194/nhess-24-4015-2024

MERZ, B.; BLÖSCHL, G.; VOROGUSHYN, S.; DOTTORI, F.; AERTS, J. C. J. H.; BATES, P.; BERTOLA, M.; KEMTER, M.; KREIBICH, H.; LALL, U.; MACDONALD, E. Causes, impacts and patterns of disastrous river floods. **Nature Reviews Earth and Environment**, v. 2, n. 9, p. 592–609, 2021. Disponível em: https://doi.org/10.1038/s43017-021-00195-3

MERZ, B.; KREIBICH, H.; SCHWARZE, R.; THIEKEN, A. Review article “assessment of economic flood damage”. **Natural Hazards and Earth System Science**, v. 10, n. 8, p. 1697–1724, 2010. Disponível em: https://doi.org/10.5194/nhess-10-1697-2010

MISHRA, A. *et al.* An Overview of Flood Concepts, Challenges, and Future Directions. **Journal of Hydrologic Engineering**, v. 27, n. 6, 2022. Disponível em: https://doi.org/10.1061/(asce)he.1943-5584.0002164

MOEL, H. De; JONGMAN, B.; KREIBICH, H.; MERZ, B. Flood risk assessments at different spatial scales. **Mitig Adapt Strateg Glob Change**, v. 20, p. 865–890, 2015. Disponível em: https://doi.org/10.1007/s11027-015-9654-z

NAJAFI, H.; SHRESTHA, P. K.; RAKOVEC, O.; APEL, H.; VOROGUSHYN, S.; KUMAR, R.; THOBER, S.; MERZ, B.; SAMANIEGO, L. High-resolution impact-based early warning system for riverine flooding. **Nature Communications**, v. 15, n. 1, p. 3726, 2024. Disponível em: https://doi.org/10.1038/s41467-024-48065-y

NEEDHAM, J.; FIELDS, W.; LEHMAN, W. The US Army Corps of Engineers Scalable Approach to Estimating Loss of Life from Flooding. *In*: 2016, Lyon, France. **III European Conference on Flood Risk Management**. Lyon, France: *[s. n.]*, 2016. p. 6.Disponível em: https://doi.org/10.1051/e3sconf/20160706003

NEEDHAM, J.; SORENSEN, J. H.; MILETI, D. S.; LANG, S. Warning and mobilization of populations at risk of dam failure. *In*: 2016, Adelaide. **ANCOLD Conference**. Adelaide: ANCOLD, 2016. p. 1–10.

NOFAL, O. M.; VAN DE LINDT, J. W. **Understanding flood risk in the context of community resilience modeling for the built environment: research needs and trends**. *[S. l.]*: Taylor and Francis Ltd., 2022. Disponível em: https://doi.org/10.1080/23789689.2020.1722546

OGUZHAN, S.; AKSOY, A. O. Experimental investigation of the effect of vegetation on dam break flood waves. **Journal of Hydrology and Hydromechanics**, v. 68, n. 3, p. 231–241, 2020. Disponível em: https://doi.org/10.2478/johh-2020-0026

OUBENNACEUR, K.; CHOKMANI, K.; NASTEV, M.; TANGUY, M.; RAYMOND, S. Uncertainty analysis of a two-dimensional hydraulic model. **Water (Switzerland)**, v. 10, n. 3, p. 1–19, 2018. Disponível em: https://doi.org/10.3390/w10030272

PANDEY, B. R.; KNOBLAUCH, H.; ZENZ, G. Potential Dam Breach Flood Assessment with the 2D Diffusion and Full Dynamic Wave Equations Using a Hydrologic Engineering Center-River Analysis System. **Water (Switzerland)**, v. 16, n. 2, 2024. Disponível em: https://doi.org/10.3390/w16020277

PAPAGIANNAKI, K. *et al.* Developing a large-scale dataset of flood fatalities for territories in the Euro-Mediterranean region, FFEM-DB. **Scientific Data**, v. 9, n. 1, p. 166, 2022. Disponível em: https://doi.org/10.1038/s41597-022-01273-x

PAPROTNY, D. **Pan-European exposure maps and uncertainty estimates from HANZE v2.0 model, 1870-2020**. *[S. l.]*: Zenodo, 2023. Disponível em: https://doi.org/10.5281/zenodo.7885990

PAPROTNY, D.; MENGEL, M. Population, land use and economic exposure estimates for Europe at 100 m resolution from 1870 to 2020. **Scientific Data**, v. 10, n. 1, p. 372, 2023. Disponível em: https://doi.org/10.1038/s41597-023-02282-0

PAPROTNY, D.; RHEIN, B.; VOUSDOUKAS, M. I.; TEREFENKO, P.; DOTTORI, F.; TREU, S.; ŚLEDZIOWSKI, J.; FEYEN, L.; KREIBICH, H. Merging modelled and reported flood impacts in Europe in a combined flood event catalogue for 1950-2020. **Hydrology and Earth System Sciences**, v. 28, n. 17, p. 3983–4010, 2024. Disponível em: https://doi.org/10.5194/hess-28-3983-2024

PATÉ-CORNELL, M. E. Uncertainties in risk analysis: Six levels of treatment. **Reliability Engineering and System Safety**, v. 54, n. 2–3, p. 95–111, 1996. Disponível em: https://doi.org/10.1016/S0951-8320(96)00067-1

PENG, J.; ZHANG, J.; SAYAMA, T. Assessment of loss of life owing to dam-failure flooding considering population distribution and evacuation. **International Journal of Disaster Risk Reduction**, v. 112, n. August, 2024. Disponível em: https://doi.org/10.1016/j.ijdrr.2024.104737

PENG, M.; ZHANG, L. M. Analysis of human risks due to dam-break floods — part 1: a new model based on Bayesian networks. **Natural Hazards**, v. 64, p. 903–933, 2012. Disponível em: https://doi.org/10.1007/s11069-012-0275-5

PENNING-ROWSELL, E.; FLOYD, P.; RAMSBOTTOM, D.; SURENDRAN, S. Estimating Injury and Loss of Life in Floods: A Deterministic Framework. **Natural Hazards**, v. 36, p. 43–64, 2005. Disponível em: https://doi.org/10.1007/s11069-004-4538-7

PETER, S. J.; SIVIGLIA, A.; NAGEL, J.; MARELLI, S.; BOES, R. M.; VETSCH, D.; SUDRET, B. Development of Probabilistic Dam Breach Model Using Bayesian Inference. **Water Resources Research**, v. 54, n. 7, p. 4376–4400, 2018. Disponível em: https://doi.org/10.1029/2017WR021176

PETRUCCI, O. Review article: Factors leading to the occurrence of flood fatalities: A systematic review of research papers published between 2010 and 2020. **Natural**

Hazards and Earth System Sciences, v. 22, n. 1, p. 71–83, 2022. Disponível em: https://doi.org/10.5194/nhess-22-71-2022

PHILIPPUS, D.; WOLFAND, J. M.; ABDI, R.; HOGUE, T. S. Raspy-cal: A genetic algorithm-based automatic calibration tool for hec-ras hydraulic models. **Water (Switzerland)**, v. 13, n. 21, p. 1–15, 2021. Disponível em: https://doi.org/10.3390/w13213061

PROSKE, D. Comparison of dam failure frequencies and failure probabilities. **Beton- und Stahlbetonbau**, v. 113, p. 2–6, 2018. Disponível em: https://doi.org/10.1002/best.201800047

PSOMIADIS, E.; TOMANIS, L.; KAVVADIAS, A.; SOULIS, K. X.; CHARIZOPOULOS, N.; MICHAS, S. Potential dam breach analysis and flood wave risk assessment using HEC-RAS and remote sensing data: A multicriteria approach. **Water (Switzerland)**, v. 13, n. 3, 2021. Disponível em: https://doi.org/10.3390/w13030364

RHEIN, B.; KREIBICH, H. Causes of the exceptionally high number of fatalities in the Ahr valley, Germany, during the 2021 flood. **Natural Hazards and Earth System Sciences**, v. 25, n. 2, p. 581–589, 2025. Disponível em: https://doi.org/10.5194/nhess-25-581-2025

RIEMBAUER, G.; WEINMANN, A.; XU, S.; EICHFUSS, S.; EBERZ, C.; NETELER, M. Germany-wide Sentinel-2 based land cover classification and change detection for settlement and infrastructure monitoring. *In*: 2021, Virtual. **Conference on Big Data from Space**. Virtual: *[s. n.]*, 2021. p. 53–56.Disponível em: https://doi.org/10.2760/125905

RISHER, P.; ACKERMAN, C.; MORRILL-WINTER, J.; FIELDS, W.; NEEDHAM, J. Levee Breach Consequence Model Validated by Case Study in Joso, Japan. *In*: 2017, San Antonio, United States. **X Association of State Dam Safety Conference**. San Antonio, United States: Association of State Dam Safety, 2017. p. 13.

RIZZO, C.; MARANZONI, A.; D'ORIA, M. Probabilistic mapping and sensitivity assessment of dam-break flood hazard. **Hydrological Sciences Journal**, 2023. Disponível em: https://doi.org/10.1080/02626667.2023.2174026

ROSGEN, D. L. A classification of natural rivers. **Catena**, v. 22, n. 3, p. 169–199, 1994. Disponível em: https://doi.org/doi.org/10.1016/0341-8162(94)90001-9

ROTTA, L. H. S.; ALCÂNTARA, E.; PARK, E.; NEGRI, R. G.; LIN, Y. N.; BERNARDO, N.; MENDES, T. S. G.; SOUZA FILHO, C. R. The 2019 Brumadinho tailings dam collapse: Possible cause and impacts of the worst human and environmental disaster in Brazil. **International Journal of Applied Earth Observation and Geoinformation**, v. 90, p. 102–119, 2020. Disponível em: https://doi.org/10.1016/j.jag.2020.102119

SALMAN, A. M.; LI, Y. Flood Risk Assessment, Future Trend Modeling, and Risk Communication: A Review of Ongoing Research. **Natural Hazards Review**, v. 19, n. 3, p. 04018011, 2018. Disponível em: https://doi.org/10.1061/(asce)nh.1527-6996.0000294

SARCHANI, S.; KOUTROULIS, A. G. Probabilistic dam breach flood modeling: the case of Valsamiotis dam in Crete. **Natural Hazards**, n. 0123456789, 2022. Disponível em: https://doi.org/10.1007/s11069-022-05446-0

SHAND, T. D.; SMITH, G. P.; COX, R. J.; BLACKA, M. Development of appropriate criteria for the safety and stability of persons and vehicles in floods. *In*: (A. Barton, Org.)2011, **34th IAHR Congress 2011 - Balance and Uncertainty: Water in a Changing World, Incorporating the 33rd Hydrology and Water Resources Symposium and the 10th Conference on Hydraulics in Water Engineering**. : Engineers Australia, 2011. p. 404–412.

SHIRVANI, M.; KESSERWANI, G. Flood-pedestrian simulator for modelling human response dynamics during flood-induced evacuation: Hillsborough stadium case study. **Natural Hazards and Earth System Sciences**, v. 21, n. 10, p. 3175–3198, 2021. Disponível em: https://doi.org/10.5194/nhess-21-3175-2021

SHOKOOHI, A.; AMIRMORADI, K. Developing a regional model to forecast human fatalities during flash floods in urban areas and its uncertainty. **Natural Hazards**, 2025. Disponível em: https://doi.org/10.1007/s11069-025-07176-5

SIAM, M. R. K.; LINDELL, M. K.; WANG, H. Modeling of multi-hazard warning dissemination time distributions: An agent-based approach. **International Journal of Disaster Risk Reduction**, v. 100, 2024. Disponível em: https://doi.org/10.1016/j.ijdrr.2023.104207

SIEGRIST, M.; GUTSCHER, H. Natural hazards and motivation for mitigation behavior: People cannot predict the affect evoked by a severe flood. **Risk Analysis**, v. 28, n. 3, p. 771–778, 2008. Disponível em: https://doi.org/10.1111/j.1539-6924.2008.01049.x

SILIÉZAR, J.; AUMOND, P.; CHAPRON, P.; PÉROCHE, M.; CAN, A. Méthode d'évaluation de l'audibilité d'un système d'alerte SAIP. *In*: 2022, Marseille. **6ème Congrès Français d'Acoustique**. Marseille: HAL, 2022. p. 1–4.Disponível em: https://hal.archives-ouvertes.fr/hal-03777367. Acesso em: 8 out. 2023.

SILVA, A. F. R.; ELEUTÉRIO, J. C. Aplicação dos modelos RCEM e LifeSim para Estimativa de Perdas de Vidas Relacionadas á Inundação Causada pela Ruptura da Barragem de Fundão (Mariana). *In*: 2021, Belo Horizonte, Minas Gerais, Brazil. **XXIV Simpósio Brasileiro de Recursos Hídricos**. Belo Horizonte, Minas Gerais, Brazil: Associação Brasileira de Recursos Hídricos, 2021. p. 1–11.

SILVA, A. F. R.; ELEUTÉRIO, J. C. Analysis of flood warning and evacuation efficiency by comparing damage and life-loss estimates with real consequences related to the São Francisco tailings dam failure in Brazil. **Natural Hazards and Earth System Sciences**, v. 23, n. 9, p. 3095–3110, 2023 a. Disponível em: https://doi.org/10.5194/nhess-23-3095-2023

SILVA, A. F. R.; ELEUTÉRIO, J. C. Effectiveness of a Dam-Breach Flood Alert in Mitigating Life Losses: A Spatiotemporal Sectorisation Analysis in a High-Density Urban Area in Brazil. **Water**, v. 15, n. 19, p. 3433, 2023 b. Disponível em: https://doi.org/10.3390/w15193433

SILVA, A. F. R.; ELEUTÉRIO, J. C. Enhancing the reliability of flood hazard mapping for embankment dam-breach events using probabilistic scenario simulations. **Under adjustments for submission**, 2025.

SILVA, A. F. R.; ELEUTÉRIO, J. C.; APEL, H.; KREIBICH, H. Assessing the impact of early warning and evacuation on human losses during the 2021 Ahr Valley flood in Germany using agent-based modelling. **Natural Hazards and Earth System Sciences**, v. 25, n. 4, p. 1501–1520, 2025. Disponível em: https://doi.org/10.5194/nhess-25-1501-2025

SILVA, T. F. das G.; VINÇON-LEITE, B.; GIANI, A.; FIGUEREDO, C. C.; PETRUCCI, G.; LEMAIRE, B.; SPERLING, E. Von; TASSIN, B.; SEIDL, M.; KHAC, V. T.; OTHERS. Modelagem da Lagoa da Pampulha: uma ferramenta para avaliar o impacto da bacia hidrográfica na dinâmica do fitoplâncton. **Engenharia Sanitária e Ambiental**, v. 21, p. 95–108, 2016.

SINGH, A.; GUNTU, R. K.; SAIRAM, N.; SHAHI, K. R.; BUCH, A.; FISCHER, M.; DHANYA, C. T.; KREIBICH, H. FLEMO $_{flash}$ – Flood Loss Estimation MOdels for companies and households affected by flash floods. **EGUsphere**, v. Preprint, n. Preprint, p. 1–20, 2025. Disponível em: https://doi.org/10.5194/egusphere-2025-1512

SINGH, V. P. **Dam breach modeling techonology**. 1. ed. *[S. l.]*: Springer Dordrecht, 1996. v. 17. Disponível em: https://doi.org/10.1007/978-94-015-8747-1

SMITH, G.; MODRA, B.; TUCKER, T.; COX, R.; FELDER, S. **Vehicle stability testing for flood flowsReport No. WRL TR2017/07**. Sydney: *[s. n.]*, 2017. Disponível em: https://doi.org/10.26190/unsworks/27416.

SMITH, G. P.; DAVEY, E. K.; COX, R. **Flood Hazard**. Water Research Laboratory, Faculty of Engineering,University of New South Wales: *[s. n.]*, 2014.

SORENSEN, J. H.; LINDELL, M. K.; BAKER, E. J.; LEHMAN, W. P. Community Response to Hurricane Threat: Estimates of Warning Issuance Time Distributions. **Weather, Climate, and Society**, v. 12, n. 4, p. 837–846, 2020. Disponível em: https://doi.org/10.1175/WCAS-D-20-0031.1

SORENSEN, J. H.; MILETI, D. S. **INTERVIEW SCHEDULE. Community Warning Issuance, Diffusion, and Protective Action Initiation Estimation**. Lakewood, Colorado: *[s. n.]*, 2015 a.

SORENSEN, J. H.; MILETI, D. S. **Influence Weights and Measures for the Factors Shaping First Alert/Warning Delay, Diffusion and Protective Action Initiation Curves for Dam Breaches , Controlled Dam Releases , and Levee Breaches or Overtopping**. Lakewood, Colorado: *[s. n.]*, 2015 b.

SORENSEN, J. H.; MILETI, D. S. **First Alert or Warning Diffusion Time Estimation for Dam Breaches, Controlled Dam Releases and Levee Breaches or Overtopping**. Lakewood, Colorado: *[s. n.]*, 2015 c.

SORENSEN, J. H.; MILETI, D. S. **First Alert and/or Warning Issuance Time Estimation for Dam Breaches, Controlled Dam Releases, and Levee Breaches or Overtopping**. Lakewood, Colorado: *[s. n.]*, 2015 d.

SORENSEN, J. H.; MILETI, D. S. **Protective Action Initiation Time Estimation for Dam Breaches, Controlled Dam Releases, and Levee Breaches or Overtopping**. Lakewood, Colorado: *[s. n.]*, 2015 e.

SUN, R.; WANG, X.; ZHOU, Z.; AO, X.; SUN, X.; SONG, M. Study of the comprehensive risk analysis of dam-break flooding based on the numerical simulation of flood routing. Part I: Model development. **Natural Hazards**, v. 73, n. 3, p. 1547–1568, 2014. Disponível em: https://doi.org/10.1007/s11069-014-1154-z

SZÖNYI, M.; ROEZER, V.; DEUBELLI, T.; ULRICH, J.; MACCLUNE, K.; LAURIEN, F.; NORTON, R. **Post Event Review Capability flood event review 'Bernd'**. Zurich, Switzerland. Zurich Insurance Company: *[s. n.]*, 2022. Disponível em: https://floodresilience.net/zurich-flood-resilience-alliance/.

TELLMAN, B.; SULLIVAN, J. A.; KUHN, C.; KETTNER, A. J.; DOYLE, C. S.; BRAKENRIDGE, G. R.; ERICKSON, T. A.; SLAYBACK, D. A. Satellite imaging reveals increased proportion of population exposed to floods. **Nature**, v. 596, n. 7870, p. 80–86, 2021. Disponível em: https://doi.org/10.1038/s41586-021-03695-w

THIEKEN, A. H.; BUBECK, P.; HEIDENREICH, A.; VON KEYSERLINGK, J.; DILLENARDT, L.; OTTO, A. Performance of the flood warning system in Germany in July 2021 – insights from affected residents. **Natural Hazards and Earth System Sciences**, v. 23, n. 2, p. 973–990, 2023. Disponível em: https://doi.org/10.5194/nhess-23-973-2023

THIEKEN, A. H.; SAMPROGNA MOHOR, G.; KREIBICH, H.; MÜLLER, M. Compound inland flood events: Different pathways, different impacts and different coping options. **Natural Hazards and Earth System Sciences**, v. 22, n. 1, p. 165–185, 2022. Disponível em: https://doi.org/10.5194/nhess-22-165-2022

THIEKEN, A. H.; ZENKER, M.; BUBECK, P. Flood-related fatalities in July 2021 in North Rhine-Westphalia, Germany: what can be learnt for future flood risk management? **Journal of Coastal and Riverine Flood RiskFlood Risk**, v. 2, p. 1–19, 2023.

TOMURA, S.; CHIBA, M.; YAMAMOTO, T.; UEMURA, F.; MASUYA, S.; OMURA, N.; YOSHIDA, T.; TAKEDA, A.; HOSHINO, T.; YAMADA, T.; NAKATSUGAWA, M. Fatality estimation by life loss evaluation model for the large-scale floods under future climate. *In*: 2020, Sapporo, Japan. **22nd Congress of the International Association for Hydro-Environment Engineering and Research-Asia Pacific Division**. Sapporo, Japan: IAHR, 2020. p. 1–8.

TSAI, C. W.; FRANCESCHINI, S. Evaluation of Probabilistic Point Estimate Methods in Uncertainty Analysis for Environmental Engineering Applications. **Journal of Environmental Engineering**, v. 131, n. 3, p. 387–395, 2005. Disponível em: https://doi.org/10.1061/(asce)0733-9372(2005)131:3(387)

TSAI, C. W.; YEH, J. J.; HUANG, C. H. Development of probabilistic inundation mapping for dam failure induced floods. **Stochastic Environmental Research and Risk Assessment**, v. 33, n. 1, p. 91–110, 2019. Disponível em: https://doi.org/10.1007/s00477-018-1636-8

TSCHIEDEL, A. da F.; PAIVA, R. C. D. de. Uncertainty assessment in hydrodynamic modeling of floods generated by dam break Avaliação de incertezas em simulações

hidrodinâmicas de ondas geradas por rompimento de barragens. **Revista Brasileira de Recursos Hídricos**, v. 30, n. 23, p. 1–17, 2018. Disponível em: https://doi.org/10.1590/2318-0331.231820170074

USACE. **HEC-LifeSim. Life Loss Estimation. User's Manual - Version 1.0.1**. Davis, California: *[s. n.]*, 2019.

USACE. **HEC-LifeSim. Life Loss Estimation. Version 2.0. Technical Reference Manual. CPD-97a**. Davis, California: *[s. n.]*, 2020. Disponível em: www.hec.usace.army.mil.

USACE. **LifeSim. Life Loss Estimation. User's Manual. Version 2.0**. Davis, California: *[s. n.]*, 2021.

USACE. **LifeSim. Version 2.1.3**. Lakewood, Colorado: Risk Management Center, Institute for Water Resources, U.S. Army Corps of Engineers, 2023. Disponível em: https://www.rmc.usace.army.mil/Software/LifeSim/

USACE. **LifeSim. Version 2.1.5**. Lakewood, Colorado: Institute for Water Resources, Risk Management Center, US Army Corps of Engineers, 2025. Disponível em: https://github.com/USACE-RMC/LifeSim. Acesso em: 23 abr. 2025.

USBR. **RCEM – Reclamation Consequence Estimating Methodology - Guidelines for Estimating Life Loss for Dam Safety Risk Analysis**. Washington, DC: *[s. n.]*, 2015.

VIANINI NETO, L. **Estudo de ruptura da barragem da Pampulha, em Belo Horizonte: Retroanálise da brecha do acidente de 1954 e ruptura hipotética nas condições atuais**. 2016. Master thesis - Federal University of Minas Gerias, Belo Horizonte, Minas Gerais, Brazil, 2016.

VINET, F.; LUMBROSO, D.; DEFOSSEZ, S.; BOISSIER, L. A comparative analysis of the loss of life during two recent floods in France: The sea surge caused by the storm Xynthia and the flash flood in Var. **Natural Hazards**, v. 61, n. 3, p. 1179–1201, 2012. Disponível em: https://doi.org/10.1007/s11069-011-9975-5

VOROGUSHYN, S.; HAN, L.; APEL, H.; NGUYEN, V. D.; GUSE, B.; GUAN, X. It could have been much worse: spatial counterfactuals of the July 2021 flood in the Ahr valley, Germany. **Natural Hazards and Earth System Sciences Discussions**, 2024. Disponível em: https://doi.org/10.5194/nhess-2024-97

WAHL, T. L. Uncertainty of Predictions of Embankment Dam Breach Parameters. **Journal of Hydraulic Engineering**, v. 130, n. 5, p. 389–397, 2004.

WANG, H. Lessons Learnt From Evacuation Modelling for Dam Failure Consequence Assessments. *In*: 2019, Auckland, New Zealand. **ANCOLD Conference**. Auckland, New Zealand: ANCOLD, 2019. p. 9.

WANG, Y.; FU, Z.; CHENG, Z.; XIANG, Y.; CHEN, J.; ZHANG, P.; YANG, X. Uncertainty analysis of dam-break flood risk consequences under the influence of non-structural measures. **International Journal of Disaster Risk Reduction**, v. 102, p. 104265, 2024. Disponível em: https://doi.org/10.1016/j.ijdrr.2024.104265

WASKO, C.; NATHAN, R.; STEIN, L.; O'SHEA, D. Evidence of shorter more extreme rainfalls and increased flood variability under climate change. **Journal of Hydrology**, v. 603, n. September, p. 126994, 2021. Disponível em: https://doi.org/10.1016/j.jhydrol.2021.126994

WORLEY, L. C.; UNDERWOOD, K. L.; VARTANIAN, N. L. V.; DEWOOLKAR, M. M.; MATT, J. E.; RIZZO, D. M. Semi-automated hydraulic model wrapper to support stakeholder evaluation: A floodplain reconnection study using 2D hydrologic engineering center's river analysis system. **River Research and Applications**, v. 38, n. 4, p. 799–809, 2022. Disponível em: https://doi.org/10.1002/rra.3946

XU, Y.; ZHANG, L. M. Breaching Parameters for Earth and Rockfill Dams. **Journal of Geotechnical and Geoenvironmental Engineering**, v. 135, n. 12, p. 1957–1970, 2009.

YARI, A.; OSTADTAGHIZADEH, A.; ARDALAN, A.; ZAREZADEH, Y.; RAHIMIFOROUSHANI, A.; BIDARPOOR, F. Risk factors of death from flood: Findings of a systematic review. **Journal of Environmental Health Science and Engineering**,

v. 18, n. 2, p. 1643–1653, 2020. Disponível em: https://doi.org/10.1007/s40201-020-00511-x

YAZDANI, M.; GENCARELLI, C. N.; SALVATI, P.; MOLINARI, D. An empirical flood fatality model for Italy using random forest algorithm. **International Journal of Disaster Risk Reduction**, v. 98, n. October, 2023. Disponível em: https://doi.org/10.1016/j.ijdrr.2023.104110

ZENZ, G.; GOLDGRUBER, M. 2th International BENCHMARK WORKSHOP ON NUMERICAL ANALYSIS OF DAMS, 2nd-4th October, 2013, Graz-AUSTRIA. *In*: 2013, **Anais [...]**. *[S. l.: s. n.]*Disponível em: www.atcold.at

ZHAI, G.; FUKUZONO, T.; IKEDA, S. An empirical model of fatalities and injuries due to floods in Japan. **Journal of the American Water Resources Association**, v. 42, n. 4, p. 863–875, 2006. Disponível em: https://doi.org/10.1111/j.1752-1688.2006.tb04500.x

ZHANG, A. T.; GU, V. X. Global Dam Tracker: A database of more than 35,000 dams with location, catchment, and attribute information. **Scientific Data**, v. 10, n. 1, 2023. Disponível em: https://doi.org/10.1038/s41597-023-02008-2

ZHANG, J.; XU, W.; LIAO, X.; ZONG, S.; LIU, B. Global mortality risk assessment from river flooding under climate change. **Environmental Research Letters**, v. 16, n. 6, 2021. Disponível em: https://doi.org/10.1088/1748-9326/abff87

ZHANG, L.; PENG, M.; CHANG, D.; XU, Y. **Dam failure mechanisms and risk assessment**. *[S. l.]*: John Wiley & Sons, 2016. Disponível em: https://doi.org/10.1002/9781118558522

ZHANG, R.; LIU, D.; DU, E.; XIONG, L.; CHEN, J.; CHEN, H. An agent-based model to simulate human responses to flash flood warnings for improving evacuation performance. **Journal of Hydrology**, v. 628, 2024. Disponível em: https://doi.org/10.1016/j.jhydrol.2023.130452